UNIVERSIDAD DE CHILE
FACULTAD DE CIENCIAS FÍSICAS Y MATEMÁTICAS
DEPARTAMENTO DE INGENIERÍA MATEMÁTICA

ESTUDIO, MODELAMIENTO Y DESARROLLO DE MÉTODOS DE CONTROL PARA SISTEMAS DE REGULACIÓN BIOLÓGICA INTRACELULAR

TESIS PARA OPTAR AL GRADO DE DOCTOR EN CIENCIAS DE LA INGENIERÍA
MENCIÓN MODELACIÓN MATEMÁTICA
EN COTUTELA CON LA UNIVERSIDAD DE NIZA-SOPHIA ANTIPOLIS

GUILLERMO OCTAVIO ESPINOZA ARMIJO

PROFESOR GUÍA :
ALEJANDRO MAASS SEPÚLVEDA

MIEMBROS DE LA COMISIÓN:
XAVIER BRESSAUD
MAURICIO GONZÁLEZ CANALES
SERVET MARTÍNEZ AGUILERA
ELISABETH PÉCOU GAMBAUDO
ANNE SIEGEL
EDGARDO UGALDE SALDAÑA

SANTIAGO - CHILE
DICIEMBRE 2010

ESTUDIO, MODELAMIENTO Y DESARROLLO DE MÉTODOS DE CONTROL PARA SISTEMAS DE REGULACIÓN BIOLÓGICA INTRACELULAR

Esta tesis se centra en el marco de los sistemas dinámicos biológicos. Su objetivo central radica en el hecho de que a partir de un estudio matemático formal es posible inferir y responder interesantes preguntas biológicas.

El primer problema abordado son las conjeturas de Thomas, las cuales establecen que una condición necesaria para la existencia de ciclos atractores (resp. multiestabilidad) es la presencia de circuitos negativos (resp. positivos) en el grafo regulatorio. Se comienza probando una serie de lemas con el fin de dar condiciones sobre el grafo de transición, junto con una formula general para el signo. Con ello es posible dar una prueba alternativa a un teorema de Remy et al. basada en la segunda conjetura en el caso booleano. En el segundo caso, encontramos condiciones para la existencia general de ciclos. Además se define el "grafo de transición extendido", el cual contiene no solo información de la dinámica sino que también de la estructura del grafo regulatorio.

En el segundo problema se muestra que el método de desincronización propuesto por Pécou se puede simular de forma numérica estable. En esta dirección, se aplica con éxito el algoritmo al modelo de Goodwin con función de regulación positiva y negativa, mostrándose teóricamente cómo inducir comportamiento periódico mediante la adición de una nueva ecuación. La inducción del caos del tipo Shilnikov o Lorenz, según la naturaleza de los valores propios, se muestra mediante la construcción de las órbitas homoclínicas y la sensibilidad a las condiciones iniciales.

Finalmente, se propone un modelo matemático para los procesos de incorporación, flujo, almacenamiento y tráfico de metales pesados Cu, Zn, Mn y Fe en *Halobacterium NRC-1*. Se muestra formalmente la existencia de estados estacionarios. Además, se derivan condiciones de monotonía para la existencia de respuestas globales en estado estacionario, independiente de la elección de los parámetros. Junto con los resultados teóricos, se desarrollan simulaciones para responder preguntas biológicas centrales sobre el crecimiento y la muerte de la *archaea* a altas concentraciones de metales, y la respuesta celular ante el estrés producido por incrementos sucesivos y alternados de metales.

Agradecimientos

En primer lugar doy gracias a mis directores de tesis Alejandro Maass y Elisabeth Pécou por el apoyo constante en mi formación como científico. Agradezco a los evaluadores de la tesis Anne Siegel y Edgardo Ugalde, así como también a los miembros del jurado.

Deseo tambien expresar mi gratitud al laboratorio J.A. Dieudonné, de la Universidad de Nice-Sophia Antipolis y al departamento de Ingeniería Matemática de la Universidad de Chile, donde la tesis fue escrita, por su hospitalidad, apoyo y buena disponibilidad, a sus profesores y funcionarios.

De manera muy especial quisiera agradecer a mi familia, Alejandra, mis hijos, mis padres y hermanos, por su apoyo irrestricto durante este largo proceso. Han sido bastantes años en los cuales no siempre ha resultado todo muy fácil, sin embargo ellos siempre han estado conmigo, al igual que mis amigos matemáticos (p-grupo) con quienes he compartido momentos muy importantes, en especial a Daniel, José, Angela y Laura con quienes estuve durante mi estadía en Niza.

Contents

Contents

Contents

List of Figures

1 General Introduction

During the past years science has evolved into a more complex state where in order to understand key phenomena it is necessary to integrate the knowledge from different areas such as mathematics, biology, computer science, chemistry and physics. Nowadays it is better to understand the whole picture rather than the sum of pieces (holism instead of reduction); and at this scenario it is mandatory the existence of interdisciplinary groups working together on the study of complex biological processes, moving away the frontiers of knowledge.

The need to give sense to complex interactions has led some researchers to shift from a component-level to a system-level perspective. With the progress in high-throughput technologies and bioinformatics in recent years, it is possible to determine to what extent genetic or environmental manipulation of a biological system affects the expression of thousands of genes and proteins. This form of study requires a shift from a conventional individual approach (divide-and-conquer approach) towards an integrated approach. The integrated approach led to an emerging field called Systems biology.

For our purposes, we can define Systems biology as a biology-based inter-disciplinary study field that focuses on complex interactions in biological systems. Mathematical models are being used in support of this, continuing a long tradition inherited from genetics, biochemistry, evolutionary biology and ecology. Systems biology has been created to reveal the dynamic interrelationship between system components, in order to enable the discovery of novel biology [SB07]. Moreover, it tries to understand biological systems within the consistent framework of knowledge built up from the molecular level to the system level [K01]. Even, from a mathematical point of view, we can understand Systems biology as the application of dynamical systems theory to molecular biology, in order to obtain theoretical results for the cellular behavior. For that reason, Systems biology have had in the last twenty years a tremendous importance and development, as well as the scientific disciplines associated with it.

Several topics where Systems biology has made its contribution can be found in the literature: metabolic pathways, microarray analysis, cell development and differentiation, or target drugs design, among others are novel examples [Ka06]. One of the first and most important discoveries was the model explaining the lac operon [JM61]. Thanks to the system point of

view it was possible to understand in a simpler form the central mechanism at which the cell can transform the lactose into glucose as a way to survive in environments with low sugar concentrations. Along with the above, several organisms, such as bacteria and archaea mainly (*E. coli, S. cerevisiae and P. aeruginosa*), have been studied as toy experimental models in order to understand their central mechanisms, searching similarities and differences between them.

Finally, the Systems biology approach often involves the development of mechanistic models, such as the reconstruction of dynamical systems from the quantitative properties of their elementary building blocks. For instance, some cellular processes and interactions can be modelled as a graph, which can be analyzed mathematically using methods coming from chemical kinetics and control theory, for example. However, due to the large number of parameters, variables and constraints, these mathematical models often need to be solved using numerical and computational techniques. In Figure 1.1 we can observe a schematic representation for Systems biology interactions.
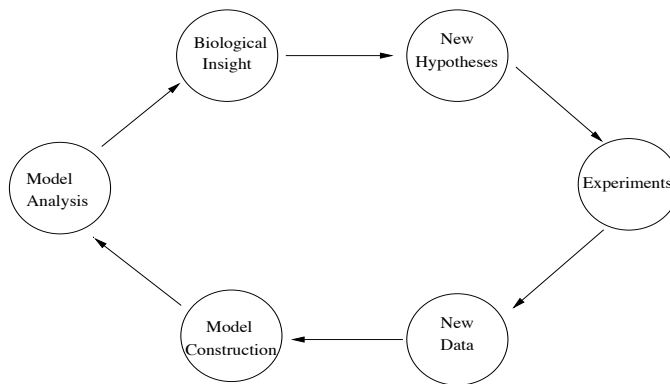
Figure 1.1: Systems biology diagram of research.

1.1 Models as dynamical systems

Most mechanistic models in Systems biology can be regarded as some form of dynamical system. A dynamical system describes the states of a biological system and how these states change in time. It can be abstractly visualized as a state space, upon which is imposed a temporal dynamics: given a particular state as an initial condition, the dynamics defines the trajectory taken over time from that starting point.

Dynamical systems usually depend on parameters. In abstractly visualizing a dynamical system, therefore, one should always keep in mind the parameter space that accompanies the

state space, the dynamics on the state space cannot be defined without first specifying the parameter values, thereby fixing a point in the parameter space. As this point varies, so do the dynamics.

1.1.1 Continuous models

A type of model that is frequently used is one in which the state of a molecular component, x, is its concentration in some cellular compartment (cytoplasm, membrane, biofilm, etc), which we will also denote by x and treat as a function of time, $x(t)$. The temporal dynamics are then described by an ordinary differential equation (ODE) for the rate of production of x. This is how the biochemistry of enzymes has been modelled, which provides a foundation for models of molecular networks [A07].

For example, if x is produced at a (zero order) rate of b units per second and consumed at a (first order) rate of c per second, then

$$\frac{dx}{dt} = b - cx.$$

In this case, the dynamical system has a one dimensional state space, consisting of the single state variable x, and a two dimensional parameter space, consisting of the two parameters b and c, which can be readily solved.

Most dynamical systems arising in Systems biology are nonlinear (complex regulatory functions following Michaelis-Menten scheme) and cannot be solved explicitly (except possibly at steady state). They have to be studied by simulation, for which parameter values must be specified (the parameter problem).

More recently, it has been possible to measure noise in individual cells, revealing the impact of both molecular stochasticity ("intrinsic noise") and cell-to-cell variability ("extrinsic noise") [PB06]. Extrinsic noise can sometimes be modelled as a probability distribution on the initial conditions of a deterministic model or by adding external noise terms, as in the Langevin approach. Molecular stochasticity, however, requires some form of stochastic master equation in which the state of a component is described by the probability distribution of the number of molecules of component x, as a function of time, and the dynamics are described by stochastic differential equations.

1.1.2 Discrete models

Differential equation models are familiar in the physical sciences, biochemistry and physiology. Biologists, however, often find it convenient to describe gene expression in terms of discrete states (on/off or low/high) and the development of microarray technology allows mRNA levels to be quantified into multiple discrete levels.

Genetic manipulations also lead naturally to causal inferences expressed in Boolean logic: "in the absence of X, Y becoming low leads to high Z". These kinds of data and reasoning can be modelled by dynamical systems with discrete states, where the temporal dynamics are given by discrete transitions between states, rather than being parametrised by a global clock, t. When states are composed of many discrete variables (for example, many genes), state transitions may take place synchronously, with each variable being updated simultaneously, or asynchronously, with variables being updated independently of each other.

Thinking in terms of dynamical systems draws attention to the state of the system. Deciding how the state should be represented, whether coarsely as Boolean levels or at fine grain in an agent-based description or somewhere in between as concentrations, and how time and space should be modelled, should depend not on the disciplinary prejudices of the modeler but on the nature of the experimental data and the kinds of biological questions that are being asked [A07].

1.2 Analysis, control and simulations of biomolecular systems

Theoretical Systems biology has worked in the conceptual basis of complicated biological problems in order to find novel solutions. In this searching, other areas of the knowledge as the mathematics has been raised as fundamental pieces in the modelling and understanding of biological processes such as homeostasis, robustness, differentiation and regulation.

If we focus only on the mathematical point of view, there emerge three fundamental topics about cellular modelling: (1) The development of models for the analysis of experimental data in order to prove conjectures; (2) Robustness and network motifs for the control of biological systems; (3) Computational methods and simulations to corroborate theoretical results. In the following we are going to explain each one of these areas.

The analysis of the dynamical behavior is essential to understand the mechanisms behind

the stability and robustness of the system, and the functionalities of the circuits. Fundamental questions about cellular response to environmental perturbations, or why certain network motifs explain observed functions need to be answered.

In general, it is common that biologists represent their results in terms of graphs. These graphs can contain information about genes (genetic networks), proteins structures (amino acid conformation), metabolic fluxes or species interactions (trophic networks). Recently, the study of graphs structures as motifs have received great attention because they can be viewed as biological properties emerging from real systems [A07]. In this line, the comparison between random graphs and regulatory networks confirm the existence of predominant structures that are preserved under the evolution, and the functional analysis of these structures (motifs) are essential in order to obtain results over dynamical properties which permits to compare different organisms [T81].

For that reason, one of the first natural problems lie in how we are able to obtain this graph structure. In general, biological experiments give us as a result biochemical interactions or expression profiles (microarrays). In the first case, it is possible to construct a set of differential deterministic or stochastic equations using the polynomial law formalism. Once we have the system of equations it is not complicated to deduce the Jacobian matrix, even in the discrete case there exists a formula for a discrete Jacobian matrix obtained from the discrete regulatory functions. In the second case, maximal entropy methods are used to infer correlations matrices and with them adjacency matrix can be obtained [L06].

Obviously, the use of regulatory graphs as mathematical objects enables us to find and explore more complex properties that cannot be concluded using only partial biological information. Additionally, since graph theory has been widely studied, different specific results from random graph or small world networks (social networks) among others can be used, implying new information in biological networks and vice-versa.

As we have mentioned before robustness to fluctuations and stability are important properties in biological systems, and in order to study this kind of challenging problems it is crucial to describe them in the language of control theory, so that we can abstract essential parts of the system within the common language of biology and engineering [K01]. Moreover, the importance of the control scheme lies in two facts: complex engineering systems can be found in biological systems, and questions about cellular response to environmental changes, cellular mechanisms to modulate stochastic perturbations, or if it is possible to destroy in some sense the natural stability creating chaos and implying apoptosis can be answered.

During the last years the mathematical study of control systems in biology has reached great interest. Novel works of Uri Alon [A07] and Eduardo Sontag [S05] have shed some

new lights on the problematic, specially in the control of feed-forward and feedback circuits motifs, and in the input/output control of monotone and near monotone systems.

In general, if we compare random networks with real regulatory networks we can observe that from the latest emerge special structures that made it different. Particularly, special interest has acquired three nodes circuits (triangles) called feed-forward circuits, in which two genes regulates a third, and feedback circuits or single loops as a factor stabilizing the systems.

These two types of regulatory circuits have been extensively studied, because they recurrently appear in several networks as patterns (E. coli and yeast). A possible explanation of the phenomena is that in some sense evolution may have been selected them by their specific dynamical function. In this line it can be proved for example that negative feedback (negative auto-regulation) has an speed up in the time response implying robustness to external changes, meanwhile positive feedback slows the response and tends to increase cell-cell variability. For the other side, the feed-forward loops produces changes in the time delay, filtering out brief spurious pulses of signal.

By contrast, Sontag [S07] has proved that intracellular regulatory systems are essentially monotone or close to be monotone. Again the dynamical property is related with graph structures, in this case positive circuits in the regulatory graph (spin sign assignment) imply monotonicity of the system. Dynamical behavior of monotone systems is ordered and non chaotic, and as a consequence the trajectories of the solutions (evolution of the states) converge to the steady states independent of the parameters for the model, besides consistent response to perturbations.

As we have seen before, the mathematical study of biological systems plays an important role in the discovery of emerging properties such as the biological organization of life, which is the intrinsic and ultimate core of Systems biology. However, this is not always possible, there exists systems where the mathematical formalization could not be solved analytically due to the large number of components or the intrinsic complexity by itself. In this scenario an important tool is the computational simulation of the mathematical models.

One of the best and novel examples of computational simulation of mathematical models have to do with the stochastic simulation algorithm. Stochastic modelling has been recently used since it is a more plausible model for real interacting particle systems. In this case, stochastic chemical kinetics describes the time evolution of a well stirred chemically reacting system from where we can derive, by applying probabilistic laws, the chemical master equations (CME). CME can be solved analytically for only a few simple cases, and even numerical solutions are prohibitively difficult in other cases so special simulations techniques, as the

application of the Gillespie algorithms, need to be used in order to solve efficiently the master stochastic equations.

But the simulation is not only used as a testing for mathematical results, in general molecular experiments in biology are extremely expensive as a cause of the repeatability, the technology and the materials employed. In this direction, the design of in-silico experiments for the prediction of the behavior under different environmental conditions is crucial to reduce the number of experiences.

Additionally, the use of special softwares and programs solving problems in database storing data, parameter optimization, hypotheses generator, bifurcation analysis, and data visualization are needed.

As a resume, the system level understanding, specially simulation, control and analysis may lead us to a more complete knowledge of the cellular behavior.

1.3 Main results of the thesis

This thesis is focused in the framework of biological dynamical systems, more specifically in the study, analysis and development of control methods for intracellular regulatory networks. For that reason the aim of this work lies in the fact that from an abstract mathematical study it is possible to infer basic molecular properties and with them answer biological questions.

Mainly three different problems have been studied. The first problem has to deal with the study of Boolean regulatory networks and the Thomas conjecture, the second problem is centered in control methods for non-linear homeostatic systems, more specifically the desynchronization of the Goodwin model, and the third problem is concerned with the mathematical modelling and analysis of metal stress response in *Halobacterium NRC-1* using differential equations. To facilitate access to the individual topics, the chapters are rendered as self-contained as possible. In the following we describe in more details each chapter.

In Chapter 2, we have centered our attention in the study of the Thomas conjecture in Boolean regulatory networks. Boolean networks are defined by the dynamic of a Boolean function $f : \{0, 1\}^n \to \{0, 1\}^n$, represented by the Transition graph, where n corresponds to the number of components (genes and proteins) and $0, 1$ are the states of these components, that is, restriction 0 means that the gene is "off" and 1 that the gene is "on".

The Thomas conjecture relates dynamical properties of the Transition graph, with asyn-

chronous updating, and topological structures or motifs in the regulatory network deduced from the discrete version of the Jacobian matrix. In this scenario, it can be proved for example that negative circuits in the regulatory graph are necessary for the existence of an attractive cycle in the transition graph for f (Homeostasis), and positive circuits are necessary for the existence of multi-stability (cell differentiation). Basically, we are interested in both, find general conditions over the circuits in the graph and give an alternative proof to the first conjecture.

In particular, we have obtained some conditions for the existence of cycles in the Transition graph. In this direction, we studied two cases: attractive cycles and arbitrary cycles. In the first case we made an alternative proof for a theorem of Remy et al. [RRT05] based in the second conjecture. In the second case, we found two conditions for the existence of general cycles. In both cases we derived an interesting formula for the sign function of cycles. Using these conditions we have defined a new graph for the dynamic called Extended Transition graph, which incorporates more information in the vertices, implying a nice method for the partial construction of circuits in the regulatory graph.

Additionally, we have studied necessary and sufficient conditions for both conjectures in a special case when the regulatory graph is composed basically by an isolated circuit. Under these assumptions we have proved, in a constructive way, that if the isolated circuit is positive then there are at least two fixed points and if the isolated circuit is negative then there exists a trap cycle.

In the case of a positive isolated circuit we used a relation between positive circuits in the regulatory graph and the existence of an spin sign assignment for the vertices. This assignment gives us information about the values of the positions for the state $x \in \{0, 1\}^n$, and as we have two possible assignments then we have two different states that correspond to the fixed points. Besides, a well known result of Sontag et al. [ESS06] established that the existence of positive circuits imply that the function f is monotone, property related with global convergence of the trajectories.

Chapter 3 is devoted to the study of non-linear effects in the desynchronization of homeostatic systems. One of the motivation of this work can be explained as follows, let us consider a therapeutic context where the objective is to perturb a hostile organism to kill it. A possible method consists in poisoning the organism by provocating the increase in the concentration of a metabolite up to a lethal level. However this method is difficult to implement because the metabolism has many mechanisms precisely intended to moderate "excesses" (by saturation or homeostatic mechanisms for example). In this context, the central idea is to propose a method in order to disorganize the metabolism.

Inspired in a paper of Pecora and Carroll about master slave synchronization (early 90s) [PC90], where in order to stabilize a chaotic system of non-linear differential equations, it is possible to eliminate one of the equations and take the respective variable as a constant in the others. As a result the reduced system presents stability to the initial conditions loosing the chaotic behavior.

In the opposite direction, our idea is to take a system, known to be stable, and induce the chaotic behavior by adding a new differential equation for one of its constants. The main theorem in this chapter establishes a method to induce chaos in stable systems by periodic orbits. Moreover, since the proof of the theorem is constructive, it is possible to formulate explicitly the new general equation, with the advantage that our method can be programmable.

We start the chapter by introducing the most important ideas of homeostatic systems, desynchronization of stable vector fields and chaos by periodic orbits. Then, we study the construction of the theoretical method in order to prove that the desynchronization can be realized in a stable way on the numerical context. At this point and for illustrative purposes we have chosen the Goodwin model with negative and positive feedback, because of its global stability property, and the synchronized Lorenz model.

The second part contains the spectral and the stability analysis of the desynchronization method applied to the Goodwin model and to the reduced two dimensional Lorenz model, which has lost its chaotic behavior. In both models we have used the proposed method, programmed in $C++$, to induce chaos of Shilnikov or Lorenz type, although the method depends on the nature of the eigenvalues, complex or real. In both scenarios conditions ensuring the chaotic behavior are stated, finding relations between the real or complex eigenvalues and the stable or unstable periodic orbits. Additionally the algorithm is tested in the simplified stable Lorenz model, as an application about how it is possible to recover the chaotic behavior of the original Lorenz model.

With regards to the biological implementation of the method, as a form to design specific drugs, we can say that we are far away to find a solution to the complete problem because of the complexity of the real model. However, we believe that the problem itself deserves our attention in the future, maybe with other classes of models, or maybe integrating interconnected systems.

Finally, Chapter 4 is about metal stress response in *Halobacterium NRC-1*, an extremophile archaea which lives in hyper-salinity environments. The major goal is to study and understand mathematically how the cellular mechanism works allowing the archaea to survive under these extreme conditions. Inspired in biological knowledge extracted from the top

down study of Baliga et al. [B06] we constructed a mathematical model in order to understand the key role of each one of the genes and proteins involved in the mechanisms for traffic, storage, efflux, extrusion and uptake of heavy metals.

Based in the continuous framework of differential equations and the power law formalisms, we are able to propose an ordinary differential equations system describing the four essential processes which are described by two modules, one dealing with the traffic and extrusion (copper-zinc), and the other with the uptake and storage of metal ions (manganese-iron). From the biological point of view many different questions are relevant. In particular, we deal with the question of cellular growth and death at high metal concentrations, and the question of cellular response under successive and alternate metal stress attack. Both questions have been formulated in a personal communication with professor Baliga, and they are essential in order to understand the adaptability of the system to the medium. For that reason we used our proposed model, with an additional equation for the growth, in order to answer this type of biological questions.

We prove in a formal way that both modules, $E(I)$ (copper-zinc extrusion) and $U(I)$ (manganese-iron uptake), present a unique equilibrium state depending on the initial amount of external metal ions. Meanwhile, in the other two cases with recycling, $E(II)$ and $U(II)$, we found a finite number of steady states. In addition, a comment on homeostatic behavior is realized, according to the various kinetic parameters (degradation, synthesis and affinity), by the existence of negative circuits in the associated regulatory graph (Thomas conjecture), and it is determined either by the convergence to the steady state or small oscillations around a given value, independent of the considered parameters (or little, weak homeostasis condition).

To conclude, we derived monotonicity conditions for the existence of global convergence to the steady states. The problem is that in general biological models are not monotone because the associated regulatory graphs have inconsistent arcs (negative circuits). For that reason, in both modules $E(I)$ and $U(I)$, we have used a decomposition technique proposed by Sontag et al. [ESS06] for near monotone systems (engineering perspective). This implies that the controlled system with fixed control variables induces a globally asymptotically stable equilibrium depending on the external metal ions concentrations. Concluding that the trajectories for the autonomous systems (without control) in both modules are globally attractive to its unique equilibrium (robustness).

Bibliography

[A07] Alon, U.: An introduction to Systems biology. Chapman & Hall, 2007.

[B06] Baliga, N.S., Kaur, A., Pan, M., Meislin, M., Facciotti, M., El-Gewely, R.: A system view of haloarchaeal strategies to withstand stress from transition metals. Genome Research 16, 841-854, 2006.

[ESS06] Enciso, G.A., Smith, H.L., Sontag, E.: Nonmonotone systems decomposable into monotone systems with negative feedback. J. Differential equations 224, 205-227, 2006.

[JM61] Jacob, F., Monod, J.: Genetic regulatory mechanisms in the synthesis of proteins. J Mol Biol. 3: 3186, 1961.

[Ka06] Kaneko, K.: Life: An Introduction to Complex Systems Biology. Springer, 2006.

[K01] Kitano, H.: Foundation of Systems biology. Edited by H. Kitano, 2001.

[L06] Lezon, T., Banavar, J.R., Cieplak, M., Maritan, A., Fedoroff, N.V.: Using entropy maximization to infer genetic interaction networks from gene expression patterns. Proc. Natl. Acad. Sci. USA 103:190339038, 2006.

[PB06] Palsson, Bernhard O.: Systems Biology: Properties of Reconstructed Networks. Cambridge University Press, 2006.

[PC90] Pecora, L. M., Carroll, T. L.: Synchronization in chaotic systems. Phys. Rev. Lett. 64, 821-824, 1990.

[RRT05] Remy, E., Ruet, P., Thieffry, D.: Graphics requirements for multistability and attractive cycles in a Boolean dynamical framework. Advances in Applied Mathematics 41(3): 335-350, 2008.

[SB07] Schmid, A.K. and Baliga, N.: Prokaryotic Systems biology. Cell engineering 5: Systems biology. Springer, 395-423, 2007.

[S05] Sontag, E.: Notes on mathematical biology. 2005-2006.

[S07] Sontag, E.: Monotone and near-monotone biochemical networks. Syst. Sybth. Biol 1, 59-87, 2007.

[T81] Thomas, R.: On the relation between the logical structure of systems and their ability to generate multiple steady states and sustained oscillations. In Series in Synergetics, volume 9, pages 180-193. Springer, 1981.

2 Study of circuits in Boolean regulatory networks.

In this chapter we revisit a well known conjecture proposed by the biologist R. Thomas relating the structure of signed regulatory graphs with its dynamical asymptotic behavior. The conjecture establishes that a necessary condition for the existence of an attractive cycle (resp. multistability) is the presence of a negative (resp. positive) circuit in this graph. Both properties are commonly associated to the biological phenomena of homeostasis and cell differentiation respectively.

Different proofs have been proposed in different contexts and mathematical formalisms: continuous case ([G98], [S03], [S05]), Boolean case [RRT05] and general discrete case ([R07], [RC07]). In particular, we will focus on regulatory models described by Boolean maps $f : \{0,1\}^n \to \{0,1\}^n$, and for these we revisited both conjectures. Our purpose is to give alternatives simple and elementary proofs to some of these old conjectures.

Following the definitions and notations in [RRT05] we first prove a series of lemmas in order to give conditions on the transition graph for the existence of signed edges in the regulatory graph, which includes a new sign formula. These general properties allow us to provide another proof for the second Thomas conjecture in the Boolean case that we think is very simple and make appear a kind of "cohomological idea" behind the sign assignment in the regulatory graph. It is also shown that in a particular case of an isolated circuit, that is, a regulatory graph consisting purely of a circuit, both Thomas conjectures are also sufficient. This last case was motivated in [RMCT03].

Additionally, we study general properties relating cycles in the transition graph to circuits in the regulatory graph. In this direction, we have proved, under some assumptions, a path reduction lemma which permit us to show that the existence of cycles in the transition graph implies the existence of circuits in the regulatory graph.

Finally, using these conditions, we propose a formal method to construct an extended transition graph from the Boolean map f. This new graph takes into account not only the

information of the dynamics of f, but also the structure of the signed regulatory graph, combining both. The spirit is to avoid the "problem" of changing from one graph to the other and produce conditions "à la Thomas" on this graph. For the moment this is just a discussion.

2.1 Introduction

Nowadays, genetic regulatory networks are typical instances of what is now commonplace to call a complex system. This term can be described in abstract as a set of elements of the same nature, called entities, related by interactions that create a graph, eventually oriented or labeled by a sign. Other similar systems include metabolic networks, ecological networks, neural networks, social networks, etc.

From a mathematical point of view a regulatory network is constructed from a dynamical system that represents the evolution in time of the values of the entities in such network. From a biological point of view the notion of regulatory network "even if is more intuitive" is classical in modelling and is less formal.

The dynamical systems considered in the literature to model biological systems range from continuous models (formalism of differential equations) to Boolean systems (maps in the discrete Boolean hypercube). Also the way the dynamical system evolves is part of the problem and at least two types of evolution has been considered: asynchronous and synchronous, being the first one considered more "biological" or "realistic". In this section we just comment on all previous models but we concentrate on Boolean systems. We avoid the discussion about the construction of such dynamical systems, but we have to mention that it is a big area of research nowadays.

Once a biological situation is transformed into a dynamical system, several questions are natural. In particular, its asymptotic behavior and thus the existence of periodic orbits and fixed points. At the same time it is relevant to relate such behavior with the biological features of the modelled system. For instance, one associates stable periodic orbits to homeostatic behavior in biology and the existence of several stable orbits to cell differentiation.

In this direction, the biologist René Thomas in 1981 [T81] go further. He proposes that the "topological structure" of the regulatory signed graph(s) can serve as a source of information to know whether a particular asymptotic behavior occurs. We will explain below his conjectures.

The ideas of René Thomas have inspired several mathematicians in the last 30 years, but essentially his intuition is still not deeply understood mathematically, even if several progresses exist in different cases, some of them quite general. Our motivation is to revisit his conjecture in the Boolean case trying to build a mathematical framework to relate "dynamics with topological structure" of the associated signed regulatory graph(s).

2.2 Biological regulatory networks

Often biological interactions are represented by using graphs, essentially because this class of models fits well with experimentation. Therefore, a common problem in biology and a mathematical challenge is to understand these kind of graphs and in some cases the dynamical properties that can be deduced from them when elements of the graph evolve with time

Formally a graph $G = (V, E)$ consists of two sets, vertices V and edges E. The vertices or nodes represent biological entities like genes or products of them as proteins, and the edges represent interactions between them. Moreover, in the case of regulatory interactions the graph can be directed and signed $(+1, -1)$, which indicates activatory or inhibitory effect respectively.

To a biological network one seldom associates a dynamical model, explaining the behavior of the system in time. One uses either differential equations $\dot{x} = f(x)$, Boolean maps $f : \{0, 1\}^n \to \{0, 1\}^n$ or other discrete, continuous or stochastic models. In both frameworks the concentration or absolute quantities of the elements are measured by the value of x in the face space that depends on the model. An important question that remains is if it is possible to obtain or infer dynamical information from the graph structure.

The biochemical processes are known to be marked by the effect of noise and uncertainty, which justify the use of stochastic tools. The use of partial differential equations and delay is particularly justified for eukaryotic cells, in which the organized structures are sensible to diffusion phenomena and non instantaneous molecular transport. The prokaryotic cells are also described more exactly for models including this type of aspects.

The main limitation of all these approaches come from their precision degree. Making the models extremely difficult to handle analytically and expensive in calculation time in order to make numerical simulations. They are useful for systems of low dimension. This is in particular why the ordinary differential equations formalism and discrete formalism are still useful to handle biological systems like regulatory networks.

Each one of these models have some advantages, however we can classify them in three groups: continuous models, discrete models and stochastic models. The latest have received great attention because many recent works on gene expression insist on the importance of stochastic effects, these are manifested in the variation of expression levels from one cell to another. However, in this thesis we will only use deterministic models.

2.2.1 Continuous model

The continuous modelling of biological interaction networks is commonly related to a system of ordinary differential equations of the type:

$$(2.2.1) \qquad \frac{dx}{dt} = F(x)$$

where $x = (x_1, \ldots, x_n)$ represents concentrations of different biological entities in the network (typically concentrations of genes, proteins or metabolites) and $F : \mathbb{R}^n \to \mathbb{R}^n$ is a non linear function taking into account the interactions of such entities. Oftenly, $F(x) = G(x) - \Gamma x$, where Γ is a diagonal matrix containing degradation rates.

The solutions of (2.2.1) starting from different initial conditions must reflect the dynamics of such biological entities in the underlying process (under modelling). The underlying assumption is that the biological variables are continuous and evolve "deterministically". One of the main problems, us stated before, in analyzing such system are on one hand the size of the system (nowadays $n >> 200$ for metabolic modelling) and on the other the impossibility to have exact values of parameters of the map F. Among others, this reason has forced the community interested in this area to develop strategies of analysis that rely on the "topological properties" of the interactions [Sg07].

The interaction signed directed graph associated with the system (2.2.1) at point $x \in \mathbb{R}^n$, that we call "regulatory graph", is constructed as follows: its vertices are $V = \{1, \ldots, n\}$ or generically $V = \{g_1, \ldots, g_n\}$, where g_i represents the i-th biological entity (g is used for gene). There is an arrow from g_j to g_i if $\frac{\partial F_i}{\partial x_j}(x) \neq 0$. Denote this graph by $\mathcal{G}(x)$. Moreover, one associates to each arrow a sign given by the sign of the partial derivative.

Most of modern efforts to understand the asymptotic behavior of solutions of (2.2.1) are based on the study of topological properties of $\mathcal{G}(x)$. We will describe later in this section the conjectures about this kind of dynamics and the graph.

Continuous models are also those using partial differential equations or even piecewise linear equations, we do not consider them here. For a review on them see [J02].

2.2.2 Discrete model

Another approach to model the dynamics of biological interaction networks is to think that each biological entity can take a finite number of states and that during the process it evolves depending on its own state and the state of some other entities in the network or neighbors (all of them are possible). This approach has been extensively studied (see for example [A01], [RMCT03], [RRT05], [RR08], [R07], [RC07]) principally due to the nature of available biological information (microarrays data for example).

Formally a "discrete dynamical system" is given by:

$$f : \Omega \to \Omega$$

where $\Omega \subset E_1 \times \ldots \times E_n$ and each E_i represents the state space for the i-th entity x_i, for $x \in \Omega$, $f(x) = (f_1(x), \ldots, f_n(x))$ with $f_i : \Omega \to E_i$. A classical state space is $\Omega = \{0, 1\}^n$, where 0 is interpreted as inactive and 1 as active.

As in the continuous case to each $x \in \Omega$ one can associate a signed directed interaction graph $\mathcal{G}(x)$ that will be defined in 2.3 for Boolean networks (where $\Omega = \{0, 1\}^n$).

A particular feature in the discrete case is the way the dynamics evolves. It can be defined "synchronously", that is, starting from $x \in \Omega$ one goes to $f(x) \in \Omega$; or "asynchronously": at each time one chooses by some mechanism a position $i \in \{1, \ldots, n\}$ and moves $x = (x_1, \ldots, x_n)$ to $(x_1, \ldots, x_{i-1}, f_i(x), x_{i+1}, \ldots, x_n)$. That is, one only changes coordinate i of x according to f.

As we will observe later, the most natural type of dynamics modelling biological networks is the asynchronous one.

2.2.3 Biological motivation: Thomas conjectures

Either in the continuous or discrete case, as we mentioned before, when the size of the network is large, it is very difficult to deduce any property of the asymptotic behavior of the dynamics. In particular, the characterization of limit cycles. This last question has become very relevant in studying biological networks since one can relate "intuitively" such behavior to particular biological phenomena. For example, the coexistence of multiple stable limit cycles (called multi-stationary) is related with "cell differentiation"; and the "homeostasis phenomenon" is oftenly associated to the existence of a unique stable or globally stable limit

cycle.

In this framework, in the early 80s, the biologist René Thomas [T81] enounced two conjectures relating the structure of a signed graph with its dynamical asymptotic behavior:

1. **First Thomas conjecture**: A necessary condition for multistability (i.e., the existence of several stable fixed points) in the dynamics (transition graph) is the existence of a positive circuit in the regulatory graph (the sign of a circuit being the product of the signs of its edges);

2. **Second Thomas conjecture**: A necessary condition for the existence of an attractive cycle in the dynamics (transition graph) is the existence of a negative circuit in the regulatory graph (odd number of negative edges).

These conjectures have been proved to be true by many authors, starting by considering some special cases and hypotheses in the network (see [R95], [P95], [G98], [CD02]) and finally during the last five years more general answers to the conjectures have been proved.

In the continuous case C. Soulé [S03] has proved the first conjecture using a fixed point theory approach (Gale-Nikaidô Theorem). The proof of Soulé Theorem is certainly elegant but we should note that it gives no information about a sufficient condition for the first conjecture.

In the discrete case Remy et al. [RRT05] have proved both conjectures in the Boolean case using the Jacobian matrix conjecture and ideas in its proof [SD05]. Meanwhile Richard et al. ([R07], [RC07]) have proved the general discrete case (not only Boolean). Particular results for the necessary and sufficient conditions in the discrete case were proved in special cases such as when the function f is monotone [A01] and when the regulatory graph is composed of an isolated circuit [RMCT03].

Main efforts nowadays are to understand sufficient conditions for the two cases in Thomas conjectures. In the rest of this chapter, our intention is to explore new proofs to the conjectures in the Boolean case that can provide ideas about the conditions to be used as "sufficient conditions".

In Section 2.3 we introduce some basic notations and definitions about the dynamics, transition graphs, regulatory graphs, attractors, circuits, cycles and the sign functions. In Section 2.4 we will restrict our attention to elementary properties about the existence of edges and a sign formula for circuits in the regulatory graph. Section 2.5 is devoted to the study of the second Thomas conjecture, we give an alternative proof using the developed tools and

we study sufficient conditions in the case where the regulatory graph is an isolated circuit. Finally, in Section 2.6.1 we study the relation between cycles in the transition graph and circuits in the regulatory graph, giving several conditions in order to construct an extended transition graph with signs for the Boolean map f.

2.3 Boolean Networks model

In this section we restrict our attention to basic discrete models, where $\Omega = \{0,1\}^n$, called Boolean networks. In this context we will study Thomas conjectures.

2.3.1 Definitions

Now we proceed to introduce formally the main definitions used in the rest of this chapter, we follow mainly the notations in [RRT05]. For a number $\alpha \in \{0,1\}$, we denote by $\overline{\alpha}$ its negation or equivalently by $\overline{\alpha} = \alpha + 1$, where the sum is modulo 2.

Definition 2.3.1. *[Set negation] For a vector $x = (x_1, \ldots, x_n) \in \{0,1\}^n$ and a set $I \subseteq \{1, \ldots, n\}$, $\overline{x}^I$ is defined by*

$$\overline{x_i}^I = \begin{cases} x_i & \text{if } i \notin I \\ \overline{x_i} & \text{if } i \in I \end{cases}$$

for all $i \in \{1, \ldots, n\}$.

In other words,

$$\overline{x}^I = x + e_{j_1} + \ldots + e_{j_r},$$

where $I = \{j_1, \ldots, j_r\}$, e_j is the canonical n-vector with a 1 in position j, and the sums are modulo 2. If the set $I = \{j\}$ (singleton) we write $\overline{x}^j$ instead of $\overline{x}^{\{j\}}$.

The distance d on $\{0,1\}^n$ is the usual Hamming distance, that counts the number of mismatches between two vectors x and y. Another way to do that is to sum (modulo 2) the two vectors and then count the number of nonzero positions.

We are interested in the dynamics of a map $f : \{0,1\}^n \to \{0,1\}^n$ where $f(x) = (f_1(x), \ldots, f_n(x))$ and $x = (x_1, \ldots, x_n) \in \{0,1\}^n$. In biological systems one possible interpretation is that each x_i is the state (1 = active, 0 = inactive) of a gene or a regulatory product. This is why we write $g_1, \ldots, g_n$ to mention the entities associated to variables $x_1, \ldots, x_n$ respectively.

2.3.2 Asynchronous dynamics

In what follows we fix $f : \{0, 1\}^n \to \{0, 1\}^n$. For $x \in \{0, 1\}^n$ we denote by $Com(x)$ the set of positions which may switch or commute their values, i.e.,

$$Com(x) = \{i : f_i(x) \neq x_i\}.$$

Clearly, $Com(x) = \emptyset$ means that x is a fixed point of f ($f(x) = x$). We will differentiate later when this set has one or various points. As we have mentioned before, the asynchronous dynamics of a Boolean network induced by f is not unique. Several rules for updating the states are possible.

The synchronous dynamics is given by the iteration of f, that is, one goes from $x \in \{0, 1\}^n$ to $f(x) = (f_1(x), \ldots, f_n(x))$ in one step. From a biological point of view, the synchronous hypothesis is not desirable because for example the change in the expression levels arises from the phenomena of synthesis and degradations that are not instantaneous and synchronized processes. So, it is necessary a delay in order to allow the correct change of concentrations.

For that reason, René Thomas in [T81] introduced the asynchronous dynamics associated to f. The idea is that only one position of a given $x \in \{0, 1\}^n$ changes at each step. Formally choose $i \in Com(x)$ and change x by $\overline{x}^i$. As many states can be a successor of the state x, we cannot describe the dynamics by a simple iteration. For that reason the asynchronous dynamics is represented by a graph called the transition graph of f.

Definition 2.3.2. *[Transition graph] Let $f : \{0, 1\}^n \to \{0, 1\}^n$ be a map. The transition graph $\mathcal{T}(f)$ associated to the asynchronous dynamics of f is defined as a directed graph where the nodes or vertices correspond to the states of the network $\{0, 1\}^n$, and the edges are defined by the set $\{(x, \overline{x}^i) : x \in \{0, 1\}^n, i \in Com(x)\}$.*

Remark 2.3.3. *By definition of $Com(x)$, in the transition graph $\mathcal{T}(f)$ loops are forbidden, that is transitions of the form (x, x). Generally, the fact that $Com(x) = \emptyset$ indicates steady states of the system.*

2.3.3 Types of attractors

One of the essential aspects in the mathematical study of the dynamics of Boolean networks is the analysis of attractors or more generally the asymptotic behavior of such systems. As usual, we will distinguish three types of attractors: stationary states, periodic orbits and aperiodic orbits. In the last one we generally make a distinction between the chaotic and non

chaotic orbits (some details in the continuous case are given in Chapter 3). In the following, we will make the formal definition of the first two types of attractors.

In the Boolean framework, a stationary state of the network is a fixed point of f, i.e. a point $x \in \{0,1\}^n$ such that $f(x) = x$. We observe that $f(x) = x$ is not formally allowed in the asynchronous dynamics.

In order to define periodic orbits we need to state previously the concept of path. A path in the transition graph of f is a sequence of states $(x^1, \ldots, x^r)$ in $\{0,1\}^n$ such that for each $i = 1, \ldots, r-1$ there exists $\varphi(i) \in \{1, \ldots, n\}$ such that

$$\varphi(i) \in Com(x^i) \text{ and } x^{i+1} = \overline{x^i}^{\varphi(i)}$$

A path is completely described by an initial state x^1 and a function $\varphi : \{1, \ldots, r-1\} \to \{1, \ldots, n\}$, called the strategy of the path, verifying the condition $\varphi(i) \in Com(x^i)$.

A path $(x^1, \ldots, x^r, x^1)$ with $r \geq 2$ is called a cycle (for f) and is denoted by $(x^1, \ldots, x^r)$. A cycle C is completely described by one of its points and its strategy φ, which satisfies $\overline{x^r}^{\varphi(r)} = x^1$, so we write $C = (x^1, \ldots, x^r, \varphi)$.

A cycle $C = (x^1, \ldots, x^r, \varphi)$ is said to be attractive if for all $i \in \{1, \ldots, r\}$, $Com(x^i) = \{\varphi(i)\}$. Equivalently, the distance between x^i and $f(x^i)$ is 1 or $f(x^i) = \overline{x^i}^{\varphi(i)}$. In other words, when you reach an attractive cycle you cannot escape anymore. Using this last definition of attractive cycle, we will redefine stationary states for f as those without successors in the transition graph of f.

We are interested in properties involving these two types of attractors, because both are related with the Thomas conjectures. For that reason in the following we will introduce the concept of circuits in the regulatory graph (defined in Subsection 2.3.4).

2.3.4 Discrete Jacobian matrices

As we have mentioned in 2.2.1, in the continuous model, to each x in the face space Ω we can associate in a natural way an interaction graph $\mathcal{G}(x)$ using the Jacobian matrix related to the map $F(x)$. A similar construction can be used in the discrete Boolean case. In this purpose we define the discrete version of the Jacobian matrix associated to f as follows,

Definition 2.3.4. *The discrete Jacobian matrix $J(x)$ of f at point $x \in \{0,1\}^n$ is given by,*

$$J_{i,j}(x) = \begin{cases} 1 & \text{if } f_i(x) \neq f_i(\overline{x}^j) \\ 0 & \text{otherwise} \end{cases}$$

where $i, j \in \{1, \ldots, n\}$.

Now it is possible to associate to the dynamics of f a signed directed graph, whose adjacency matrix is the transpose of $J(x)$. More precisely,

Definition 2.3.5. *[Regulatory graph associated to f] Given $x \in \{0,1\}^n$, we define the regulatory graph $\mathcal{G}(x)$ at point x as follows. Its set of vertices is denoted by $\{g_1, \ldots, g_n\}$ (reflecting the fact that they are genes or other regulatory objects) and there exists an edge from g_j to g_i if and only if $J_{i,j}(x) \neq 0$. The sign of the edge from g_j to g_i, denoted by $\epsilon_{j,i}$, will be 1 if $x_j = f_i(x)$, and -1 otherwise.*

A path, in the regulatory graph is a sequence of connected vertices of $\mathcal{G}(x)$

$$g_{i_1} \xrightarrow{\epsilon_{i_1,i_2}} g_{i_2} \xrightarrow{\epsilon_{i_2,i_3}} \cdots \xrightarrow{\epsilon_{i_{k-1},i_k}} g_{i_k} \xrightarrow{\epsilon_{i_k,i_{k+1}}} g_{i_{k+1}}$$

and the sign of such path is the product of the signs of the corresponding edges: $\Pi_{j=1}^{k} \epsilon_{i_j,i_{j+1}}$. If $i_{k+1} = i_1$ one speaks about a circuit and the sign of the circuit.

To avoid confusions with definitions in Subsection 2.3.3, we mention that in general we manage two graphs. The first one (transition graph) represents the dynamics of f and its vertices correspond to the different states in $\{0,1\}^n$. Meanwhile, the regulatory graph represents the interaction between variables.

Example 2.3.6. *Let $f : \{0,1\}^2 \to \{0,1\}^2$ be the Boolean map given by the following table:*

x	$f(x)$	$Com(x)$
$(0,0)$	$(1,1)$	$\{1,2\}$
$(0,1)$	$(0,1)$	$\emptyset$
$(1,0)$	$(1,0)$	$\emptyset$
$(1,1)$	$(0,0)$	$\{1,2\}$

In Figure 2.1 we show the transition graph for both asynchronous and synchronous dynamics, and, the corresponding regulatory graph.
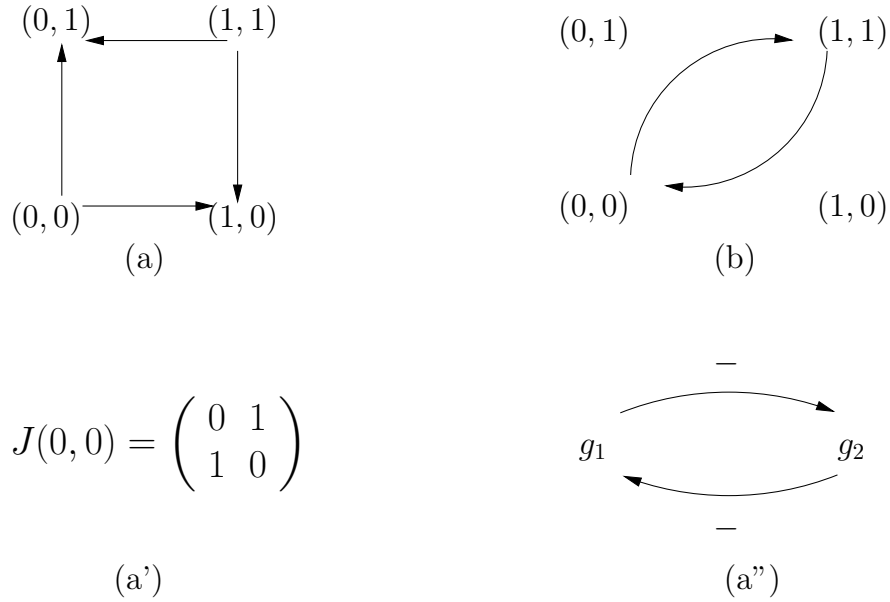
Figure 2.1: (a) Transition graph for asynchronous dynamics of f. (b) Synchronous dynamics of f. (a') The Jacobian matrix associated to f. (a") Regulatory graph associated to f in the state $x = (0, 0)$

In general, we know that if $J_{i,j}(x) \neq 0$ then there exists an edge from the vertex g_j to g_i in the regulatory graph, and from the definition of the Jacobian matrix we have that $f_i(\overline{x}^j) \neq f_i(x)$. Rewriting the function f_i in terms of the elements in the set $Com(x)$ as

$$f_i(x) = (x + e_{r_1} + \ldots + e_{r_k})_i$$

where $Com(x) = \{r_1, \ldots, r_k\}$, we can conclude that the previous differences can be expressed as follows

$$f_i(\overline{x}^j) = (x + e_j + e_{s_1} + \ldots + e_{s_l})_i \neq (x + e_{r_1} + \ldots + e_{r_k})_i = f_i(x)$$

where $Com(\overline{x}^j) = \{s_1, \ldots, s_l\}$. We recall that all sums are modulo 2.

To conclude this section, we will define the global regulatory graph for a map f, as the union of all the local regulatory graphs $\mathcal{G}(x)$, $x \in \{0, 1\}^n$, associated to f.

Definition 2.3.7. *[Union of graphs] Let $G = (V, E)$ and $G' = (V, E')$ be two directed graphs with the same set of vertices. We call the union of G and G' to the graph $(V, E \cup E')$, denoted by $G \cup G'$.*

Now, we define the global regulatory graph as follows:

Definition 2.3.8. *[Global regulatory graph associated to f] For a map $f : \{0, 1\}^n \to \{0, 1\}^n$*

we define the regulatory graph $\mathcal{G}(f)$ of f as,

$$\mathcal{G}(f) = \cup_{x \in \{0,1\}^n} \mathcal{G}(x)$$

Given a cycle $C = (x^1, \ldots, x^r, \varphi)$ in the transition graph $\mathcal{T}(f)$, we denote by $\mathcal{G}(C)$ the regulatory graph associated to the union of the regulatory graphs of points in the cycle, i.e., $\mathcal{G}(C) = \mathcal{G}(x^1) \cup \ldots \cup \mathcal{G}(x^r)$. In the same context, given a path $P = (x^1, \ldots, x^r, \varphi)$ in $\mathcal{T}(f)$ we denote by $\mathcal{G}(P) = \mathcal{G}(x^1) \cup \ldots \cup \mathcal{G}(x^r)$ to the associated regulatory graph.

Observation 2.3.9. *Note that the global regulatory graph $\mathcal{G}(f)$ or the graphs associated to paths or cycles in $\mathcal{T}(f)$ can contain positive and negative interactions from a node i to a node j (so it is a multigraph). The notions of sign of paths and circuits in $\mathcal{G}(f)$, $\mathcal{G}(C)$ or $\mathcal{G}(P)$ extend naturally.*

2.4 Sign formula for circuits in a regulatory graph

As we have seen before, the Thomas conjectures establish relations between the dynamics of f or its transition graph and the structure of its associated regulatory graph $\mathcal{G}(f)$. More specifically the sign of its circuits. In this direction, the next lemma provides a general formula for the sign function, which will be useful to study the second Thomas conjecture.

Lemma 2.4.1. *Given a Boolean map $f : \{0,1\}^n \rightarrow \{0,1\}^n$. If $J_{i,j}(x) \neq 0$ then the following expression holds:*

$$(2.4.1) \qquad \qquad \epsilon_{j,i} = sgn(\overline{x_j} - x_j) sgn(f_i(\overline{x}^j) - f_i(x))$$

where

$$sgn(x) = \begin{cases} 1 & x > 0 \\ 0 & x = 0 \\ -1 & x < 0 \end{cases}$$

Proof. We need to analyze two cases, positive edges and negative edges. If we are in the presence of a positive edge, i.e. $x_j = f_i(x)$, we must have that $\overline{x_j} = f_i(\overline{x}^j)$ because $J_{i,j}(x) \neq 0$. Thus, $\overline{x_j} - x_j = f_i(\overline{x}^j) - f_i(x)$ and the desired expression for $\epsilon_{j,i}$ holds.

In the other case, if we are in the presence of a negative edge, i.e. $x_j \neq f_i(x)$, we have that $f_i(\overline{x}^j) - f_i(x) = x_j - \overline{x_j}$. Thus, the product of signs in the formula is -1.

So the value of $\epsilon_{j,i}$ in (2.4.1) gives us another way to describe the sign of an edge. $\square$

In the previous section we have seen that the sign of a circuit is defined as the product of the signs of the edges it contains. In order to simplify the computations, we would like to have in certain cases an annihilation property. For that reason it would be better to eliminate f from the formula of $\epsilon_{j,i}$ given in previous lemma and write all the expressions in terms of x and the strategy φ. Before we need a preliminary lemma.

Lemma 2.4.2. *Let $f : \{0,1\}^n \rightarrow \{0,1\}^n$ be a Boolean map. Let $x \in \{0,1\}^n$ and $j \in Com(x)$. Denote $y = \overline{x}^j$ and take $i \in Com(y)$. We have $J_{i,j}(x) \neq 0$ if and only if $i \notin Com(x)\backslash\{j\}$. This is, a condition for the existence of an edge between g_j and g_i in $\mathcal{G}(x)$.*

Proof. In order to prove the result we consider two cases:

1. $\underline{i = j}$:

   $$(2.4.2) \qquad J_{i,j}(x) = J_{j,j}(x) \neq 0 \quad \text{iff} \quad f_j(x) \neq f_j(\overline{x}^j)$$
   $$(2.4.3) \qquad\qquad\qquad\qquad\qquad\qquad (y)_j \neq f_j(y)$$
   $$(2.4.4) \qquad\qquad\qquad\qquad\qquad\qquad (y)_i \neq f_i(y)$$

   where (2.4.3) is true since $j \in Com(x)$ and $y = \overline{x}^j$, (2.4.4) is always true since $i \in Com(y)$ and is also true that $j \notin Com(x)\backslash\{j\}$, so the equivalence holds.

2. $\underline{i \neq j}$:

   $$(2.4.5) \qquad\qquad J_{i,j}(x) \neq 0 \quad \text{iff} \quad f_i(x) \neq f_i(\overline{x}^j)$$
   $$(2.4.6) \qquad\qquad\qquad\qquad\qquad\qquad f_i(x) \neq f_i(y)$$
   $$(2.4.7) \qquad\qquad\qquad\qquad\qquad\qquad f_i(x) \neq \overline{y_i}$$
   $$(2.4.8) \qquad\qquad\qquad\qquad\qquad\qquad f_i(x) \neq \overline{x_i},$$

   where (2.4.6) and (2.4.8) come from $y = \overline{x}^j$, and (2.4.7) from the assumption $i \in Com(y)$. Using the above characterization, we shall have established the lemma if we prove that $f_i(x) \neq \overline{x_i}$ iff $i \notin Com(x)$. For the first implication since $f_i(x) \neq \overline{x_i}$ we have $f_i(x) = x_i$, which implies that $i \notin Com(x)$. In the opposite direction if we assume $i \notin Com(x)$ then $f_i(x) = x_i \neq \overline{x_i}$ which completes the proof.

$\square$

In particular if we have an attractive cycle $C = (x^1, \ldots, x^r, \varphi)$ in $\mathcal{T}(f)$, where by definition

$Com(x^i) = \{\varphi(i)\}$, then either for some $i \in \{1,\ldots,r\}$, $\varphi(i) = \varphi(i+1)$ and thus $x^j = x^{j+2}$ for any $j \in \{1,\ldots,r\}$ (here the sums of indices are in the cycle), or for any $i \in \{1,\ldots,r\}$, $\varphi(i) \neq \varphi(i+1)$, which means that $\varphi(i+1) \notin Com(x^i)$. One deduces from Lemma 2.4.2 that $J_{\varphi(i+1),\varphi(i)}(x^i) \neq 0$ for any $i \in \{1,\ldots,r\}$. In other words, there is a circuit in $\mathcal{G}(f)$.

A second consequence of previous two lemmas is that given a path $P = (x^1,\ldots,x^r,\varphi)$ in $\mathcal{T}(f)$ with $\varphi(i+1) \notin Com(x^i)\backslash\{\varphi(i)\}$ for $i \in \{1,\ldots,r-2\}$, then there is a path in $\mathcal{G}(f)$ induced by P given by:

- Vertices: $g_{\varphi(1)},\ldots,g_{\varphi(r-1)}$.

- There is an edge from $g_{\varphi(i)}$ to $g_{\varphi(i+1)}$ and the sign is determined from the one in $\mathcal{G}(x^i)$.

We will call this signed path $\mathcal{P}(P)$. Analogously one induces a circuit $\mathcal{C}(C)$ from a cycle C in $\mathcal{T}(f)$. The next proposition allows to compute the sign of $\mathcal{P}(P)$.

Proposition 2.4.3. *Let $P = (x^1,\ldots,x^r,\varphi)$ be a path in the transition graph $\mathcal{T}(f)$. If for all $i \in \{1,\ldots,r-2\}$, $\varphi(i+1) \notin Com(x^i)\backslash\{\varphi(i)\}$, then the sign of the edge between $g_{\varphi(i)}$ and $g_{\varphi(i+1)}$ in $\mathcal{G}(x^i)$ is given by the following expression:*

$$\epsilon_{\varphi(i),\varphi(i+1)} = sgn[(\overline{x^i}^{\varphi(i)} - x^i)_{\varphi(i)}]sgn[(\overline{x^{i+1}}^{\varphi(i+1)} - x^{i+1})_{\varphi(i+1)}]$$

and the sign of $\mathcal{P}(P)$ is given by

$$sgn(\mathcal{P}(P)) = s_1 s_{r-1}$$

where $s_i = sgn[(\overline{x^i}^{\varphi(i)} - x^i)_{\varphi(i)}]$ for $i \in \{1,\ldots,r-1\}$.

Proof. Let $i \in \{1,\ldots,r-2\}$. From Lemma 2.4.1 and Lemma 2.4.2 the expression for the sign $\epsilon_{\varphi(i),\varphi(i+1)}$ in $\mathcal{G}(x^i)$, under the hypothesis $J_{\varphi(i+1),\varphi(i)}(x^i) \neq 0$ is:

$$\epsilon_{\varphi(i),\varphi(i+1)} = sgn[(\overline{x^i}^{\varphi(i)} - x^i)_{\varphi(i)}]sgn[f_{\varphi(i+1)}(\overline{x^i}^{\varphi(i)}) - f_{\varphi(i+1)}(x^i)].$$

We only need to prove that $f_{\varphi(i+1)}(\overline{x^i}^{\varphi(i)}) = (\overline{x^{i+1}}^{\varphi(i+1)})_{\varphi(i+1)}$ and $f_{\varphi(i+1)}(x^i) = (x^{i+1})_{\varphi(i+1)}$. Since $x^i \in P$, $x^{i+1} = \overline{x^i}^{\varphi(i)}$, so

$$f_{\varphi(i+1)}(\overline{x^i}^{\varphi(i)}) = f_{\varphi(i+1)}(x^{i+1}) = (x^{i+1} + e_{\varphi(i+1)} + e_{j_1} + \ldots + e_{j_m})_{\varphi(i+1)} = (\overline{x^{i+1}}^{\varphi(i+1)})_{\varphi(i+1)}$$

where $Com(x^{i+1}) = \{\varphi(i+1), j_1,\ldots,j_m\}$.

For the second equality, we analyze two cases. Assume $\varphi(i) \neq \varphi(i+1)$, then the dynamics from x^i to x^{i+1} does not move coordinate $\varphi(i+1)$, thus we have

$$f_{\varphi(i+1)}(x^i) = (x^i + e_{\varphi(i)} + e_{r_1} + \ldots + e_{r_s})_{\varphi(i+1)} = (x^i)_{\varphi(i+1)} = (x^{i+1})_{\varphi(i+1)},$$

where $Com(x^i) = \{\varphi(i), r_1, \ldots, r_s\}$. If $\varphi(i) = \varphi(i+1)$, then

$$f_{\varphi(i+1)}(x^i) = f_{\varphi(i)}(x^i) = (\overline{x^{i}}^{\varphi(i)})_{\varphi(i)} = (x^{i+1})_{\varphi(i)} = (x^{i+1})_{\varphi(i+1)}.$$

This proves the desired formula.

Using the above formula, the sign in $\mathcal{P}(P)$ of the edge from $g_{\varphi(i)}$ to $g_{\varphi(i+1)}$ is given by $\epsilon_{\varphi(i),\varphi(i+1)} = s_i s_{i+1}$, for $i \in \{1, \ldots, r-2\}$. Then, by cancelation, one gets:

$$sgn(\mathcal{P}(P)) = \Pi_{i=1}^{r-2} s_i s_{i+1} = s_1 s_{r-1}.$$

$\square$

Moreover, this annihilation sign property is similar to the rule for the consistent spin assignment problem, which establishes a relation between monotone functions and positive circuits [Sg07].

2.5 Negative circuits: the second Thomas conjecture

In this section we give a simple proof for the second Thomas conjecture in the Boolean case. In a particular case (isolated circuit) we show that the condition for this conjecture is also sufficient.

There exist several proofs to this conjecture with different additional hypotheses, see for example [A01], [CD02], and also in the general case, see [RMCT03], [RRT05]. Here we provide another proof that we think is very simple and explores a kind of "cohomological idea" behind the sign assignment in $\mathcal{G}(f)$.

2.5.1 Proof of the second Thomas conjecture

Let $f : \{0,1\}^n \to \{0,1\}^n$ be a Boolean map and $C = (x^1, \ldots, x^r, \varphi)$ an attractive cycle in $\mathcal{T}(f)$. Thomas conjecture states that a necessary condition for the existence of an attractive cycle in $\mathcal{T}(f)$ is the existence of a circuit in $\mathcal{G}(f)$ with negative sign. Recall that $\mathcal{G}(f)$ is the superposition of all signed graphs $\mathcal{G}(x)$ for $x \in \{0,1\}^n$, then the desired circuit comes from the combination of edges in different $\mathcal{G}(x)'s$.

Theorem 2.5.1. *Let $f : \{0,1\}^n \to \{0,1\}^n$ be a Boolean map. Suppose f has an attractive cycle $C = (x^1, \ldots, x^r, \varphi)$ in $\mathcal{T}(f)$, then $\mathcal{G}(C) = \mathcal{G}(x^1) \cup \ldots \cup \mathcal{G}(x^r)$ has a negative circuit.*

Proof. Consider the attractive cycle $C = (x^1, \ldots, x^r, \varphi)$. In order to prove the theorem we need to analyze two cases.

If $\varphi(i) = \varphi(i+1)$ for some $i \in \{1, \ldots, r\}$ then from Lemma 2.4.2 there exists an edge from $g_{\varphi(i)}$ to $g_{\varphi(i+1)}$, whose sign is given by the formula in Proposition 2.4.3

$$\epsilon_{\varphi(i),\varphi(i+1)} = sgn[(\overline{x^i}^{\varphi(i)} - x^i)_{\varphi(i)}]sgn[(\overline{x^{i+1}}^{\varphi(i+1)} - x^{i+1})_{\varphi(i+1)}]$$

which is always -1 because

$$\overline{x^{i+1}}^{\varphi(i+1)} = \overline{\overline{x^i}^{\varphi(i)}}^{\varphi(i+1)} = \overline{\overline{x^i}^{\varphi(i)}}^{\varphi(i)} = x^i.$$

Concluding the existence of a negative self loop in $\mathcal{G}(C)$ with vertex $g_{\varphi(i)}$.

If $\varphi(i) \neq \varphi(i+1)$ for all $i \in \{1, \ldots, r\}$ then there exist $k, l \in \{1, \ldots, r\}$ with $k < l$, such that $\varphi(k) = \varphi(l)$ and $\varphi(j) \neq \varphi(k)$ for $j \in \{k+1, \ldots, l-1\}$. The last statement is a consequence of the fact that, since C is a cycle, after one complete turn of the cycle the $\varphi(i)$-coordinate of x^i must change at least two times, one to move from x^i to x^{i+1} and another to come back. In the following we will prove that the path $P = (x^k, \ldots, x^l, x^{l+1}, \varphi) \subset C$ in $\mathcal{T}(f)$ induces a negative circuit $\mathcal{C}$ in $\mathcal{G}(C)$:

$$g_{\varphi(k)} \to g_{\varphi(k+1)} \to \cdots \to g_{\varphi(l)} = g_{\varphi(k)}.$$

Since C is an attractive cycle and $\varphi(i+1) \neq \varphi(i)$ one has that $\varphi(i+1) \notin Com(x^i) \backslash \{\varphi(i)\} = \emptyset$. Therefore, from Lemma 2.4.2 there exists an edge from $g_{\varphi(j)}$ to $g_{\varphi(j+1)}$ for every $j \in \{k, \ldots, l-1\}$, where $\varphi(l) = \varphi(k)$. Then the circuit $\mathcal{C}$ is well defined and its sign is given by

the formula in Proposition 2.4.3:

$$
\begin{aligned}
sgn(\mathcal{C}) &= \Pi_{j=k}^{l-1}\epsilon_{\varphi(j),\varphi(j+1)} = \Pi_{j=k}^{l-1}s_j s_{j+1} = s_k s_l \\
&= sgn[(\overline{x^k}^{\varphi(k)} - x^k)_{\varphi(k)}]sgn[(\overline{x^l}^{\varphi(l)} - x^l)_{\varphi(l)}] \\
&= sgn[(\overline{x^k}^{\varphi(k)} - x^k)_{\varphi(k)}]sgn[(\overline{x^l}^{\varphi(k)} - x^l)_{\varphi(k)}]
\end{aligned}
$$

But, since $\varphi(j) \neq \varphi(k)$ for any $j \in \{k+1, \ldots, l-1\}$ it follows that coordinate $\varphi(k)$ of x^l is the same as coordinate $\varphi(k)$ of $x^{k+1} = \overline{x^k}^{\varphi(k)}$. So, $(x^l)_{\varphi(k)} \neq (x^k)_{\varphi(k)}$ which implies $sgn(\mathcal{C}) = -1$. We have found a circuit in $\mathcal{G}(f)$ with negative sign, which completes the proof.

$\square$

Example 2.5.2. *Consider the Boolean map $f : \{0,1\}^3 \to \{0,1\}^3$,*

x	000	100	110	010	001	101	111	011
$f(x)$	001	110	010	000	101	100	111	011

whose transition graph $\mathcal{T}(f)$ has an attractive cycle

$$
C = (100, 110, 010, 000, 001, 101, \underbrace{(2,1,2,3,1,3)}_{\varphi}))
$$

and two fixed points at 011 and 111.

From Theorem 2.5.1 there exists a negative circuit in $\mathcal{G}(C)$. In fact, as $\varphi(1) = \varphi(3) = 2$, $\varphi(2) = \varphi(5) = 1$ and $\varphi(4) = \varphi(6) = 3$ then the respective circuits

$$
g_2 \to g_1 \to g_2, \; g_1 \to g_2 \to g_3 \to g_1 \text{ and } g_3 \to g_1 \to g_3
$$

are negatives. In Figures 2.2 and 2.3 we can see an illustration of graphs $\mathcal{T}(f)$ and $\mathcal{G}(C)$ respectively.

Example 2.5.3. *Consider the following Boolean map $f : \{0,1\}^3 \to \{0,1\}^3$,*

x	000	100	110	010	001	101	111	011
$f(x)$	001	101	100	000	001	111	110	000
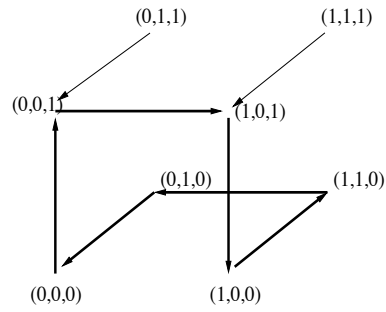
Figure 2.2: Transition graph associated to f in Example 2.5.2.
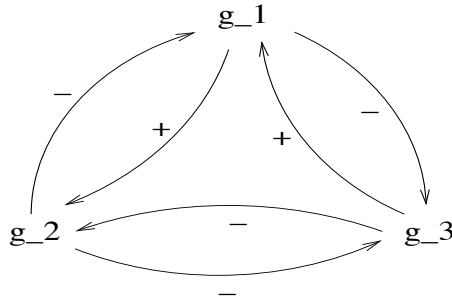
Figure 2.3: Regulatory graph $\mathcal{G}(C)$ associated to f in Example 2.5.2.

The transition graph of f, $\mathcal{T}(f)$, can be seen in Figure 2.4. This graph has one attractive cycle

$$C = (100, 101, 111, 110, \underbrace{(3, 2, 3, 2)}_{\varphi})$$

and one fixed point at 001. In Figure 2.5 we can see the regulatory graph $\mathcal{G}(f)$, which consists of one negative circuit and one positive loop.
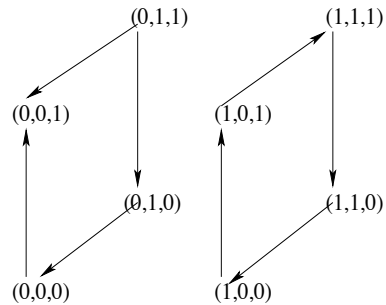
Figure 2.4: Transition graph associated to f in Example 2.5.3.
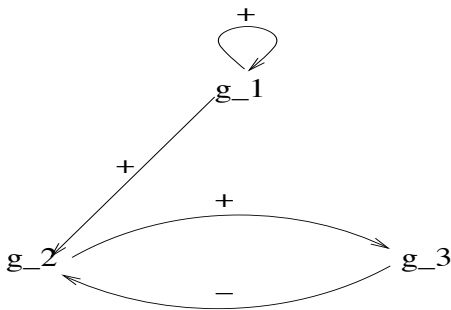
Figure 2.5: Regulatory graph associated to f at point (111) in Example 2.5.3.

2.5.2 Sufficient condition for isolated circuits

Nowadays, it would be desirable to understand completely the relation between the dynamics of f and the structure of its regulatory graph. In order to understand the sufficient condition for both Thomas conjectures we restrict our attention to the simplest case of regulatory graphs consisting of one isolated circuit $\mathcal{C}$. That is, for a Boolean map f, the regulatory graph associated to f, $\mathcal{G}(f)$, has no other edge between the vertices of $\mathcal{C}$ than the edges of $\mathcal{C}$ itself. Under this assumption, we reformulate a discussion of Remy et al. [RMCT03] about the dynamical study of isolated circuits.

In [RMCT03], the authors have first proposed a graph-based representation of the discrete dynamics of genetic regulatory networks. Additionally, they have shown how the structure of the synchronous dynamical graphs can be analytically computed in terms of elementary cycles. From them, they could then derive the structure of the corresponding asynchronous dynamical graphs.

The main idea behind the proof is to discover the Boolean map f from $\mathcal{G}(f)$. In this direction, we will find a rule to calculate either the fixed points of f when the isolated circuit is positive or the attractive cycle when the isolated circuit is negative. That is, in a constructive way, the converse (sufficient condition) of the Thomas conjectures will be proved. We begin with a lemma which gives us a general characterization.

Lemma 2.5.4. *Let f be a Boolean function and $x \in \{0,1\}^n$. If $J_{i,j}(x) \neq 0$ then the following equivalences are satisfied:*

$$i \notin Com(x) \iff f_i(x) = x_i \iff \begin{cases} x_i = x_j & \text{if } \epsilon_{j,i} = +1 \\ x_i \neq x_j & \text{if } \epsilon_{j,i} = -1 \end{cases}$$

Proof. In order to prove both equivalences the proof splits naturally into three parts.

(1) $i \notin Com(x) \implies f_i(x) = x_i$.

(2) $f_i(x) = x_i \implies \begin{cases} x_i = x_j & \text{if } \epsilon_{j,i} = +1 \\ x_i \neq x_j & \text{if } \epsilon_{j,i} = -1 \end{cases}$.

(3) $\begin{cases} x_i = x_j & \text{if } \epsilon_{j,i} = +1 \\ x_i \neq x_j & \text{if } \epsilon_{j,i} = -1 \end{cases} \implies i \notin Com(x)$.

The first implication follows directly from the definition of $Com(x)$.

For the second implication, since $J_{i,j}(x) \neq 0$, it follows from Lemma 2.4.1 that the sign of the edge between g_j and g_i is given by the expression

$$\epsilon_{j,i} = sgn[(\overline{x}^j)_j - x_j]sgn[f_i(\overline{x}^j) - f_i(x)].$$

Assuming $x_i = f_i(x)$, the last term in the sign formula is transformed into $sgn[f_i(\overline{x}^j) - x_i]$. Moreover, since $J_{i,j}(x) \neq 0$ we have that $f_i(\overline{x}^j) \neq f_i(x) = x_i$, which implies that $f_i(\overline{x}^j) = \overline{x_i}$. We thus get

(2.5.1) $$\epsilon_{j,i} = sgn[\overline{x_j} - x_j]sgn[\overline{x_i} - x_i].$$

Applying (2.5.1) we conclude that if the sign is $+1$ then $x_j = x_i$ and if the sign is -1 then $x_j \neq x_i$.

Finally, to prove (3) we proceed by contradiction. Suppose that $i \in Com(x)$, that is, $x_i \neq f_i(x)$. As before, from the sign formula if we assume that $x_j = x_i$ then $x_j \neq f_i(x)$ and $\epsilon_{j,i} = -1$, a contradiction. In the same manner, if we assume that $x_j \neq x_i$ then $x_j = f_i(x)$ and $\epsilon_{j,i} = +1$. This contradicts our assumption, and the proof is complete. $\square$

The main feature of Lemma 2.5.4 is that it allows one to prove the sufficient condition for both Thomas conjectures on the special case of isolated circuits. Thus, the following result can be established.

Proposition 2.5.5. *Let $f : \{0,1\}^n \to \{0,1\}^n$ be a Boolean map. Assume $\mathcal{G}(f) = \mathcal{G}(x)$ for all $x \in \{0,1\}^n$ and that it consists of an isolated circuit $\mathcal{C}$ with vertex set $\{g_1, \ldots, g_n\}$ and an edge from g_i to g_{i+1} for $i \in \{1, \ldots, n\}$, $g_{n+1} = g_1$. If the isolated circuit is positive then f has more than one fixed point; and if the isolated circuit is negative then f contains an attractive cycle (that is not a fixed point).*

Proof. The proof consists in the construction of the fixed points and the attractive cycle. By

hypotheses, for all $x \in \{0,1\}^n$, $\mathcal{G}(x)$ has the following form:

$$\mathcal{C} = g_1 \xrightarrow{\epsilon_{1,2}} g_2 \xrightarrow{\epsilon_{2,3}} \ldots \xrightarrow{\epsilon_{n-1,n}} g_n \xrightarrow{\epsilon_{n,1}} g_1,$$

which implies $J_{i+1,i}(x) \neq 0$ for all $i \in \{1, \ldots, n-1\}$ and $J_{1,n}(x) \neq 0$.

We begin by constructing iteratively two points $\hat{x}^1$ and $\hat{x}^2$ as follows:

$$(\hat{x}^1)_1 = 0 \text{ and } (\hat{x}^2)_1 = 1$$

as initial conditions and for $k \in \{1,2\}$ and $1 < i < n - 1$

$$\begin{cases} (\hat{x}^k)_{i+1} = (\hat{x}^k)_i & \text{if } \epsilon_{i,i+1} = +1 \\ (\hat{x}^k)_{i+1} \neq (\hat{x}^k)_i & \text{if } \epsilon_{i,i+1} = -1 \end{cases}$$

1. Assume the isolated circuit $\mathcal{C}$ is positive. We will prove that $\hat{x}^1$ and $\hat{x}^2$ are fixed points. By hypotheses, $J_{i+1,i}(x) \neq 0$ for all $x \in \{0,1\}^n$ and $i \in \{1, \ldots, n-1\}$. In particular for $\hat{x}^1$ we have $J_{i+1,i}(\hat{x}^1) \neq 0$. According to Lemma 2.5.4 and by construction of the points, it follows that $f_{i+1}(\hat{x}^1) = (\hat{x}^1)_{i+1}$. Therefore, it only remains to prove that $f_1(\hat{x}^1) = (\hat{x}^1)_1$.

   As the circuit is positive, we have an even number of negative edges, which implies by construction that there exist an even number of changes in the positions of $\hat{x}^1$, so we need to consider two cases: If $\epsilon_{n,1} = +1$, the even number of changes happen between positions 1 to $n-1$ then $(\hat{x}^1)_1 = (\hat{x}^1)_n$ and Lemma 2.5.4 implies that $f_1(\hat{x}^1) = (\hat{x}^1)_1$. On the other hand, if $\epsilon_{n,1} = -1$, between positions 1 and $n-1$ have occurred an odd number of changes then $(\hat{x}^1)_1 \neq (\hat{x}^1)_n$ and again Lemma 2.5.4 implies that $f_1(\hat{x}^1) = (\hat{x}^1)_1$. The same reasoning applies for $\hat{x}^2$, thus we get the desired fixed points.

2. Assume the isolated circuit $\mathcal{C}$ is negative. We will prove that the following cycle C starting from $\hat{x}^1$ is attractive:

$$C = \{\hat{x}^1, \overline{\hat{x}^1}^{\{1\}}, \overline{\hat{x}^1}^{\{1,2\}}, \ldots, \underbrace{\overline{\hat{x}^1}^{\{1,\ldots,n\}}}_{\hat{x}^2}, \overline{\hat{x}^2}^{\{1\}}, \overline{\hat{x}^2}^{\{1,2\}}, \ldots, \underbrace{\overline{\hat{x}^2}^{\{1,\ldots,n\}}}_{\hat{x}^1}\}.$$

   Since the circuit is negative, we have an odd number of negative edges which implies, by construction, that there exist an odd number of changes in the positions of $\hat{x}^1$. The proof runs inductively over the points of the cycle.

   Basis: We will show that $f(\hat{x}^1) = \overline{\hat{x}^1}^1$. As before we need to consider two cases: If $\epsilon_{n,1} = +1$, the odd number of changes occur between positions 1 to $n - 1$ then

$(\hat{x}^1)_1 \neq (\hat{x}^1)_n$. By the negation of Lemma 2.5.4 we get $f_1(\hat{x}^1) \neq (\hat{x}^1)_1$. For the second case, if $\epsilon_{n,1} = -1$, between positions 1 and $n-1$ have occurred an even number of changes so $(\hat{x}^1)_1 = (\hat{x}^1)_n$ and again using the negation of Lemma 2.5.4 we get $f_1(\hat{x}^1) \neq (\hat{x}^1)_1$. It is important to note that since positions 2 to n of $\hat{x}^1$ are consistent with their signs, they do not change when f is applied, concluding that $f(\hat{x}^1) = \overline{\hat{x}^1}^1$.

Inductive step: Suppose the assertion is true until position i, that is, $f(\overline{\hat{x}^1}^{\{1,\dots,i-1\}}) = \overline{\hat{x}^1}^{\{1,\dots,i\}}$. We will show that $f(\overline{\hat{x}^1}^{\{1,\dots,i\}}) = \overline{\hat{x}^1}^{\{1,\dots,i+1\}}$. By induction hypotheses we have changed the first i positions of $\hat{x}^1$ consistently with its sign $\epsilon_{k,k+1}$, $k \in \{1,\dots,i\}$. In the same way, positions $i+2$ to n are consistent with its sign so they do not change, concluding that $f_k(\overline{\hat{x}^1}^{\{1,\dots,i\}}) = (\overline{\hat{x}^1}^{\{1,\dots,i\}})_k$, $k \in \{1,\dots,i,i+2,\dots,n\}$. Therefore, we only need to study position $i+1$.

$$
\begin{pmatrix} x_1 \\ \vdots \\ x_{i-1} \\ x_i \\ \vdots \\ x_n \end{pmatrix}
\xrightarrow{\epsilon_{n,1}}
\begin{pmatrix} \overline{x_1} \\ \vdots \\ x_{i-1} \\ x_i \\ \vdots \\ x_n \end{pmatrix}
\cdots
\begin{pmatrix} \overline{x_1} \\ \vdots \\ \overline{x_{i-1}} \\ x_i \\ \vdots \\ x_n \end{pmatrix}
\xrightarrow{\epsilon_{i-1,i}}
\begin{pmatrix} \overline{x_1} \\ \vdots \\ \overline{x_{i-1}} \\ \overline{x_i} \\ \vdots \\ x_n \end{pmatrix}
\cdots
\begin{pmatrix} \overline{x_1} \\ \vdots \\ \overline{x_{i-1}} \\ \overline{x_i} \\ \vdots \\ x_n \end{pmatrix}
\xrightarrow{\epsilon_{n-1,n}}
\begin{pmatrix} \overline{x_1} \\ \vdots \\ \overline{x_{i-1}} \\ \overline{x_i} \\ \vdots \\ \overline{x_n} \end{pmatrix}
$$

As before, we consider two cases: If $\epsilon_{i,i+1} = +1$, we have by construction that $(\hat{x}^1)_{i+1} = (\hat{x}^1)_i$, but $(\hat{x}^1)_i \neq (\overline{\hat{x}^1}^{\{1,\dots,i\}})_i$ and $(\hat{x}^1)_{i+1} = (\overline{\hat{x}^1}^{\{1,\dots,i\}})_{i+1}$, then $(\overline{\hat{x}^1}^{\{1,\dots,i\}})_i \neq (\overline{\hat{x}^1}^{\{1,\dots,i\}})_{i+1}$. Hence, by the negation of Lemma 2.5.4 we conclude that $f_{i+1}(\overline{\hat{x}^1}^{\{1,\dots,i\}}) \neq (\overline{\hat{x}^1}^{\{1,\dots,i\}})_{i+1}$. In an equivalent way we prove that if $\epsilon_{i,i+1} = -1$ then $(\overline{\hat{x}^1}^{\{1,\dots,i\}})_i = (\overline{\hat{x}^1}^{\{1,\dots,i\}})_{i+1}$ and using the negation of Lemma 2.5.4 we get $f_{i+1}(\overline{\hat{x}^1}^{\{1,\dots,i\}}) \neq (\overline{\hat{x}^1}^{\{1,\dots,i\}})_{i+1}$. That is, $f(\overline{\hat{x}^1}^{\{1,\dots,i\}}) = \overline{\hat{x}^1}^{\{1,\dots,i+1\}}$.

Finally, we apply again previous inductive argument, with $\hat{x}^1$ replaced by $\hat{x}^2$, to obtain that $i+1 \in Com(\overline{\hat{x}^2}^{\{1,\dots,i\}})$ for $i \in \{1,\dots,n-1\}$. Thus, we have proved that the cycle C is attractive, and the proof is complete.

$\square$

Observation 2.5.6. *Notice that in the last proof we use, even if it appears to be hidden, all the hypotheses: C has n vertices and the signs are constant independently of x.*

In order to illustrate the last result we will show some examples:

Example 2.5.7. *(n = 3) Suppose that the regulatory graph is composed by a positive isolated circuit which has the following form:*

$$g_1 \xrightarrow{+1} g_2 \xrightarrow{+1} g_3 \xrightarrow{+1} g_1$$

If we apply the construction proposed in Proposition 2.5.5, we can obtain two fixed points, $(0,0,0)$ and $(1,1,1)$. This is because the edges are positive and Lemma 2.5.4 says that $x_i = x_{i+1}$.

Additionally, from the structure of the regulatory graph we can deduce the other values of the function f. In fact, it is not hard to prove that since all the edges have the form $g_i \xrightarrow{+1} g_{i+1}$, the Jacobian matrix satisfies $J_{i+1,i}(x) \neq 0$, which finally implies that $f_{i+1}(x) \neq f_{i+1}(\overline{x}^i)$.

If we choose the point x as $(0,0,0)$ and $(1,1,1)$, we conclude that the function f is defined as:

x	000	100	010	001	111	011	101	110
$f(x)$	000	010	001	100	111	101	110	011

Example 2.5.8. *(n = 2) In this case the regulatory graph consists of an isolated positive circuit having the form*

$$g_1 \xrightarrow{-1} g_2 \xrightarrow{-1} g_1.$$

Again by the construction used in Proposition 2.5.5, the two fixed points are $(0,1)$ and $(1,0)$, because both edges are negative and Lemma 2.5.4 says that $x_i \neq x_{i+1}$. Besides, as before $J_{i+1,i}(x) \neq 0$ which implies that $f_{i+1}(x) \neq f_{i+1}(\overline{x}^i)$. Then using the points $(0,1)$ and $(1,0)$ the function f has the following form:

x	00	10	01	11
$f(x)$	11	10	01	00

Example 2.5.9. *(n = 3) Suppose we have a regulatory graph composed by a negative isolated circuit*

$$g_1 \xrightarrow{+1} g_2 \xrightarrow{-1} g_3 \xrightarrow{+1} g_1.$$

In this case since the circuit is negative we expect that f presents an attractive cycle. From Proposition 2.5.5 we can generate the starting point $\hat{x}^1 = (0,0,1)$, because the edge between g_2 and g_3 is negative so $(\hat{x}^1)_2 \neq (\hat{x}^1)_3$. In the same way we obtain that $\hat{x}^2 = (1,1,0)$. Then

we conclude that the attractive cycle has the following form:

$$\hat{x}^1 = 001, \overline{\hat{x}^1}^{\{1\}} = 101, \overline{\hat{x}^1}^{\{1,2\}} = 111, \overline{\hat{x}^1}^{\{1,2,3\}} = 110 = \hat{x}^2$$

$$\overline{\hat{x}^2}^{\{1\}} = 010, \overline{\hat{x}^2}^{\{1,2\}} = 000, \overline{\hat{x}^2}^{\{1,2,3\}} = 001 = \hat{x}^1$$

Moreover, it is not difficult to see that the function f satisfying the condition has the following form:

x	000	100	010	001	111	011	101	110
$f(x)$	001	011	000	101	110	100	111	010

Observation 2.5.10. *The main problem of this strategy is that in the general case it does not apply. However, it is possible to prove a weaker result for regulatory graphs with minimal circuits and restricted fixed points. That is, both Thomas conjectures are stable under projection, and this enables to relax the assumptions under which they are valid (for more details see [RR08]).*

2.6 From the transition to the regulatory graphs

In the previous sections we have shown a series of lemmas and propositions in order to prove that the existence of an attractive cycle in the transition graph implies the existence of a negative circuit in the regulatory graph. Moreover, from the first Thomas conjecture we know that multistability implies the existence of a positive circuit in the regulatory graph [RRT05].

In general, different examples (examples 2.5.2, 2.5.3, 2.5.9) illustrate that under the presence of a cycle in $\mathcal{T}(f)$, there exists a circuit in $\mathcal{G}(f)$. This empirical result, together with the fact that in general the hypothesis of attractivity is too strong, motivates the study of general cycles and the idea of an extended transition graph which incorporates the information of the signed regulatory graph. Therefore, the main objective of this section is to find conditions that permit us to understand the relation of general cycles in $\mathcal{T}(f)$ with circuits in $\mathcal{G}(f)$.

2.6.1 Cycles: general framework

Let $f : \{0,1\}^n \to \{0,1\}^n$ be a Boolean map and $C = (x^1, \ldots, x^r, \varphi)$ a cycle in the transition graph $\mathcal{T}(f)$. Since C is not necessarily attractive we cannot assume that the sets $Com(x^i)$

has a unique point as before. So, $|Com(x)| \geq 1$.

From the definition of a cycle, we have that for all $i \in \{1, \ldots, r\}$ it is satisfied that $\varphi(i) \in Com(x^i)$ and $x^{i+1} = \overline{x^i}^{\varphi(i)}$. For that reason, if we use Lemma 2.4.2 for x^i, $\varphi(i)$, x^{i+1} and $\varphi(i+1)$, one deduces that the condition for the existence of an edge between vertices $g_{\varphi(i)}$ and $g_{\varphi(i+1)}$ is

$$(2.6.1) \qquad \qquad \varphi(i+1) \notin Com(x^i) \backslash \{\varphi(i)\}.$$

In Section 2.5 we have proved that when the cycle is attractive the expression (2.6.1) is always satisfied because $Com(x^i)$ has a single element $\varphi(i)$, so the desired edge exists. However, in general we do not know if there exists an edge between two nodes generated by the strategy φ.

The main result of this section shows that a cycle in the transition graph implies the existence of a circuit in the regulatory graph. In order to prove the last assertion, we have divided the proof into a sequence of lemmas: (i) a reduction lemma for cycles in $\mathcal{T}(f)$ and (ii) a lemma for the existence of edges in $\mathcal{G}(f)$ with vertex set $\{g_{\varphi(1)}, \ldots, g_{\varphi(r)}\}$.

Lemma 2.6.1. *Let $f : \{0,1\}^n \rightarrow \{0,1\}^n$ be a Boolean map and consider a cycle $C = (x^1, \ldots, x^r, \varphi)$ of length $r > 2$ in $\mathcal{T}(f)$. If there exists $\varphi(j)$ such that for all $i \in \{\varphi(1), \ldots, \varphi(r)\}$ and $x \in \{x^1, \ldots, x^r\}$*

$$(2.6.2) \qquad \qquad J_{i,\varphi(j)}(x) = 0 \text{ or equivalently } f_i(x) = f_i(\overline{x}^{\varphi(j)}),$$

then C can be reduced to another cycle $\bar{C}$ of length $r - 2$.

Proof. The proof consists in the construction of a reduced cycle $\bar{C}$. Let $\varphi(j)$ be as in the hypotheses and $k \in \{1, \ldots, r\} \backslash \{j\}$ such that $\varphi(k) = \varphi(j)$ (it exists since in the cycle such component changes at least twice).

In what follows we will show that the path starting from x^j with strategy $\{\varphi(j+1), \ldots, \varphi(k-1), \varphi(k+1)\}$ is well defined. Using Lemma 2.4.2 for x^j, $\varphi(j)$, x^{j+1} and $\varphi(j+1)$ and (2.6.2) one deduces that $\varphi(j+1) \in Com(x^j) \backslash \{\varphi(j)\}$, since $J_{\varphi(j+1),\varphi(j)}(x^j) = 0$, which implies that the state $y^1 = \overline{x^j}^{\varphi(j+1)}$ is in the dynamics. Let $y^2 = \overline{y^1}^{\varphi(j+2)}$ be the next state. To continue, it is also necessary to prove that y^2 is in the dynamics, that is, $\varphi(j+2) \in Com(y^1)$ or equivalently $(y^1)_{\varphi(j+2)} \neq f_{\varphi(j+2)}(y^1)$.

From (2.6.2), taking $x = x^{j+2} \in C$ and $i = \varphi(j+2)$, it follows that

$$f_{\varphi(j+2)}(x^{j+2}) = f_{\varphi(j+2)}(\overline{x^{j+2}}^{\varphi(j)}) = f_{\varphi(j+2)}(\overline{\overline{x^j}^{\{\varphi(j),\varphi(j+1)\}}}^{\varphi(j)}) = f_{\varphi(j+2)}(\overline{x^j}^{\varphi(j+1)}) = f_{\varphi(j+2)}(y^1).$$

Moreover, we have that $f_{\varphi(j+2)}(x^{j+2}) \neq (x^{j+2})_{\varphi(j+2)}$, because $\varphi(j+2) \in Com(x^{j+2})$, and $(x^{j+2})_{\varphi(j+2)} = (\overline{x^j}^{\{\varphi(j),\varphi(j+1)\}})_{\varphi(j+2)} = (y^1)_{\varphi(j+2)}$, concluding that $\varphi(j+2) \in Com(y^1)$.

In the same way, it is possible to prove in the general case that for $y^l = \overline{x^j}^{\{\varphi(j+1),\dots,\varphi(j+l)\}}$, $l \in \{1,\dots,k-j-1\}$, we have that $\varphi(j+l+1) \in Com(y^l)$. In fact, it is only necessary to use (2.6.2) with $x = x^{\varphi(j+l+1)}$ and $i = \varphi(j+l+1)$, which implies that

$$
\begin{aligned}
f_{\varphi(j+l+1)}(x^{j+l+1}) &= f_{\varphi(j+l+1)}(\overline{x^{j+l+1}}^{\varphi(j)}) = f_{\varphi(j+l+1)}(\overline{\overline{x^j}^{\{\varphi(j),\dots,\varphi(j+l)\}}}^{\varphi(j)}) \\
&= f_{\varphi(j+l+1)}(\overline{x^j}^{\{\varphi(j+1),\dots,\varphi(j+l)\}}) = f_{\varphi(j+l+1)}(y^l).
\end{aligned}
$$

That is, we can conclude as before that since $f_{\varphi(j+l+1)}(x^{j+l+1}) \neq (x^{j+l+1})_{\varphi(j+l+1)} = (y^l)_{\varphi(j+l+1)}$, we have $\varphi(j+l+1) \in Com(y^l)$, for $l \in \{1,\dots,k-j-1\}$.

To finish the construction of the reduced path, we have that $x^{k+1} = \overline{x^k}^{\varphi(k)} = \overline{x^j}^{\{\varphi(j),\dots,\varphi(k)\}}$, but since $\varphi(j) = \varphi(k)$, it follows that $x^{k+1} = \overline{x^j}^{\{\varphi(j+1),\dots,\varphi(k-1)\}} = y^{k-j-1}$. Additionally, from the definition and the last assertion we have that $x^{k+2} = \overline{x^{k+1}}^{\varphi(k+1)} = \overline{y^{k-j-1}}^{\varphi(k+1)}$, that is, $\varphi(k+1) \in Com(y^{k-j-1})$. Summarizing, the path P_1 from x^j to x^{k+2} with strategy $\{\varphi(j+1),\dots,\varphi(k-1),\varphi(k+1)\}$ (without $\varphi(j)$ and $\varphi(k)$) is in $\mathcal{T}(f)$.

It is important to note that since C is well defined, the paths P_2 from x^1 to x^j with strategy $\{\varphi(1),\dots,\varphi(j-1)\}$ and P_3 from x^{k+2} to x^1 with strategy $\{\varphi(k+2),\dots,\varphi(r)\}$ are also well defined. Therefore, if we define the cycle $\bar{C}$ as

$$\bar{C} = (x^1, \{\varphi(1),\dots,\varphi(j-1),\varphi(j+1),\dots,\varphi(k-1),\varphi(k+1),\dots,\varphi(r)\}),$$

then we conclude that $\bar{C}$ is in $\mathcal{T}(f)$ and has length $r-2$. This is because the new strategy does not take into account $\varphi(j)$ and $\varphi(k)$, which completes the proof. $\qquad\square$

In what follows it is necessary the following definition. A cycle $(x^1,\dots,x^r,\varphi)$ in $\mathcal{T}(f)$ is of minimal length if there is no other cycle in $\mathcal{T}(f)$ of length strictly smaller than r.

Lemma 2.6.2. *Let $f : \{0,1\}^n \to \{0,1\}^n$ be a Boolean map. If there exists a cycle $C = (x^1,\dots,x^r,\varphi)$, $r \geq 2$, of minimal length (not necessarily attractive) in $\mathcal{T}(f)$ then for all $j \in \{\varphi(1),\dots,\varphi(r)\}$, there exist $i \in \{\varphi(1),\dots,\varphi(r)\}$, $i \neq j$, and $x \in \{x^1,\dots,x^r\}$ such that $J_{i,j}(x) \neq 0$. That is, there exists an edge from g_j to g_i.*

Proof. We remark that if $C = (x^1, x^2, \varphi)$ then $\varphi(1) = \varphi(2)$ and by Lemma 2.4.2 there is an edge from $g_{\varphi(1)}$ to $g_{\varphi(1)}$ since $\varphi(1) \notin Com(x^1) \backslash \{\varphi(1)\}$.

Now we proceed by contradiction. Thus assume there is $\varphi(j) \in \{\varphi(1), \dots, \varphi(r)\}$ such that for all $i \in \{\varphi(1), \dots, \varphi(r)\}$ and $x \in \{x^1, \dots, x^r\}$, $J_{i,\varphi(j)}(x) = 0$. Using Lemma 2.6.1 there exists a cycle,

$$\bar{C} = (x^1, \{\varphi(1), \dots, \varphi(j-1), \varphi(j+1), \dots, \varphi(k-1), \varphi(k+1), \dots, \varphi(r)\}),$$

which is well defined and has length $r - 2$, which contradicts the minimality hypothesis. $\square$

Using both previous lemmas, we get the following theorem:

Theorem 2.6.3. *Let* $f : \{0,1\}^n \to \{0,1\}^n$ *be a Boolean map. Suppose there is a cycle* $C = (x^1, \dots, x^r, \varphi)$ *in* $\mathcal{T}(f)$, $r \geq 2$, *then* $\mathcal{G}(C) = \mathcal{G}(x^1) \cup \dots \cup \mathcal{G}(x^r)$ *has a circuit.*

Proof. The proof is divided into three cases:

(i) If $C = (x^1, x^2, \varphi)$ then $\varphi(1) = \varphi(2)$ and from Lemma 2.4.2 there is a self loop in $g_{\varphi(1)}$ since $\varphi(1) \notin Com(x^1) \backslash \{\varphi(1)\}$.

(ii) If C has minimal length then by Lemma 2.6.2 for all $j \in \{\varphi(1), \dots, \varphi(r)\}$ there exist $i \in \{\varphi(1), \dots, \varphi(r)\}$, $i \neq j$, and $x \in \{x^1, \dots, x^r\}$ such that $J_{i,j}(x) \neq 0$. That is, since sets are finite there exists a circuit in $\mathcal{G}(f)$ with vertex set $\{g_{\varphi(1)}, \dots, g_{\varphi(r)}\}$.

(iii) Finally, if C has no minimal length then Lemma 2.6.1 gives a reduction scheme for the cycle until one of the following happens: the resulting cycle has minimal length $r > 2$ and we apply Lemma 2.6.2 or it has the form $\bar{C} = (x^1, x^2, \varphi)$. Whatever the case there exists a circuit in $\mathcal{G}(C)$, which proves the proposition $\square$

In order to illustrate the last results we will show an example of a regulatory graph deduced from a cycle.

Example 2.6.4. *Let* $f : \{0,1\}^3 \to \{0,1\}^3$ *be the following Boolean map,*

x	000	100	010	001	111	011	101	110
$f(x)$	000	010	001	100	111	101	110	011

whose transition graph $\mathcal{T}(f)$ is defined in Figure 2.6. It is not difficult to see that f induces a non attractive cycle $C = \{100, 110, 010, 011, 001, 101\}$ and two fixed points 000 and 111.
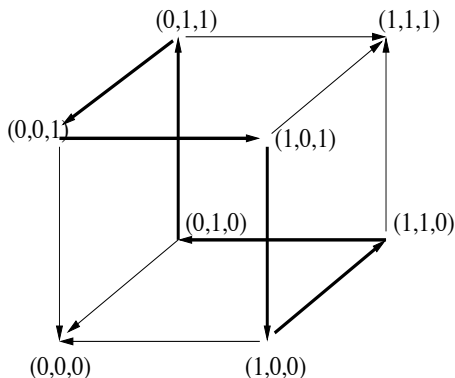
Figure 2.6: Transition graph $\mathcal{T}(f)$ in Example 2.6.4.

Since the transition graph has a cycle, it follows from Proposition 2.6.3 that the regulatory graph $\mathcal{G}(f)$ has a circuit. Additionally, the sign of the circuit is given by the existence of the two fixed points, as we can see in Figure 2.7.
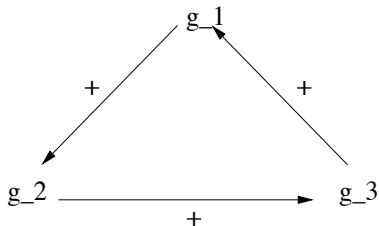
Figure 2.7: Regulatory graph at the point $(1, 0, 0)$, $\mathcal{G}((1, 0, 0))$ in Example 2.6.4.

The last example shows that the attractiveness hypothesis is essential for the presence of a negative circuit in the regulatory graph. In general, we only have a "correspondence" between cycles in $\mathcal{T}(f)$ and circuits in $\mathcal{G}(f)$.

2.6.2 Extended transition graph

The last subsection motivates the idea of an "extended transition graph", which takes into account not only the information of the states and the dynamics of the system (transition graph) but also information on the existence of signed edges in the regulatory graph. That is, an extended graph combining both dynamics and structure.

In this direction, we will start by recalling previous general results for the existence of edges in the regulatory graph and their corresponding signs. In fact, combining the edge

condition with the previous characterization for the sign, we are able to obtain a simplified expression for the sign formula depending only on the states.

In what follows, we use Lemma 2.4.2 to find a simplified version for the sign formula in Lemma 2.4.1, based on the equivalences of Lemma 2.5.4.

Lemma 2.6.5. *Let $f : \{0,1\}^n \to \{0,1\}^n$ be a Boolean map, $x \in \{0,1\}^n$ and $j \in Com(x)$. Denote $y = \overline{x}^j$. For $i \in Com(y)$, if $J_{i,j}(x) \neq 0$ then the following expression holds for the sign:*

(2.6.3)
$$\epsilon_{j,i} = (-1)^{x_j + \overline{x}_i^j} = (-1)^{x_j + y_i}$$

where the operations are modulo 2.

Proof. In order to prove the result we consider two cases:

1. $\underline{i \neq j}$: By hypotheses, since $J_{i,j}(x) \neq 0$ and using Lemma 2.4.2 for x, $j \in Com(x)$, $y = \overline{x}^j$ and $i \in Com(y)$ one deduces that $i \notin Com(x)\backslash\{j\}$. More specifically, it follows that $i \notin Com(x)$ because we are in the case $i \neq j$. Then, Lemma 2.5.4 implies that:

(2.6.4)
$$\begin{cases} x_i = x_j & \text{if } \epsilon_{j,i} = +1, \\ x_i \neq x_j & \text{if } \epsilon_{j,i} = -1. \end{cases}$$

We are now in position to prove the sign formula. If $\epsilon_{j,i} = +1$ then $x_i = x_j$, it follows directly that $x_j + x_i = x_j + y_i$ is always 0. On the other hand, if $\epsilon_{j,i} = -1$ then $x_j \neq x_i$ and as before the sum $x_j + x_i = x_j + y_i$ is always 1. That is, the expression for the sign holds:
$$\epsilon_{j,i} = (-1)^{x_j + y_i}$$

2. $\underline{i = j}$: By hypotheses, since $J_{i,i}(x) \neq 0$, it follows by the sign formula in Lemma 2.4.1 that
$$\epsilon_{i,i} = sgn(\overline{x}_i^i - x_i)sgn(f_i(\overline{x}^i) - f_i(x)) = sgn(y_i - x_i)sgn(f_i(y) - f_i(x)).$$

The last expression is always -1 because $i \in Com(x)$ and $i \in Com(y)$, then it follows that $x_i \neq f_i(x)$ and $y_i \neq f_i(y)$ respectively.

To conclude, it is sufficient to show that the new formula for the sign gives the same result. Since $x_i + \overline{x}_i^i = x_i + y_i$ is always 1, we have that $\epsilon_{i,i} = (-1)^{x_i + y_i} = -1$. That is, the sign expression holds and the proof is complete

□

Finally, the previous lemma and Lemma 2.4.2 allow us to define a signed transition graph $\bar{\mathcal{G}}$ which incorporates the dynamics of the Boolean map f and the signed regulatory graph.

Definition 2.6.6. *[Extended transition graph] Let $f : \{0,1\}^n \rightarrow \{0,1\}^n$ be a Boolean map. We define the extended transition graph $\bar{\mathcal{G}} = (\bar{V}, \bar{E})$ as follow:*

- *A node $v \in \bar{V}$ is defined as a 3-tuple $(x, y, Com(x))$, where $x \in \{0,1\}^n$ and $y = \bar{x}^j$ with $j \in Com(x)$.*

- *Given two nodes $v_j = (x, y, Com(x))$, $y = \bar{x}^j$, $j \in Com(x)$, and $v_i = (y, z, Com(y))$, $z = \bar{y}^i$ and $i \in Com(y)$. Then, there exists an edge in $\bar{E}$ between v_j and v_i if and only if $i \notin Com(x)\backslash\{j\}$.*

Finally, the sign of the edge from v_j to v_i is calculated by the formula $\epsilon_{j,i} = (-1)^{x_j + y_i}$

Remark 2.6.7. *It is important to note that from Definition 2.6.6 we build the extended transition graph using exclusively the dynamical information of the Boolean map f.*

The following example illustrates the construction of the extended transition graph $\bar{\mathcal{G}}$.

Example 2.6.8. *Let $f : \{0,1\}^3 \rightarrow \{0,1\}^3$ be a Boolean map, which is defined by the following table:*

x	000	100	010	001	111	011	101	110
$f(x)$	011	000	111	011	100	111	000	100

In what follows, we will describe in details the construction of the extended transition graph choosing two different points for which we generate their corresponding edges.

Consider $x^1 = 100$. Since $f(100) = 000$, it follows that $Com(100) = \{1\}$. As $|Com(100)| = 1$, it is possible to define $y^1 = \bar{x}^1 = 000$ and conclude that the first node of the extended transition graph is $(100, 000, \{1\})$. In order to define the second node we take $y^1 = 000$ and compute $f(000) = 011$. As $Com(000) = \{2,3\}$, there exist two possibilities to choose the second node, $z^1 = 010$ or $z^2 = 001$. If we consider the first choice the second node will be $(000, 010, \{2,3\})$ and from the second choice the third node will be $(000, 001, \{3,2\})$.

Once we have the nodes, we proceed to verify the existence of a signed edge between them: (i) $(100, 000, \{1\})$ and $(000, 010, \{2,3\})$. Since $2 \notin Com(100)\backslash\{1\}$, it follows that there exists

an edge between the nodes with sign $\epsilon_{1,2} = (-1)^{x_1^1 + y_2^1} = (-1)^{1+0} = -1$. (ii) $(100, 000, \{1\})$ and $(000, 001, \{3, 2\})$. Again, since $3 \notin Com(100)\backslash\{1\}$, it follows that there exists an edge between the nodes with sign $\epsilon_{1,3} = (-1)^{x_1^1 + y_3^1} = (-1)^{1+0} = -1$. That is,

$$(100, 000, \{1\}) \xrightarrow{-1} (000, 010, \{2, 3\}) \text{ and } (100, 000, \{1\}) \xrightarrow{-1} (000, 001, \{3, 2\})$$

Consider $x^2 = 101$. Since $f(101) = 000$, we have $Com(101) = \{1, 3\}$, which implies that there exist two possibles nodes in the extended transition graph $(101, 001, 1, 3)$ and $(101, 100, \{3, 1\})$. From the first election, if we define $y^2 = 001$ and since $f(001) = 011$, we have $Com(011) = \{2\}$. It follows that the third node will be $(001, 011, \{2\})$. Meanwhile, for the second node election, if we consider $y^3 = 100$ and since $f(100) = 000$, we have $Com(100) = \{1\}$. Hence, the fourth node will be $(100, 000, \{1\})$.

As before, we need to verify the existence of the edges between the nodes: (iii) $(101, 001, 1, 3)$ and $(001, 011, \{2\})$. Since $2 \notin Com(101)\backslash\{1\}$, there exists an edge with sign $\epsilon_{3,1} = (-1)^{x_1^2 + y_2^2} = (-1)^{1+0} = -1$. (iv) $(101, 100, \{3, 1\})$ and $(100, 000, \{1\})$. Since $1 \in Com(101)\backslash\{3\}$, it follows that there exists no edge. That is,

$$(101, 001, \{1, 3\}) \xrightarrow{-1} (001, 011, \{2\})$$

In Figure 2.8 we can see the usual transition graph (a) and the complete illustration about the construction of the extended transition graph (a'), which contains the information of the regulatory graph (b).

Finally, although the number of nodes in the extended transition graph is bigger than in the original, for higher dimensions it should be still possible to develop the systematic construction in order to infer the corresponding regulatory graph.

2.7 Conclusions and discussions

As we have mentioned before in the introduction, our motivation has been to explore the Thomas intuition in the Boolean case, trying to find a good mathematical framework to relate "dynamics with topological structure" of the associated signed regulatory graph(s), as source of information to know whether a particular asymptotic behavior occurs.
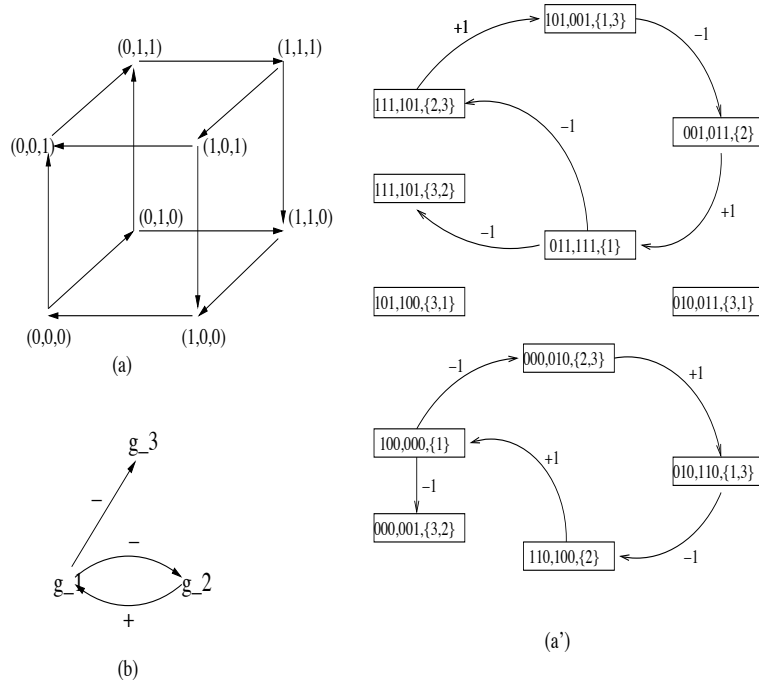
Figure 2.8: (a) Transition graph $\mathcal{T}(f)$. (a') Extended transition graph associated to f. (b) Associated Regulatory graph. In Example 2.6.8.

Following definitions and notations described in [RRT05], we have shown a series of properties in order to give conditions in the transition graph for the existence of signed edges in the regulatory graph, which include a new sign formula for the circuits. These properties allow us to provide an elementary proof for the second Thomas conjecture in the Boolean case that we think is very simple and make appears a kind of "cohomological idea" behind the sign assignment in the regulatory graph. It is also shown, in a constructive way, that in the particular case of an isolated circuit (regulatory graph consisting purely of a circuit) both Thomas conjectures are also sufficient.

Inspired by the proof of the second Thomas conjecture, we have studied the relation between cycles in the transition graph and circuits in the regulatory graph. In this direction, we have proved that the existence of a cycle $C = (x^1, \ldots, x^r, \varphi)$ in the transition graph (not necessarily attractive) implies the existence of a circuit in the regulatory graph. In order to show the last assertion, we have proved a path reduction lemma for cycles in $\mathcal{T}(f)$ and a lemma for the existence of edges in $\mathcal{G}(f)$ with vertex set $\{g_{\varphi(1)}, \ldots, g_{\varphi(r)}\}$. This confirms that the attractiveness hypothesis is essential for the presence of a negative circuit in the regulatory graph.

Finally, from Lemmas 2.4.2, 2.4.1 and 2.5.4, we are able to propose a formal method for the construction of an extended signed transition graph from the Boolean map f. This new

graph takes into account not only the information of the dynamics of f (transition graph), but also the structure of the signed regulatory graph, combining both. The spirit behind this new graph is to avoid the "problem" of changing from one graph to the other and produce conditions "à la Thomas".

Several aspects can be addressed in future work. Stronger results are certainly possible in order to completely understand the relation between the dynamics and the structure of the regulatory graph. In fact, the crucial problem about sufficient conditions in both Thomas conjectures has not yet proved even in the particular case of Boolean maps. Some efforts have been made on the study of positive and negative circuits of the regulatory graph and the fixed points in the case of discrete neural networks [A04], where necessary and sufficient conditions have been proved.

Further results seem possible when focussing on particular classes of Boolean maps. For that reason, our next challenge will be the study of possible relationships between the number of fixed points and the structure of circuits of the regulatory graph under the additional hypothesis of monotonicity for the Boolean map (among others). The objective is to find restrictions where sufficient conditions can be obtained for both Thomas conjectures.

In this direction, we think that the use of the extended transition graphs together with the interpretation of the cohomological equation relating cycles in the transition graph and circuits in the regulatory graph could help to understand dynamically the complete theoretical framework.

Bibliography

[A01] Aracena, J.: Modèles mathématiques discrets associés à des systeèmes biologiques. These de doctorat, Université Joseph Fourier, Grenoble, 2001.

[A04] Aracena, J., Demongeot, J., Goles E.: Positive and negative circuits in discrete neural networks. IEEE transactions on neural networks, Vol. 15 (1):77-83, 2004

[CD02] Cinquin, P., Demongeot, J.: Positive and negative feedback: striking a balance between necessary antagonists. Journal Theoretical Biology 216:229-241, 2002.

[J02] De Jong, H.: modelling and simulation of genetic regulatory system: A literature review. Journal of Computational Biology, 9(1):67-103, 2002.

[JG03] De Jong H., Gouzé J.-L., Hernández C., Page M., Sari T., Geiselmann H., Qualitative simulation of genetic regulatory networks using piecewise-linear models. Journal Math. Biol., Vol. 66: 301-340, 2003.

[GM90] Goles, E., Martínez, S.: Neural and automata networks. Dynamical behavior and applications. Mathematics and its Applications, 58. Kluwer Academic Publishers Group, Dordrecht, 1990.

[G98] Gouzé, J.-L.: Positive and negative circuits in dynamical systems. Journal of Biologycal Systems, 6:11-15, 1998.

[P95] Plahte, E., Mestl, T., Omholt, W.S.: Feedback circuits, stability and multistationary in dynamical systems. Journal of Biologycal Systems, 3:409-413, 1995.

[RMCT03] Remy, E., Mossé, B., Chaouiya, C., Thieffry, D.: A description of dynamical graphs associated to elementary regulatory circuits. Bioinformatics, 19(2):172-178, 2003.

[RRT05] Remy, E., Ruet, P., Thieffry, D.: Graphics requirements for multistability and attractive cycles in a Boolean dynamical framework. Advances in Applied Mathematics 41(3): 335-350, 2008.

Bibliography

[RR08] Remy, E., Ruet, P.: From minimal signed circuits to the dynamics of Boolean regulatory networks Bioinformatics 24: i220-i226, 2008.

[R95] Robert, F.: Les systemes dynamiques discrets. Volume 19 of Mathematiques et Applications. Springer, 1995.

[SD05] Shih, M.-H., Dong, J.-L.: A combinatorial analogue of the Jacobian problem in automata networks. Advances in Applied Mathematics, 34(1):30-46, 2005.

[Sg07] Sontag, E.: Monotone and near-monotone biochemical networks. Syst. Sybth. Biol 1, 59-87, 2007.

[S03] Soulé, C.: Graphics requirements for multistationarity. ComplexUs, 1:123-133, 2003.

[S05] Soulé, C.: Mathematical approaches to gene regulation and differentiation. Manuscript, 2005.

[T81] Thomas, R.: On the relation between the logical structure of systems and their ability to generate multiple steady states and sustained oscillations. In Series in Synergetics, volume 9, pages 180-193. Springer, 1981.

[R07] Richard, A.: On the link between oscillations and negative circuits in discrete genetic regulatory networks. JOBIM, Marseille, France, 2007.

[RC07] Richard, A., Comet, J.P.: Necessary conditions for multistability in discrete dynamical systems. Discrete Applied Mathematics, 155(18):2403-2413, 2007.

3 Numerical implementation of a Desynchronization method on Homeostatic systems: The Goodwin model

We show that the method of desynchronization proposed in [P06] can be simulated in a numerical stable way. We apply with success the algorithm to the simplest differential equations model of a feedback loop regulatory structure, namely the Goodwin model. Moreover, we show theoretically how to induce periodic behavior by adding a negative feedback, we propose a simulation algorithm and apply it to the Goodwin model with positive or negative regulatory function, inducing a Shilnikov or Lorenz type of chaos by building of homoclinic orbits.

The algorithm is robust against variations of parameters and numerical uncertainty. One outcome is, for instance, in the Lorenz type situation, trajectories visiting, in a chaotic order, neighborhoods of four given stable states of the initial system. We illustrate the results by applying with success the algorithm to the simplest differential equations model of a feedback loop regulatory structure, namely the Goodwin model, as well as to the master-slave synchronized Lorenz equations as an illustrative example.

In this context, the Goodwin model is the simplest differential equations modelling the dynamics of a regulatory negative feedback circuit. The model has been fundamentally important in biology, because it has explained the working mechanism of the circadian clock and other types of biological phenomena.

Additionally, from a mathematical point of view, we have done an spectral analysis on the desynchronized Goodwin model in order to obtain a relation between the eigenvalues of the differential model and the stability of the model. In this direction, we have naturally classified the eigenvalues into two classes, purely real or complex, depending ultimately on the choice of the parameters: synthesis (K_i) and degradation (γ_i). Finally, we use this

eigenvalue classification in the construction of the Poincaré map which allows us to find some inequalities between the model parameters in the stability analysis, which implies different types of attractors: sink, saddle or source.

3.1 Introduction

In this chapter we introduce, compute and analyze the numerical implementation of a desynchronization method on homeostatic systems, which has been developed by E. Pécou. In [P06] it was showed how to induce self-disorganization inside a stable, parameter-dependent, system by adding a feedback on the parameter.

For a long time, in biology, the study of stable systems has reached great attention and in particular the study of homeostatic systems, which are stable under the change of the parameters (external cellular stress condition). However, our motivation moves on an opposite direction, the possibility of inducing chaos from the initial conditions in order to do unstable the system.

For example, let us consider a therapeutic context where the objective is to perturb a hostile organism to kill it. A possible method consists in poisoning the organism by provoking the increase in the concentration of a metabolite up to a lethal level. However, this method is difficult to implement because the metabolism has many mechanisms precisely intended to moderate "excesses" (by saturation or homeostatic mechanisms for example).

In this context, E. Pécou has proposed a novel method in order to disorganize the metabolism by introducing a new differential equation into the original system. In [P06], it was proved that given a parametrized system of differential equations, that is a smooth family of smooth vector fields

$$\frac{dx}{dt} = F_\lambda(x) \quad x \in \mathbb{R}^n, \, n \geq 2, \, \lambda \in]a,b[,$$

having a globally stable equilibrium state x_λ, it is possible to build a differential equation for the parameter $\frac{d\lambda}{dt} = g(\lambda, x)$, such that the vector field $G = (g(\lambda, x), F_\lambda(x))$ defined on $]a,b[\times\mathbb{R}^n$ exhibits Lorenz-type or Shilnikov-type of chaos depending on the nature of the eigenvalues.

The precise statement is recalled in Theorem 3.2.1. Since the proof gave a constructive method for the feedback equation, a natural question, addressed in this chapter, is to provide the corresponding numerical algorithm (Section 3.3). In this direction, we show that the construction is structurally stable, and thus numerically observable.

In Sec. 3.4.1, we illustrate our methods on the classical dynamical model of biomolecular regulatory networks, namely the Goodwin equations. Those equations (Eq. 3.4.1) model the dynamics of a sequence of biochemical reactions in which one product at one step is consumed at the following step and the last product regulates (inhibits or activates) the first chemical reaction (typically, the transcription of a gene). Regulation is modelled by a non-linear sigmoid function characterized by a threshold parameter θ. To understand why this sigmoid function appears, one can consult [TO78], where a derivation of those equations, starting with the biological processes, is made. We have chosen as control parameters, first, the threshold θ, and, second, the maximum reaction rate $V_{\max}$ of the regulated variable.

The Goodwin model with negative regulation function is well known for having a unique equilibrium point which is stable for a wide range of parameter values. At first sight, we choose a set of parameters which set the system in the Lorenz type of situation, and apply the algorithm. The results show trajectories which oscillate between four states in an unpredictable order, and moreover, this order is sensitive to initial conditions.

Another numerical experiment consists in applying the algorithm by adding a feedback on the parameter $V_{\max}$, we create sustained oscillations with cooperativity index 4. This result is interesting since it is known that the Goodwin model with negative regulation cannot exhibit oscillations when it applies to a three-variable system with low "cooperativity index" (less than 8) (See [C99] for instance for a detailed review on necessary conditions for oscillations in negative feedbacks).

3.2 Inducing chaos in stable systems: Mathematical results

3.2.1 Master-slave synchronization

At the beginning of the 90s Pecora and Carroll [PC90] introduced a novel notion of synchronization for dynamical systems. Roughly speaking, this notion established that two identical systems can be coupled in such a way that the solution of one always converges to the solution of the other, independently of the initial conditions. This property was called Master-slave (M-S) synchronization to avoid confusion to other well studied types of synchronization.

In what follows and in order to motivate the main concepts we introduce the celebrated

Lorenz model:

$$(L) \begin{cases} \dot{x} &= \sigma(y - x) \\ \dot{y} &= (\tau - z)x - y \\ \dot{z} &= xy - bz \end{cases}$$

This system is known for exhibiting chaotic behavior for some values of σ, τ and b (for instance 10, 28 and 8/3 respectively). Pecora and Carroll ([PC90], [PC91]) proved that given any solution $(x(t), y(t), z(t))$ of the Lorenz model, the following reduced subsystem of two variables

$$(L_x) \begin{cases} \dot{Y} &= (\tau - Z)x(t) - Y \\ \dot{Z} &= x(t)Y - bZ, \end{cases}$$

has all its trajectories $(Y(t), Z(t))$ asymptotically converging to $(y(t), z(t))$, that is:

$$\lim_{t \to +\infty} ||Y(t) - y(t)|| = 0; \quad \lim_{t \to +\infty} ||Z(t) - z(t)|| = 0$$

They referred to this property as synchronization of (L) by the x-variable. Moreover, they described a more surprising fact for this particular system when any function is substituted by $x(t)$ inside the equations in the reduced system (L_x), any two solutions (Y_1, Z_1) and (Y_2, Z_2) would eventually converge one to the other, that is:

$$\lim_{t \to +\infty} ||Y_1(t) - Y_2(t)|| = 0; \quad \lim_{t \to +\infty} ||Z_1(t) - Z_2(t)|| = 0,$$

and this property was called absolute M-S synchronization.

Additionally, in the same paper, Pecora and Carroll also reported that z is not a synchronizing coordinate, and they have discriminated between synchronizing and non-synchronizing coordinates by a criterion of non positivity of the Lyapunov exponents which gives finally a necessary condition (for a full treatment we refer the reader to [BT97]).

3.2.2 Desynchronization of stable vector fields

Taking the reverse point of view, suppose we have a system of differential equations showing global asymptotic stability, and which depends on a parameter λ. Is it possible to break the asymptotic stability by adding a differential equation for the parameter? In the M-S synchronized Lorenz example the answer is yes because we only need to restore the differential equation for x to get chaos.

In [P06], Pécou has proved the previous situation in a more general case and the author has

explained in a constructive way how to create a function g for the new differential equation. In general: given $n \geq 2$ and a one-parameter family of vector fields on $\mathbb{R}^n$, $F_\lambda(x)$, $\lambda \in I$ interval subset of $\mathbb{R}$, such that for each λ, F_λ has a global asymptotically stable equilibrium point x_λ, it is possible to construct a vector field on $\mathbb{R}^{n+1}$ of the form $G(\lambda, x) = (g(\lambda, x), F_\lambda(x))$ which exhibits chaotic behavior. More precisely,

Theorem 3.2.1. *[Theorem 1, [P06]] Let $]a, b[\subset \mathbb{R}$ and $U \subset \mathbb{R}^n$ $(n \geq 2)$ be open sets and let $\{ F_\lambda \, , \, \lambda \in]a, b[\}$ be a C^k-family of C^k-vector fields defined on U $(k \geq 1$, or $k = +\infty)$. Assume that for each $\lambda \in I$, there exists $x_\lambda^* \in U$ which is a hyperbolic, globally attracting singularity for the differential equation:*

$$\frac{dx}{dt} = F_\lambda(x),$$

that is $F_\lambda(x_\lambda^*) = 0$, the Jacobian $J_\lambda = D_{x_\lambda^*} F_\lambda$ has all its eigenvalues with negative real parts, and the basin of x_λ^* contains U. Assume furthermore that

> *(i) J_λ has only one real eigenvalue ρ with maximum negative real part or only one pair of complex conjugate eigenvalues $\rho \pm i\omega$ with maximum real part and*

> *(ii) there exists λ_0 such that*
> $$\partial_\lambda F_\lambda(x_\lambda^*)|_{\lambda = \lambda_0} \neq 0.$$

Then, there exists a C^∞-map $g : I \times U \to \mathbb{R}$ such that the vector field $G(\lambda, x) = (g(\lambda, x), F_\lambda(x))$ is chaotic. More precisely, the flow of G has a homoclinic orbit and the first return map in a local section to the homocline has a countable set of horseshoes, and thus, a positive topological entropy.

Condition (i) is generic, and condition (ii) says that the vector field has an order 1 dependence on the parameter. Before to start the proof we recall the definition of a homoclinic orbit

Definition 3.2.2 (Homoclinic orbit)**.** *A homoclinic orbit is a trajectory of a flow of a dynamical system which joins a saddle equilibrium point to itself. More precisely, a homoclinic orbit lies in the intersection of the stable manifold and the unstable manifold of an equilibrium.*

Sketch of the proof: The substance of the proof lies in the construction of a homoclinic orbit in the (λ, x)-phase space: we perturb the degenerated vector field $G_0 = (0, F_\lambda)$ so that a chosen stable singular point $M_0 = (\lambda_0, x_{\lambda_0}^*)$ becomes a saddle singular point with a one-dimensional unstable manifold. Then, either one (or two) separatrix (separatrices) of M_0

are transformed into one or two homoclinic curve(s). Details can be found in [P06], and the numerical building is explained below.

Once we have shown how to build a homoclinic orbit, the proof splits into two parts: (a) when the less contracting eigenvalue of the Jacobian J_{λ_0} is not real and has a complex conjugate eigenvalue (referred to as the "complex" case, or the Shilnikov-like situation); (b) when the less contracting eigenvalue of J_{λ_0} is real (this is the "real" case, or the Lorenz-like situation).

In the complex case, the existence of one homoclinic orbit directly implies the existence of chaos, like in the Shilnikov model of chaos (see [S65],[S70],[W88]): the first return map to a cross section of the homoclinic orbit is shown to have an infinite number of horseshoes. In the real case, two homoclinic orbits are necessary, and after an arbitrary small perturbation, we get a Lorenz type of chaos with a strange attractor in the vicinity of the union of the homoclinic orbits ([R89], [R92]). □

Notation: A vector in $\mathbb{R}^n$ is usually denoted by x. A vector in $\mathbb{R}^{n+1}$ is denoted by (λ, x) to emphasize the role of the λ-axis. Given a set $A \subset \mathbb{R}^n$, we denote $Cl(A)$, its topological closure, $Int(A)$, its topological interior, and ∂A, its topological boundary. $B_r(x)$ is the standard notation for the open n-ball with radius $r > 0$ centered at a point x. Its boundary is the n-sphere, denoted by $S_r(x)$.

Additionally, to simplify the notations we assume that $I \times U =]-1, 1[\times B_1(0)$ and $\Gamma = \{(\lambda, x_\lambda^*), \lambda \in I\}$ is a straight line through $(0, 0)$ which does not intersect $\{-1\} \times Cl(U)$ nor $\{1\} \times Cl(U)$, is not parallel to the λ-axis, $F_\lambda(x_\lambda^*) = 0$ and $DF_{lambda}(x_\lambda^*)$ has eigenvalues with negative real parts, that is, Γ is a straight line with non zero slope in the direction of λ. We denote by F the vector field in $I \times U$ defined by $F(\lambda, x) = (0, F_\lambda(x))$.

3.2.3 Construction of the homoclinic orbit

According to hypothesis (i) of Theorem 3.2.1, two situations can occur: either there exists a unique real eigenvalue with a maximal real part or a unique pair of complex conjugate eigenvalues with a maximum real part. Our proof runs differently according to each situation: in the complex case, we construct a homoclinic connection to find the Shilnikov classical situation ([S65], [S70]). The real case is a reconstruction of the Lorenz situation ([BT97], [MP02]). Nonetheless, in both cases, we use the following construction of a homoclinic curve.

Proposition 3.2.3 (Proposition 1, [P06])**.** *There exists a C^∞-map $g : I \times U \to \mathbb{R}$ such that*

the vector field G defined on $I \times U$ by

$$G(\lambda, x) = (g(\lambda, x), F_\lambda(x))$$

has a saddle singular point at $(0,0)$ and one separatrix of its one-dimensional unstable manifold is a homoclinic curve.

In the following we explain how the function g is built. The global picture to have in mind is that g is 0 (and so the vector field G is vertical), except in two disjoint cylindrical domains with axes parallel to the λ direction. Inside these domains g is constructed so as to satisfy the following definition of elementary dynamical block.
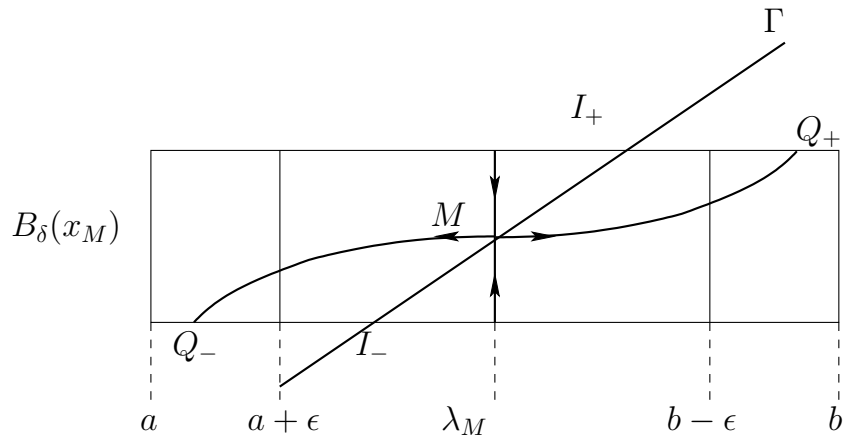
Figure 3.1: Elementary dynamical block B.

Definition 3.2.4 (Elementary block). *Let $M = (\lambda_M, x_M) \in \Gamma$, the set of singular points. Consider a and b such that $-1 < a < \lambda_M < b < 1$ and choose $\epsilon > 0$ such that $a + \epsilon < \lambda_M < b - \epsilon$.*

We call elementary dynamical block the cylinder $C_\delta = [a, b] \times \bar{B}_\delta(x_M)$ ($\delta < 1$) together with a vector field

$$G : \begin{array}{ccc} C_\delta & \to & \mathbb{R}^{n+1} \\ (\lambda, x) & \to & (g(\lambda, x), F_\lambda(x)) \end{array}$$

satisfying:

- *M is a saddle singular point for G with a 1 dimensional unstable manifold.*

- *$g|_{\partial C_\delta} \equiv 0$.*

- *The connected component of the unstable manifold of M containing M in C_δ intersects the boundary of C_δ at two points Q_- and Q_+ such that $Q_- \in]a, a + \epsilon[\times S_\delta(x_M)$ and $Q_+ \in]b - \epsilon, b[\times S_\delta(x_M)$*

See Figure 3.1.

Given μ, δ, let

$$h_{\mu,\delta}(r) = \begin{cases} \mu & \text{if } r < \delta \\ \frac{\mu}{2}(1 + cos(\frac{\pi r^2}{\delta^2})) & \text{else} \end{cases},$$

and

$$\Lambda(\lambda) = \frac{(\lambda - \lambda_M)(b - \lambda)^2(\lambda - a)^2}{(b - \lambda_M)^2(\lambda_M - a)^2}.$$

Finally, we can conclude the following expression for the function $g_{\mu,\delta}$:

$$g_{\mu,\delta}(\lambda, x) = \Lambda(\lambda)h(||x - x_M||),$$

where δ and μ are two positive real numbers respectively, called the radius of the block and the injection speed.

Now, for a suitable choice of parameters a, b, δ and μ, one can render the singular point M unstable, with an unstable manifold almost parallel to the direction λ in the neighborhood of M, and the vector field projection on this direction is quite larger than the projection on the other directions. Therefore, a small perturbation about M is driven by the flow away from M with a speed almost parrallel to the λ axis. By construction, the amplitude of this speed decreases when moving away from M, and it vanishes at the boundaries of the cylinder, where the flow is orthogonal to the direction $(0, \lambda)$. Constructing $g_{\mu,\delta}$ as an assembly of suitable blocks one can manage that M is a homoclinic point for the modified vector field.

Observation 3.2.5. *Notice that the map $g_{\mu,\delta}$ is C^1, positive in $]\lambda_M, b[\times B_\delta$, negative in $]a, \lambda_M[\times B_\delta$ and null on $\partial(]a, b[\times B_\delta)$. Moreover, the differential of $g_{\mu,\delta}$ with respect to λ at the point (λ_M, x_M), singular point of (G), is μ.*

Example 3.2.6. *In order to explain the construction of the different blocks and the homoclinic orbit we will consider as an illustrative example the following dynamical system:*

$$(3.2.1) \qquad \begin{cases} \frac{dY}{dt} = (-1 + \lambda)(\alpha(Y - \lambda) + \beta Z) \\ \frac{dZ}{dt} = (-1 + \lambda)(-\beta(Y - \lambda) + \alpha Z) \end{cases}$$

It is linear, with a fixed point $(Y, Z) = (\lambda, 0)$. It is stable if $\lambda < 1, \alpha > 0$, and this is a focus if $\beta < 0$.

We would like to desynchronize this system, with the block construction discussed above.

3.2. INDUCING CHAOS IN STABLE SYSTEMS: MATHEMATICAL RESULTS

We thus consider the modified vector field:

$$(3.2.2) \qquad \begin{cases} \frac{d\lambda}{dt} &= \quad g_{\mu,\delta}(\lambda, Y, Z) \\ \frac{dY}{dt} &= \quad (-1+\lambda)\left(\alpha(Y-\lambda)+\beta Z\right) \\ \frac{dZ}{dt} &= \quad (-1+\lambda)\left(-\beta(Y-\lambda)+\alpha Z\right) \end{cases}$$

In the sequel we fix $\alpha = 1, \beta = -4$. Call $\Gamma = \{\lambda, \lambda, 0\}$. This is the set of fixed points for (3.2.1) when λ varies.

We choose $M_0 = (0,0,0)$, $M_1 = (0.25, 0.25, 0)$, $\delta = 0.05$, $\mu = 100$. Then, $a = b = 0.25$ and the explicit formula for g inside C_0 is:

$$g_{C_0}(\lambda, y, z) = 12800\lambda(0.0625 - \lambda^2)^2(1 + \cos(400\pi(y^2 + z^2))).$$

Figure 3.2 illustrates the behavior of one orbit which starts close to M_0, before the construction of the second block (that is g is still 0 in the second cylinder C_1).
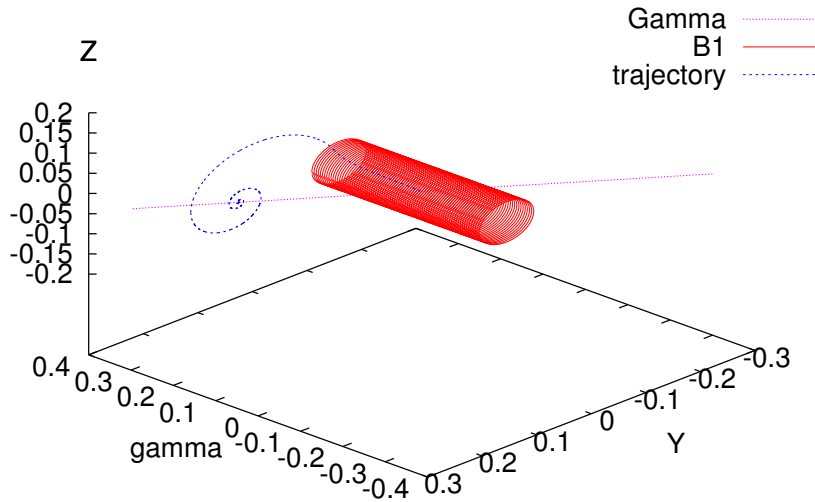
Figure 3.2: A trajectory starting in a neighborhood of M_0 for the first dynamical block

We choose some arbitrary $l > 0$, for instance $l = 0.01$, and the parameter $\mu_1 = \mu$ for the second dynamical block. Then, the second dynamical block centered at M_1 is defined by the

following function g:

$$g_{C_1}(\lambda, y, z) = \frac{(\lambda - 0.25)(0.5 - \lambda)^2(\lambda + 0.01)^2}{0.0625 * 0.063001}(1 + \cos(400\pi((y - 0.25)^2 + z^2))).$$

Figure 3.3 sketches an orbit of the complete flow.
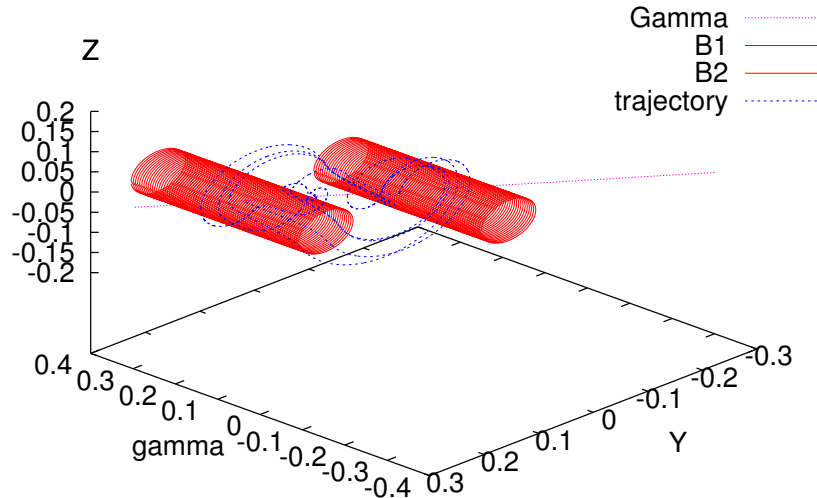
Figure 3.3: A trajectory starting in a neighborhood of M_0 for the extended dynamical system.

3.2.4 Periodic behavior

In the following, we show a new mathematical result.

Theorem 3.2.7. *Let $I \subset \mathbb{R}$ and let $\{ F_\lambda, \lambda \in]a, b[\}$ be a C^k-family of C^k-vector fields defined on $\mathbb{R}^n$ ($n \geq 2$, $k \geq 1$, or $k = +\infty$). Assume that there exist λ_0 and λ_1 in $]a, b[$ such that F_{λ_i} has a hyperbolic globally attracting singularity $x_i^* \in \mathbb{R}^n$ ($i = 0, 1$). Let $M_0 = (\lambda_0, x_0^*)$ and $M_1 = (\lambda_1, x_1^*)$.*

Then, there exist a C^∞-map $g : I \times \mathbb{R}^n \to R$, such that M_0 and M_1 are hyperbolic saddle fixed points for the vector field $G(\lambda, x) = (g(\lambda, x), F_\lambda(x))$ and for arbitrarily small invariant neighborhoods U_0 and U_1 of M_0 and M_1 respectively such that all orbits of G crossing $U_0^+ = U_0 \cap]\lambda_0, \lambda_1[\times \mathbb{R}^n$ or $U_1^- = U_1 \cap]\lambda_0, \lambda_1[\times \mathbb{R}^n$ visit alternatively U_0^+ and U_1^- for all time.

Proof. To simplify the notations, let $(\lambda_0, x_0^*) = (0, 0)$. Choose $\delta > 0$ such that both cylinders

$C_0 = [0, \lambda_1] \times B^n(0, \delta)$ and $C_1 = [0, \lambda_1] \times B^n(x_{\lambda_1}^*, \delta)$ do not intersect.

Since the property of having a hyperbolic globally attracting singularity is structurally stable, there exists $\epsilon > 0$ so that for each $\lambda \in]-\epsilon, \epsilon[$ or $\lambda \in]\lambda_1 - \epsilon, \lambda_1 + \epsilon[$, F_λ keeps this property.

First step. Suppose that there exists a map g defined for $(\lambda, x) \in [0, \lambda_1] \times \mathbb{R}^n$ such that:

(H1) M_0 and M_1 are saddle hyperbolic fixed points for $G = (g, F_\lambda)$ and $W^s(M_i) = \{\lambda_i\} \times \mathbb{R}^n$.

Let ψ_t be the flow of G.

Like in the previous section (proof of Proposition **??**), we construct "half-neighborhoods" U_0^+ and U_1^- of the saddle points M_0 and M_1.

Consider, for $\epsilon_0 \leq \epsilon$ small enough and $\eta_0 < \delta$, the $n-$disc $D^+ = \{\epsilon_0\} \times B^n(0, \eta_0)$. Let

$$V_0^+ = \bigcup_{t>0} \psi_{-t}(D^+),$$

$U_0^+ = V_0^+ \cap C_0$ and $\Pi^+ = V_0^+ \cap \partial C_0$.

In a similar way, we define, for $\epsilon_1 \leq \epsilon$ small enough and $\eta_1 < \delta$, $D^- = \{\lambda_1 - \epsilon_1\} \times B^n(x_1^*, \eta_1)$. Let $V_1^- = \bigcup_{t>0} \psi_{-t}(D^-)$, $U_1^- = V_1^- \cap C_1$ and $\Pi^- = V_1^- \cap \partial C_1$.

The following lemma holds readily.

Lemma 3.2.8. *The vector field G is tangent to the boundary of U_0^+ and U_1^-. G is transverse to $\Pi^+ \cup D^+$ and to $\Pi^- \cup D^-$ and the flow ψ_t enters U_0^+ (resp. U_1^-) through Π^+ (resp Π^-) and leaves U_0^+ (resp. U_1^-) through D^+ (resp D^-). Finally, each orbit crossing Π^+ (resp Π^-) has to cross next D^+ (resp D^-).*

For $\zeta_1 > 0$ small enough, $V_1^- \cap C_0$ contains a cylinder $]\lambda_1 - \zeta_1, \lambda_1[\times B^n(0, \delta)$. Consider a conic hyper-surface K_0 with axis $\{x = 0, \lambda \in [\epsilon_0, \lambda_1 - \zeta_1]\}$, and bounded by the $n-$discs D^+ and $\{\lambda_1 - \zeta_1\} \times B^n(0, \delta)$.

Similarly, there exists $\zeta_0 > 0$ small enough such that $V_0^+ \cap C_1$ contains $]0, \zeta_0[\times B^n(x_1^*, \delta)$. We let K_1 be a conic hyper-surface with axis $\{x = x_1^*, \lambda \in [\zeta_0, \lambda_1 - \epsilon_1]\}$, and bounded by the $n-$discs D^- and $\{\zeta_0\} \times B^n(x_1^*, \delta)$.

We define $\mathbf{K}_i$ the volume bounded by K_i, $i = 0, 1$. Suppose that g satisfies moreover that

(H2) G is transverse and in-going to K_0 and K_1.

Consider a point of D^+. Its future orbit by ψ_t stays in $\mathbf{K_0}$, then crosses $\{\lambda_1 - \zeta_1\} \times B^n(0, \delta)$, enters V_1^-, crosses Π^- and finally intersects D^-. Since the previous construction is symmetric, it is clear that the flow ψ_t induces a map from D^- to D^+. By composing both maps we get a well defined first return map on D^+. Moreover, the orbit of a point in U_0^+ crosses alternatively D^+ and D^- for all future time.
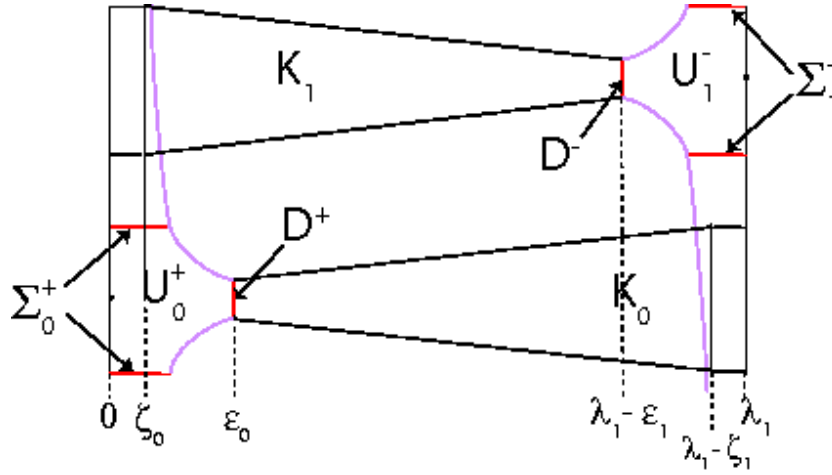
Figure 3.4: Trapping region

Second step Let us construct a map g that satisfies hypotheses (H1) and (H2).

Let us define the family of step functions:

$$\sigma_{a,k}(r) = \frac{a^k - r^k}{a^k + r^k}, \quad a > 0, \ k \in \mathbb{N}, \ r > 0$$

Those functions decrease from 1 to -1 and vanish at $r = a$. The derivative is 0 at $r = 0$ and tend to 0 when $r \to +\infty$. The steepness of the curve at $r = a$ increases with k.

Lemma 3.2.9. *There exist k and μ such that one can choose $a = ||x_1^*||/2$ and*

$$g(\lambda, x) = \begin{cases} \mu\lambda(\lambda_1 - \lambda)\sigma_{a,k}(||x||) & \text{if } \lambda \in [0, \lambda_1] \\ 0 & \sim \end{cases}$$

g **satisfies (H1):** Notice that $g(0,0) = g(\lambda_1, x_1^*) = 0$, and thus M_0 and M_1 are equilibrium points of the vector field G. A straightforward computation gives:

$$\frac{\partial g}{\partial \lambda}(0,0) = \mu\lambda_1 \quad \frac{\partial g}{\partial \lambda}(\lambda_1, x_1^*) = \mu\lambda_1 \frac{2^k - 1}{2^k + 1}$$

and

$$D_x g(0,0) = 0 \quad D_x g(\lambda_1, x_1) = 0.$$

As a consequence, the eigenvalues of $D_{(\lambda,x)}G(M_0)$ are those of $D_x F_0(0)$ and $\mu\lambda_1$. Similarly, the eigenvalues of $D_{(\lambda,x)}G(M_1)$ are those of $D_x F_{\lambda_1}(x_1^*)$ and $\mu\lambda_1 \frac{2^k-1}{2^k+1}$. Thus M_0 and M_1 are hyperbolic points with a one dimensional unstable manifold. Moreover, since $g = 0$ on $\{0\} \times \mathbb{R}^n$, the stable manifold of M_0 is $W_s(M_0) = \{0\} \times \mathbb{R}^n$. For the analogous reason, $W_s(M_1) = \{\lambda_1\} \times \mathbb{R}^n$.

For μ large enough, g satisfies (H2): We show that there exists $\mu > 0$ large enough so that G is transverse to the boundary of the cone K_0 and directed inside the cone. Denoting α the slope of K_0, this condition is satisfied as soon as for any $(\lambda, x) \in K_0$,

$$\alpha g(\lambda, x) > ||F_\lambda(x).||$$

Let $\bar{\lambda} = \min(\epsilon_0, \zeta_1)$; then for $\lambda \in [\epsilon_0, \lambda_1 - \zeta_1]$ we have $\lambda(\lambda_1 - \lambda) \geq \bar{\lambda}(\lambda_1 - \bar{\lambda})$. On the other hand, for $x \in B^n(0, \delta)$,

$$\sigma_{||x_1^*||/2,k}(||x||) \geq \sigma_{||x_1^*||/2,k}(||\delta||).$$

Thus g is minored on K_0 by:

$$g(\lambda, x) \geq C\mu,$$

where

$$C = \bar{\lambda}(\lambda_1 - \bar{\lambda})\sigma_{||x_1^*||/2,k}(||\delta||).$$

By letting

$$\mu \geq \frac{1}{\alpha C}\sup\{||F_\lambda(x)||, (\lambda, x) \in K_0\}$$

the corresponding vector field G points inward the cone K_0.

In the same way, there exist μ such that G points inward the cone K_1 and hypothesis (H2) is satisfied. $\qquad\square$

3.2.5 Lorenz model: switching master-slave synchronization

Consider the following system of equations which is the x-slave system derived from the Lorenz equations ([PC90], [PC91], [MP02])

$$(L_x) \begin{cases} \dot{Y} &= (\tau - Z)x(t) - Y \\ \dot{Z} &= x(t)Y - bZ \end{cases}$$

It is obvious that if we introduce a differential equation for the constant variable $x(t)$ having the form of the original in the Lorenz model we will recover the chaotic behavior. We tested our method of desynchronization by comparing $\widehat{L}$ to the Lorenz system. That is,

$$(\widehat{L}) \begin{cases} \dot{\lambda} &= g_{\mu,\delta}(\lambda, Y, Z) \\ \dot{Y} &= (\tau - Z)\lambda - Y \\ \dot{Z} &= \lambda Y - bZ \end{cases}$$

In this case the function $g_{\mu,\delta}(\lambda, Y, Z)$ is given by the desynchronization method.

Remark 3.2.10. *In the real case two homoclinic orbits must be built and controlled. Technically it means that we need to adjust the four dynamical blocks (real case) in the right way.*

The most difficult problem was the election of the block size. This is due to the nature of the real eigenvalues and because the Lorenz model exhibits symmetries with respect to the Z variable, so we need different values for the right and left side to avoid superposition of the orbits.

For the simulation we have chosen $\lambda = 0$ as initial point for the first block, the length of the blocks are $a = 0.18$ for the left side and $b = 0.15$ for the right side, $\delta = 0.14$, $\epsilon = 0.005$ and $l = 0.003$. The value of the first eigenvalue associated to the control equation was $\mu = 27$.

In Figure 3.5 we can see the result of the simulation. In first place we have the classical drawing of the chaotic behavior of the Lorenz model, and in the second we have the homoclinic orbit between the blocks obtained from the equation $(\widehat{L})$.

On the other hand, in Figure 3.6 we can see the transition between the blocks and the sensitivity to the initial condition, in the picture we have three different curves produced by the starting points $\lambda_1 = 0.0$ (brown), $\lambda_2 = -0.01$ (green) and $\lambda_3 = 0.001$ (orange).

"TrajLorenz"   +

"TrajLorenzD"   +
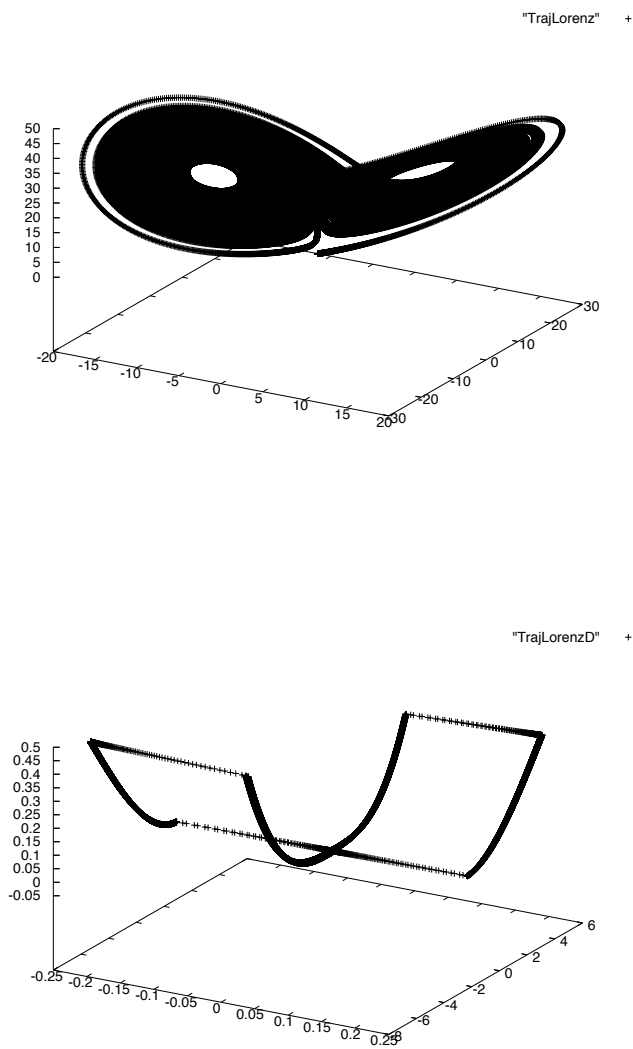
Figure 3.5: Lorenz Model: the real versus the desynchronization for the M-S Lorenz equation.
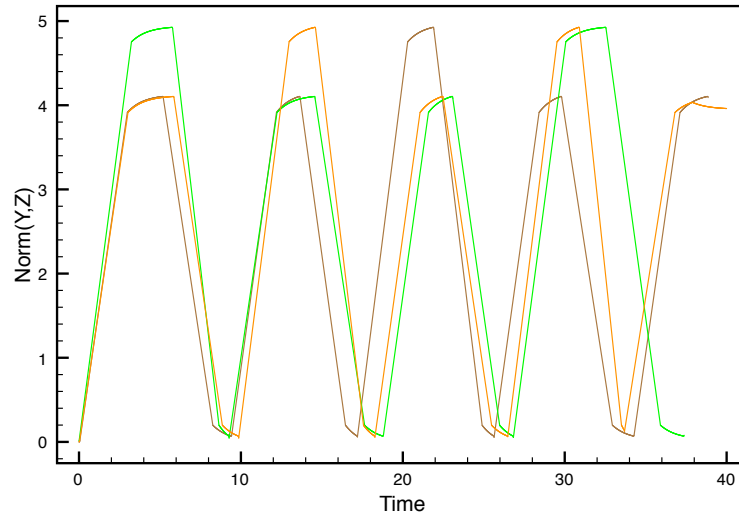
Figure 3.6: Sensitivity to the initial conditions. Chaos in the M-S Lorenz system

3.3 Desynchronization algorithm

As we have said in previous section, the main objective of this chapter is to develop a structurally stable algorithm of desynchronization which could be applied with success to different types of stable dynamical systems, in order to induce chaotic behavior by periodic orbits (numerically observable).

For that reason, in this section we explain the main features and sub-routines of the algorithm, as well as also explain the different stages from the input data to the construction of the $g_{\mu,\delta}(\lambda, x)$ function.

Later, we apply the method to the most simple homeostatic system namely the Goodwin model in order to break this homeostatic condition of stability. However, in order to illustrate and corroborate the algorithm, we also apply the method to the M-S Lorenz model in order to recover the chaotic behavior (sensitivity to initial conditions).

The algorithm also uses several known methods to find fixed points and solve systems of differential equations (as fourth order Runge-Kutta method for example). But, the principal new tool is the construction of the elementary dynamical blocks. Additionally, we have made several sub-routines in order to determine:

- The eigenvalues and to fit the constants of the model following Subsection 3.5.1.

- The first return map to exhibit chaos.

- The Lyapunov exponents that characterizes the rate of separation of infinitesimally close trajectories.

- Sensitivity to the inital conditions, where a graph shows variations with respect to the starting point close to the origin.

We recalled from [P06] that the method for creating chaos is based on the building of a homoclinic orbit, and therefore in the construction of the elementary dynamical blocks. More precisely, the task consists in finding a function $g(\lambda, x)$, such that the following extended dynamical system (3.3.1) has a homoclinic orbit.

(3.3.1)
$$\begin{cases} \frac{d\lambda}{dt} &= g(\lambda, x) \\ \frac{dx}{dt} &= F_\lambda(x) \end{cases}$$

Initial data   Our data consist in the knowledge of two equilibrium states corresponding to two parameter values:
$$M_0 = (\lambda_0, x^*_{\lambda_0}) \text{ and } M_1 = (\lambda_1, x^*_{\lambda_1})$$
for sake of simplicity, we write x_i for $x^*_{\lambda_i}$, for $i = 0, 1$. We suppose that $\lambda_0 < \lambda_1$.

Notice that we do not require the knowledge of the vector field F_λ. We only need to know that it satisfies the hypotheses of Theorem 3.2.1.

Cylinders   Let us consider a horizontal cylinder $C_0 = B^n(x_0, \delta) \times [2\lambda_0 - \lambda_1, \lambda_1]$, such that the radius δ is strictly smaller than the half-distance between x_0 and x_1. For instance, we choose $\delta = ||x_1 - x_0||/4$.

Next, for a given small $l > 0$, to be fixed later, we define another horizontal cylinder $C_1 = B^n(x_1, \delta) \times [\lambda_0 - l_a, 2\lambda_1 - \lambda_0]$.

Claim: The function g is 0 outside from the cylinders C_0 and C_1.

Dynamical block   Let $M = (\lambda_M, x_M)$ such that x_M is the stable equilibrium state of F_{λ_M}, and let $C = B^n(x_M, \delta) \times [a, b]$, where $\delta > 0$ and $a < \lambda_M < b$. We give a general formula for g inside C, denoted g_C.

Let $\mu > 0$. For all $(\lambda, x) \in C$, we set:

$$(3.3.2) \qquad g_C(\lambda, x) = \frac{(\lambda - \lambda_M)(b - \lambda)^2(a - \lambda)^2}{(b - \lambda_M)^2(a - \lambda_M)^2} h_{\mu,\delta}(\|x - x_M\|)$$

where the function $h_{\mu,\delta}$ is given by:

$$(3.3.3) \qquad h_{\mu,\delta}(r) = \begin{cases} \frac{\mu}{2}\left[1 + \cos\left(\frac{\pi r^2}{\delta^2}\right)\right] & \text{if } r \leq \delta \\ 0 & \text{if } r > \delta \end{cases}$$

Finally, we set $g_C(\lambda, x) = 0$ if $(\lambda, x) \notin C$.

A system Eq. 3.3.1 with $g = g_C$ is called a *dynamical block*. It has a saddle fixed point at M with a one-dimensional unstable manifold. The parameter μ is the derivative of g_C at M in the λ-direction. In [P06], it was proved that for any $\epsilon > 0$, there exists μ large enough, such that both unstable separatrices intersect the $n-$balls $\{b - \epsilon\} \times B_\delta(x_M)$ and $\{a + \epsilon\} \times B_\delta(x_M)$, before leaving the cylinder C.

Claim: We let $g = g_{C_0} + g_{C_1}$. There exist a parameter l, such that the system Eq. 3.3.1 has a homoclinic orbit.

3.3.1 Pseudo code: construction of the elementary dynamical blocks

In what follows, we will assume that we know the values of the eigenvalues μ, α_2, α_3 and α_4 (see Section 3.5.1 for a more detailed discussion). This is because they are useful for the study of the stability (as we can see the the following section).

The construction of the elementary blocks depends on the variables a, b for the length of the blocks, δ for the radius (block), μ for the injection speed and ϵ as an error tolerance. The output of the program will be the block function P, which contains all the previous information.

```
Const_blocks(P, a, b, delta, mu, epsilon, Goodwin, GoodwinPert) {

  for (k=1;k<N;k++) X[k]=drand48();
  X[0]=lambda_initial;

   For each fixed point
  do {
```

```
    H=tetan/(tetan+pow(z1,nc)) - e*z1/C;
    DH=-(double)nc*K1*C*tetan*pow(z1,nc-1)/pow(tetan+pow(z1,nc),2) - e;
    if (DH != 0) aux= z1 - H/DH;
    else aux= z1+0.5;
    z1=aux;

    Y[3]=z1;
    Y[2]=gamm3*Y[3]/K3;
    Y[1]=gamm2*Y[2]/K2;
    H=tetan/(tetan+pow(z1,nc)) - e*z1/C;
} while (fabs(H)>eta);

numbloc=i;
for (k=0;k<N;k++) {
    P.CM[numbloc][k]=Y[k];
    P.bg[numbloc]=P.CM[numbloc][0]-a;
    P.bd[numbloc]=P.CM[numbloc][0]+b;
    P.eps[numbloc]=epsilon;
    P.mub[numbloc]=mu;
    P.deb[numbloc]=delta;
    P.amp[numbloc]=1.0;
}
}
```

One of the biggest problems was to keep the homoclinic orbit inside the elementary block. In order to solve this problem, we first draw a cone inside the block with an angle α and we check the inequality condition between F_λ and $g_{\mu.\delta}$ (for more details see [P06]),

$$||F_\lambda|| \leq \alpha|g_{\mu,\delta}|.$$

It is important to note that we only check the condition when we have assigned a value to the function $g_{\mu,\delta}$, because outside the block its value is zero. For that reason we use the sub-functions Λ and $h_{\mu,\delta}$. These two sub-functions have several restrictions to maintain the curve inside the cone, and they depend on the parameters M (center of the block) $a, b, \epsilon, \mu, \delta$ and x the iteration point. In what follows, we present in details the pseudo-codes that construct these auxiliary functions:

```
Function g(X) {
```

```
  for (i=0;i<P.nb;i++) {
      gdex+=B(P.CM[i],P.bg[i],P.bd[i],P.eps[i],P.mub[i],P.deb[i],X);
  }
}


Function B(M, a, b, epsilon, mu, delta, X) {
  double lambda,lambdaM,z;
  lambda=X[0];lambdaM=M[0];

  if ((lambda>a) && (lambda<b)) {
      Lambda=(lambda-lambdaM)*pow((lambda-a),2)*pow((b-lambda),2)*
          h(M,a,b,epsilon,mu,delta,X)/(pow((lambdaM-a),2)*pow((b-lambdaM),2));
      return z;
  }
}


Function h(M, a, b, epsilon, mu, delta, X) {

  lambdaM=M[0];

  if ( X[0]>=lambdaM ) {
      deltabar1=(X[0]-lambdaM)*delta/((bord-lambdaM)-epsilon); //right condition
      epsilon2=epsilon*delta/((bord-lambdaM)-epsilon);
  } else {
      deltabar1=(lambdaM-X[0])*delta/((lambdaM-borg)+epsilon); //left condition
      epsilon2=epsilon*delta/((lambdaM-borg)+epsilon);
  }

  if (R<delta) {
      if (fabs(X[0]-M[0])<=epsilon) {
          if (fabs(X[1])>1.0) {
              if (R<=delta/2.0) {
                z=mu;//*(1.0+cos(M_PI*pow((R/delta),2)))/2.0;
              } else {
                if (fabs(X[0]-M[0])>=epsilon) z=mu;
                else z=0.0;
              }
          }
          if (fabs(X[1])<1.0) {
```

```
        if (R<=delta/2.0) {
          z=mu;//*(1.0+cos(M_PI*pow((R/delta),2)))/2.0;
        } else {
          if (fabs(X[0]-M[0])>=epsilon) z=mu;
          else z=0.0;
        }
      }
    }
    if ((X[0]>M[0]+epsilon) || (X[0]<M[0]-epsilon)){
      if ((R>deltabar1) && (R<=delta)){
        z=mu;
      }
      if ((R<=deltabar1)) {
        z=mu*(1.0+cos(M_PI*pow((R/delta),2)))/2.0;
      }
    }
    if ((X[0]>bord-epsilon) || (X[0]<borg+epsilon)){
      z=0.0;
    }
  }
  return z;
}
```

Remark The algorithm has been implemented using a code in $C++$ language. Codes are available upon request.

3.4 Homeostatic systems

In [T81], René Thomas conjectured that any dynamical system displaying stable oscillations must have at least one negative circuit, while any system with multiple steady states must contain a positive circuit. In the differential case, C. Soulé [So03] presented a full proof for the first part of the conjecture. However, he does not give any information about sufficient conditions in the case of positive circuits. This implies that certain other conditions are necessaries and need to be considered as the network topology or the ranges of values on specific state variables or parameters.

It is possible to rewrite the conjecture in such a way that two special biological processes

appear: homeostasis related with negative circuits and cellular differentiation related with positive circuits. We are particularly interested in the concept of homeostasis or how an organism regulates its internal environment so as to maintain a stable constant condition.

Intuitively, these biological associations make sense. For example suppose the following toy model that consists of three genes:

$$A \xrightarrow{-1} B \xrightarrow{-1} C \xrightarrow{-1} A$$
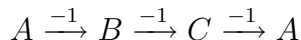
In this case we have a negative circuit between the genes A, B and C (odd number of negative edges). If the concentration of A increases, then the concentration of B decreases, which in turn will produce the increasing of the concentration of C, which finally will cause that the concentration of A decreases. Since we initially assumed A to be increasing, then we can conclude that the negative circuit promotes oscillatory behavior in the genes concentrations.

In the remainder, we will focus on homeostatic systems. It is known that homeostasis is characterized by the existence of a global stable equilibrium state. In general we can classify steady states and trap cycles as attractors. Attractors represent regions of predictability and stability in the behavior of the system. We are interested in attractors of cardinality greater than one implying cyclic behavior, which can often be identified with homeostasis of sustained oscillatory activity, as can be found in the cell cycle or circadian rhythm.

In order to apply the desynchronization method, we will restrict our attention to the three dimensional Goodwin model, which describes a transcriptional negative or positive feedback exhibiting homeostatic behavior.

3.4.1 The Goodwin model

The Goodwin model was proposed by Brian C. Goodwin at the beginning of the 60s, as a negative feedback oscillator, in order to explain via the differential equations formalism important biological processes. Roughly speaking, he described rather closely the putative molecular mechanism of the circadian clock ([G63], [G65]), and until today it has been the best and simplest example of the homeostatic behavior at cellular level. This is because the main characteristic feature in the Goodwin model is that degradation of clock-mRNA and clock protein species plays an important role in the control of the oscillator's period.

In fact, the Goodwin model has been the earliest model predicting oscillations due to negative feedback on gene expression, at a time when the part played by such regulatory
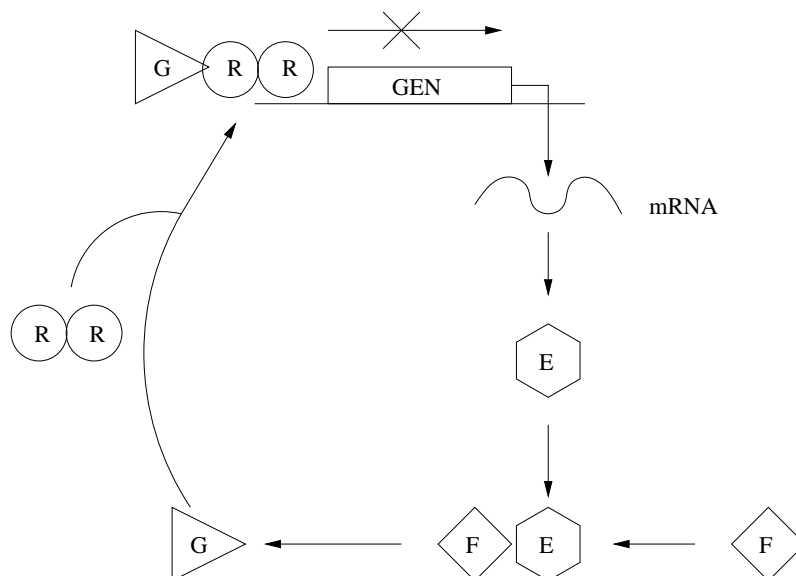
Figure 3.7: Scheme of the Goodwin model.

mechanism in the origin of circadian rhythms was not yet known. Moreover, the model has the property to be the simplest homeostatic system.

Now we proceed with an overview of the biological model: the model used here is a simplification of the originally. We have only considered 3 variables because instead of a direct regulation there exists a cascade of reactions such that the last product is the co-repressor. Hence, the submodel describes one of the most basic regulatory systems: the feedback inhibition by products of a gene.

The main components are the following: E (enzyme) and R (repressor) represent the proteins, and F and G represent the metabolites (molecules that participate as final products or intermediaries). The association between the repressor (in form of a dimmer) to the metabolite G permits the fixation of the complex to the region upstream of the coding gene for the enzyme E and then it blocked its own transcription. In Figure 3.7 we can see a graphical representation of the biological model.

From the theoretical point of view it is necessary to associate thus biological mechanism with a mathematical model. As we have exposed before there exist a lot of mathematical models describing biological processes like differential equations, boolean functions or stochastic equations, in this case we will use the first one.

The starting point is to define the variables of the system of differential equations. In our case the variables x, y and z represent the concentration of mRNA M, the enzymatic protein E, and the metabolite G (co-repressor) respectively. As a result it is not complicated to

see that the equations representing the biological model have the following form (power law formalism):

$$(3.4.1) \qquad (G_\lambda) = \begin{cases} \frac{dM}{dt} &= V_{\max} K_1 R_\lambda^{\pm}(G) - \gamma_1 M \\ \frac{dE}{dt} &= K_2 M - \gamma_2 E \\ \frac{dG}{dt} &= K_3 E - \gamma_3 G \end{cases}$$

where the constants K_i are rates of synthesis and the constants γ_i are rates of degradation.

In the previous system $R_\lambda^{\pm}(z)$ represents the regulatory function for the feedback circuit, and the sign indicates the type of regulation (positive or negative). Basically, it describes in a quantitative way how transcription depends on the co-repressor. It has been experimentally observed that this function has a sigmoidal shape and the standard analytical expression for the function is:

$$R_\lambda^{-}(z) = \frac{\lambda^n}{\lambda^n + z^n} \; ; \; R_\lambda^{+}(z) = \frac{1 + z^n}{\lambda^n + z^n}$$

where λ is a threshold parameter and n is the cooperative index.

In order to apply the desynchronization method to the Goodwin model we need to choose a constant parameter as a new variable. In the previous system we have three alternatives K_i, γ_i and λ, but the first two are not too relevant from the biological point of view. For that reason we have chosen the constant λ as the new variable. This election implies that the following differential equation needs to be added (see Subsection 3.2.3):

$$\frac{d\lambda}{dt} = g_{\mu,\delta}(\lambda, x, y, z).$$

In general, we know that the system evolves by damping equations and then we obtain an stable stationary state. Hence, in the rest of the chapter we will tackle the problem of how applying the desynchronization method to the Goodwin model. In this direction, it is not complicated to prove that all the hypotheses in Theorem 3.2.1 are satisfied. Finally we will analyze the spectrum of the Jacobian associated matrix. Besides a local stability analysis and a classification of different types of attractors will be realized.

3.5 Inducing chaos in the Goodwin model

As we have seen in previous in Section 3.2 the desynchronization method depends on some parameters like the size of the blocks and the injection speed μ. However, in order to apply the method with success, it is necessary to determine the spectrum of the system. This is because the number of blocks that need to be constructed for inducing a Lorenz (4 blocks) or Shilnikov (2 blocks) type of chaos depend on whether the eigenvalues associated to the system are purely real or complex, respectively.

For that reason, in the rest of the chapter we focus on determining conditions between the parameters of the Goodwin model in order to obtain the transition from purely real to complex eigenvalues. In Proposition 3.5.1 we get a geometrical description for the transition in the case of a Goodwin model with linear degradation. Meanwhile, in Proposition 3.5.4 and under the same restrictions we get a numerical description of the transition.

3.5.1 Spectral analysis

Consider the Goodwin equation with negative feedback (3.4.1). The desynchronization method is different according to the nature of the less contracting eigenvalues, real or complex. This property depends on the parameters K_i and γ_i. Our objective is to analyze this dependency in

$$
(3.5.1) \qquad (G) = \begin{cases} \frac{d\lambda}{dt} &= g_{\mu,\delta}(\lambda, x, y, z) \\ \frac{dx}{dt} &= V_{\max} K_1 R_\lambda^-(z) - \gamma_1 x \\ \frac{dy}{dt} &= K_2 x - \gamma_2 y \\ \frac{dz}{dt} &= K_3 y - \gamma_3 z \end{cases}
$$

where μ and δ are constant parameters, which correspond to the first eigenvalue and the block diameter, respectively.

To begin the spectral analysis of the 4-dimensional vector field, we need to find all the eigenvalues of the previous system, and study the orbit structure in the neighborhood of the homoclinic orbits. In order to do that we will first compute the Jacobian matrix DG associated to the model (G). In our case DG has the following expression:

$$DG(\lambda_M, x_M) = \begin{pmatrix} \mu & 0 & 0 & 0 \\ K_1\frac{\partial R}{\partial \lambda} & -\gamma_1 & 0 & V_{\max}K_1\frac{\partial R}{\partial z} \\ 0 & K_2 & -\gamma_2 & 0 \\ 0 & 0 & K_3 & -\gamma_3 \end{pmatrix}$$

To continue with the analysis, we need to compute the characteristic polynomial $P(\alpha)$ associated to the Jacobian matrix $DG(\lambda_M, x_M)$,

$$P(\alpha) = det(DG - \alpha I) = (\alpha - \mu)\left[(-\gamma_1 - \alpha)(-\gamma_2 - \alpha)(-\gamma_3 - \alpha) + V_{\max}K_1K_2K_3\frac{\partial R}{\partial z}\right].$$

It is not complicated to see that $\alpha_1 = \mu > 0$ is the first real eigenvalue. The other three eigenvalues can be obtained as the solution of the following equation:

(3.5.2)
$$(\gamma_1 + \alpha)(\gamma_2 + \alpha)(\gamma_3 + \alpha) - V_{\max}K_1K_2K_3\frac{\partial R}{\partial z} = 0$$

whose expansion is

$$\alpha^3 + (\gamma_1 + \gamma_2 + \gamma_3)\alpha^2 + (\gamma_1\gamma_2 + \gamma_2\gamma_3 + \gamma_1\gamma_3)\alpha + \gamma_1\gamma_2\gamma_3 - K_1K_2K_3\frac{\partial R}{\partial z} = 0.$$

Geometrical solution of $P(\alpha)$:

Let us consider the following polynomial

$$Q(\alpha) = (\alpha + \gamma_1)(\alpha + \gamma_2)(\alpha + \gamma_3),$$

and the constant
$$C = V_{\max}K_1K_2K_3\frac{\partial R}{\partial z}.$$

The problem of finding the roots of the characteristic polynomial, $P(\alpha) = 0$, is equivalent to solve $Q(\alpha) = C$, which can be solved geometrically. In this direction, if we plot the polynomial $Q(\alpha)$ (Figure 3.8) we can observe two points where the function reaches its maximum α_1 and its minimum α_2.
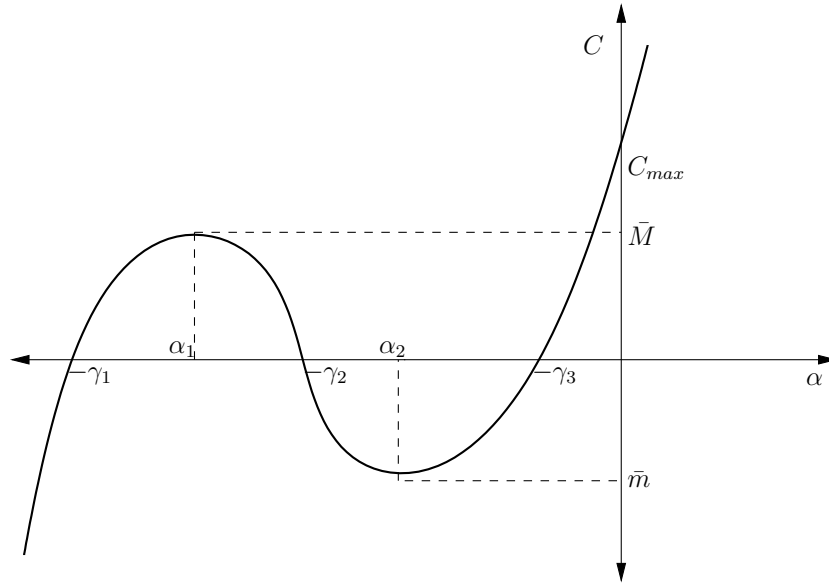
Figure 3.8: Plot of the polynomial $Q(\alpha)$.

Using the first derivative of $Q(\alpha)$

$$\frac{dQ(\alpha)}{d\alpha} = (\alpha + \gamma_2)(\alpha + \gamma_3) + (\alpha + \gamma_1)(\alpha + \gamma_3) + (\alpha + \gamma_1)(\alpha + \gamma_2),$$

we can show that

$$\alpha_1 = \frac{-(\gamma_1 + \gamma_2 + \gamma_3) - \sqrt{\gamma_1^2 + \gamma_2^2 + \gamma_3^2 - \gamma_1\gamma_2 - \gamma_1\gamma_3 - \gamma_2\gamma_3}}{3}$$

and

$$\alpha_2 = \frac{-(\gamma_1 + \gamma_2 + \gamma_3) + \sqrt{\gamma_1^2 + \gamma_2^2 + \gamma_3^2 - \gamma_1\gamma_2 - \gamma_1\gamma_3 - \gamma_2\gamma_3}}{3}.$$

If we evaluate both values α_1 and α_2 in $Q(\alpha)$ we get

$$Q(\alpha_1) = \frac{2}{27}b^3 - \frac{1}{9}b^2a - \frac{2}{27}b^2\sqrt{b^2 - ab + a^2} + \frac{2}{27}ab\sqrt{b^2 - ab + a^2} - \frac{1}{9}a^2b + \frac{2}{27}a^3 - \frac{2}{27}a^2\sqrt{b^2 - ab + a^2},$$

and

$$Q(\alpha_2) = \frac{2}{27}b^3 - \frac{1}{9}b^2a + \frac{2}{27}b^2\sqrt{b^2 - ab + a^2} - \frac{2}{27}ab\sqrt{b^2 - ab + a^2} - \frac{1}{9}a^2b + \frac{2}{27}a^3 + \frac{2}{27}a^2\sqrt{b^2 - ab + a^2}.$$

Since the expressions for α_1, α_2, $Q(\alpha_1)$ and $Q(\alpha_2)$ are not so simple, we have assumed some restrictions and simplifications in the form of the $\gamma's$. That is, we have assumed the following two cases:

- Constant degradation: $\gamma = \gamma_1 = \gamma_2 = \gamma_3$.

- Linear degradation: $\gamma_1 = \gamma$, $\gamma_2 = \gamma + a$ and $\gamma_3 = \gamma + b$.

In what follows we analyze the second case (linear degradation) because the first one can be deduced from it with $a = b = 0$. Hence, under the above assumption we can obtain the new values for α_1 and α_2,

$$\alpha_1 = \frac{-(3\gamma + a + b) - \sqrt{a^2 + b^2 - ab}}{3}$$

and

$$\alpha_2 = \frac{-(3\gamma + a + b) + \sqrt{a^2 + b^2 - ab}}{3},$$

implying that the values $\bar{M} = Q(\alpha_1)$ and $\bar{m} = Q(\alpha_2)$ are:

$$\bar{M} = \frac{2}{27}b^3 - \frac{1}{9}b^2a + \frac{2}{27}b^2\sqrt{b^2 - ab + a^2} - \frac{2}{27}ab\sqrt{b^2 - ab + a^2} - \frac{1}{9}a^2b + \frac{2}{27}a^3 + \frac{2}{27}a^2\sqrt{b^2 - ab + a^2}$$

and

$$\bar{m} = \frac{2}{27}b^3 - \frac{1}{9}b^2a - \frac{2}{27}b^2\sqrt{b^2 - ab + a^2} + \frac{2}{27}ab\sqrt{b^2 - ab + a^2} - \frac{1}{9}a^2b + \frac{2}{27}a^3 - \frac{2}{27}a^2\sqrt{b^2 - ab + a^2}.$$

Summarizing, we can obtain the following inequalities for the existence of complex and real solutions for $P(\alpha)$:

Proposition 3.5.1. *Assuming the case of linear degradation, the solutions of equation (3.5.2) can be classified in terms of $\bar{M}$ and $\bar{m}$ as follows:*

$$(3.5.3) \quad \begin{cases} \quad \text{if } \bar{m} < C < \bar{M} & P(\alpha) \text{ has 3 real eigenvalues} \\ \quad\quad \text{if } C < \bar{m} & P(\alpha) \text{ has 2 complex eigenvalues with maximal real part} \\ \text{if } \bar{M} < C < C_{max} & P(\alpha) \text{ has 1 real eigenvalue with maximal real part} \end{cases}$$

where $\bar{m} = Q(\alpha_2)$ and $\bar{M} = Q(\alpha_1)$ correspond to the minimum and maximum values of Q respectively, and $C_{max} = \gamma_1\gamma_2\gamma_3$ to the value $Q(0)$. Moreover, all these values can be computed as functions of γ_i and K_i.

Observation 3.5.2. *In the special case $\gamma_1 = \gamma_2 = \gamma_3$, we will obtain that the characteristic polynomial always has two complex eigenvalues, because the function $Q(\alpha)$ only has one zero, which at the same time corresponds to a zero for the derivative. On the other hand, the discriminant (term inside the square root) will always be non negative independently of the values of γ_i.*

Numerical solution of $P(\alpha)$:

Let us define the following constants: $B = (\gamma_1 + \gamma_2 + \gamma_3)$, $C = (\gamma_1\gamma_2 + \gamma_2\gamma_3 + \gamma_1\gamma_3)$ and $D = \gamma_1\gamma_2\gamma_3 - V_{\max}K_1K_2K_3\frac{\partial R}{\partial z}$. Using these constants we can obtain a new representation for the characteristic polynomial $P(\alpha)$:

$$(3.5.4) \qquad \alpha^3 + B\alpha^2 + C\alpha + D = 0.$$

Since the polynomial has three eigenvalues, we conclude that at least one of them need to be real. Hence, we can use numerical or exact methods in order to compute the other eigenvalues.

In order to solve numerically the above problem we use the Newton's method to find approximately one real eigenvalue with a method of localization to find the starting point of the iteration. As a result we can compute the value of $\alpha_2 \in \mathbb{R}$ and we can obtain a reduced polynomial depending on it:

$$\alpha^2 + (B + \alpha_2)\alpha + [C + (B + \alpha_2)\alpha_2] = 0$$

Now it is easy to compute the last two eigenvalues using the explicit formula for the second order polynomial. The problem is that we need the exact value because the method of desynchronization is so tie that any small change in the parameters propagates the error.

On the other hand, to find a relation between the parameters of the model and an exact formula for the eigenvalues is necessary. In general, it is not difficult to compute the solutions of a third degree polynomial. In first place, we need to define the following change of variables $\alpha = y + h$ in order to eliminate de quadratic term in (3.5.4). In our case, this is possible if we use $h = -B/3$, obtaining

$$y^3 + (C - \frac{B^2}{3})y - \frac{CB}{3} + \frac{2B^3}{27} + D = 0.$$

To continue with the reduction, we apply a second change of variables $y = u + v$ to find a new system of equations. Finally we obtain that the real root of the characteristic polynomial is given by the following expression:

$$(3.5.5) \qquad \alpha_2 = \frac{-B}{3} + \left(\frac{q - \sqrt{q^2 - 4(\frac{p}{3})^3}}{2} \right)^{1/3} + \frac{p}{3\left(\frac{q - \sqrt{q^2 - 4(\frac{p}{3})^3}}{2} \right)^{1/3}},$$

where $p = -(-B^2/3 + C)$ and $q = -(2B^3/27 - CB/3 + D)$ are deduced from the above exact method.

The last simplifications allow us to define the first discriminant Δ_1, that is,

$$\Delta_1 = q^2 - 4\left(\frac{p}{3}\right)^3.$$

It is not complicated to see that it is impossible for Δ_1 to be negative, because all the parameters in our model are positive. This implies that the restriction for the complex eigenvalues must be found in the following second degree polynomial:

$$\lambda^2 + (B + \alpha_2)\lambda + [C + (B + \alpha_2)\alpha_2],$$

which have the following roots:

(3.5.6)
$$\alpha_{3,4} = \frac{(B + \alpha_2) \pm \sqrt{\Delta_2}}{2},$$

where the expression for the second discriminant Δ_2 is given by

$$\Delta_2 = (B + \alpha_2)^2 - 4[C + (B + \alpha_2)\alpha_2].$$

At this point, it is important to note that unfortunately previous expressions for both Δ_1 and Δ_2 have different constants which make difficult a good choice for the parameters, specifically the transition between the purely real case and the complex case. For that reason, we have first obtained numerical and graphical results for the election of the definitive parameters in the model, as we can see in Figure 3.9.

Despite the last assertion about numerical results, we want to find an analytic expression that relates the parameters of the model with the nature of the complex or real eigenvalues (transition). In this direction, we have made some restrictions for the choice of the parameters, that is, we have sub-divided the study in two cases (as before):

- Constant degradation: $\gamma = \gamma_1 = \gamma_2 = \gamma_3$

- Linear degradation: $\gamma_1 = \gamma$, $\gamma_2 = \gamma + a$ and $\gamma_3 = \gamma + b$

It is only necessary to study the case of linear degradation (constant degradation can be deduced using $a = b = 0$). The following proposition established this simplification for the values of p and q introduced in equation (3.5.5).
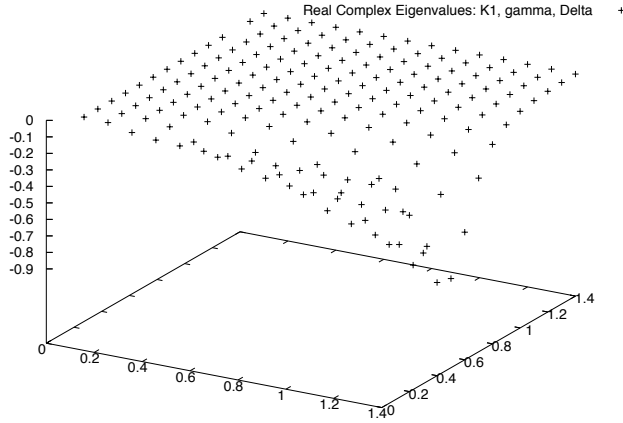
Figure 3.9: Transition of the discriminant versus constants K_i and γ_i.

Lemma 3.5.3. *Assuming the case of linear degradation we obtain that*

$$(3.5.7) \qquad p \;=\; \frac{(a+b)^2}{3} - ab \geq 0$$

$$(3.5.8) \qquad q \;=\; -\frac{(a+b)}{3}\frac{(2a-b)}{3}\frac{(a-2b)}{3} + V_{\max}K_1K_2K_3\frac{\partial R}{\partial z}$$

Proof. We first recall some previous notation: $B = (\gamma_1+\gamma_2+\gamma_3)$, $C = (\gamma_1\gamma_2+\gamma_2\gamma_3+\gamma_1\gamma_3)$ and $D = \gamma_1\gamma_2\gamma_3 - V_{\max}K_1K_2K_3\frac{\partial R}{\partial z}$ are the constants deduced from the characteristic polynomial $P(\alpha)$.

From these constants we can deduce the value of the parameters $p = -(-B^2/3 + C)$ and $q = -(2B^3/27 - CB/3 + D)$ from the explicit formula for third degree polynomial. In what follows we find a reduction for the values of p and q in the linear degradation case. We begin with the value of p:

$$
\begin{aligned}
p \;&=\; \frac{B^2}{3} - C \\[4pt]
&=\; \frac{(\gamma_1+\gamma_2+\gamma_3)^2 - 3(\gamma_1\gamma2+\gamma_2\gamma_3+\gamma_3\gamma_1)}{3} \\[4pt]
(3.5.9) \qquad &=\; \frac{(\gamma_1-\gamma_2)^2 + (\gamma_2-\gamma_3)^2 + (\gamma_3-\gamma_1)^2}{6},
\end{aligned}
$$

78

but since $\gamma_1 = \gamma$, $\gamma_2 = \gamma + a$ and $\gamma_3 = \gamma + b$, we have that

$$p = \frac{a^2 + (a-b)^2 + b^2}{6} = \frac{(a+b)^2}{3} - ab > 0,$$

whose value is zero in the case of constant degradation.

Now we find an expression for q:

$$
\begin{aligned}
q &= -\left(\frac{2B^3}{27} - \frac{BC}{3} + D\right) \\
&= \frac{-B}{3}\left(\frac{2B^2}{9} - C\right) - D \\
&= \frac{-B}{3}\left[-\gamma^2 - \frac{2\gamma}{3}(a+b) + \frac{2}{9}(a+b)^2 - ab\right] - D \\
&= -\left[\gamma + \frac{(a+b)}{3}\right]\left\{-[\gamma + \frac{(a+b)}{3}]^2 + \frac{(a^2 + b^2 - ab)}{3}\right\} - \gamma(\gamma^2 + \gamma(a+b) + ab) \\
&\quad + V_{\max}K_1K_2K_3\frac{\partial R}{\partial z} \\
(3.5.10) &= -2(\frac{a+b}{3})^3 + \frac{ab(a+b)}{3} + V_{\max}K_1K_2K_3\frac{\partial R}{\partial z}.
\end{aligned}
$$

So, from (3.5.10) we conclude that

$$q = -\frac{(a+b)}{3}\frac{(2a-b)}{3}\frac{(a-2b)}{3} + V_{\max}K_1K_2K_3\frac{\partial R}{\partial z},$$

where $\frac{\partial R}{\partial z} = -nz^{n-1}\lambda^n/(\lambda^n + z^n)^2 \leq 0$. □

From Lemma 3.5.3 we can conclude a simple formula for Δ_1 and Δ_2 in the case of constant degradation $(a = b = 0)$, because the value $p = 0$ gives us that $B^2 = 3C$, which implies that

$$\Delta_1 = (q)^2 = \left(V_{\max}K_1K_2K_3\frac{\partial R}{\partial z}\right)^2 \geq 0$$

To obtain a formula for the second discriminant we first need the value of α_2. It is not complicated to deduce using the previous information that

$$\alpha_2 = \frac{-B}{3} + (\frac{q}{2})^{1/3},$$

which allows us to compute the following expression for Δ_2

$$\begin{aligned}
\Delta_2 &= (B + \alpha_2)(B - 3\alpha_2) - 4C \\
&= -3(\frac{q}{2})^{2/3} \\
&= -3(\frac{(V_{\max} K_1 K_2 K_3 \frac{\partial R}{\partial z})}{2})^{2/3}.
\end{aligned}$$

(3.5.11)

As a consequence, in the case of constant degradation we typically have two complex eigenvalues. The unique possibility to be in the purely real case is $\frac{\partial R}{\partial z} = 0$, which is true when the value of $z \gg \lambda$ or $\lambda \gg z$.

In the case of linear degradation $(a, b \neq 0)$, we can obtain another equation between the parameters using the previous expressions for p and q. Moreover, we can deduce the sign of q, which will be greater than zero if $a \in (b/2, b)$ and $\gamma_i \geq K_i$. In this context, the following proposition shows the transition between purely real and complex eigenvalues.

Proposition 3.5.4. *For the parameters of degradation $\gamma, \gamma+a, \gamma+b$ and synthesis K_1, K_2, K_3, the inequalities for the sign of the discriminant have the following form:*

$$\Delta_1 \geq 0 \ \text{if} \ \left| 9 V_{\max} K_1 K_2 K_3 \frac{\partial R}{\partial z} \right| \geq (a + b) \left[(\frac{a}{\sqrt{2}} - \frac{b}{\sqrt{2}})^2 + a^2 + b^2 \right]$$

and

$$\Delta_2 \geq 0 \ \text{if} \ p \in \left[(15 - 6\sqrt{6})(\frac{q}{2})^{2/3}, (15 - 6\sqrt{6})(\frac{q}{2})^{2/3} \right].$$

Proof. First we solve de inequality for Δ_1. From the general formula we have that

$$\Delta_1 = q^2 - 4(\frac{p}{3})^3.$$

We need to find an expression for $\Delta_1 \geq 0$, then using the values of q and p we have

$$|q| \geq \frac{2}{3\sqrt{3}} (p)^{3/2}.$$

Solving in the case $a \in (b/2, b)$,

$$\frac{(a+b)}{3}\frac{(2a-b)}{3}\frac{a-2b}{3} + |V_{\max}K_1K_2K_3\frac{\partial R}{\partial z}| \geq \frac{2}{27}(a+b)^3$$

$$27|V_{\max}K_1K_2K_3\frac{\partial R}{\partial z}| \geq (a+b)\left[(a+b)^2 + (2a-b)(a-2b)\right]$$

$$9|V_{\max}K_1K_2K_3\frac{\partial R}{\partial z}| \geq (a+b)(a^2 - ab + b^2)$$

$$9|V_{\max}K_1K_2K_3\frac{\partial R}{\partial z}| \geq (a+b)\left[\left(\frac{a}{\sqrt{2}} - \frac{b}{\sqrt{2}}\right)^2 + \frac{a^2}{2} + \frac{b^2}{2}\right]$$

For the second inequality, $\Delta_2 \geq 0$, we can conclude

$$\Delta_2 = (B - 3\alpha_2)(B + \alpha) - 4C,$$

but in this case

$$\alpha_2 = \frac{-B}{3} + \left(\frac{q}{2}\right)^{1/3} + \frac{p}{3(\frac{q}{2})^{1/3}}.$$

So as we did in the other case, we can find the next expression,

$$
\begin{aligned}
\Delta_2 &= \frac{4}{3}B^2 - \left[\left(\frac{q}{2}\right)^{1/3} + \frac{p}{3(\frac{q}{2})^{1/3}}\right]^2 - 4C \\
&= 4p - \left[\left(\frac{q}{2}\right)^{1/3} + \frac{p}{3(\frac{q}{2})^{1/3}}\right]^2 \\
&= -\left[\frac{p}{3(\frac{q}{2})^{1/3}} - 5\left(\frac{q}{2}\right)^{1/3}\right]^2 + 24(\frac{q}{2})^{2/3}
\end{aligned}
$$

and the corresponding inequality is

$$4\left(\frac{q}{2}\right)^{2/3} \geq \left[\frac{p}{3(\frac{q}{2})^{1/3}} - 5\left(\frac{q}{2}\right)^{1/3}\right]^2.$$

Finally, we prove the relation

$$
\begin{aligned}
24\left(\frac{q}{2}\right)^{2/3} &\geq \left[\frac{p - 15(\frac{q}{2})^{2/3}}{3(\frac{q}{2})^{1/3}}\right]^2 \\
216\left(\frac{q}{2}\right)^{4/3} &\geq \left[p - 15\left(\frac{q}{2}\right)^{2/3}\right]^2 \\
6\sqrt{6}\left(\frac{q}{2}\right)^{2/3} &\geq |p - 15\left(\frac{q}{2}\right)^{2/3}|.
\end{aligned}
$$

Solving the inequality, we have

$$p \in \left[(15 - 6\sqrt{6}) \left(\frac{q}{2} \right)^{2/3}, (15 + 6\sqrt{6}) \left(\frac{q}{2} \right)^{2/3} \right].$$

$\square$

3.6 Stability condition: real eigenvalues in the Goodwin model

The study of homoclinic equations was begun by L.P. Shilnikov in a series of papers in the 60s ([S65], [S70],). However, the subject was largely left untouched in the West until the recent upsurgence of interest in the study of chaos [W88]. Most of the early work on the subject considered systems of ordinary differential equations of low dimension, proving results about homoclinic systems in $n = 2, 3$ dimensions.

The main idea behind the proofs of the classical theorems is the construction of a Poincaré return map on a suitable surface near the fixed point. This map is the composition of two components. Near to the fixed point, we assume that the behaviour is governed by the linearization of the system about the fixed point. Away from the fixed point, we only consider those trajectories that remain close to the homoclinic orbit (in both phase space and parameter space) and thus approximate this part of the map with an affine map near to the homoclinic orbit. We will not consider this in detail here, but the method used is extended to general ordinary differential equation systems (for more details see [W88]).

In this direction, in Section 3.4.1, using the Jacobian matrix deduced from the desynchronized Goodwin model, we found a condition between the model parameters to get four real eigenvalues: μ, which is the control parameter for the injection speed and the eigenvalue associated to the new differential equation, and $\alpha_2, \alpha_3, \alpha_4$, which are the other three real eigenvalues satisfying the first inequality in (3.5.3).

Here, we use these eigenvalues in order to analyze and characterize mathematically the stability of the desynchronized Goodwin model. For that reason, we will first show the construction of the Poincaré map. Later, we will explain some numerical results to corroborate the existence of chaos. Finally, we will study how to find a relation between the four real eigenvalues and the stable or unstable periodic orbits.
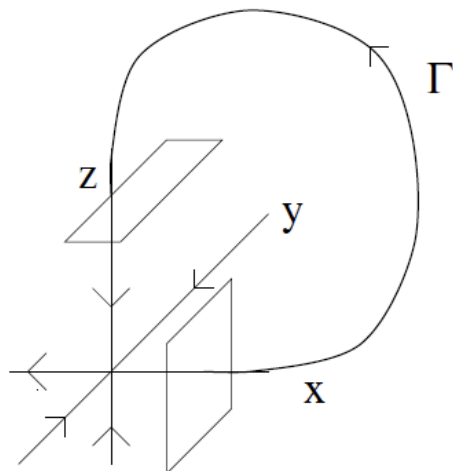
Figure 3.10: Homoclinic orbit associated to a saddle point, together with Poincaré surfaces.

3.6.1 Construction of the Poincaré map for the Goodwin model with real eigenvalues

In general, in the construction of the Poincaré map we can distinguish two cases for the analysis (the other cases can be obtained by translation and time reversal):

$$H1: \quad \mu, \alpha_4 > 0; \alpha_2, \alpha_3 < 0$$
$$H2: \quad \mu > 0; \alpha_2, \alpha_3, \alpha_4 < 0.$$

In this section we will work under hypothesis $H2$, because we need that the stable manifold lies outside the unstable manifold. However, all the main techniques work under both conditions and there only exist differences in the stability analysis conclusion.

Consider the linearized system of differential equation for the four real eigenvalues $\mu, \alpha_2, \alpha_3, \alpha_4$,

$$(3.6.1) \qquad \frac{dx}{dt} = \alpha_2 + f_2(\lambda, x, y, z; \nu)$$

$$(3.6.2) \qquad \frac{dy}{dt} = \alpha_3 + f_3(\lambda, x, y, z; \nu)$$

$$(3.6.3) \qquad \frac{dz}{dt} = \alpha_4 + f_4(\lambda, x, y, z; \nu)$$

$$(3.6.4) \qquad \frac{d\lambda}{dt} = \mu + f_1(\lambda, x, y, z; \nu),$$

where the functions f_i are C^2 and vanish along with their first derivative at the origin. The previous system has a fixed point at the origin with eigenvalues μ, α_2, α_3 and α_4. Moreover, we

can compute the exact solution from the above system, $\lambda(t) = \lambda_0 \exp(\mu t)$, $x(t) = x_0 \exp(\alpha_2 t)$ $y(t) = y_0 \exp(\alpha_3 t)$ and $z(t) = z_0 \exp(\alpha_4 t)$.

In general the analysis have the following steps: We set up the domains for the Poincaré map, then we compute P_0^L and P_1^L, and finally we examine the dynamics of $P^L = P_1^L \circ P_0^L$.
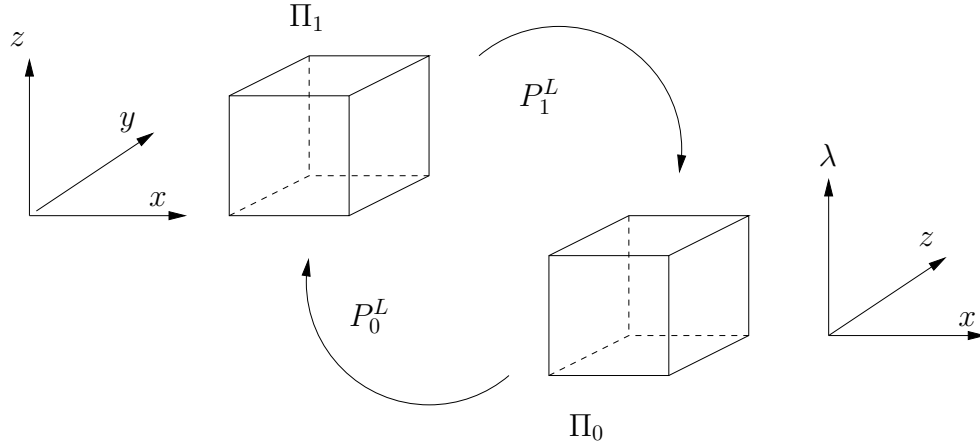
Figure 3.11: Construction of the Poincaré map $P^L = P_1^L \circ P_0^L$.

We define the two domains in which the functions P_0 and P_1 are constructed (see Figure 3.11):

$$(3.6.5) \qquad \Pi_0 \;=\; \{(\lambda, x, y, z) \in \mathbb{R}^4 / |x| \leq \epsilon, |z| \leq \epsilon, y = \epsilon, 0 < \lambda < \epsilon\}$$

$$(3.6.6) \qquad \Pi_1 \;=\; \{(\lambda, x, y, z) \in \mathbb{R}^4 / |x| \leq \epsilon, |y| \leq \epsilon, |z| \leq \epsilon, \lambda = \epsilon\}$$

The time of flight T from Π_o to Π_1 is given by the equation

$$\epsilon = \lambda_0 \exp(\mu t)$$

then we have that

$$T = \frac{1}{\mu} log(\frac{\epsilon}{\lambda_0}).$$

The first map that we construct is $P_0^L : \Pi_0 \to \Pi_1$ such that:

$$\begin{pmatrix} x \\ \epsilon \\ z \\ \lambda \end{pmatrix} \rightarrow \begin{pmatrix} x(\frac{\epsilon}{\lambda})^{\frac{\alpha_2}{\mu}} \\ \epsilon(\frac{\epsilon}{\lambda})^{\frac{\alpha_3}{\mu}} \\ z(\frac{\epsilon}{\lambda})^{\frac{\alpha_4}{\mu}} \\ \epsilon \end{pmatrix}$$

where we replace the value of the time by T to obtain the second expression.

3.6. STABILITY CONDITION: REAL EIGENVALUES IN THE GOODWIN MODEL

From Section 3.2a in [W88], and the definition of Π_1 on some open set $U \subset \Pi_1$, we compute the map $P_1^L : U \subset \Pi_1 \to \Pi_0$ in the following way:

$$
\begin{pmatrix} x \\ y \\ z \\ \epsilon \end{pmatrix} \rightarrow
\begin{pmatrix} 0 \\ 0 \\ 0 \\ \epsilon \end{pmatrix} +
\begin{pmatrix} a & b & c & 0 \\ 0 & 0 & 0 & 0 \\ d & e & f & 0 \\ g & h & i & 0 \end{pmatrix}
\begin{pmatrix} x \\ y \\ z \\ 0 \end{pmatrix} +
\begin{pmatrix} j\nu \\ 0 \\ k\nu \\ l\nu \end{pmatrix}.
$$

where all the variables in the matrix are real constants and ν is the parameter of control.

Finally the Poincaré map defined by $P^L = P_1^L \circ P_0^L : V \subset \Pi_0 \to \Pi_0$ is obtained:

$$
\begin{pmatrix} x \\ z \\ \lambda \end{pmatrix} \rightarrow
\begin{pmatrix}
ax(\frac{\epsilon}{\lambda})^{\frac{\alpha_2}{\mu}} + b\epsilon(\frac{\epsilon}{\lambda})^{\frac{\alpha_3}{\mu}} + cz(\frac{\epsilon}{\lambda})^{\frac{\alpha_4}{\mu}} + i\nu \\
dx(\frac{\epsilon}{\lambda})^{\frac{\alpha_2}{\mu}} + e\epsilon(\frac{\epsilon}{\lambda})^{\frac{\alpha_3}{\mu}} + fz(\frac{\epsilon}{\lambda})^{\frac{\alpha_4}{\mu}} + k\nu \\
gx(\frac{\epsilon}{\lambda})^{\frac{\alpha_2}{\mu}} + h\epsilon(\frac{\epsilon}{\lambda})^{\frac{\alpha_3}{\mu}} + iz(\frac{\epsilon}{\lambda})^{\frac{\alpha_4}{\mu}} + \nu
\end{pmatrix},
$$

where $V = (P_0^L)^{-1}(U)$.

To simplify the system we define the following new variables:

$$
\begin{aligned}
A &= a(\tfrac{\epsilon}{\lambda})^{\frac{\alpha_2}{\mu}}, & B &= b(\tfrac{\epsilon}{\lambda})^{\frac{\alpha_3}{\mu}+1}, & C &= x(\tfrac{\epsilon}{\lambda})^{\frac{\alpha_4}{\mu}}, \\
D &= d(\tfrac{\epsilon}{\lambda})^{\frac{\alpha_2}{\mu}}, & E &= e(\tfrac{\epsilon}{\lambda})^{\frac{\alpha_3}{\mu}+1}, & F &= f(\tfrac{\epsilon}{\lambda})^{\frac{\alpha_4}{\mu}}, \\
G &= x(\tfrac{\epsilon}{\lambda})^{\frac{\alpha_2}{\mu}}, & H &= h(\tfrac{\epsilon}{\lambda})^{\frac{\alpha_3}{\mu}+1}, & I &= i(\tfrac{\epsilon}{\lambda})^{\frac{\alpha_4}{\mu}}.
\end{aligned}
$$

As a result, we have now a new reduced system of equations with three variables,

$$
\begin{aligned}
x &= Ax\lambda^{\frac{|\alpha_2|}{\mu}} + B\lambda^{\frac{|\alpha_3|}{\mu}} + Cz\lambda^{\frac{|\alpha_4|}{\mu}} + i\nu \\
z &= Dx\lambda^{\frac{|\alpha_2|}{\mu}} + E\lambda^{\frac{|\alpha_3|}{\mu}} + Fz\lambda^{\frac{|\alpha_4|}{\mu}} + k\nu \\
\lambda &= Gx\lambda^{\frac{|\alpha_2|}{\mu}} + H\lambda^{\frac{|\alpha_3|}{\mu}} + Iz\lambda^{\frac{|\alpha_4|}{\mu}} + \nu
\end{aligned}
$$

and it is possible to find the solution as a function of ν, with some restrictions over the parameters.

In the rest of the section we assume that the value of λ is small (close to the origin). We first solve the equations and find the singular points for P^L,

$$
(3.6.7) \qquad x = \frac{B\lambda^{\frac{|\alpha_3|}{\mu}} + Cz\lambda^{|\alpha_4|}\mu + i\nu}{1 - A\lambda|\alpha_2|\mu}.
$$

We assume that λ is small enough such that the denominator in (3.6.7) is one,

$$(3.6.8) \qquad z = \frac{DB\lambda^{\frac{|\alpha_2+\alpha_3|}{\mu}} + Di\nu\lambda^{\frac{|\alpha_2|}{\mu}} + E\lambda^{|\alpha_3|}\mu + k\nu}{1 - DC\lambda^{\frac{|\alpha_4|}{\mu}} - F\lambda|\alpha_4|\mu}.$$

Again we assume that the value of λ is small enough such that the denominator in (3.6.8) can be taken to be 1. Finally we can obtain a fixed point expression in terms of λ for the equation (3.6.7), replacing the previous values of x and z.

$$
\begin{aligned}
\lambda - \mu \;=\; & G\left[B\lambda^{\frac{|\alpha_3|}{\mu}} + C(DB\lambda^{\frac{|\alpha_2+\alpha_3|}{\mu}} + Di\nu\lambda^{\frac{|\alpha_2|}{\mu}} + E\lambda^{|\alpha_3|}\mu + k\nu)\lambda^{\frac{|\alpha_4|}{\mu}} + i\nu\right]\lambda^{\frac{|\alpha_2|}{\mu}} \\
(3.6.9) \qquad & + H\lambda^{\frac{|\alpha_3|}{\mu}} + I\left[DB\lambda^{\frac{|\alpha_2+\alpha_3|}{\mu}} + Di\nu\lambda^{\frac{|\alpha_2|}{\mu}} + E\lambda^{|\alpha_3|}\mu + k\nu\right]\lambda^{\frac{|\alpha_4|}{\mu}} \quad (\star)
\end{aligned}
$$

Graphically we can show the solutions of (3.6.9) for μ sufficiently small and near zero. In contrast, for the analytic analysis we need to examine the slope of the right hand side of (3.6.9) at $\lambda = 0$, which is given by the expression:

$$
\begin{aligned}
\frac{d(\star)}{d\lambda} \;=\; & GB\frac{2|\alpha_2|}{\mu}\lambda^{\frac{2|\alpha_2|}{\mu}-1} + GCBD\frac{|2\alpha_2+\alpha_3+\alpha_4|}{\mu}\lambda^{\frac{|2\alpha_2+\alpha_3+\alpha_4|}{\mu}-1} + GCDi\nu\frac{|2\alpha_3+\alpha_4|}{\mu}\lambda^{\frac{|2\alpha_3+\alpha_4|}{\mu}-1} \\
& + GEC\frac{|\alpha_2+\alpha_3+\alpha_4|}{\mu}\lambda^{\frac{|\alpha_2+\alpha_3+\alpha_4|}{\mu}-1} + GCk\nu\frac{|\alpha_2+\alpha_4|}{\mu}\lambda^{\frac{|\alpha_2+\alpha_4|}{\mu}-1} + Gi\nu\frac{|\alpha_2|}{\mu}\lambda^{\frac{|\alpha_2|}{\mu}-1} \\
& + H\frac{|\alpha_3|}{\mu}\lambda^{\frac{|\alpha_3|}{\mu}-1} + IBD\frac{|\alpha_2+\alpha_3+\alpha_4|}{\mu}\lambda^{\frac{|\alpha_2+\alpha_3+\alpha_4|}{\mu}-1} + IDi\nu\frac{|\alpha_2+\alpha_4|}{\mu}\lambda^{\frac{|\alpha_2+\alpha_4|}{\mu}-1} \\
& (3.6.10) E\frac{|\alpha_3+\alpha_4|}{\mu}\lambda^{\frac{|\alpha_3+\alpha_4|}{\mu}-1} + Ik\nu\frac{|\alpha_4|}{\mu}\lambda^{\frac{|\alpha_4|}{\mu}-1}.
\end{aligned}
$$

We know that P_1^L is invertible so that the determinant is different from zero, i.e., $I(AE - BD) + G(BF - CE) + H(CD - AF) \neq 0$. This implies that I, G and H cannot be all three equal to zero. Therefore, at $\lambda = 0$, (3.6.10) takes the values:

$$\frac{d(\star)}{d\lambda} = \begin{cases} 0 & \text{if } 2|\alpha_2| > \mu,\ |\alpha_3| > \mu \text{ and } |\alpha_4| > \mu \\ \infty & \text{if } 2|\alpha_2| < \mu \text{ or } |\alpha_3| < \mu \text{ or } |\alpha_4| < \mu \end{cases}$$

3.6.2 Existence of chaos: computational results for Goodwin model

We first show the results for the simulation in the "real" case (model with real eigenvalues) using the algorithm of desynchronization, as we can see in Figure 3.12. In the first plot we can see the homoclinic orbits between the four blocks, in a 2D view, meanwhile in the second plot we have the 3D representation. We have chosen λ, x and z as variables.

The parameters used in the simulation are the following: $n = 4$, $\mu = 20$, $\epsilon = 0.03$, $\delta = 0.006$, $l = 0.02$, $a = b = 0.25$, $K_1 = K_2 = K_3 = 0.32$, and $\gamma_1 = 0.17$, $\gamma_2 = 0.18$, $\gamma_3 = 0.19$.

An easy way to observe and measure the effect of chaos in the Poincaré map is realizing perturbations on the initial conditions. That is, inside a ball of size ϵ choose different points describing different orbits. In Table 3.1 we can see that small differences on the initial conditions create different trajectories for the homoclinic orbits.

Since we are in the real case and we have four blocks, in two different quadrants, we can describe all the trajectories by a code where 0 (resp. 1) means that we are in the first (resp. second) part. Differences in the code imply different trajectories, being a numerical proof for the existence of Chaos of Lorenz type. Here we show the graphical results in Figure 3.13.

We have chosen three different but close starting points to show the chaotic effect. In the graph we can see three curves with different transitions between the block, so as a consequence of the chaos we have sensitivity. It is the same if we show the code generated by the orbits.

Code	x value	y value	z value
001101	1.15501	5.85506	19.5635
001010	1.16001	5.86006	19.5685
001010	1.16501	5.86506	19.5735
001010	1.17001	5.87006	19.5785
00100100	1.17501	5.87506	19.5835
01001001	1.18001	5.88006	19.5885
01001001	1.18501	5.88506	19.5835

Table 3.1: Code $0, 1$ describing different trajectories for x, y, z perturbed starting points

Finally, the geometry of the Poincaré map and the Möbius effect can be seen in Figure 3.14. In the simulation we can see numerical results about the structural stability of the chaotic orbit. In fact, in the second plot we can see how the cube is deformed by the effect of the homoclinic orbit, in this case the torsion is a consequence of the Möbius strip.
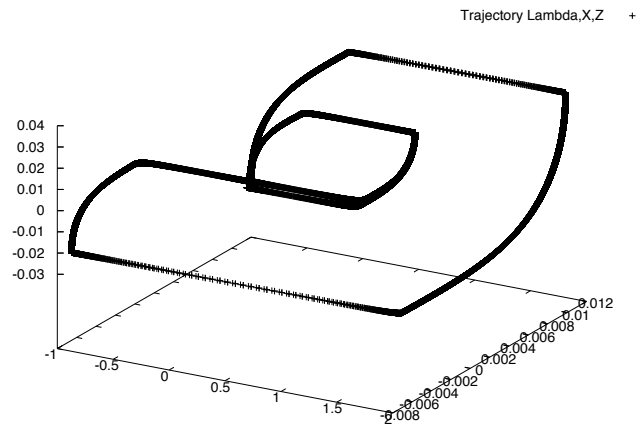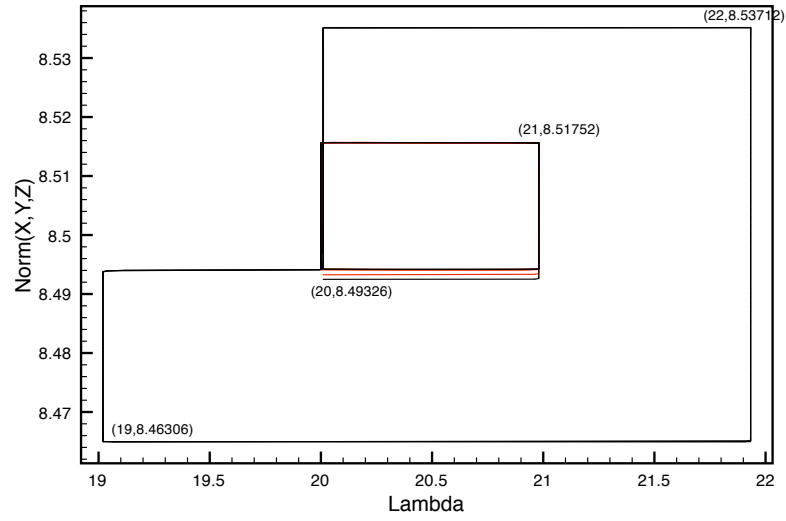
Figure 3.12: Real Case: Orbits generated by the program for the desynchronization of Goodwin model with 4 blocks.
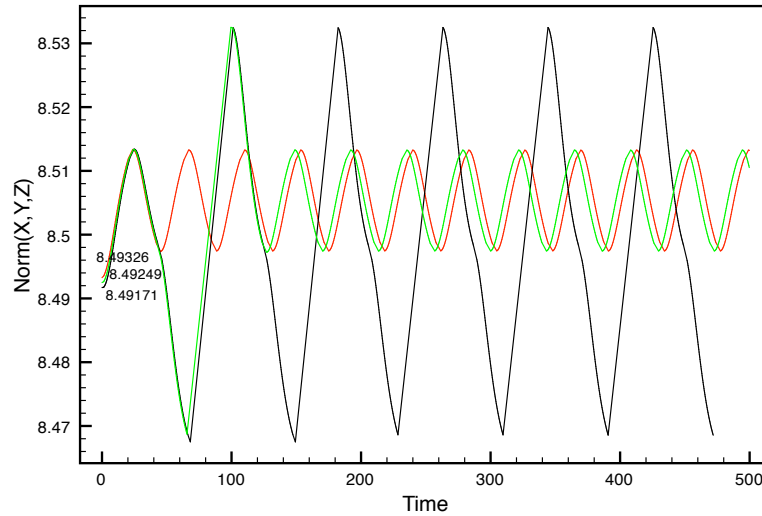
Figure 3.13: Sensitivity to the initial conditions, chaos in the real case

3.6.3 Stability analysis of the periodic orbits for the Goodwin model

At this point, we have information about the Poincaré map and some computational simulations reenforcing the idea of chaotic behavior of the synchronized Goodwin model. For that reason in this section we analyze the stability of the periodic orbits. We start by the construction of the Jacobian matrix related to the Poincaré map P^L.

From equation (3.6.7) we can obtain the values for the following Jacobian matrix:

$$(3.6.11) \qquad DP^L = \begin{pmatrix} A\lambda^{\frac{|\alpha_2|}{\mu}} & C\lambda^{\frac{|\alpha_4|}{\mu}} & Ax\frac{|\alpha_2|}{\mu}\lambda^{\frac{|\alpha_2|}{\mu}-1} + B\frac{|\alpha_3|}{\mu}\lambda^{\frac{|\alpha_3|}{\mu}-1} + Cz\frac{|\alpha_4|}{\mu}\lambda^{\frac{|\alpha_4|}{\mu}-1} \\ D\lambda^{\frac{|\alpha_2|}{\mu}} & F\lambda^{\frac{|\alpha_4|}{\mu}} & Dx\frac{|\alpha_2|}{\mu}\lambda^{\frac{|\alpha_2|}{\mu}-1} + E\frac{|\alpha_3|}{\mu}\lambda^{\frac{|\alpha_3|}{\mu}-1} + Fz\frac{|\alpha_4|}{\mu}\lambda^{\frac{|\alpha_4|}{\mu}-1} \\ G\lambda^{\frac{|\alpha_2|}{\mu}} & I\lambda^{\frac{|\alpha_4|}{\mu}} & Gx\frac{|\alpha_2|}{\mu}\lambda^{\frac{|\alpha_2|}{\mu}-1} + H\frac{|\alpha_3|}{\mu}\lambda^{\frac{|\alpha_3|}{\mu}-1} + Iz\frac{|\alpha_4|}{\mu}\lambda^{\frac{|\alpha_4|}{\mu}-1} \end{pmatrix}$$

The stability is determined by considering the nature of the eigenvalues of DP^L. First we compute the characteristic polynomial $P(\gamma)$:

$$det(DP^L - \gamma I).$$

Solving the equation for γ we obtain the following polynomial:

$$P(\gamma) = -\gamma^3 + tr(DP^L)\gamma^2 - [ae + ai + ei + hf + db + gc]\gamma + det(DP^L) = 0.$$
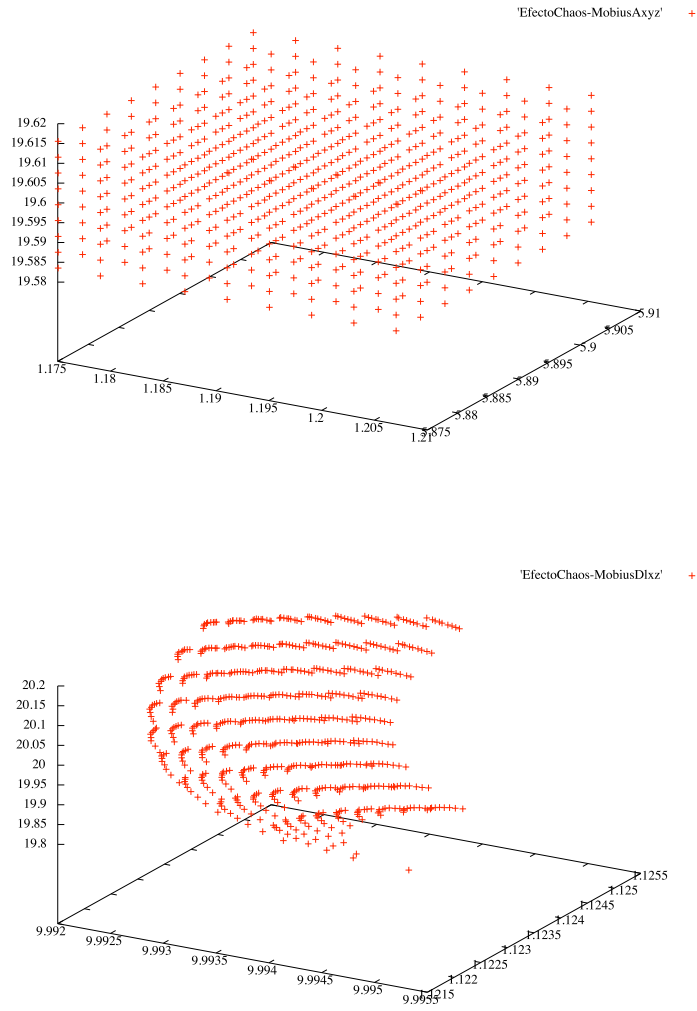
Figure 3.14: First return map for the Goodwin model with real eigenvalues.

3.6. STABILITY CONDITION: REAL EIGENVALUES IN THE GOODWIN MODEL

We want to find the solutions γ of the previous equation or at least a formula that governs the size of the solutions depending on λ and the eigenvalues. For that reason we compute the discriminant of the polynomial. It is known that if the polynomial has the form $p(x) = ax^3 + bx^2 + cx + d$, then the discriminant will be:

$$\Delta = b^2c^2 - 4ac^3 - 4b^2d - 27a^2d^2 + 18abcd.$$

In our case, if we use the previous formula we can deduce that the discriminant is

$$\Delta = tr(DP^L)^2\mathcal{C} - 4\mathcal{C}^3 - 4tr(DP^L)^2det(DP^L) - 27det(DP^L)^2 + 18\mathcal{C}tr(DP^L)det(DP^L)$$

where $\mathcal{C} = ae + ai + ei + hf + db + gc$, $tr(\cdot)$ is the trace function of a matrix and $det(\cdot)$ is the determinant.

We need to compute the expression for $tr(DP^L)$ and $det(DP^L)$, using the matrix (3.6.11) and the values for x (3.6.7) and z (3.6.8):

$$
\begin{aligned}
tr(DP^L) \;=\;& A\lambda^{\frac{|\alpha_2|}{\mu}} + F\lambda^{\frac{|\alpha_4|}{\mu}} + G\frac{|\alpha_2|}{\mu}\left[B\lambda^{\frac{|\alpha_2+\alpha_3|}{\mu}-1} + CDi\nu\lambda^{\frac{|2\alpha_2+\alpha_4|}{\mu}-1} + CE\lambda^{\frac{|\alpha_2+\alpha_3+\alpha_4|}{\mu}-1}\right. \\
&+\; Ck\nu\lambda^{\frac{|\alpha_2+\alpha_4|}{\mu}-1} + i\nu\lambda^{\frac{|\alpha_2|}{\mu}-1}\bigg] + H\frac{|\alpha_3|}{\mu}\lambda^{\frac{|\alpha_3|}{\mu}-1} + I\frac{|\alpha_4|}{\mu}\left[DB\lambda^{\frac{|\alpha_2+\alpha_3+\alpha_4|}{\mu}-1}\right. \\
&+\; Di\nu\lambda^{\frac{|\alpha_2+\alpha_4|}{\mu}-1} + E\lambda^{\frac{|\alpha_3+\alpha_4|}{\mu}-1} + k\nu\lambda^{\frac{|\alpha_4|}{\mu}-1}\bigg].
\end{aligned}
$$

(3.6.12)

For the matrix determinant, it is easy to see that, no matter the value of the constants, the final expression is equivalent to

$$
\begin{aligned}
det(DP^L) \;=\;& AFG\frac{|\alpha_2|}{\mu}\left[B\lambda^{\frac{|2\alpha_2+\alpha_3+\alpha_4|}{\mu}-1} + BCD\lambda^{\frac{|3\alpha_2+\alpha_3+2\alpha_4|}{\mu}-1} + CDi\nu\lambda^{\frac{|3\alpha_2+2\alpha_4|}{\mu}-1}\right. \\
&+\; CE\lambda^{\frac{|2\alpha_2+\alpha_3+2\alpha_4|}{\mu}-1} + Ck\nu\lambda^{\frac{|2\alpha_2+2\alpha_4|}{\mu}-1} + i\nu\lambda^{\frac{|2\alpha_2+\alpha_4|}{\mu}-1}\bigg] + AFH\frac{|\alpha_3|}{\mu}\lambda^{\frac{|\alpha_2+\alpha_3+\alpha_4|}{\mu}-1} \\
&+\; AFI\frac{|\alpha_4|}{\mu}\left[BD\lambda^{\frac{|2\alpha_2+\alpha_3+2\alpha_4|}{\mu}-1} + Di\nu\lambda^{\frac{|2\alpha_2+2\alpha_4|}{\mu}-1} + E\lambda^{\frac{|\alpha_2+\alpha_3+2\alpha_4|}{\mu}-1}\right. \\
&+\; k\nu\lambda^{\frac{|\alpha_2+2\alpha_4|}{\mu}-1}\bigg].
\end{aligned}
$$

(3.6.13)

Using equations (3.6.12) and (3.6.13), we can do the analysis for the size of the trace and the determinant, when λ is small. In general, we can find different inequalities for the

eigenvalues if we know the values of the exponents.

$$tr(DP^L) = \begin{cases} \text{small} & |\alpha_2| > \mu \wedge |\alpha_3| > \mu \wedge |\alpha_4| > \mu \\ \text{large} & |2\alpha_2 + \alpha_3 + \alpha_4| < \mu. \end{cases}$$

and

$$det(DP^L) = \begin{cases} \text{small} & |\alpha_2 + \alpha_3 + \alpha_4| > \mu \\ \text{large} & |3\alpha_2 + \alpha_3 + 2\alpha_4| < \mu. \end{cases}$$

In resume, we have the following result for the stability of periodic orbits in the desynchronized Goodwin model with real eigenvalues.

Theorem 3.6.1. *In the desynchronized Goodwin model with real eigenvalues μ, α_2, α_3 and α_4, and under the hypothesis $H2$. When the value of λ is small enough we can conclude that the eigenvalues can be made arbitrarily small or large, so the singular point in the Poincaré map can be of three different forms:*
Sink: if $|\alpha_2| > \mu, |\alpha_3| > \mu, |\alpha_4| > \mu$.
Saddle: if $|\alpha_2| + |\alpha_3| + |\alpha_4| > \mu$ and $|2\alpha_2| + |\alpha_3| + |\alpha_4| < \mu$.
Source: if $|3\alpha_2| + |\alpha_3| + |2\alpha_4| < \mu$.

3.7 Stability condition: complex eigenvalues in the Goodwin model

In the last section we have studied stability conditions in the Goodwin model with purely real eigenvalues. However, we know that for a certain range in the parameters there exist complex eigenvalues, more specifically two purely complex and two real. That is, using the equations of the desynchronized Goodwin model we can deduce the Jacobian matrix, and from this matrix we can obtain four eigenvalues, in our case denoted by $\mu, \alpha_2 \in \mathbb{R}$ and $\rho \pm iw \in \mathbb{C}$.

As before, here we develop the mathematical analysis of the complex desynchronized Goodwin model. For that reason, we will first show the construction of the Poincaré map. Later, we will explain some numerical results to corroborate the existence of chaos. Finally, we will study how to find a relation between the complex eigenvalues and the stable or unstable periodic orbits.

3.7.1 Construction of the Poincaré map for the Goodwin model with complex eigenvalues

Consider the following linearized system of differential equations:

$$
(3.7.1) \qquad \frac{dx}{dt} = \rho x - wy + f_1(\lambda, x, y, z; \nu)
$$

$$
(3.7.2) \qquad \frac{dy}{dt} = wx + \rho y + f_2(\lambda, x, y, z; \nu)
$$

$$
(3.7.3) \qquad \frac{dz}{dt} = \alpha_2 + f_3(\lambda, x, y, z; \nu)
$$

$$
(3.7.4) \qquad \frac{d\lambda}{dt} = \mu + f_4(\lambda, x, y, z; \nu)
$$

where the functions f_i are C^2 and vanish along with their first derivative at the origin. Here $(\lambda, x, y, z) = (0, 0, 0, 0)$ is an hyperbolic fixed point with the eigenvalues of the vector field linearized about the origin, hence, the origin has a three dimensional stable manifold and one dimensional unstable manifold. Additionally, we make the following assumptions,

$$
H1: \qquad \mu, \alpha_2 > 0; \rho < 0; w \neq 0.
$$
$$
H2: \quad \mu > 0; \alpha_2, \rho < 0; w \neq 0; \mu > -\rho > 0.
$$

In the rest of the section we will work under the hypothesis $H2$, and the additional condition $\rho > \alpha_2$. Because, we need that the stable manifold lies outside the unstable manifold.

As we did before in the real case, we first define the sets Π_0 and Π_1

$$
(3.7.5) \quad \Pi_0 = \{(\lambda, x, y, z) \in \mathbb{R}^4 / \epsilon \exp(\frac{2\pi\rho}{w}) \leq x \leq \epsilon, |z| \leq \epsilon, y = 0, 0 < \lambda < \epsilon\}
$$
$$
(3.7.6) \quad \Pi_1 = \{(\lambda, x, y, z) \in \mathbb{R}^4 / \lambda = \epsilon\}
$$

The linearized flow generated by the solution is given by:

$$
\begin{aligned}
x(t) &= \exp(\rho t)(x_0 coswt - y_0 senwt) \\
y(t) &= \exp(\rho t)(x_0 senwt + y_0 coswt) \\
z(t) &= z_0 \exp(\alpha_2 t) \\
\lambda(t) &= \lambda_0 \exp(\mu t).
\end{aligned}
$$

The time of flight T from Π_o to Π_1 is found solving the equation

$$
\epsilon = \lambda_0 \exp(\mu t)
$$

then we have that

$$T = \frac{1}{\mu} log(\frac{\epsilon}{\lambda_0}).$$

We need to compute the Poincaré function P^L in the complex case and we need to compute P_0^L and P_1^L. First $P_0^L : \Pi_0 \to \Pi_1$ is defined by

$$
\begin{pmatrix} x \\ 0 \\ z \\ \lambda \end{pmatrix} \to \begin{pmatrix} x(\frac{\epsilon}{\lambda})^{\frac{\rho}{\mu}} cos(\frac{w}{\mu} ln(\frac{\epsilon}{\lambda})) \\ x(\frac{\epsilon}{\lambda})^{\frac{\rho}{\mu}} sin(\frac{w}{\mu} ln(\frac{\epsilon}{\lambda})) \\ z(\frac{\epsilon}{\lambda})^{\frac{\alpha_2}{\mu}} \\ \epsilon \end{pmatrix}.
$$

Now we make the computation of $P_1^L : \Pi_1 \to \Pi_0$

$$
\begin{pmatrix} x \\ y \\ z \\ \epsilon \end{pmatrix} \to \begin{pmatrix} a & b & c & 0 \\ d & e & f & 0 \\ g & h & i & 0 \\ 0 & 0 & 0 & 0 \end{pmatrix} \begin{pmatrix} x \\ y \\ z \\ 0 \end{pmatrix} + \begin{pmatrix} \bar{x} \\ 0 \\ 0 \\ 0 \end{pmatrix}
$$

where $\bar{x} = \epsilon(1 + \exp(2\pi\rho))/2$.

With the previous information we obtain the map P^L defined as the composition of the other two, i.e. $P^L = P_1^L \circ P_0^L : V \subset \Pi_0 \to \Pi_0$.

$$
\begin{pmatrix} x \\ z \\ \lambda \end{pmatrix} \to \begin{pmatrix} ax(\frac{\epsilon}{\lambda})^{\frac{\rho}{\mu}} cos(\frac{w}{\mu} ln\frac{\epsilon}{\lambda}) + bx(\frac{\epsilon}{\lambda})^{\frac{\rho}{\mu}} sin(\frac{w}{\mu} ln\frac{\epsilon}{\lambda}) + cz(\frac{\epsilon}{\lambda})^{\frac{\alpha_2}{\mu}} + \bar{x} \\ dx(\frac{\epsilon}{\lambda})^{\frac{\rho}{\mu}} cos(\frac{w}{\mu} ln\frac{\epsilon}{\lambda}) + ex(\frac{\epsilon}{\lambda})^{\frac{\rho}{\mu}} sin(\frac{w}{\mu} ln\frac{\epsilon}{\lambda}) + fz(\frac{\epsilon}{\lambda})^{\frac{\alpha_2}{\mu}} \\ gx(\frac{\epsilon}{\lambda})^{\frac{\rho}{\mu}} cos(\frac{w}{\mu} ln\frac{\epsilon}{\lambda}) + hx(\frac{\epsilon}{\lambda})^{\frac{\rho}{\mu}} sin(\frac{w}{\mu} ln\frac{\epsilon}{\lambda}) + iz(\frac{\epsilon}{\lambda})^{\frac{\alpha_2}{\mu}} \end{pmatrix}.
$$

In order to study the trajectories of the Poincaré map, it is necessary to solve the equations in (3.7.1). However, it is not hard to see that the system is unsolvable, so we need to realize a simplification to study another equivalent problem.

To begin we first make a simplification such that the term $sin(\cdot)$ is eliminated. Additionally, we introduce a control variable ν and constants j, k,

$$
\begin{pmatrix} x \\ z \\ \lambda \end{pmatrix} \to \begin{pmatrix} x(\frac{\epsilon}{\lambda})^{\frac{\rho}{\mu}} pcos(\frac{w}{\mu} ln\frac{\epsilon}{\lambda} + \phi_1) + cz(\frac{\epsilon}{\lambda})^{\frac{\alpha_2}{\mu}} + j\nu + x_0 \\ x(\frac{\epsilon}{\lambda})^{\frac{\rho}{\mu}} qcos(\frac{w}{\mu} ln\frac{\epsilon}{\lambda} + \phi_2) + fz(\frac{\epsilon}{\lambda})^{\frac{\alpha_2}{\mu}} + k\nu \\ x(\frac{\epsilon}{\lambda})^{\frac{\rho}{\mu}} rcos(\frac{w}{\mu} ln\frac{\epsilon}{\lambda} + \phi_3) + iz(\frac{\epsilon}{\lambda})^{\frac{\alpha_2}{\mu}} + \nu \end{pmatrix}.
$$

Defining new variables we can obtain a second simplification

$$
\begin{aligned}
\delta &= \frac{-\rho}{\mu}; \gamma = \frac{-\alpha_2}{\mu}; \xi = \frac{-w}{\mu} \\
\alpha &= p\epsilon^{-\delta}; \bar{\alpha} = c\epsilon^{-\gamma} \\
\beta &= q\epsilon^{-\delta}; \bar{\beta} = f\epsilon^{-\gamma} \\
\zeta &= r\epsilon^{-\delta}; \bar{\zeta} = i\epsilon^{-\gamma} \\
\Phi_i &= \frac{w}{\mu} ln\epsilon + \phi_i.
\end{aligned}
$$

So finally the Poincaré map can be defined as:

$$
\begin{pmatrix} x \\ z \\ \lambda \end{pmatrix} \rightarrow \begin{pmatrix} \alpha x \lambda^\delta cos(\xi ln\lambda + \Phi_1) + \bar{\alpha}z\lambda^\gamma + j\nu + x_0 \\ \beta x \lambda^\delta cos(\xi ln\lambda + \Phi_2) + \bar{\beta}z\lambda^\gamma + k\nu \\ \zeta x \lambda^\delta cos(\xi ln\lambda + \Phi_3) + \bar{\zeta}z\lambda^\gamma + \nu \end{pmatrix}
$$

The next step is to compute the singular points of the Poincaré map. We start by calculating the variables x, z and λ in the equation (3.7.1).

$$
x = \frac{\bar{\alpha}z\lambda^\gamma + j\nu + x_0}{1 - \alpha\lambda^\delta}cos(\xi ln\lambda + \Phi_1).
$$

Since λ is small enough as we want, then the denominator is 1,

$$
z = \frac{\beta(j\nu + x_0)\lambda^\delta cos(\xi ln\lambda + \Phi_2) + k\nu}{1 - \beta\bar{\alpha}\lambda^{\delta+\gamma} - \bar{\beta}\lambda^\gamma}.
$$

Again assuming the simplification the denominator is 1, and we get

$$
\begin{aligned}
\lambda &= \zeta[\bar{\alpha}(\beta(j\nu + x_0)\lambda^\delta cos(\xi ln\lambda + \Phi_2) + k\nu)\lambda^\gamma + j\nu + x_0)\lambda^\delta cos(\xi ln\lambda + \Phi_3)] \\
&+ \bar{\zeta}[\beta(j\nu + x_0)\lambda^\delta cos(\xi ln\lambda + \Phi_2) + k\nu]\lambda^\gamma + \nu.
\end{aligned}
$$

Since the previous problem is in general hard to solve, it is possible to write a program in order to find the solution for λ to be a fixed point and then we can obtain the values of z and x.
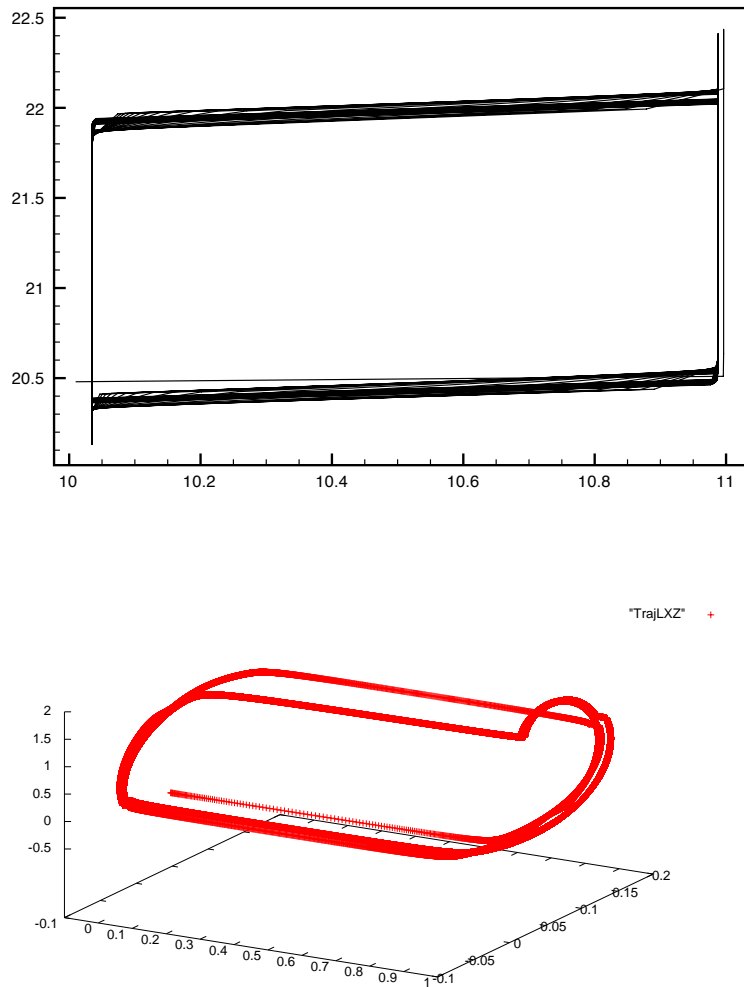
Figure 3.15: Complex Case: Orbits generated by the method for the desynchronization of Goodwin model with 2 blocks.

3.7.2 Existence of chaos: Computational results

As we have explained in Section 3.3 about the program of desynchronization, we have used it to realize several simulations.

We first show the results for the simulation in the "complex" case using the program of desynchronization, as we can see in Figure 3.15. In the first plot we can see the homoclinic orbits between the two blocks, in a 2D view, meanwhile in the second plot we have the 3D representation. We have chosen λ, x and z as variables.

The parameters used in the simulation are the following: $n = 3$, $\mu = 20$, $\epsilon = 0.05$, $\delta = 0.1$, $a = b = 1.0$, $K_1 = K_2 = K_3 = 1.0$, and $\gamma_1 = 0.1$, $\gamma_2 = 0.2$, $\gamma_3 = 0.3$.
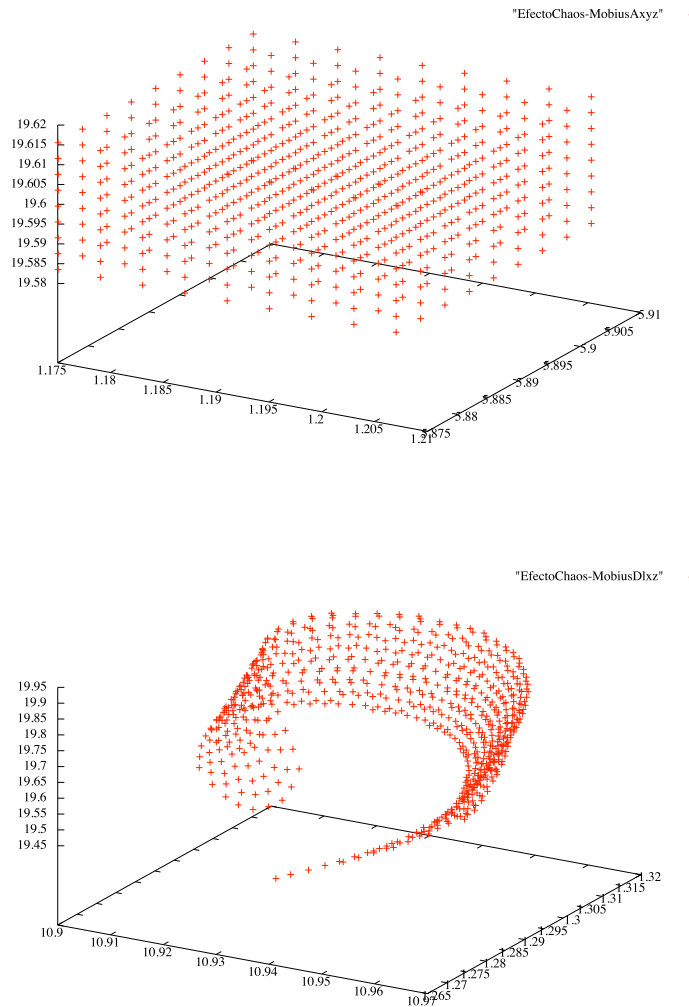
Figure 3.16: The global effect of the stable manifold.

In the "complex" case we can prove numerically the existence of chaos by the geometry of the Poincaré map and its circular effect (for more details see [W88]).

In general the idea is to show that P^L contains an invariant Cantor set on which it is topologically conjugate to the shift map. In this case we have considered a cube Π_0 near the origin as we can see in Figure 3.16, then we have applied the function P^L to all the points inside the cube at the same interval of time. Finally we have plotted the image of the set Π_1 concluding spiral behavior.

In the first plot we have a cube near the origin of the x, y, z system where the value of λ is constant and equal to ϵ. After iterate the program between Π_0 and Π_1 by the time of flight.

In the second plot we can see how the cube is deformed by the effect of the homoclinic orbit, the torsion is a consequence of the Möbius strip.

Finally, following the same principle, it is also possible to create a feedback on the parameter $V_{\max}$, instead of θ. The result is illustrated in Fig. 3.18. Recall that the method sustaining algorithm is based on the principle of creating a trapping region in phase space which is toroidal. Inside, orbits are forced to "turn around" indefinitely. This fact explains why the trajectories have a periodic behavior. Nonetheless, they are not exactly periodic, and might exhibit irregularities, as exhibited in the figure.
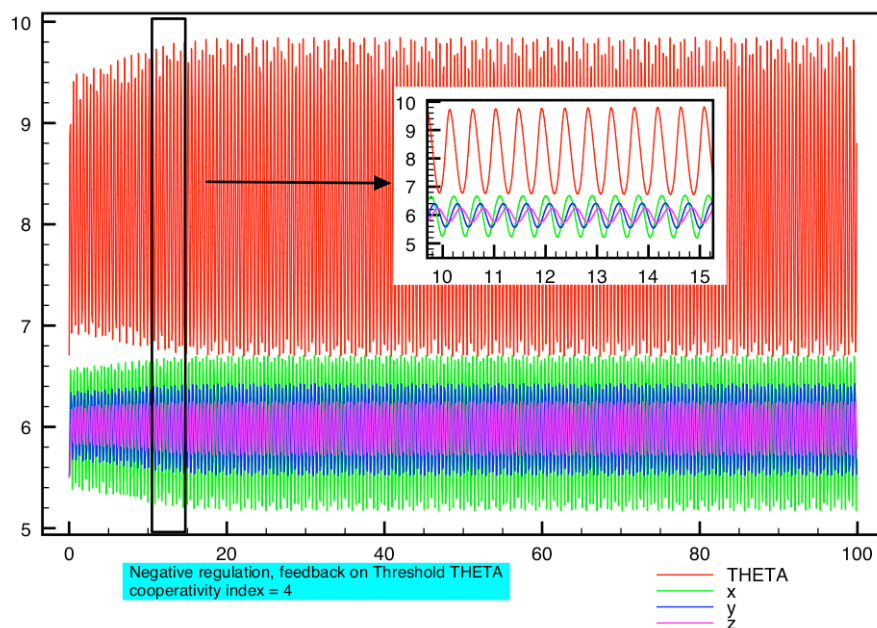
Figure 3.17: Phase space of the negative Goodwin model with 3 variables and cooperativity index $n = 4$. *(left)* simulation of the original system; *(right)* simulation of the system with a feedback on θ, as constructed with the algorithm. Parameters are: $V_{\max} = 80\,\mathrm{Mol}.l^{-1}t^{-1}$, $K_2 = K_3 = \gamma_1 = \gamma_2 = \gamma_3 = 10\,t^{-1}$. The algorithm runs with μ between 29 (picture) and 35.

3.7.3 Stability analysis of the periodic orbits for the Goodwin model

We continue with the stability analysis of the periodic orbits. We will prove that the system presents a Shilnikov type condition.
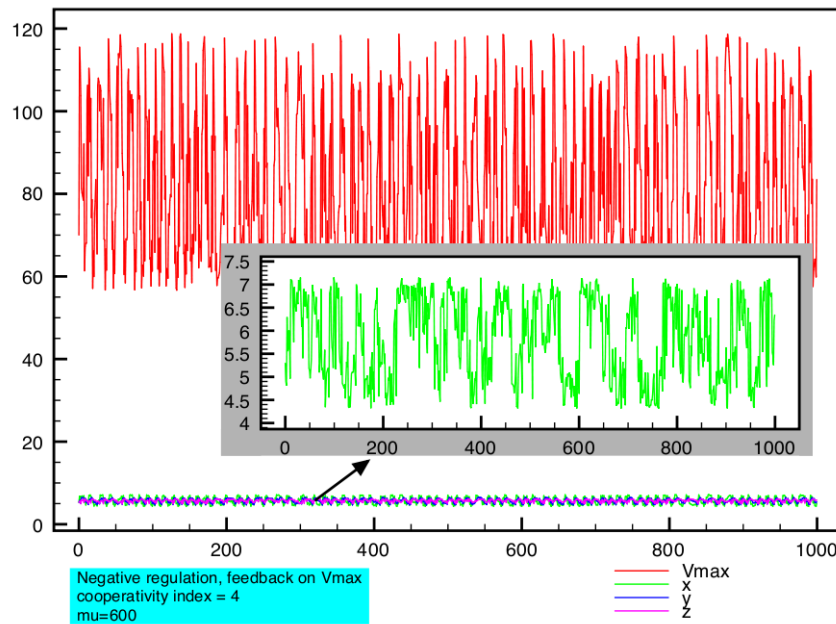
Figure 3.18: Time series showing a periodic behavior created in the negative Goodwin model with 3 variables and cooperativity index $n = 4$ by a feedback on V_{max}. Other parameters are:$\theta = 7\,\text{Mol}.l^{-1}$, $K_2 = K_3 = \gamma_1 = \gamma_2 = \gamma_3 = 10\,t^{-1}$. The algorithm runs with μ between 409 and 608. The simulation shown is for $\mu = 600$ (down).

From equation (3.6.7) we can obtain the values of the Jacobian matrix for the system P^L:

$$DP^L = \begin{pmatrix} \alpha\lambda^\delta cos(\xi ln\lambda + \Phi_1) & \bar{\alpha}\lambda^\gamma & \alpha x\delta\lambda^{\delta-1}cos(\xi ln\lambda + \Phi_1) - \alpha x\xi\lambda^{\delta-1}sin(\xi ln\lambda + \Phi_1) + \bar{\alpha}\gamma z\lambda^{\gamma-1} \\ \beta\lambda^\delta cos(\xi ln\lambda + \Phi_2) & \bar{\beta}\lambda^\gamma & \beta x\delta\lambda^{\delta-1}cos(\xi ln\lambda + \Phi_2) - \beta x\xi\lambda^{\delta-1}sin(\xi ln\lambda + \Phi_2) + \bar{\beta}\gamma z\lambda^{\gamma-1} \\ \zeta\lambda^\delta cos(\xi ln\lambda + \Phi_3) & \bar{\zeta}\lambda^\gamma & \zeta x\delta\lambda^{\delta-1}cos(\xi ln\lambda + \Phi_3) - \zeta x\xi\lambda^{\delta-1}sin(\xi ln\lambda + \Phi_3) + \bar{\zeta}\gamma z\lambda^{\gamma-1} \end{pmatrix}.$$

The stability is determined by considering the nature of the eigenvalues of the Jacobian matrix DP^L. In our case, it is only necessary to compute the determinant of the matrix, because it is the expression that governs the eigenvalues.

For time-continuous systems, the question about local stability can be answered without explicitly computing the eigenvalues of the Jacobian matrix, using the theorem of Routh and Hurwitz [H64]. This theorem establishes that the real parts of all roots of a polynomial are negative if and only if certain conditions (inequalities) are fulfilled, which in general can be easily tested. The procedure involves the construction of an special array with $n + 1$ rows which are computed from the constants coefficients and a posteriori analysis on its values.

In our case we have a polynomial of third degree so the conditions for local stability, that

is, to have eigenvalues with negative real part are:

$$\begin{cases} -tr(DP^L) > 0 \\ -tr(DP^L)C + det(DP^L) > 0 \end{cases}$$

where C is a value depending on the matrix.

It is not complicated to prove that the stability only depends on the value of $det(DP^L)$. However, for general high order systems, the analytical expression for the determinant is extremely complicated. In these cases it is only necessary to compute the order of λ in the previous expression. Finally in the desynchronized Goodwin model we have:

$$det(DP^L) \approx \lambda^{3\delta+2\gamma-1}.$$

Summarizing, we have the following result for the system stability:

Theorem 3.7.1. *In the desynchronized Goodwin model with complex eigenvalues μ, α_2 and $\rho \pm iw$, and under the hypothesis H2, if λ is sufficiently small, we can conclude that the Shilnikov condition for the periodic orbits is:*

$$\begin{array}{ll} \text{stable periodic orbit} & -3\rho - 2\alpha_2 > \mu \\ \text{unstable periodic orbit} & -3\rho - 2\alpha_2 < \mu \end{array}.$$

In Theorem 3.7.1 we can see that the value of μ, for stable periodic orbits, depends on the other eigenvalues α_2 and ρ (real part of both complex eigenvalues). Hence, the previous result is a generalization for the second order system case [W88].

3.7.4 Relation between the model parameters

As we have seen before, in our desynchronized model we have the presence of various parameters related with: the block size (a, b, δ), constants of the original Goodwin model (γ_1, γ_2, γ_3, K_1, K_2, K_3); and the control value μ, eigenvalue associated to the new differential equation for λ.

In order to study the existence of a relation between the parameters, we want to get an idea about the size of the "wiggles". In general, we know that if the wiggles are small then the 1-loop periodic orbits are only visible for a narrow range of parameters. In contrast, if the size of the wiggles are large enough, we might expect to have greater likelihood of observing the periodic orbits.

First we remain some of the notations:

$$\delta = \frac{-\rho}{\mu}, \gamma = \frac{-\alpha_2}{\mu}, \xi = \frac{-w}{\mu}$$

where $\mu, \alpha_2, \rho \pm iw$ are the eigenvalues of the desynchronized Goodwin model.

From the solution (3.7.7) of the singular points for the Poincaré map we have that

$$
\begin{aligned}
\lambda - \nu = {} & \zeta\bar{\alpha}(\beta(j\nu + x_0)\lambda^\delta cos(\xi ln\lambda + \Phi_2) + k\nu)\lambda^\gamma + j\nu + x_0)\lambda^\delta cos(\xi ln\lambda + \Phi_3) \\
& + \bar{\zeta}(\beta(j\nu + x_0)\lambda^\delta cos(\xi ln\lambda + \Phi_2) + k\nu)\lambda^\gamma.
\end{aligned}
$$

In general, if we omit the constants, we can say that the order of the previous expression is:

$$\lambda - \nu \approx \lambda^{2\delta + \gamma} + \lambda^{\delta + \gamma}$$

Now we impose the following condition for the expression in the *cos* function:

$$\xi ln\lambda_{i+1} - \xi ln\lambda_i = \pi$$

which implies that the quotient between $\lambda's$ is:

$$\frac{\lambda_{i+1}}{\lambda_i} = exp(\frac{\pi}{\xi}).$$

The principal idea to find the limit when i goes to infinity for the quotient between ν's, which give us the size of the oscillations in the periodic orbits. That is,

$$\lim_{i\to\infty} \frac{\nu_{i+1}}{\nu_i} \approx -\lim_{i\to\infty} \frac{\lambda_{i+1}^{2\delta+\gamma}}{\lambda_i^{2\delta+\gamma}} = -exp\left(\frac{\pi}{\xi}\right)^{2\delta+\gamma}$$

and we can conclude that

$$\lim_{i\to\infty} \frac{\nu_{i+1}}{\nu_i} \approx -exp\left(\frac{2\rho + \alpha_2}{w}\right)$$

where $\rho, \alpha_2 < 0; w \neq 0$.

Proposition 3.7.2. *The size of the oscillations, computed as the limit between consecutive ν's, can be expressed in terms of the eigenvalues in the following way*

$$\lim_{i\to\infty} \frac{\nu_{i+1}}{\nu_i} = -exp\left(\frac{2\rho + \alpha_2}{w}\right)$$

where ρ, α_2, w depend on the values of the constants $\gamma_1, \gamma_2, \gamma_3, K_1, K_2, K_3$ of the original Good-

win model.

If we define the quantity $\eta = 2\rho + \alpha_2/w$, we would be able to see that when the values γ_i's increases or the values K_i's decreases, the value of η goes to $-\infty$, so it is more probable to observe periodic orbits.

3.8 Conclusions and future work

In this chapter we have developed an algorithm for the desynchronization of stable systems following the structure described in the constructive proof of the main theorem in [P06] (Theorem 3.2.1).

Since the algorithm depends on certain parameters of the model and the nature of the eigenvalues (purely real or complex), we have done both the spectral and the stability analysis in order to obtain the best election for the model's parameters, which generate and maintain the periodicity of the homoclinic orbits and the sensitivity to the initial conditions (the chaotic behavior).

As a first control example we made the desynchronization of the M-S Lorenz model with the aim of testing the method against the well known chaotic behavior. In the Lorenz case we have always real eigenvalues, independent of the parameters hence, we have applied the four block method in order to create two homoclinic orbits with an additional problem related to the magnitude of the eigenvalues for the simulation. Finally we have obtained similar results to compare the method with the right choice of parameters.

However, we have center our attention in the most simple homeostatic biological system, the Goodwin model, in which we induce periodicity and chaos by negative feedback. As a first task, in the Goodwin model was necessary to differentiate between the nature of the eigenvalues, purely real or complex, in order to realize the formal block construction: four blocks in the real case and two in the complex case. Additionally, we found a relation between the parameters of the model, and depending on the case, we have constructed the homoclinic orbit. Finally, we made the stability analysis showing Shilnikov and Lorenz type condition of chaotic behavior by the construction of the respective Poincaré map.

Another numerical experiment consists in applying the algorithm by adding a feedback on the parameter $V_{\max}$, we create sustained oscillations with cooperativity index 4 (Figure 3.17). This result is interesting since it is known that the Goodwin model with negative regulation

cannot exhibit oscillations when it applies to a three-variable system with low "cooperativity index" (less than 8) as noted in [C99].

The originality of our method relies on the fact that 1) it targets the dynamics of regulation and 2) it acts on the "software" of the organism, inducing a self-disorganization. Moreover, from the work presented here we have learnt that the type of feedback proposed by the method might be very simple: essentially, alternatively positive and negative action on the parameter. This type of action is encountered in natural regulatory systems.

With regards to the biological implementation of the algorithm, as a form to design specific drugs, we can say that we are far away to find a solution to the complete problem because of the complexity of the real model. However, we believe that the problem itself deserves our attention in the future, maybe with other class of models, or maybe integrating interconnected system.

Bibliography

[BT97] Balmforth N., Tresser, C., Worfolk, P., Wu, C.: Master-slave synchronization and the Lorenz equations. Chaos 7 (3), 1997.

[C99] Conrad, E.: Mathematical models of biochemical oscillations. PhD thesis, Virginia Tech, 1999.

[Go02] Goldbeter, A.: Computational approaches to cellular rhythms. Nature, vol 14, 2002.

[G63] Goodwin, B. C.: Temporal organization in cells Academic Press, New York, 1963.

[G65] Goodwin, B. C.: Oscillatory behavior in enzymatic control processes. Advances in Enzyme Regulation, Pergamon Press, Oxford, 425-438, 1965.

[H64] Hurwitz, A.: On The Conditions Under Which An Equation Has Only Roots With Negative Real Parts. Selected Papers on Mathematical Trends in Control Theory, 1964.

[MP02] Martens, M., Pécou, E., Tresser, C., Wolfolk, P. On the geometry of master-slave synchronization. Chaos 12 (2), 316-324, 2002.

[P06] Pécou, E.: Desynchronization of one-parameter families of stable vector fields. Nonlinearity 19, 261-276, 2006.

[PC90] Pecora, L. M., Carroll, T. L.: Synchronization in chaotic systems. Phys. Rev. Lett. 64, 821-824, 1990.

[PC91] Pecora, L. M., Carroll, T. L.: Driving systems with chaotic signals. Phys. Rev. A 44, 2374-2383, 1991.

[R89] Robinson, C: Homoclinic bifurcation to a transitive attractor of Lorenz type. Nonlinearity 2, 495-518, 1989.

[R92] Robinson, C: Homoclinic bifurcation to a transitive attractor of Lorenz type, II. SIAM J. of Math. Anal. 23, 1255-1268, 1992.

[S65]   Shilnikov, L. P.: A case of the existence of a denumerable set of periodic motions. Sov. Mat. Dokl. 6, 163-166, 1965.

[S70]   Shilnikov, L. P.: A contribution to the problem of the structure of an extended neighborhood of a rough equilibrium state of saddle-focus type-case. Math. USSR, Sbornik. 10, 91-102, 1970.

[So03] Soulé, C.: Graphics requirements for multistationarity. ComplexUs 1, 123-133, 2003.

[T81]   Thomas, R.: On the relation between the logical structure of systems and their ability to generate multiple steady states and sustained oscillations. In Series in Synergetics, volume 9, pages 180-193. Springer, 1981.

[TO78] Tyson, J.J., Othmer H.G.: The dynamics of feedback control circuits in biochemical pathways. Progress in Th. Biology 5, 1-62, 1978.

[W88]   Wiggins, S.: Global Bifurcations and Chaos, Analytical Methods. Applied Mathematical Sciences 73. Springer, 1988.

4 A mathematical model for metal stress response in *Haloarchaeal*.

In [B06], Baliga and coworkers reconstructed the physiological behaviors of *Halobacterium NRC-1*, an extremophile archaea which lives in hypersaline environments. Using a system level study (top-down approach) they proposed a biological model identifying four mechanisms that play a central role in conferring resistance to excess of heavy metals.

In this chapter we propose a mathematical model accounting for the dynamics of uptake, efflux, storage and traffic of transition heavy metals $Cu(II)$, $Zn(II)$, $Mn(II)$ and $Fe(II)$ in *Halobacterium NRC-1* based on the framework of differential equations and the power law formalism. Since there are a lot of variables and parameters, we have sub-divided the whole system in two independent modules, one solving the traffic and extrusion of $Cu(II)$ and $Zn(II)$, and the other dealing with the uptake and storage of $Mn(II)$ and $Fe(II)$. Moreover, each one of the modules have been divided in two classes: (I) without and (II) with re-utilization of exported metal ions.

For both modules and their respective classes we prove in a formal way that the systems present stable stationary states. The homeostatic behavior is characterized, according to the various kinetic parameters (degradation, synthesis and affinity). Additionally, we derive monotonicity conditions for the existence of global steady state responses, independently of the choice of the parameters. Together with the theoretical results, we develop several simulations to obtain numerical solutions for the system of differential equations and graphical representations for the trajectory of each element in the modules.

Finally, from the biological point of view many particular questions are relevant to be tested with the model. In particular, we address the question of cellular growth and death at high metal ions concentrations, and the question of cellular response under successive and alternate metal stress attacks. Both questions are essential in order to understand the adaptability of the system to the medium. In this direction, we extend and simulate our model with an additional equation for the growth. Additionally, this work try to extend a previous model developed in [P06] for the behavior of the cop operon, which takes into

account only information about copper mechanisms in bacteria showing that homeostasis is a result of transient dynamics.

4.1 Introduction

Transition heavy metals such as $Mn(II)$, $Cu(II)$, $Zn(II)$, $Fe(II)$, $Co(II)$ and $Ni(II)$ are important for essential biological processes in all organisms. They are effective in trace amounts, nonetheless, when their concentrations abnormally increase, for instance because of a sudden change in the environment or a failure of the regulatory mechanisms, severe damages can occur to the cell. For these reasons there is an increasing interest in the different molecular processes that the cell uses to regulate the metal stress response, and maintain homeostasis. However, they are not completely known yet.

Organisms usually avoid metal toxicity through selective uptake, traffic and efflux of metal ions and enzymatic conversion of metals into non or less toxic redox states. Defects in metal traffic can cause serious illness such as Menkes and Wilson diseases ([H99], [F99], [L99], [M01]).

In order to decipher metal-protein specialization from transcriptional responses, one requires the knowledge of genes that respond to a specific metal as well as the proteins that mediate the metal regulation. In general, we can use a reductionist approach and analyze the effect of each transition metal in the cell, but a top-down level system approach enables full appreciation of a global stress response of this type, thereby helping in distinguishing putative direct changes from indirect responses ([Ha01], [B02], [B04]).

The deepening of the system level understanding eventually leads to mathematical models of corresponding degree of precision, that are useful in the re-engineering of microbes in view of industrial, environmental and medical purposes [B07].

In a system approach, measurements and analysis of all the components at the same time provide integral information about how the different transition metal ions with the proteins act inside the cell to regulate and to control the metal stress response. However, when we need to solve conflicts of biological hypotheses or to provide precise interpretation of non-intuitive data, the mathematical modeling approach can be useful.

The main objective of this chapter is to understand how homeostasis is achieved and show some theoretical properties related with the steady states such as robustness, monotonicity and convergence to equilibrium by building a mathematical model, accompanied by simulations, based on the most complete description at the biomolecular level of metal stress response done for *Haloarchaeal NRC-1* [B06].

In the simulations we do not use real values for concentrations, affinities and degradation rates because only few of them have been measured and the others are still unknown.

However, we have considered qualitative relationships between them and some restrictions compatible with biological reality. Therefore, we have been able to establish qualitatively similar results as those obtained in [B06] by experiments (see Figure 4.1).

The chapter is organized as follows: Section 4.2 contains a brief summary of the biological model under study built by Baliga et al. Section 4.3 provides a detailed exposition about how we have constructed the mathematical model. Sections 4.4 is devoted to the mathematical analysis of the steady states and homeostasis behavior, and Section 4.5 deals with monotonicity and the global stability analysis. Finally Section 4.6 contains the main results and simulations obtained by the programs *xDim* ([MM], differential equation solver) and *Cell Designer* ([K03], [K07]).

Moreover, two important biological questions dealing with cellular growth and death under different metal stress, and the cellular response under successive and alternate stress of metals are treated. In order to answer these two questions we have simulated how the Cu/Zn module responds to successive and alternative external stress of copper and zinc ions. In the other case, we have added to our model an additional equation. This equation introduces a new variable, which is constant in the original model, dealing with the cellular growth problem. Our point of view sheds some new lights on the way a cell would react to environmental perturbations such as cellular stress by subletal metal concentrations.
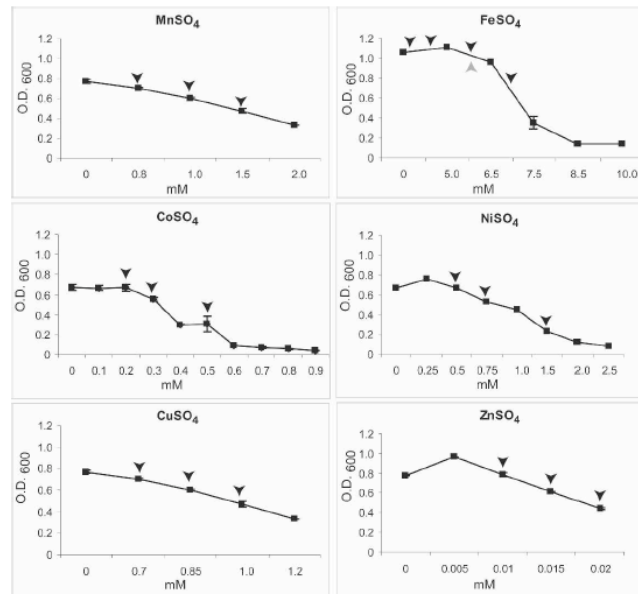
Figure 4.1: Picture from Baliga et al. work [B07]: At higher concentrations all metal were growth inhibitory.

4.2 Overview of the biological model

In [B06], using microarray analysis, the authors investigated transcription level changes for $2,400$ genes exposed for 5 hours to at least three different metal concentrations, and they reconstructed both the physiological behaviors and the regulatory interaction networks of *Halobacterium NRC-1*, in subletal levels of $Mn(II)$, $Fe(II)$, $Co(II)$, $Ni(II)$, $Cu(II)$ and $Zn(II)$.

Halobacterium NRC-1 is an extremophile archaea, which requires environments with nearly saturated salt conditions ($\sim 4.5M$) and an optimal temperature observed at $37^{o}C$ to survive and grow. Typical habitats comprise marine salterns, salt evaporation ponds and hypersaline lakes, where high cells densities and rapid evaporation can lower oxygen tension and deplete nutrient concentrations [B07].

In what follows we briefly discuss the main biological results obtained from the top-down system level approach in [B06]. In order to explain the generalities of the model we separate the global metal stress response structure into four modules: $Cu(II)$, $Zn(II)$, $Mn(II)$, $Fe(II)$, each one of them representing an important regulatory mechanism for metal uptake, efflux and traffic. However, later in the mathematical model and the corresponding analysis we take into account the interactions between them.

DNA microarrays were used to assess global transcriptional responses to environmental and genetic perturbations in *Halobacterium NRC-1*. We know that at abnormally high concentrations all metals are growth-inhibitory. This growth-arrest phenotype is perhaps one of the resistance mechanisms to the regular occurrence of stressful conditions in its dynamic hypersaline environment.

The physiological response reconstruction was made through simultaneous analysis of transcript level changes, along with a variety of independent databases. In general, over 20% of all genes responded transiently within minutes of exposure to heavy metals, perhaps reflecting immediate large-scale physiological adjustments to maintain homeostasis.

Moreover, 1/3 transcriptional changes elicited by the various transition metals were related to oxidative stress managements, including deshydrogenases activation, ion scavenging, protein turnover, DNA replication and repair. These observations are consistent with the property of transition metals to catalyze production of reactive oxygen species (ROS).

While several of these phenomena constitute a general stress response, up-regulator of active efflux of Co, Ni, Cu and Zn, down-regulation of Mn uptake and up-regulation of Fe

chelation, confer resistance to the respective metals.

Finally it is hypothesized that at least four mechanisms play a central role in conferring resistance to the six transition metals, and for the convenience of the reader we repeat the relevant material from [B06] and other articles (an example for *Bacillus Subtilis* can be seen in [Mo05]), thus making our work self-contained.

In the following we will use the standard notation for genes and proteins. The genes will be denoted with their first letter name in minuscule, e.g. $yvgX$, and the proteins will be denoted with their first letter name in majuscule, e.g. $YvgX$.

4.2.1 $Cu(II)$ resistance

The regulatory mechanism of resistance to $Cu(II)$ excess involves:

- Two P_1 ATPase transporters $YvgX$ and $ZntA$, which pump copper ions out of the cell.

- Two metallochaperones $VNG0702H$ and $VNG2581H$, which safely transport copper (and also zinc) inside the cell. In what follows the metallochaperones will be denoted by Ch.

- A regulator $VNG1179C$ from a Lpr family regulator with a putative metal binding TRASH (traffic, resistance and sensing of heavy metals) domain, which up-regulates the transcription of $VNG0702/2581H$ and $YvgX$. We observe that the regulator of $ZntA$ will be analyzed in Section 4.2.2.

TRASH domain [E03] is a well conserved cysteine motif (signature CxCxC) that is involved in metal coordination. TRASH is encoded by multiple prokaryotic genomes and is present in transcriptional regulators. The domain constitutes a novel component in metal traffic and heavy metal resistance. However the regulation of $VNG1179C$ is unknown.

Observation 4.2.1. *In the literature we have not found evidence about the presence of an operon in the regulation of the system, so in our model we have assumed that the genes are not co-regulated in the genome.*

Now we describe the model in details (see Figure 4.2 for a graphical description). The mechanism that the cell uses to import the copper from the exterior is not known. We have assumed the existence of a regulatory function with a threshold parameter which traduces the fact that a minimal external pressure is necessary to allow permeability. On the other

hand, we have assumed that the chemical reaction is irreversible, as in the copper model described in [Sz03]. In summary, uptake is represented by the following equation:

$$Cu_{ext} \rightarrow Cu_{int}.$$
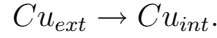
Once copper ions are inside the cell, they bind to the putative metallochaperones Ch producing the complex $ChCu$. The special behavior of this archaea is characterized in the copper mechanism because the chaperones can bind to both copper and zinc ions, and in general the presence of zinc activates all the regulatory machinery for the copper traffic, so we include here the zinc reaction too,

$$Cu_{int} + Ch \rightarrow ChCu,$$

$$Zn_{int} + Ch \rightarrow ChZn.$$
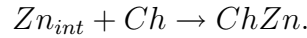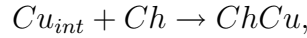
Additionally the model needs a basal concentration of the protein Ch to start the transcription machinery of the copper chaperones and the copper efflux ATPase $YvgX$, this fact was proved experimentally and different simulations of our mathematical model show the same conclusion (more details in Section 4.6).

The complexes $ChCu$ and $ChZn$ deliver Cu and Zn ions respectively to the protein with TRASH domains $VNG1179C$ ([To05], [Sz03]), which will be denoted from now as TD,

$$ChCu + TD \rightleftarrows TDCu + Ch,$$

$$ChZn + TD \rightleftarrows TDZn + Ch,$$
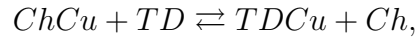
which in turn activates transcription of both chaperones Ch,

$$TDCu \rightarrow Ch,$$
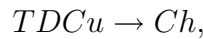
and the $YvgX$ protein,

$$TDCu \rightarrow YvgX,$$
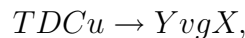
where the complex $TDCu$ produces (positive regulation) chaperone and transport protein. The regulatory mechanisms that involves the complex $TDZn$ will be analyzed in Subsection 4.2.3.

In the above model, the metal-binding domain works on DNA next to the genes as a $Cu(II)$ sensor to modulate activity of $VNG1179C$. This is functionally similar to the modulation of

the activity of the human $Cu(II)$-translocating ATPase $ATP7B$, whose abnormal function results in $Cu(II)$ accumulation leading to Wilson's disease ([H99], [L99]).

Efflux of $Cu(II)$ by the P_1 ATPase $YvgX$ is a key mechanism for withstanding $Cu(II)$ toxicity. Recent experiments realized in absence of this protein have shown poor growth in presence of $Cu(II)$ and $Zn(II)$. However, we will see in the next subsection that it is not the only system used by the cell to control the traffic of toxic metals. The main reactions associated to efflux are:

$$ChCu + YvgX \rightleftarrows YvgXCu + Ch,$$

and

$$YvgXCu \longrightarrow (Cu_e)^* + YvgX,$$
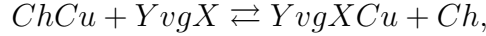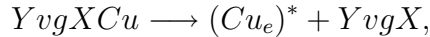
where $(Cu_e)^*$ corresponds to external copper ions exported by the cell. In the model we mainly assumed that $(Cu_e)^*$ cannot be absorbed again by the cell. However we have done other simulations (see Section 4.6) where, in order to compare this effect, we allow to the metal ions return into the cell. Additionally, there exists degradation of the complexes which release copper to the internal medium.
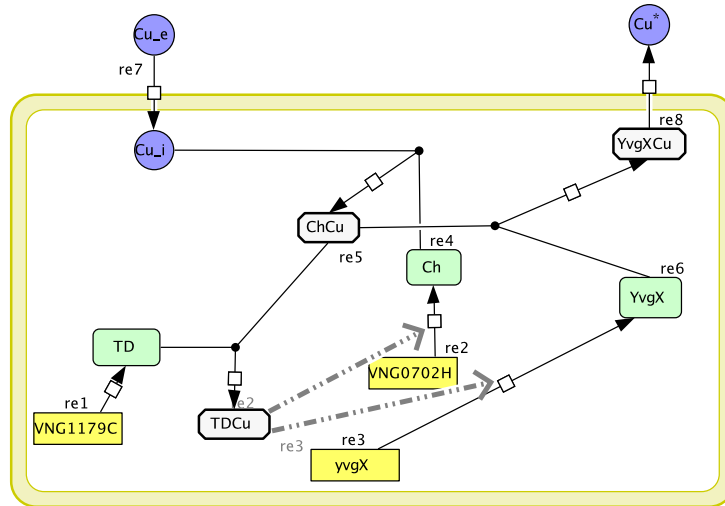
Figure 4.2: Scheme of the $Cu(II)$ resistance model which involves three genes: $VNG1179C$, $VNG0702H$ and $yvgX$. The metallochaperones $VNG0702H/2581H$ (Ch in scheme) transfer copper ions to $VNG1179C$, a protein exhibiting TRASH domain (TD in scheme), and its complex up-regulates the production of the metallochaperones and $YvgX$, which releases Cu from the cell.

4.2.2 $Zn(II)$ resistance

In terms of oxidative stress, $Zn(II)$ seems to be the most damaging among metals. In particular, its high toxicity was experimentally proven in *Halobacterium NRC-1*. For that reason, intracellular zinc levels are tightly regulated by zinc enzymes expression and zinc transporters.

As for copper, the zinc uptake mechanism is unknown, for that reason we have used a regulatory function with a threshold to simulate the process:

$$Zn_{ext} \rightarrow Zn_{int}.$$
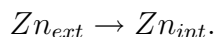
As stated in the previous subsection, the chaperones $VNG0702H$ and $VNG2581H$, common to Cu and Zn ions, are the transporters:

$$Zn_{int} + Ch \rightarrow ChZn.$$
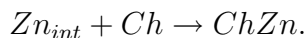
The traffic system uses $ZntA$, another P_1 ATPase of broad specificity, that confers resistances to Co, Ni, Cu and Zn. Experimental evidence shows that $ZntA$ protein is upregulated at steady state only in the presence of $Zn(II)$ [B06], however the regulator involved is unknown and it has not been characterized in the reference paper.

For that reason and inspired by previous evidence ([Ch07], [Y05]) we assume that transcription of $zntA$ gene is activated by $ZntR$ protein, a metal responsive transcriptional regulator. The binding of $Zn(II)$ ions to $ZntR$ is produced by the action of the metallochaperones Ch, as in the copper model, i.e.,

$$ChZn + ZntR \rightleftarrows ZntRZn + Ch.$$
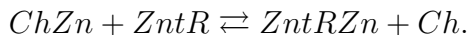
As the mechanism of regulation is unknown, the concentration of $ZntR$ needs to be in a basal level in order to produce the reactions. This process converts the complex $ZntRZn$ into a strong transcriptional activator of the gene $zntA$, resulting in the increasing efflux of zinc ions. The associated reaction is given by:

$$ZntRZn \rightarrow ZntA,$$
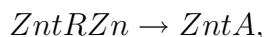
where we have assumed a positive regulation.

In the experimental test it was investigated how the cell reacts under the elimination of $ZntA$ protein, and the result was a poor growing in the presence of metals. As a consequence, it was proved that there exists a correlation between the amount of $ZntA$ and the amount of heavy metal expulsed from the cell. The associated reaction is:

$$ZntAZn \longrightarrow (Zn_e)^* + ZntA,$$
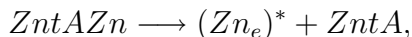
where $(Zn_e)^*$ corresponds to external zinc ions exported out of the cell.
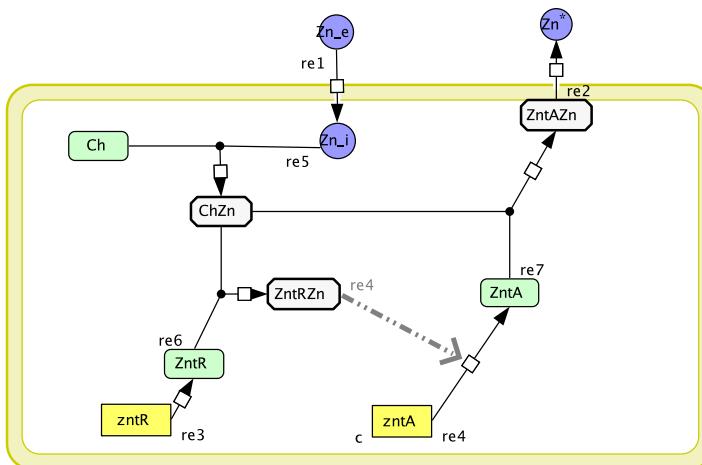
Figure 4.3: Scheme of the $Zn(II)$ resistance model with two genes: $zntR$ (unknown regulator) and $zntA$. Metallochaperones transport zinc ions to both proteins $ZntR$ and $ZntA$. $ZntR$ regulates positively the production of $ZntA$, the traffic protein which confers resistance to $Zn(II)$, $Cu(II)$, $Co(II)$ and $Ni(II)$.

4.2.3 Link between the $Cu(II)$ and the $Zn(II)$ mechanisms.

In general, it is known that certain organisms require multiple mechanisms for clearing $Cu(II)$ from the cells in order to reduce its toxicity. For example, this is the case of the Cop operon in *E. Coli* [Sz03], where $P-$type ATPase $CopA$, Cu-oxidase $CueO$ and multicomponent copper transport system $CusCFBA$ are related.

In *Halobacterium NRC-1*, as we have seen before, it was experimentally shown that in the presence of zinc, the copper mechanism is activated. Thus, the zinc ions need to be incorporated in the study of the copper mechanism.

For example, the protein $ZntA$, involved in the zinc extrusion mechanism (Subsection 4.2.2) can export copper out from the cell. The following chemical reactions summarize the

process:

$$ZntA + ChCu \longrightarrow ZntACu + Ch,$$

and

$$ZntACu \longrightarrow (Cu_e)^* + ZntA.$$
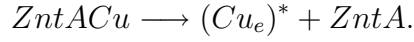
Moreover, as we have seen before, the internal zinc can bind to the chaperone Ch forming the complex $ChZn$, which can interact with TD protein in order to regulate the production of Ch and $YvgX$. That is,

$$ChZn + TD \rightleftarrows TDZn + Ch,$$

$$TDZn \rightarrow Ch,$$

$$TDZn \rightarrow YvgX.$$
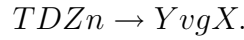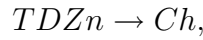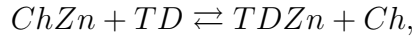
It was proved by biological experiments that these additional mechanisms make the release of copper outside from the cell a more efficient system [B06]. In the simulations of Section 4.6 we will see that the curve for the concentration of external copper grows faster than the curve for the concentration of external zinc. This behavior is consistent with two biological forces: zinc is necessary inside the cell from multiple mechanisms and copper is exported by two different proteins $YvgX$ and $ZntA$.

As a consequence, it is necessary to incorporate and study both extrusion mechanisms into a single module, called Cu/Zn module.

Assumptions:

Baliga and co-authors have assumed that one or both of these putative chaperones are constitutively present in the cell at a basal level, trafficking $Cu(II)$ ions to appropriate ligands. Moreover, they did not find evidence for the regulation of $VNG1179C$ (TD) and $ZntR$. However, the idea of a basal concentration for the chaperones and the regulators with TRASH domain is not generally accepted in a model with differential equations. In contrast, to construct a more realistic model we have assumed the existence of a negative auto-regulation for both TD and Ch which is consistent with the empirical evidence. In fact, when the amount of free TD and Ch is small (as in the case of absent of ion stress or in the case of maximum stress) then the production of both proteins will increase, in the contrary case the amount will be relatively constant.

On the other hand, as it is unknown the existence of an operon (as in the case of Cop operon in *E. Coli*) we will omit in the final equation the reaction of the type

$$X + O \rightleftarrows XO \rightarrow Y,$$
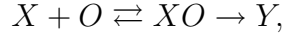
by considering only reactions of the type

$$X \rightarrow Y.$$
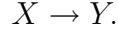
In the last case, we can obtain a regulatory function using the Michaelis-Menten reduction (quasi-steady state approximation), in order to consider the effect of one protein or complex in the regulation of the other. This reduction simplifies the model and the mathematical analysis, however, it will be necessary to consider the effect of the binding regions when we take into account the growth effect, in which case, the amount ρ_0 will depend on the number n of archaeas present in the medium.

4.2.4 $Fe(II)$ resistance

Iron is an essential micronutrient for almost all organisms, and given its limited bio-availability, micro-organisms have developed sophisticated mechanisms to scavenge this metal ion from their environment. In most bacteria, the iron-responsive transcriptional regulator Fur is responsible for coordinating the expression of iron uptake and storage functions.

In this model we can distinguish two main processes: $Fe(II)$ uptake and detoxification (see Figure 4.4 for graphical details). In general, the uptake mechanism is not well known, because the transcriptional regulators have not been identified yet. However, different experiments [B06] have shown that $Mn(II)$ up-regulates and $Zn(II)$ down-regulates putative siderophore (an iron chelating compound) biosynthesis and $Fe(II)$ uptake. For that reason we assume that we have an unknown regulator denoted by FeR. FeR protein can be bound to Mn, Fe and Zn forming the following compounds:

$$FeR + Mn \rightarrow FeRMn,$$

$$FeR + Fe \rightarrow FeRFe,$$

$$FeR + Zn \rightarrow FeRZn.$$
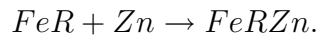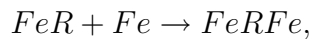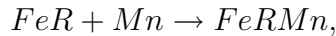
The complexes $FeRMn$ and $FeRZn$ act over the regulated transcriptional domain of an

uptake protein that we denote FeU, up-regulating and down-regulating respectively. The associated reactions are:

$$(4.2.1) \qquad\qquad FeRMn + R_1 \rightleftarrows R_1FeRMn \rightarrow FeU,$$

$$(4.2.2) \qquad FeRZn + R_1 \rightleftarrows R_1FeRZn \rightarrow \emptyset \text{ (block the production of } FeU\text{),}$$

where R_1 represents the regulated transcription domain of FeU. The last arrow in (4.2.1) means that the complex $FeRMn$ binds to the gene region R_1 producing (positive regulation) the uptake protein FeU. Meanwhile, the last arrow in (4.2.2) implies that complex $FeRZn$ down regulates the production of the uptake protein. For that reason in our case the symbol $\emptyset$ means no production.

Observation 4.2.2. *The presence of Fe is not necessary in the regulation of the uptake protein, hence we can conclude that manganese simulates iron deficiency. For that reason, to better understand the behavior of the system we study the whole Fe/Mn module*

Chelation of $Fe(II)$ by the ferritin $DpsA$ is a mechanism for detoxifying the cell from $Fe(II)$. Transcription of $DpsA$ is up-regulated in the presence of Co, Fe, Zn and down-regulated by Mn and Fe deficiency conditions. Increase in $dpsA$ transcription during ferric stress, on the other hand, in conjunction with its property to store iron in its nontoxic $Fe(III)$ form, points to a regulatory mechanism that ensures increased abundance of $DpsA$ to minimize its toxicity in the cell ([R02], [Z04], [Se00]). This can be summarized in the following reactions:

$$FeRFe + R_2 \rightleftarrows R_2FeRFe \rightarrow DpsA,$$

$$FeRZn + R_2 \rightleftarrows R_2FeRZn \rightarrow DpsA,$$

$$(4.2.3) \qquad FeRMn + R_2 \rightleftarrows R_2FeRMn \rightarrow \emptyset \text{ (block the production of } DpsA\text{),}$$
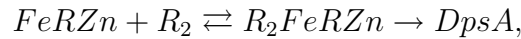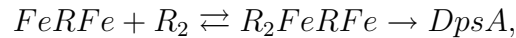
where R_2 represents the regulated transcription domain of $DpsA$. Similarly as we have explained before, $FeRFe$ and $FeRZn$ exert a positive regulation over the production of $DpsA$, meanwhile in (4.2.3), $FeRMn$ down regulates it (symbol $\emptyset$).

Finally, detoxification and storage can be represented as follow:

$$DpsA + Fe \longrightarrow DpsAFe,$$

$$DpsAFe \longrightarrow DpsA + Fe(III).$$
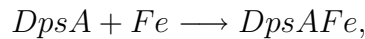
Observation 4.2.3. *In the description for detoxification and storage, we are not interested*

in what happens with $Fe(III)$. Even in the case that there exists another special mechanisms dealing with this metal ion, it is not complicated to incorporate the effect in our model. That is, in our model $Fe(III)$ is not reused.

Figure 4.4: Scheme of the $Fe(II)$ resistance model: Three genes are involved in the central mechanism feR, feU and $dpsA$. We have an unknown regulator protein FeR working in presence of $Mn(II)$, $Fe(II)$ and $Zn(II)$, regulating the FeU protein dealing with the iron uptake and $DpsA$ protein dealing with the iron detoxification.

4.2.5 $Mn(II)$ resistance

In contrast with the iron uptake, before the biological study in [B06] little was known about manganese uptake system.

The uptake mechanism for minimizing $Mn(II)$ toxicity is composed of the putative Mn-dependent autorepressor protein $SirR$, from the $MntR$ family regulator, which can bind to either $Mn(II)$ or $Fe(II)$,

$$SirR + Mn \rightleftarrows SirRMn,$$

$$SirR + Fe \rightleftarrows SirRFe,$$

and three subunits of Mn-uptake ABC transporters $ZurA$, $ZurM$ and $YcdH$ (transmenbrane protein), whose genes are gathered in the zur operon.

In the uptake system, the operation of the zur operon was not clearly established. We know that the proteins observed are three: $ZurA$, $ZurM$ and $YcdH$ [He99]. $ZurA$ is an ABC transporter and it is in charge of the manganese uptake; the $ZurM$ protein displays

high similarities with hydrophobic membrane proteins associated with ABC transporters; and $YcdH$ is an adhesion protein. We can summarize all the previous information in the following reaction:

$$ZurA + Mn_{ext} \rightleftarrows ZurAMn \rightarrow ZurA + Mn_{int}.$$

At the beginning it was thought that $SirR$ protein in presence of either $Mn(II)$ or $Fe(II)$ up-regulates the expression of the zur operon (result obtained from regulatory inference programs *cMonkey, Inferelator*). However, after multiple experiments it was understood that it actually down-regulates the expression of the operon. The explanation for this phenomenon, contradicting previous results that show correlated growing, is the negative regulatory action of the $SirR$ protein over itself. This explains the behavior and the results previously found in the biological experiments:

$$SirRMn + R_3 \rightleftarrows R_3SirRMn,$$

$$SirRMn + R_4 \rightleftarrows R_4SirRMn,$$

$$R_3 \longrightarrow SirR,$$
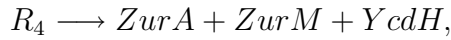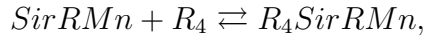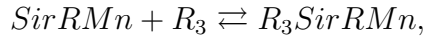
$$R_4 \longrightarrow ZurA + ZurM + YcdH,$$

where R_3 and R_4 correspond to the regulatory sites of proteins $SirR$ and $ZurA$ respectively. In this case, the last two pseudo-reactions show the idea of negative regulation, that is, in normal condition the archaea produces $SirR$ and $ZurA - ZurM - YcdH$ proteins, however under the presence of manganese inside the cell and the formation of complex $SirRMn$, the production of both proteins are blocked.

Finally, $SirR$ may also impose this regulation upon binding $Fe(II)$, but its function might be blocked upon binding either $Co(II)$ or $Ni(II)$. However, its transcriptional control seems to only have impact on conferring resistance to $Mn(II)$ and none of the other metals.

4.3 The mathematical model

In general, it is difficult to construct a model for a global system because we do not have real biological data. In theory, knowing all the biological actors and all the local interactions allow to construct a precise and fine tuned mathematical model coherent with reality. Such a model enables to do in-silico experiments, faster and inexpensive, as in virtual biology for example. The drawback of this approach is that the model might be too complex to extract
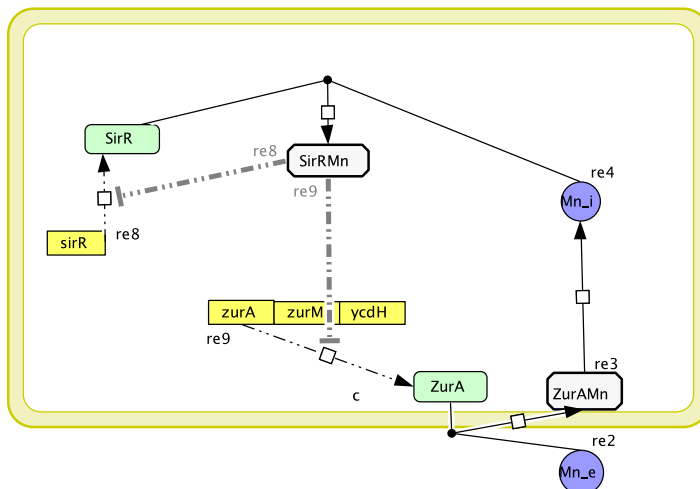
Figure 4.5: Scheme of the $Mn(II)$ resistance model: In the presence of either $Mn(II)$ or $Fe(II)$, $SirR$ protein down-regulates itself and the operon $zurA/zurM/ycdH$ as a mechanism for metal stress resistance. $ZurA$ is the ABC transporter dealing with the manganese uptake.

relevant information, applicable to other situations. This is the reason why in the literature we find simple models, even toy models, which reflect only a few aspects of the system which can be understood.

In this section we construct a mathematical model for *Halobacterium NRC-1* based on the biological information of Section 4.2, which has been translated into chemical equations, in order to obtain a formal description of the processes and shed new lights on the cellular behavior.

We use the differential equation formalism, working under the following assumptions: we have a population of cells and our variables account for a mean behavior. As a result we can neglect stochastic fluctuations and assume that all the variables of the system evolve continuously and in a deterministic way. We have neglected the spatial effect, like compartmentalization or (spatial) diffusion.

If we analyze the biological network of interactions, it seems natural to divide the whole system into two modules: one dealing with the uptake regulatory process, which involves $Mn(II)$ and $Fe(II)$, and the other dealing with the trafficking regulation, with actors $Cu(II)$ and $Zn(II)$. A key point to be analyzed mathematically is the measure and the comparison of their influence on the whole system. Since we do not know particular regulatory networks for cobalt and nickel, we have omitted both metals in the final analysis.

We have supposed that reactions are governed by mass-action kinetics and we have used

mass balance analysis to build the system of polynomial differential equations governing the dynamics (see [Sa01] for more details). This is the standard approach in the context of power law formalism. In the literature we did not find information about the quantity of metal ions joined to the proteins, so we have made the assumption of one metal ion by protein in all the equations, but it can be considered as a parameter, that is, we could define q as the number of metal ions joined to a protein and then use the polynomial formalism.

One exception is made for mass action kinetics, which concerns the uptake process. In fact, since the precise mechanism is not known in the case of $Cu(II)$ and $Zn(II)$ or the transporter is not an ABC transporter we adapt the equations to the experimental observation by using ad-hoc functions. In this direction, to mimic the threshold effect (uptake occurs once external concentration overpasses a given range), we use positive sigmoid shaped regulatory functions, satisfying the following properties: (i) $\mathbf{R}_i(0) = 0$; (ii) $\mathbf{R}_i$ is small for concentration lower than a threshold θ_i; (iii) $\mathbf{R}_i$ grows proportionally to the concentration between θ_i and a second threshold θ_i'; and (iv) $\mathbf{R}_i$ saturates for concentrations greater than θ_i'. Typically the function $\mathbf{R}_i$ has the following form:

$$(4.3.1) \qquad\qquad \mathbf{R}_i(x) = \frac{\tau_i x^n}{x^n + \theta_i}$$

where θ_i is the threshold parameter, n corresponds to the cooperative coefficient and τ_i is the saturation constant at high concentrations, $x >> \theta_i$.

In what follows, we will show in details the equations for both modules: Cu/Zn module where regulation is mainly achieved by control of the traffic and efflux of metal ions, and Mn/Fe module where regulation is mainly achieved by the control of uptake and storage of metal ions. We have analyzed separately each of the individual control processes for metal ions following the differential approach, in order to calibrate and find the value of some parameters.

In both modules, Cu/Zn and Mn/Fe, we have assumed an external source of metal ions with concentrations $\sigma_i(t)$, $i = 1, \ldots, 4$, for $Cu(II)$, $Zn(II)$, $Mn(II)$ and $Fe(II)$, respectively. This value corresponds to the derivative of the sum of total intracellular and extracellular metal concentrations. That is, they represent the velocity at which the metal ions from the external source enter into the system (open system) and enrich the medium.

4.3.1 Cu/Zn **resistance module**

Variables and parameters

The module constructed in this subsection has a lot of components, for that reason we use several variables to refer us to each one of them. Before introducing the variables, we define abbreviations of the nomenclature to denote some components.

Let us denote by Cu_{ext} and Zn_{ext} the metal ions available at the extracellular medium, Cu_{int} and Zn_{int} internal free metal ions, and Cu^* and Zn^* the exported metal ions. The variables Cu_{int} and Zn_{int} are unreal because it is not possible to find free copper or zinc inside the cell, however for us they will play the role of storage or internal cellular use.

In the analysis we distinguish two classes of models: (i) class $E(I)$, where extruded metals are not reused. (ii) Class $E(II)$, where recapture of Cu^* and Zn^* is allowed. In class $E(II)$, we simple make a change in the system of differential equations removing the two equations for Cu^* and Zn^*. Other authors use variables with time delay in order to exhibit the previous property.

Table 4.1 summarizes the abbreviations and Table 4.2 introduces the variables x_i used in the construction of the first module:

Table 4.1: Abbreviation in the Cu/Zn module.

Name	Abbreviation	Name	Abbreviation
Internal copper	Cu_{int}	Internal zinc	Zn_{int}
Exported copper	$(Cu)^*$	Exported zinc	$(Zn)^*$
External copper	Cu_{ext}	External zinc	Zn_{ext}
Copper regulator	TD	Copper traffic protein	$YvgX$
Zinc regulator	$ZntR$	Zinc traffic protein	$ZntA$
Chaperone	Ch	Chaperone bound copper	$ChCu$
Chaperone bound zinc	$ChZn$	TD bound copper	$TDCu$
TD bound zinc	$TDZn$	$YvgX$ bound copper	$YvgXCu$
$ZntR$ bound zinc	$ZntRZn$	$ZntA$ bound copper	$ZntACu$
$ZntA$ bound zinc	$ZntAZn$		

The second important part of the module corresponds to the parameters used in the reactions. Degradation rates of the proteins are denoted $\bar{\delta}$, while δ represents degradation rates of the protein-metal complexes. We have affinity reactions constants: K_X between proteins, CC_X from internal free metal to protein X. Finally, for the proteins with unknown regulators we have assumed that it production is proportional to the amount of internal metal ions. For example, the amount of TD is assumed to be auto-regulated in presence of copper.

Table 4.2: Variables for the Cu/Zn module.

Variable	Abbreviation	Variable	Abbreviation
x_1	Cu_{int}	x_2	Zn_{int}
x_3	$ChCu$	x_4	$ChZn$
x_5	$TDCu$	x_6	$TDZn$
x_7	$YvgXCu$	x_8	$ZntRZn$
x_9	$ZntACu$	x_{10}	$ZntAZn$
x_{11}	Ch	x_{12}	TD
x_{13}	$YvgX$	x_{14}	$ZntR$
x_{15}	$ZntA$	x_{16}	$(Cu)^*$
x_{17}	$(Zn)^*$	x_{18}	Cu_{ext}
x_{19}	Zn_{ext}		

In the same way this mechanism is applied to the chaperone protein production Ch and the regulatory proteins TD and $ZntR$.

4.3.2 Cu/Zn module equations

Using the previous scheme we can derive the equations for the model. The reactions involved in the biological model have been constructed. Notice that the dot over the variables means time derivative.

Class $E(I)$

$$
\left.
\begin{array}{rcl}
\dot{x}_{18} & = & \sigma_1(t) - \mathbf{R}_1(x_{18}) \\
\dot{x}_{19} & = & \sigma_2(t) - \mathbf{R}_2(x_{19})
\end{array}
\right\}
\quad
\begin{array}{c}
\text{external copper ions} \\
\text{external zinc ions}
\end{array}
$$

$$
\left.
\begin{array}{rcl}
\dot{x}_{16} & = & \mathbf{R}_3(x_7) + \mathbf{R}_4(x_9) \\
\dot{x}_{17} & = & \mathbf{R}_5(x_{10})
\end{array}
\right\}
\quad \text{extrusion}
$$

$$
\left.
\begin{array}{rcl}
\dot{x}_1 & = & \mathbf{R}_1(x_{18}) + \delta_{Ch}x_3 + \delta_{TD}x_5 + \delta_Y x_7 + \delta_{ZA}x_9 - CC_{Ch}(x_{11} - x_3 - x_4)x_1 \\
\dot{x}_2 & = & \mathbf{R}_2(x_{19}) + \delta_{Ch}x_4 + \delta_{TD}x_6 + \delta_{ZR}x_8 + \delta_{ZA}x_{10} - CC_{Ch}(x_{11} - x_3 - x_4)x_2
\end{array}
\right\}
\quad \text{internal ions}
$$

$$
\left.
\begin{array}{rcl}
\dot{x}_3 & = & CC_{Ch}(x_{11} - x_3 - x_4)x_1 - K_{TD}(x_{12} - x_5 - x_6)x_3 - K_Y(x_{13} - x_7)x_3 \\
& & - K_{ZA}(x_{15} - x_9 - x_{10})x_3 - \delta_{Ch}x_3 \\
\dot{x}_4 & = & CC_{Ch}(x_{11} - x_3 - x_4)x_2 - K_{TD}(x_{12} - x_5 - x_6)x_4 - K_{ZR}(x_{14} - x_8)x_4 \\
& & - K_{ZA}(x_{15} - x_9 - x_{10})x_4 - \delta_{Ch}x_4 \\
\dot{x}_5 & = & K_{TD}(x_{12} - x_5 - x_6)x_3 - \delta_{TD}x_5 \\
\dot{x}_6 & = & K_{TD}(x_{12} - x_5 - x_6)x_4 - \delta_{TD}x_6 \\
\dot{x}_7 & = & K_Y(x_{13} - x_7)x_3 - \mathbf{R}_3(x_7) - \delta_Y x_7 \\
\dot{x}_8 & = & K_{ZR}(x_{14} - x_8)x_4 - \delta_{ZR}x_8 \\
\dot{x}_9 & = & K_{ZA}(x_{15} - x_9 - x_{10})x_3 - \mathbf{R}_4(x_9) - \delta_{ZA}x_9 \\
\dot{x}_{10} & = & K_{ZA}(x_{15} - x_9 - x_{10})x_4 - \mathbf{R}_5(x_{10}) - \delta_{ZA}x_{10}
\end{array}
\right\}
\quad
\begin{array}{l}
\text{transport} \\
\text{and} \\
\text{efflux}
\end{array}
$$

$$
\left.
\begin{array}{rcl}
\dot{x}_{11} & = & \frac{G}{1 + \alpha_1(x_{11} - x_3 - x_4)} + \frac{Ax_5 + Bx_6}{AB + Ax_5 + Bx_6} - \bar{\delta}_{Ch}(x_{11} - x_3 - x_4) - \delta_{Ch}x_3 - \delta_{Ch}x_4 \\
\dot{x}_{12} & = & \frac{G}{1 + \alpha_2(x_{12} - x_5 - x_6)} - \bar{\delta}_{TD}(x_{12} - x_5 - x_6) - \delta_{TD}x_5 - \delta_{TD}x_6 \\
\dot{x}_{13} & = & \frac{Ax_5 + Bx_6}{AB + Ax_5 + Bx_6} - \bar{\delta}_Y(x_{13} - x_7) - \delta_Y x_7 + \mathbf{R}_3(x_7) \\
\dot{x}_{14} & = & \frac{G}{1 + \alpha_3(x_{14} - x_8)} - \bar{\delta}_{ZR}(x_{14} - x_8) - \delta_{ZR}x_8 \\
\dot{x}_{15} & = & \frac{x_8}{\beta + x_8} - \bar{\delta}_{ZA}(x_{15} - x_9 - x_{10}) - \delta_{ZA}x_9 - \delta_{ZA}x_{10} + \mathbf{R}_4(x_9) + \mathbf{R}_5(x_{10})
\end{array}
\right\}
\quad
\begin{array}{l}
\text{protein} \\
\text{generation}
\end{array}
$$

where A, B, G, α_1, α_2, α_3 and β are the constants inside each regulatory function.

Class $E(II)$

Equations $\dot{x}_{16}$ and $\dot{x}_{17}$ are removed and the extruded metal ions are incorporated into the external concentrations as follows:

$$\left. \begin{aligned} \dot{x}_{18} &= \sigma_1(t) - \mathbf{R}_1(x_{18}) + \mathbf{R}_3(x_7) + \mathbf{R}_4(x_9) \\ \dot{x}_{19} &= \sigma_2(t) - \mathbf{R}_2(x_{19}) + \mathbf{R}_5(x_{10}) \end{aligned} \right\} \text{ external ions}$$

The diagram

Figure 4.6 depicts all interactions between proteins, metal ions and genes of the respective module with their abbreviations. In the model we have three genes and five proteins related with the trafficking. Both regulatory proteins, $VNG1179C$ (TD) and $ZntR$, have production rates depending on the amount of free proteins because the exact regulatory mechanism is unknown. Hence, we assume that at high concentrations of free proteins the production is blocked and when the amount of free protein is small we get a basal production.

4.3.3 Mn/Fe resistance module

Variables and parameters

As before, let us denote by Mn_{ext} and Fe_{ext} the metal ions available at the extracellular medium, and Mn_{int} and Fe_{int} the free internal metal ions. As in the Cu/Zn module, here the variables Mn_{int} and Fe_{int} mean internal cellular use or storage.

The module has been divided in two classes: (i) class $U(I)$, where we do not have metal exportation mechanisms, even in a passive way, (ii) class $U(II)$, where we assume metal ions extrusion in a passive way. In the second case, we use regulatory functions with threshold parameters in order to model the unknown mechanism.

We introduce some preliminary notations in the Mn/Fe uptake regulatory mechanism. We will denote by FeR the general ferric uptake regulator, because according to the study there exists different types of regulators, such as $DtxR$ with 68.4% identity in a 19 nucleotides overlap, additionally the protein for the ferric uptake will be denoted by FeU. Table 4.3 summarizes all the abbreviations and Table 4.4 defines the variables, with their corresponding names, used in the construction of the second module.

For consistency between the modules we have assumed the same parameters for degradations, affinity reactions constants and reversible reactions with DNA.
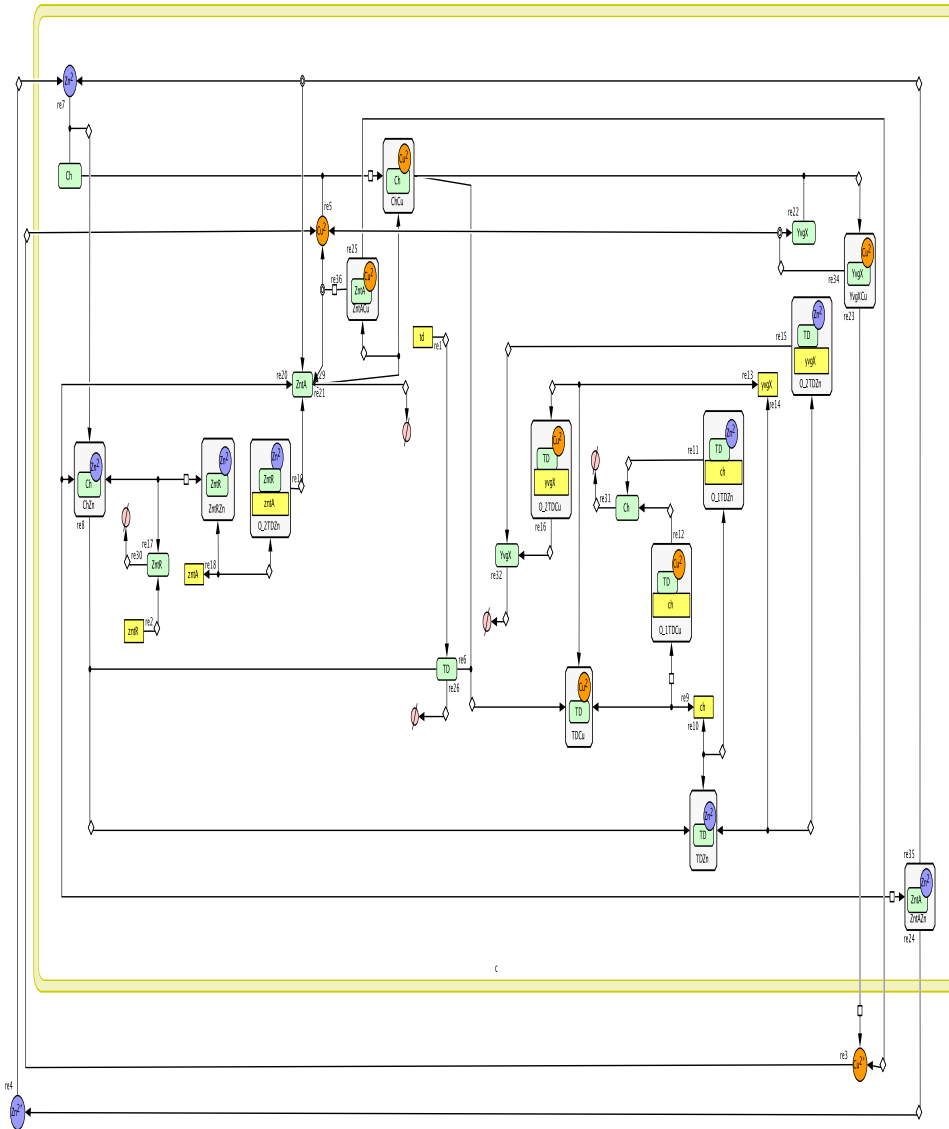
Figure 4.6: Complete module for the Cu/Zn traffic and efflux mechanism. To draw the biological network we use CellDesigner (Kitano et al. [K07]) for the graphical representation. In the picture, the yellow squares represent the genes, the blue squares represent the proteins and the white squares represent the intermediary interactions such as, protein-protein, protein-ion or protein joined to regulatory sites. Meanwhile in circles have been represented the metal ions, and the yellow line represents the limit between extracellular and intracellular environments.

Table 4.3: Abbreviation in the Mn/Fe module.

Name	Abbreviation	Name	Abbreviation
Internal manganese	Mn_{int}	Internal iron	Fe_{int}
External manganese	Mn_{ext}	External iron	Fe_{ext}
Mn uptake protein	$ZurA$	protein regulator	$SirR$
Fe detoxification	$DpsA$	Fe uptake protein	FeU
protein regulator	FeR	$ZurA$ bound manganese	$ZurAMn$
FeU bound iron	$FeUFe$	$SirR$ bound manganese	$SirRMn$
$SirR$ bound iron	$SirRFe$	FeR bound manganese	$FeRMn$
FeR bound iron	$FeRFe$	$DpsA$ bound iron	$DspAFe$

Table 4.4: Variables for the Mn/Fe module

Variable	Name	Variable	Name
x_1	Mn_{int}	x_2	Fe_{int}
x_3	$ZurAMn$	x_4	$FeUFe$
x_5	$SirRMn$	x_6	$SirRFe$
x_7	$FeRMn$	x_8	$FeRFe$
x_9	$DspAFe$	x_{10}	$ZurA$
x_{11}	$SirR$	x_{12}	$DpsA$
x_{13}	FeU	x_{14}	FeR
x_{15}	Mn_{ext}	x_{16}	Fe_{ext}

4.3.4 Mn/Fe module equations

Class $U(I)$

$$\left.\begin{array}{rcl}
\dot{x_{15}} &=& \sigma_3(t) - K_{ZA}(x_{10} - x_3)x_{15} \\
\dot{x_{16}} &=& \sigma_4(t) - K_{FU}(x_{13} - x_4)x_{16}
\end{array}\right\} \quad \begin{array}{c} \text{external manganese ions} \\ \text{external ferric ions} \end{array}$$

$$\left.\begin{array}{rcl}
\dot{x}_1 &=& D_{ZA}x_3 + \delta_{ZA}x_3 + \delta_{SR}x_5 + \delta_{FR}x_7 \\
&-& CC_{SR}(x_{11} - x_5 - x_6)x_1 - CC_{FR}(x_{14} - x_7 - x_8)x_1 \\
\dot{x}_2 &=& D_{FU}x_4 + \delta_{FU}x_4 + \delta_{SR}x_6 + \delta_{FR}x_8 + \delta_{DA}x_9 \\
&-& CC_{SR}(x_{11} - x_5 - x_6)x_2 - CC_{FR}(x_{14} - x_7 - x_8)x_2 - CC_{DA}(x_{12} - x_9)x_2
\end{array}\right\} \quad \text{internal ions}$$

$$\left.\begin{array}{rcl}
\dot{x}_3 &=& K_{ZA}(x_{10} - x_3)x_{15} - \delta_{ZA}x_3 - D_{ZA}x_3 \\
\dot{x}_4 &=& K_{FU}(x_{13} - x_4)x_{16} - \delta_{FU}x_4 - D_{FU}x_4
\end{array}\right\} \quad \text{uptake}$$

$$\left.\begin{array}{rcl}
\dot{x}_5 &=& CC_{SR}(x_{11} - x_5 - x_6)x_1 - \delta_{SR}x_5 \\
\dot{x}_6 &=& CC_{SR}(x_{11} - x_5 - x_6)x_2 - \delta_{SR}x_6 \\
\dot{x}_7 &=& CC_{FR}(x_{14} - x_7 - x_8)x_1 - \delta_{FR}x_7 \\
\dot{x}_8 &=& CC_{FR}(x_{14} - x_7 - x_8)x_2 - \delta_{FR}x_8 \\
\dot{x}_9 &=& CC_{DA}(x_{12} - x_9)x_2 - \delta_{DA}x_9
\end{array}\right\} \quad \begin{array}{l} \text{transport} \\ \text{and} \\ \text{efflux} \end{array}$$

$$
\begin{aligned}
\dot{x}_{10} &= \frac{G}{1+\gamma_1(x_{11}-x_5-x_6)} - \bar{\delta}_{ZA}(x_{10}-x_3) - \delta_{ZA}x_3 \\
\dot{x}_{11} &= \frac{G}{1+\gamma_2(x_{11}-x_5-x_6)} - \bar{\delta}_{SR}(x_{11}-x_5-x_6) - \delta_{SR}x_5 - \delta_{SR}x_6 \\
\dot{x}_{12} &= \frac{C_1}{1+x_7} + \frac{x_8}{A_1+x_8} - \bar{\delta}_{DA}(x_{12}-x_9) - \delta_{DA}x_9 \\
\dot{x}_{13} &= \frac{x_7}{A_2+x_7} - \bar{\delta}_{FU}(x_{13}-x_4) - \delta_{FU}x_4 \\
\dot{x}_{14} &= \frac{G}{1+\alpha(x_{14}-x_7-x_8)} - \bar{\delta}_{FR}(x_{14}-x_7-x_8) - \delta_{FR}x_7 - \delta_{FR}x_8
\end{aligned} \Bigg\} \text{ protein generation}
$$

Class $U(II)$

Equations $\dot{x}_{15}$ and $\dot{x}_{16}$ are modified with the incorporation of regulatory functions for the extruded metal ions in a passive way.

$$
\begin{aligned}
\dot{x}_{15} &= \sigma_3(t) + \mathbf{R}_6(x_1) - K_{ZA}(x_{10}-x_3)x_{15} \\
\dot{x}_{16} &= \sigma_4(t) + \mathbf{R}_7(x_2) - K_{FU}(x_{13}-x_4)x_{16}
\end{aligned} \Bigg\} \text{ external ions}
$$

$$
\begin{aligned}
\dot{x}_1 &= -\mathbf{R}_6(x_1) + D_{ZA}x_3 + \delta_{ZA}x_3 + \delta_{SR}x_5 + \delta_{FR}x_7 \\
&\quad - CC_{SR}(x_{11}-x_5-x_6)x_1 - CC_{FR}(x_{14}-x_7-x_8)x_1 \\
\dot{x}_2 &= -\mathbf{R}_7(x_2) + D_{FU}x_4 + \delta_{FU}x_4 + \delta_{SR}x_6 + \delta_{FR}x_8 + \delta_{DA}x_9 \\
&\quad - CC_{SR}(x_{11}-x_5-x_6)x_2 - CC_{FR}(x_{14}-x_7-x_8)x_2 - CC_{DA}(x_{12}-x_9)x_2
\end{aligned} \Bigg\} \text{ internal ions}
$$

The diagram

Figure 4.7 depicts the interaction network for the Mn/Fe module. We put all the interactions between the protein and the metal ions, including these among the intermediary compounds. In the model we can see the double negative circuit for $SirR$ and $ZurA$, and the storage regulation mechanism by $DpsA$ protein.
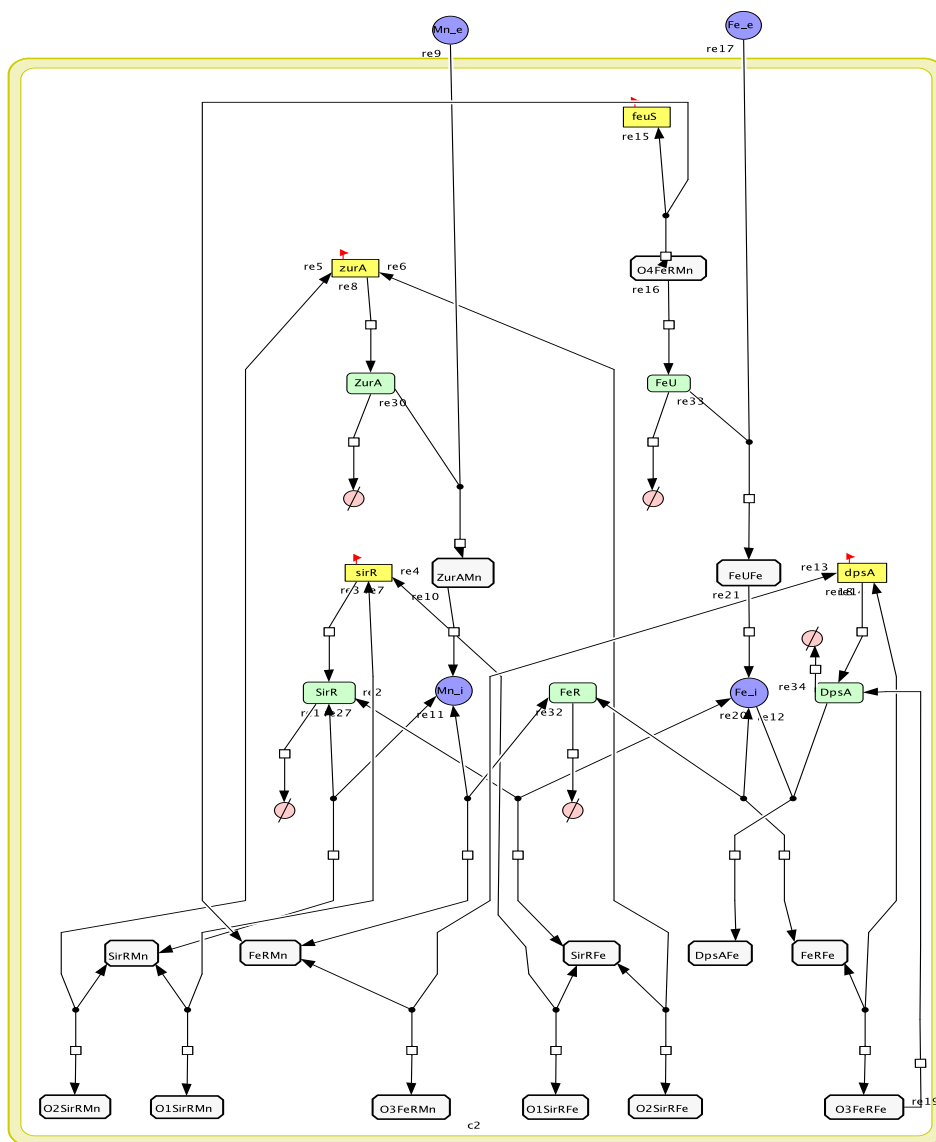
Figure 4.7: Complete module for Mn/Fe uptake mechanism. We use the same box notation to denote the genes, proteins and intermediary states as in Figure 4.6

4.4 Mathematical analysis

One of the advantages of the differential approach is that there exists a mathematical machinery to prove biological properties like existence of equilibrium states, convergence and homeostasis. In fact, the cellular metal resistance to external stress is a phenomenon of "equilibrium" in which the cellular growth and death are involved.

In Section 4.3 we have constructed two modules for the metal stress response in *Halobacterium NRC-1*, one dealing with the extrusion and the other with the uptake of metal ions, with more than 50 differential equations. In what follows, we use both modules in order to deduce mathematical properties that improve biological knowledge. This will be discussed later in Sections 4.6 and 4.7.

4.4.1 Steady state analysis

The steady state analysis consists in determining the existence of equilibrium states. In Chapter 2, we have defined different types of attractors in the continuous and discrete framework. It is important from the biological point of view to know in which parameters the stable state depends, especially to analyze the homeostatic behavior, which allows to understand how the equilibrium state evolves when some parameters like the external metal concentrations change.

Because we are concerned with steady states, we analyze the case when there is no external source of metal, that is $\sigma_i(t) = 0$, $i = 1, \ldots, 4$, for all time $t > 0$. So, we have a constant amount of metals introduced at time $t = 0$.

Suppose we have the following system of differential equations $\dot{x} = F(x)$. The steady states are the points $\bar{x}$ where all the derivatives are zero, that is $F(\bar{x}) = 0$. Since we have divided the complete model into two modules and each module in two classes, we have made the analysis for each one separately.

Cu/Zn **module:**

1. **Class $E(I)$:**

   From the first two equations (external ions) we get that the amount of extracellular metal ions, $x_{18} = Cu_{ext}$ and $x_{19} = Zn_{ext}$, are zero because the form of functions

describing the trajectories of the metal ions in 4.3.1.

Let C_{int} be the total amount of internal copper ions, i.e. the sum of internal free copper with the copper bound to the different proteins. In our case, the expression for this quantity is $C_{int} = Cu_{int} + ChCu + TDCu + YvgXCu + ZntACu$. Using the corresponding equations, we can conclude that the derivative for the total intracellular copper is:

(4.4.1)
$$\dot{C_{int}} = \mathbf{R}_1(x_{18}) - \mathbf{R}_3(x_7) - \mathbf{R}_4(x_9).$$

At the equilibrium, the previous equation will be zero. However, we know that $Cu_{ext} = x_{18} = 0$ and since the regulatory functions are positive, we get that the unique possibility at steady state will be $x_7 = x_9 = 0$.

Using the same arguments we can define $Z_{int} = Zn_{int} + ChZn + TDZn + ZntRZn + ZntAZn$, the intracellular free zinc plus protein-ion compounds, and we have

(4.4.2)
$$\dot{Z_{int}} = \mathbf{R}_2(x_{19}) - \mathbf{R}_5(x_{10}),$$

which is equal to zero at the equilibrium, concluding that $x_{10} = 0$.

Equation $\dot{x}_7 = 0$ reads:

$$K_Y(x_{13} - x_7)x_3 - \mathbf{R}_3(x_7) - \delta_Y x_7 = 0$$

which implies $x_3 = 0$ or $x_{13} = 0$. In the same way equations $\dot{x}_9 = 0$ and $\dot{x}_{10} = 0$ read:

$$K_{ZA}(x_{15} - x_9 - x_{10})x_3 - \mathbf{R}_4(x_9) - \delta_{ZA}x_9 = 0$$

which implies $x_3 = 0$ or $x_{15} = 0$, and $\dot{x}_{10} = 0$ leads to

$$K_{ZA}(x_{15} - x_9 - x_{10})x_4 - \mathbf{R}_5(x_{10}) - \delta_{ZA}x_{10} = 0$$

which implies $x_4 = 0$ or $x_{15} = 0$. Let us examine all different possibilities.

a) If $YvgX = x_{13} = 0$. By equation $\dot{x}_{13} = 0$, it follows that

$$\frac{Ax_5 + Bx_6}{AB + Ax_5 + Bx_6} = 0,$$

then we deduce that $x_5 = x_6 = 0$, since $A, B > 0$. From equation $\dot{x}_{12} = 0$, we get immediately that x_{12} is the positive solution of a second degree polynomial $\alpha_2 \bar{\delta}_{TD} x_{12}^2 + \bar{\delta}_{TD} x_{12} - G = 0$, whose solution is

$$x_{12} = \frac{-\delta_{TD} + \sqrt{\bar{\delta}_{TD}^2 + 4G\alpha_2\bar{\delta}_{TD}}}{2\alpha_2\bar{\delta}_{TD}} > 0,$$

because all the constants are positive.

On the other hand, equation $\dot{x}_5 = 0$ implies $x_3 = 0$. Equally, $\dot{x}_6 = 0$ gives $x_4 = 0$. We conclude from equation $\dot{x}_{11} = 0$ that x_{11} is the positive solution of a second degree polynomial $\alpha_1 \bar{\delta}_{Ch} x_{11}^2 + \bar{\delta}_{Ch} x_{11} - G = 0$, whose solution is

$$x_{11} = \frac{-\bar{\delta}_{Ch} + \sqrt{\bar{\delta}_{Ch}^2 + 4G\alpha_1\bar{\delta}_{Ch}}}{2\alpha_1\bar{\delta}_{Ch}} > 0.$$

As $x_4 = 0$, we easily derive that $x_8 = 0$ and as we have done before from $\dot{x}_{14} = 0$

$$x_{14} = \frac{-\bar{\delta}_{ZR} + \sqrt{\bar{\delta}_{ZR}^2 + 4G\alpha_3\bar{\delta}_{ZR}}}{2\alpha_3\bar{\delta}_{ZR}} > 0.$$

From equation $\dot{x}_3 = 0$ we obtain $x_1 = 0$ and, in parallel, $x_2 = 0$ since $x_{11} \neq 0$. Finally, we get $x_{15} = 0$, and $x_{16} = Cu^*$ and $x_{17} = Zn^*$ (external amount of extruded copper and zinc) are constant and equal to the initial external amount of metal ions $\tilde{C}u$ and $\tilde{Z}n$, respectively.

b) If $x_{13} \neq 0$, then $x_3 = 0$. Using equation $\dot{x}_5 = 0$, we find $x_5 = 0$.

- *First step:* Using the last five equations, we express x_{11}, x_{12}, x_{13}, x_{14} and x_{15} in terms of the other variables. We find:

$$x_{15} = \frac{1}{\bar{\delta}_{ZA}} \frac{x_8}{\beta + x_8}; \quad x_{13} = \frac{1}{\bar{\delta}_Y} \frac{x_6}{A + x_6};$$

$$x_{14} = \frac{-(\bar{\delta}_{ZR} + \alpha_3\delta_{ZR}x_8) + \sqrt{(\bar{\delta}_{ZR} + \alpha_3\delta_{ZR}x_8)^2 + 4\alpha_3\bar{\delta}_{ZR}[(\bar{\delta}_{ZR} - \delta_{ZR})x_8 + (\delta_{ZR} - \bar{\delta}_{ZR})\alpha_3 x_8^2 + G]}}{2\alpha_3\bar{\delta}_{ZR}}$$

$$x_{12} = \frac{-(\bar{\delta}_{TD} + \alpha_2 \delta_{TD} x_6) + \sqrt{(\bar{\delta}_{TD} + \alpha_2 \delta_{TD} x_6)^2 + 4\alpha_2 \bar{\delta}_{TD}[(\bar{\delta}_{TD} - \delta_{TD})x_6 + (\delta_{TD} - \bar{\delta}_{TD})\alpha_2 x_6^2 + G]}}{2\alpha_2 \bar{\delta}_{TD}}$$

$$G - \left[-\frac{x_6}{A + x_6} + \bar{\delta}_{Ch}(x_{11} - x_4) + \delta_{Ch} x_4 \right](1 + \alpha_1(x_{11} - x_4)) = 0$$

- *Last step:* The only non trivial remaining equations are $\dot{x}_1 = \dot{x}_2 = \dot{x}_4 = \dot{x}_6 = \dot{x}_8 = 0$. Equation $\dot{x}_1 = 0$ gives $x_1 = 0$ or $x_{11} = x_4$. But if the second option holds, then, by equation $\dot{x}_2 = 0$, we have $x_4 = x_6 = x_8 = 0$ and consequently $x_{13} = 0$, which is excluded. Thus $x_1 = 0$.

  The next four equations are not independent and they have the following form:

  $$
  \begin{aligned}
  0 &= \delta_{CH} x_4 + \delta_{TD} x_6 + \delta_{ZR} x_8 - CC_{Ch}(x_{11} - x_4)x_2 \\
  0 &= CC_{Ch}(x_{11} - x_4)x_2 - K_{TD}(x_{12} - x_6)x_4 - K_{ZR}(x_{14} - x_8)x_4 - K_{ZA} x_{15} x_4 - \delta_{Ch} x_4 \\
  0 &= K_{TD}(x_{12} - x_6)x_4 - \delta_{TD} x_6 \\
  0 &= K_{ZR}(x_{14} - x_8)x_4 - \delta_{ZR} x_8,
  \end{aligned}
  $$

  and if we sum them we obtain that $K_{ZA} x_{15} x_4 = 0$, which implies either that $x_{15} = 0$ or $x_4 = 0$.

  If $x_4 = 0$, then from $\dot{x}_8 = 0$ we get that $x_8 = 0$. Additionally, since $x_7 = x_9 = x_{10} = 0$, from $\dot{x}_{15} = 0$ we have that $x_{15} = 0$.

  In the other case, if $x_{15} = 0$ again from $\dot{x}_{15} = 0$ we get that $x_8 = 0$, and as $x_{14} = YvgX \neq 0$ from $\dot{x}_8 = 0$ we have that $x_4 = 0$. Hence, whatever the case, the only possible solutions are $x_6 = 0$, because $x_{12} = TD \neq 0$, $x_8 = 0$ and $x_{13} = 0$.

  $\square$

Proposition 4.4.1. *The class $E(I)$ for the Cu/Zn module admits a unique equilibrium state. In this state, all concentrations are zero, except the variables for proteins with basal rate production (Ch) or with unknown regulator (TD, ZntR):*

$$Ch = x_{11} = \frac{-1 + \sqrt{1 + \frac{4G\alpha_1}{\delta_{Ch}}}}{2\alpha_1} > 0,$$

$$TD = x_{12} = \frac{-1 + \sqrt{1 + \frac{4G\alpha_2}{\bar{\delta}_{TD}}}}{2\alpha_2} > 0,$$

$$ZntR = x_{14} = \frac{-1 + \sqrt{1 + \frac{4G\alpha_3}{\bar{\delta}_{ZR}}}}{2\alpha_3} > 0,$$

where all the constants $\alpha_1, \alpha_2, \alpha_3, \delta, \bar{\delta}$ and G are positive.

Additionally, since $C_{int} + x_{16} + x_{18} = \tilde{C}u$ and $Z_{int} + x_{17} + x_{19} = \tilde{Z}n$, we have that the external amount of extruded metal ions, $x_{16} = \tilde{C}u$ and $x_{17} = \tilde{Z}n$, where $\tilde{C}u = Cu_{ext}(0)$ and $\tilde{Z}n = Zn_{ext}(0)$, respectively.

Observation 4.4.2. *One of the consequences of Proposition 4.4.1 is that at steady state the Cu/Zn module maintains the chaperone Ch and regulatory proteins, TD and $ZntR$, in a basal concentration different from zero, which can be understood as a form to be prepared for another "cycle". This is useful for the archaea when it is submitted to different pulses of external metal ions (stress condition), as we can observe in Section 4.6, Figure 4.25.*

Observation 4.4.3. *In the case when the constant value σ_1 is different from zero the homeostatic condition $\dot{C}_{int} = 0$ cannot be verified with an equilibrium at the interior of the cell. That is, in order to satisfy the equation $\dot{C}_{int} = 0$, it must be kept a movement of metal ions inside the cell. Result that could be interesting from the biological point of view.*

Observation 4.4.4. *Continuing with the equation $\dot{C}_{int} = 0$, and using $x_{18} = 0$ with σ_1 constant but different from zero, we deduce the following equation $\sigma_1 = \mathbf{R}_3(x_7) + \mathbf{R}_4(x_9) = \frac{\tau_3 x_7^n}{\theta_3 + x_7^n} + \frac{\tau_4 x_9^n}{\theta_4 + x_9^n}$. A necessary condition for the existence of a solution is that $0 \leq \sigma_1 \leq \tau_3 + \tau_4$, because the regulatory functions $\mathbf{R}_3$ and $\mathbf{R}_4$ are limited by the constants τ_3 and τ_4, respectively. Hence, the idea of extremal homeostatic capabilities of the system can be explored.*

Class $E(II)$:

Unlike the previous analysis, in this case we can only deduce from equations $\dot{x}_{18} = 0$ and $\dot{x}_{19} = 0$ that there exist solutions, different from zero, for the variables x_{18}, x_{19}, x_7, x_9 and x_{10}. For these variables the steady state can be obtained numerically and only depends on the external amount of metal ions, i.e.

(4.4.3) $$x_7 = f_7(x_{18}), \quad x_9 = f_9(x_{18}), \quad x_{10} = f_{10}(x_{19}).corcho$$

However, we can reduce significantly the difficulty of the above problem assuming that the regulatory functions $\mathbf{R}_i(\cdot)$ are linear functions depending on some threshold parameter, that

is:

$$\mathbf{R}_i(x) = \frac{\tau_i x^n}{\theta_i + x^n} \sim \begin{cases} \tau_i & \text{if } x \geq \theta_i \\ \frac{\tau_i}{\theta_i} x & \text{if } x < \theta_i \end{cases},$$

where θ_i is the constant threshold parameter and τ_i is the saturation constant for high concentrations, $x >> \theta_i$. This simplification seems natural if we assume that the extruded metal ions need to be proportional to the concentration of the protein-ion complex $YvgXCu$, $ZntACu$ or $ZntAZn$.

Under the previous assumption we get the following regulatory functions at small concentrations:

$$\mathbf{R}_1(x_{18}) = \frac{\tau_1}{\theta_1} x_{18}, \ \mathbf{R}_2(x_{19}) = \frac{\tau_2}{\theta_2} x_{19},$$

$$\mathbf{R}_3(x_7) = \frac{\tau_3}{\theta_3} x_7, \ \mathbf{R}_4(x_9) = \frac{\tau_4}{\theta_4} x_9 \text{ and } \mathbf{R}_5(x_{10}) = \frac{\tau_5}{\theta_5} x_{10},$$

which are replaced in eqs. x_{18} and x_{19}. We get:

(4.4.4)
$$\dot{x}_{18} = -\frac{\tau_1}{\theta_1} x_{18} + \frac{\tau_3}{\theta_3} x_7 + \frac{\tau_4}{\theta_4} x_9 = 0$$

and

(4.4.5)
$$\dot{x}_{19} = -\frac{\tau_2}{\theta_2} x_{19} + \frac{\tau_5}{\theta_5} x_{10} = 0.$$

Meanwhile, at high concentrations we found the following restrictions between the saturation constants:

$$-\tau_1 + \tau_3 + \tau_4 = 0$$

and

$$-\tau_2 + \tau_5 = 0.$$

In what follows we compute the value for the other variables. We first define the artificial variables $C_{int} = Cu_{int} + ChCu + TDCu + YvgXCu + ZntACu$ and $Z_{int} = Zn_{int} + ChZn + TDZn + ZntRZn + ZntAZn$ for the total amount of intracellular copper and zinc, respectively. From equations (4.4.8) and (4.4.2) we can deduce the existence of two conservation equations where the following relations for x_{18} and x_{19} are satisfied:

(4.4.6)
$$C_{int} + x_{18} = Cu_{ext}(0) = \tilde{C}u,$$
(4.4.7)
$$Z_{int} + x_{19} = Zn_{ext}(0) = \tilde{Z}n$$

where the constants $\tilde{C}u$ and $\tilde{Z}n$ correspond to the initial external condition for copper and zinc, respectively.

Now, we proceed to deduce the values for x_5 and x_6. It is not hard to see that the expression $x_4\dot{x}_5 - x_3\dot{x}_6 = 0$ gives us the relation

(4.4.8)
$$\frac{x_5}{x_6} = \frac{x_3}{x_4} = C,$$

where C is a constant. So, we have that $x_5 = Cx_6$ and $x_3 = Cx_4$.

From $\dot{x}_5 = 0$ we get that

$$(x_{12} - x_3 - x_4) = \frac{\delta_{TD}x_5}{K_{TD}x_3},$$

and if we replace this value in $\dot{x}_{17} = 0$ we deduce that x_5 is the positive real solution of a second degree polynomial

$$-G + \left(\frac{\bar{\delta}_{TD}\delta_{TD}}{K_{TD}x_3} + \delta_{TD}(1 + \frac{1}{C})\right)x_5 + \left(\frac{\bar{\delta}_{TD}\delta_{TD}}{K_{TD}x_3} + \delta_{TD}(1 + \frac{1}{C})\right)\frac{\alpha_2\delta_{TD}}{K_{TD}x_3}x_5^2 = 0,$$

concluding that

$$x_5 = \frac{K_{TD}x_3}{2\alpha_2\delta_{TD}}\left\{-1 + \sqrt{1 + \frac{4G\alpha_2}{\bar{\delta}_{TD} + K_{TD}x_3(1 + \frac{1}{C})}}\right\} > 0.$$

In the same form, we can compute x_6 as the positive real solution of a second degree polynomial depending on x_4, concluding that

$$x_6 = \frac{K_{TD}x_4}{2\alpha_2\delta_{TD}}\left\{-1 + \sqrt{1 + \frac{4G\alpha_2}{\bar{\delta}_{TD} + K_{TD}x_4(1 + C)}}\right\} > 0,$$

where G is the constant inside the regulatory function used for protein with unknown regulation and basal concentration.

The expression $x_4\dot{x}_9 - x_3\dot{x}_{10} = 0$ gives the equation:

$$x_3\mathbf{R}_5(x_{10}) + \delta_{ZA}x_3x_{10} = x_4\mathbf{R}_4(x_9) + \delta_{ZA}x_4x_9.$$

However, since $\frac{x_3}{x_4} = C$, we conclude the following identity between x_9 and x_{10}

$$C = \frac{\mathbf{R}_4(x_9) + \delta_{ZA}x_9}{\mathbf{R}_5(x_{10}) + \delta_{ZA}x_{10}}.$$

The last expression can be simplified if we assume the reduction for the regulatory functions

at small or high concentrations. In this way, we can obtain that

(4.4.9)
$$C = \left(\frac{\frac{\tau_4}{\theta_4} + \delta_{ZA}}{\frac{\tau_5}{\theta_5} + \delta_{ZA}} \right) \frac{x_9}{x_{10}}$$

or

(4.4.10)
$$C = \frac{\tau_4 + \delta_{ZA} x_9}{\tau_5 + \delta_{ZA} x_{10}},$$

respectively.

In order to obtain an expression for x_9 and x_{10} from equation $\dot{x}_{15} = 0$ we first need an explicit formula for x_8. As we have done before, from equation $\dot{x}_8 = 0$ we have that

$$(x_{14} - x_8) = \frac{\delta_{ZR} x_8}{K_{ZR} x_4},$$

and from $\dot{x}_{14} = 0$ we conclude that x_8 is the positive real solution of the following second degree polynomial

$$-G + \left(\frac{\bar{\delta}_{ZR} \delta_{ZR}}{K_{ZR} x_4} + \delta_{ZR} \right) x_8 + \left(\frac{\bar{\delta}_{ZR} \delta_{ZR}}{K_{ZR} x_4} + \delta_{ZR} \right) \frac{\alpha_3 \delta_{ZR}}{K_{ZR} x_4} x_8^2 = 0.$$

That is,

$$x_8 = \frac{K_{ZR} x_4}{2\alpha_3 \delta_{ZR}} \left\{ -1 + \sqrt{1 + \frac{4G\alpha_3}{\bar{\delta}_{ZR} + K_{ZR} x_4}} \right\} > 0.$$

Now, we return over x_9 and x_{10}. From equation (4.4.9) for small concentrations we get that

$$x_{10} = \frac{x_9 \left(\frac{\tau_4}{\theta_4} + \delta_{ZA} \right)}{C \left(\frac{\tau_5}{\theta_5} + \delta_{ZA} \right)}.$$

Moreover, from $\dot{x}_9 = 0$ we deduce that $(x_{15} - x_9 - x_{10}) = \frac{\mathbf{R}_4(x_9) + \delta_{ZA} x_9}{K_{ZA} x_3}$, and using $\dot{x}_{15} = 0$ we obtain that

$$x_9 = \frac{\frac{x_8}{\beta + x_8}}{\frac{\bar{\delta}_{ZA} \left(\frac{\tau_4}{\theta_4} + \delta_{ZA} \right)}{K_{ZA} x_3} + \left(\delta_{ZA} - \frac{\tau_4}{\theta_4} \right) + \frac{\left(\frac{\tau_5}{\theta_5} - \delta_{ZA} \right) \left(\frac{\tau_4}{\theta_4} + \delta_{ZA} \right)}{C \left(\frac{\tau_5}{\theta_5} + \delta_{ZA} \right)}}.$$

From equation $\dot{x}_7 = 0$ we have that

$$(x_{13} - x_7) = \frac{\left(\frac{\tau_3}{\theta_3} + \delta_Y \right) x_7}{K_Y x_3},$$

and replacing this value in $\dot{x}_{13} = 0$ we get a polynomial expression for x_7, that is

$$x_7 = \left(\frac{(A + \frac{B}{C})x_5}{AB + (A + \frac{B}{C})x_5} \right) \left(\frac{K_Y x_3}{\bar{\delta}_Y(\frac{\tau_3}{\theta_3} + \delta_Y + (\delta_Y - \frac{\tau_3}{\theta_3})K_Y x_3)} \right)$$

At this point, it is important to note that all the other variables depend exclusively on x_3 and x_4.

Finally from the last equations, $\dot{x}_{12} = 0$ to $\dot{x}_{15} = 0$, we can deduce that

$$x_{12} = x_3 \left(1 + \frac{1}{C} \right) + \frac{1}{2\alpha_2} \left\{ -1 + \sqrt{1 + \frac{4G\alpha_2}{\bar{\delta}_{TD} + K_{TD}x_3(1 + \frac{1}{C})}} \right\},$$

$$x_{13} = x_7 + \frac{(\frac{\tau_3}{\theta_3} + \delta_Y)x_7}{x_3},$$

$$x_{14} = x_8 + \frac{\delta_{ZR}x_8}{K_{ZR}x_4},$$

$$x_{15} = \frac{x_8}{\beta + x_8} + (\bar{\delta}_{ZA} - \delta_{ZA})(x_9 + x_{10}) + \frac{\tau_4}{\theta_4}x_9 + \frac{\tau_5}{\theta_5}x_{10},$$

and from equation $\dot{x}_{11} = 0$, the variable x_{11} is the positive real solution of the following polynomial

$$\frac{G}{1 + \alpha_1(x_{11} - (1 + \frac{1}{C})x_3)} + \frac{(A + \frac{B}{C})x_5}{AB + (A + \frac{B}{C})x_5} - \bar{\delta}_{Ch}(x_{11} - (1 + \frac{1}{C})x_3) - \delta_{Ch}(1 + \frac{1}{C})x_3 = 0,$$

where G, A, B are constants inside the regulatory functions with unknown regulator and C is the constant defined in (4.4.8).

Using all the previous results it is possible to obtain the value of x_1 and x_2 in terms of the external metal ions concentrations.

$$x_1 = \frac{\bar{\delta}_{Ch} \left(\frac{\tau_1}{\theta_1}x_{18} + \delta_{Ch}x_3 + \delta_{TD}x_5 + \delta_Y x_7 + \delta_{ZA}x_9 \right)}{CC_{Ch}(x_{11} - \delta_{Ch}(1 + C)x_3)},$$

$$x_2 = \frac{\bar{\delta}_{Ch} \left(\frac{\tau_2}{\theta_2}x_{19} + \delta_{Ch}x_4 + \delta_{TD}x_6 + \delta_{ZR}x_8 + \delta_{ZA}x_{10} \right)}{CC_{Ch}(x_{11} - \delta_{Ch}(1 + \frac{1}{C})x_4)}.$$

However, as we have seen before C_{int} and Z_{int} are calculated as the sum of all internal

complexes with copper and zinc. Hence, we can rewrite

$$C_{int} = \sum_{i=0}^{3} x_{2i+1} = \sum_{i=0}^{6} f_{2i+1}(x_{18}, x_{19}),$$

$$Z_{int} = \sum_{i=1}^{4} x_{2i} = \sum_{i=1}^{7} f_{2i}(x_{18}, x_{19}),$$

where the functions f_i correspond to the expressions, previously calculated, for the variables depending on x_{18} and x_{19}. These last two expressions imply that we can find the values of x_{18} and x_{19} as the solution of a polynomial system of two equations as follows

$$\begin{cases} x_{18} & + & \sum_{i=0}^{4} f_{2i+1}(x_{18}, x_{19}) & = & \tilde{C}u \\ x_{19} & + & \sum_{i=1}^{5} f_{2i}(x_{18}, x_{19}) & = & \tilde{Z}n \end{cases}$$

As a conclusion we obtain the existence of a finite number of equilibriums depending on $\tilde{C}u$ and $\tilde{Z}n$, initial external condition of metal ions concentration, which correspond to the positive real solutions of the above system. Summarizing we have the following proposition:

Proposition 4.4.5. *The class $E(II)$ for the Cu/Zn module satisfies:*

1. *At the equilibrium, x_{18} and x_{19} correspond to the positive real solutions of the following polynomial system:*

$$\begin{cases} x_{18} & + & \sum_{i=0}^{3} f_{2i+1}(x_{18}, x_{19}) & = & \tilde{C}u \\ x_{19} & + & \sum_{i=1}^{4} f_{2i}(x_{18}, x_{19}) & = & \tilde{Z}n \end{cases},$$

   where $\tilde{C}u$ and $\tilde{Z}n$ correspond to the initial external conditions for metal ions of copper and zinc, respectively, and the functions $f_i(\cdot, \cdot)$ correspond to the expressions for the other variables depending on x_{18} and x_{19}.

2. *For each couple of values of the initial external metal ions concentrations for copper and zinc ($\tilde{C}u$ and $\tilde{Z}n$) there exists a finite number of possible equilibrium states.*

Observation 4.4.6. *From the last proposition we conclude that the number of steady states is finite and that eventually, depending on the real parameters, is unique.*

Observation 4.4.7. *In Figures 4.22 and 4.23 we can observe that the trajectories converge to the stationary state depending on the initial external condition.*

Mn/Fe **module:**

1. **Class $U(I)$:**

   The analysis for the Mn/Fe module is different because of the nature of the differential equations. As we have done before in the steady state analysis for the Cu/Zn module, we take the first two equations, $\dot{x}_{15}$ and $\dot{x}_{16}$, for the external amount of manganese and iron ions respectively. So, at the steady state we conclude that $x_{15} = 0$ or $x_{10} = x_3$ and $x_{16} = 0$ or $x_{13} = x_4$.

   Independently of the previous case, from the equations $\dot{x}_3 = 0$ and $\dot{x}_4 = 0$ we conclude that the values of x_3 and x_4 are also zero.

   Since $x_3 = x_4 = 0$ the solutions $x_{10} = x_3$ and $x_{13} = x_4$ both zero are not allowed. In fact, from equations $\dot{x}_{10} = 0$ the unique possibility would be that the constant $G = 0$ and from equations $\dot{x}_{13} = 0$ we could conclude that $x_7 = 0$ which implies from $\dot{x}_7 = 0$ that $x_{14} = x_8$ (because we assume that $x_1 \neq 0$), and combined with $\dot{x}_8 = 0$ we conclude that $x_8 = x_{14} = 0$, concluding as before from $\dot{x}_{14} = 0$ that the unique possibility would be constant $G = 0$. For that reason, in what follows we will assume that $x_{10}x_3 = 0$ and $x_{13} \neq x_4 = 0$.

   As we have done before in the analysis of steady states for the Cu/Zn module, we define the total amount of intracellular manganese, denoted by M_{int}, as the sum of Mn_{int} (free manganese), $ZurAMn$, $SirRMn$ and $FeRMn$. That is, in terms of the variables we have that $M_{int} = x_1 + x_3 + x_5 + x_7$ and we obtain that:

   $$(4.4.11) \qquad \dot{M}_{int} = K_{ZA}(x_{10} - x_3)x_{15} = -\dot{x}_{15}.$$

   Hence, we deduce that the total amount of intracellular manganese plus the total amount of extracellular manganese will be constant:

   $$M_{int} + x_{15} = Mn_{ext}(t = 0) = \tilde{M}n,$$

   which implies that at steady state we have

   $$(4.4.12) \qquad x_1 + x_5 + x_7 = \tilde{M}n.$$

   Moreover, we obtain the same result when we want to calculate $\dot{F}_{int}$ for the total amount of intracellular iron ions. F_{int} is equal to the sum of Fe_{int} (free iron), $FeUFe$, $SirRFe$, $FeRFe$, $DpsAFe$, whose derivative is $\dot{F}_{int} = \dot{x}_2 + \dot{x}_4 + \dot{x}_6 + \dot{x}_8 + \dot{x}_9$. As for

the manganese, we can deduce the following expression:

$$(4.4.13) \qquad \dot{F}_{int} = K_{FU}(x_{13} - x_4)x_{16} = -\dot{x}_{16}.$$

Again, we deduce that the total amount of intracellular iron plus the total amount of extracellular iron will be constant:

$$F_{int} + x_{16} = Fe_{ext}(t = 0) = \tilde{F}e,$$

which implies that at steady state we have

$$(4.4.14) \qquad x_2 + x_6 + x_8 + x_9 = \tilde{F}e.$$

In what follows, our idea is to deduce minimal relations between the variables, more specifically in terms of x_1 and x_2, internal metal ion concentrations, which are assumed to be different from zero. The last assumption is consistent with the necessity of control internal metal ions in order to activate diverse essential processes.

We recall the equations for x_5, x_6, x_7, x_8, x_9:

$$(4.4.15) \qquad \dot{x}_5 = CC_{SR}(x_{11} - x_5 - x_6)x_1 - \delta_{SR}x_5$$
$$(4.4.16) \qquad \dot{x}_6 = CC_{SR}(x_{11} - x_5 - x_6)x_2 - \delta_{SR}x_6$$
$$(4.4.17) \qquad \dot{x}_7 = CC_{FR}(x_{14} - x_7 - x_8)x_1 - \delta_{FR}x_7$$
$$(4.4.18) \qquad \dot{x}_8 = CC_{FR}(x_{14} - x_7 - x_8)x_2 - \delta_{FR}x_8$$
$$(4.4.19) \qquad \dot{x}_9 = CC_{DA}(x_{12} - x_9)x_2 - \delta_{DA}x_9$$

If we apply the cross multiplication $x_2 \cdot (4.4.15) - x_1 \cdot (4.4.16)$, we deduce that $-\delta_{SR}x_5x_2 + \delta_{SR}x_6x_1 = 0$ which implies the conservation relation:

$$\frac{x_5}{x_1} = \frac{x_6}{x_2}.$$

In the same way, we can obtain applying $x_2(4.4.17) - x_1(4.4.18)$ that $-\delta_{FR}x_7x_2 + \delta_{FR}x_8x_1 = 0$, which implies the relation:

$$\frac{x_7}{x_1} = \frac{x_8}{x_2}.$$

Both relations are true in the case that all variables are different from zero. It is obvious that since we have assumed that $x_1 \neq 0$ and $x_2 \neq 0$, it is not possible that x_5, x_6, x_7, x_8, x_9 to be zero. This is because in that hypothetical case x_{11}, x_{12}, x_{14} would

need to be zero, which is not possible. On the other hand, from both conservation relations we can conclude that

(4.4.20)
$$\frac{x_1}{x_2} = \frac{x_5}{x_6} = \frac{x_7}{x_8} = C,$$

where C is a positive constant.

It is not complicated to deduce the other values as functions of x_1 and x_2. From equation (4.4.15) we obtain that

$$(x_{11} - x_5 - x_6) = \frac{\delta_{SR} x_5}{CC_{SR} x_1},$$

and if we combine the last expression with (4.4.20) and $\dot{x}_{11} = 0$, we get that x_5 is the positive solution of the following second degree polynomial

$$\left(\frac{\bar{\delta}_{SR}}{CC_{SR} x_1} + C + 1 \right) \frac{\gamma_2 \delta_{SR}^2}{CC_{SR} x_1} x_5^2 + \left(\frac{\bar{\delta}_{SR}}{CC_{SR} x_1} + C + 1 \right) \delta_{SR} x_5 - G = 0,$$

where G is the constant inside the regulatory function for proteins with unknown regulator and C is the constant defined in (4.4.20). That is,

(4.4.21)
$$x_5 = \frac{CC_{SR} x_1}{2\gamma_2 \delta_{SR}} \left\{ -1 + \sqrt{1 + \frac{4G\gamma_2}{\bar{\delta}_{SR} + CC_{SR} x_1 (1 + \frac{1}{C})}} \right\} > 0,$$

and since $x_6 = \frac{x_5}{C}$, we get

(4.4.22)
$$x_6 = \frac{CC_{SR} x_2}{2\gamma_2 \delta_{SR}} \left\{ -1 + \sqrt{1 + \frac{4G\gamma_2}{\bar{\delta}_{SR} + CC_{SR} x_2 (1 + C)}} \right\} > 0,$$

where all the constants G, C, γ_2, δ_{SR}, $\bar{\delta}_{SR}$ and CC_{SR} are positive.

Using the values for x_5 and x_6, we can obtain from $\dot{x}_{10} = 0$ that

$$\frac{G}{1 + \gamma_1 \frac{\delta_{SR} x_5}{CC_{SR} x_1}} - \bar{\delta}_{ZA} x_{10} = 0,$$

which implies that

$$x_{10} = \frac{GCC_{SR} x_1}{\bar{\delta}_{ZA}(CC_{SR} x_1 + \gamma_1 \delta_{SR} x_5)},$$

and from $\dot{x}_{11} = 0$ that

$$x_{11} = (C + 1)x_5 + \frac{\delta_{SR} x_5}{CC_{SR} x_1}.$$

In the same form, we can deduce the values for x_7 and x_8 at steady state. From equation (4.4.17) we obtain that

$$(x_{14} - x_7 - x_8) = \frac{\delta_{FR}x_7}{CC_{FR}x_1},$$

and if we combine the last expression with (4.4.20) and $\dot{x}_{14} = 0$, we get that x_7 is the positive solution of a second degree polynomial of the form:

$$\left(\frac{\bar{\delta}_{FR}}{CC_{FR}x_1} + C + 1\right) \frac{\alpha\delta_{FR}^2}{CC_{FR}x_1}x_7^2 + \left(\frac{\bar{\delta}_{FR}}{CC_{FR}x_1} + C + 1\right)\delta_{FR}x_7 - G = 0.$$

That is,

$$(4.4.23) \qquad x_7 = \frac{CC_{FR}x_1}{2\alpha\delta_{FR}}\left\{-1 + \sqrt{1 + \frac{4G\alpha}{\bar{\delta}_{FR} + CC_{FR}x_1(1 + \frac{1}{C})}}\right\} > 0,$$

and since $x_8 = \frac{x_7}{C}$, we get

$$(4.4.24) \qquad x_8 = \frac{CC_{FR}x_2}{2\alpha\delta_{FR}}\left\{-1 + \sqrt{1 + \frac{4G\alpha}{\bar{\delta}_{FR} + CC_{FR}x_2(1 + C)}}\right\} > 0,$$

where all the constant G, C, α, δ_{FR}, $\bar{\delta}_{FR}$ and CC_{FR} are positive.

Additionally, from $\dot{x}_{13} = 0$, we have that

$$x_{13} = \frac{x_7}{\bar{\delta}_{FU}(A_2 + x_7)}.$$

At this point it still remains to obtain the values for x_9 and x_{12}. We first take equation $\dot{x}_9 = 0$ to get

$$(x_{12} - x_9) = \frac{\delta_{DA}x_9}{CC_{DA}x_2},$$

and replacing this value on $\dot{x}_{12} = 0$ and using $x_7 = Cx_8$, we deduce the following equation,

$$\frac{C_1}{1 + x_7} + \frac{x_8}{A_1 + x_8} - \frac{\delta_{DA}\bar{\delta}_{DA}x_9}{CC_{DA}x_2} - \delta_{DA}x_9 = 0.$$

Using the corresponding values for x_7 and x_8, which depend on x_1 and x_2 respectively, we obtain that

$$x_9 = \left(\frac{C_1 A_1 + (C_1 + 1)x_8 + Cx_8^2}{(1 + Cx_8)(A_1 + x_8)}\right) \frac{1}{\left(\frac{\bar{\delta}_{DA}\delta_{DA}}{CC_{DA}x_2} - \delta_{DA}\right)}.$$

On the other hand, from the equations (4.4.12) and (4.4.14), and the conservation

relation in (4.4.20), we have that $x_2 + x_6 + x_8 = \frac{\tilde{Mn}}{C}$. From the last expression we get the following equation

$$x_9 = \tilde{Fe} - \frac{\tilde{Mn}}{C},$$

where $C = \frac{Mn_{int}}{Fe_{int}} = \frac{SirRMn}{SirRFe} = \frac{FeRMn}{FeRFe}$.

Finally, we construct the following two polynomial depending exclusively on x_1 and x_2:

(4.4.25)
$$\begin{cases} P_1(x_1) &= x_1 + x_5(x_1) + x_7(x_1) - \tilde{Mn}, \\ P_2(x_2) &= x_2 + x_6(x_2) + x_8(x_2) + x_9(x_2) - \tilde{Fe}. \end{cases}$$

The values for x_1 and x_2 at the equilibrium can be calculated from (4.4.25) as the positive real roots.

Additionally, we only need to find the real solutions for the first polynomial, because we have the conservation equation (4.4.20) for the variables x_2, x_6 and x_8. Therefore, we get the expression

$$x_2 + x_6(x_2) + x_8(x_2) = \frac{x_1 + x_5(x_1) + x_7(x_1)}{C} = \frac{\tilde{Mn}}{C},$$

which implies that

$$x_9 = \tilde{Fe} - \frac{\tilde{Mn}}{C}.$$

Thus, we have the following proposition about the existence and unicity of an equilibrium state depending on the initial external amount of metal ions.

Proposition 4.4.8. *The class $U(I)$ for the Mn/Fe module at the equilibrium satisfies that $x_{15} = Mn_{ext} = 0$, $x_{16} = Fe_{ext} = 0$, $x_3 = ZurAMn = 0$ and $x_4 = FeUFe = 0$. The other variables can be deduced for each couple of constant values $\tilde{Mn}$ and $\tilde{Fe}$, which correspond to the initial external amount of metal ions. $Mn_{int} = x_1$ corresponds to the positive real roots of the polynomial*

(4.4.26)
$$P_1(x_1) = x_1 + x_5(x_1) + x_7(x_1) - \tilde{Mn} = 0.$$

which has a unique positive real solution.

Additionally, x_2, x_6 and x_8 satisfy

$$x_2 + x_6(x_2) + x_8(x_2) = \frac{x_1 + x_5(x_1) + x_7(x_1)}{C} = \frac{\tilde{Mn}}{C},$$

implying that

$$x_9 = \tilde{F}e - \frac{\tilde{M}n}{C}.$$

Proof. Let us first define the following polynomial:

$$Q(x_1) = x_1 + x_5(x_1) + x_7(x_1).$$

It follows directly that $P_1(x_1) = Q(x_1) - \tilde{M}n$, therefore the problem of finding the roots of $P_1(x_1) = 0$ is equivalent to solve $Q(x_1) = \tilde{M}n$, which can be solved geometrically. Hence, in what follows we analyze Q.

From (4.4.21) and (4.4.23) we obtain that $Q(x_1)$ satisfies:

$$
\begin{aligned}
Q(x_1) &= x_1 \left\{ 1 + \frac{CC_{SR}}{2\gamma_2 \delta_{SR}} \left[-1 + \sqrt{1 + \frac{4G\gamma_2}{\bar{\delta}_{SR} + CC_{SR}x_1(1 + \frac{1}{C})}} \right] \right. \\
&\left. + \frac{CC_{FR}}{2\alpha\delta_{FR}} \left[-1 + \sqrt{1 + \frac{4G\alpha}{\bar{\delta}_{FR} + CC_{FR}x_1(1 + \frac{1}{C})}} \right] \right\},
\end{aligned}
$$

which can be reduced to

$$\overline{Q}(x_1) = (1 - a_1 - a_2) + a_1\sqrt{1 + \frac{b_1}{c_1 + x_1}} + a_2\sqrt{1 + \frac{b_2}{c_2 + x_1}}$$

where $a_1 = \frac{CC_{SR}}{2\gamma_2\delta_{SR}}$, $b_1 = \frac{4G\gamma_2}{CC_{SR}(1+1/C)}$, $c_1 = \frac{\bar{\delta}_{SR}}{CC_{SR}(1+1/C)}$, $a_2 = \frac{CC_{FR}}{2\alpha\delta_{FR}}$, $b_2 = \frac{4G\alpha}{CC_{FR}(1+1/C)}$ and $c_2 = \frac{\bar{\delta}_{FR}}{CC_{FR}(1+1/C)}$ are positive constants. That is, we deduce that

$$Q(x_1) = x_1 \cdot \overline{Q}(x_1).$$

In the rest of the proof, we will study the polynomial $\overline{Q}$ in order to deduce properties of Q. It is not complicated to see that $\overline{Q}(x_1)$ intersects the y-axis at the point $1 + \xi_1 a_1 + \xi_2 a_2$, where ξ_1 and ξ_2 are two positive constants, since both terms inside the root square $(1 + \frac{b1}{c1+x_1})$ and $(1 + \frac{b1}{c1+x_1})$ are bigger than 1 at $x_1 = 0$. Moreover, when x_1 goes to ∞, $\overline{Q}(x_1)$ converges asymptotically to 1, and $\overline{Q}$ is strictly decreasing because

$$\frac{d\overline{Q}(x_1)}{dx_1} = -\frac{a_1 b_1}{2\sqrt{1 + \frac{b_1}{c_1+x_1}}(c_1 + x_1)^2} - \frac{a_2 b_2}{2\sqrt{1 + \frac{b_2}{c_2+x_1}}(c_2 + x_1)^2} < 0,$$

concluding that $\overline{Q}$ has no positive real root. This implies that $\overline{Q}$ has the form showed in Figure 4.8 left.

From the above considerations, the polynomial $Q(x_1)$ has the following properties: (i) $Q(0) = 0$, (ii) $Q(-\infty) = -\infty$ and $Q(\infty) = \infty$, (iii) Q is an strictly increasing function because

$$\frac{dQ(x_1)}{dx_1} = (1 - a_1 - a_2) + \sqrt{1 + \frac{b_1}{c_1 + x_1}} \left\{ a_1 - \frac{x_1 a_1 b_1}{(c_1 + b_1 + x_1)(c_1 + x_1)} \right\}$$

$$(4.4.27) \qquad + \sqrt{1 + \frac{b_2}{c_2 + x_1}} \left\{ a_2 - \frac{x_1 a_2 b_2}{(c_2 + b_2 + x_1)(c_2 + x_1)} \right\} > 0,$$

which implies that Q has a unique real root, which is zero (Figure 4.8 right).

Finally, since the values for x_1 needs to be positive and real, we have that for each external manganese input, $\tilde{M}n$, there exists a unique positive real equilibrium state.
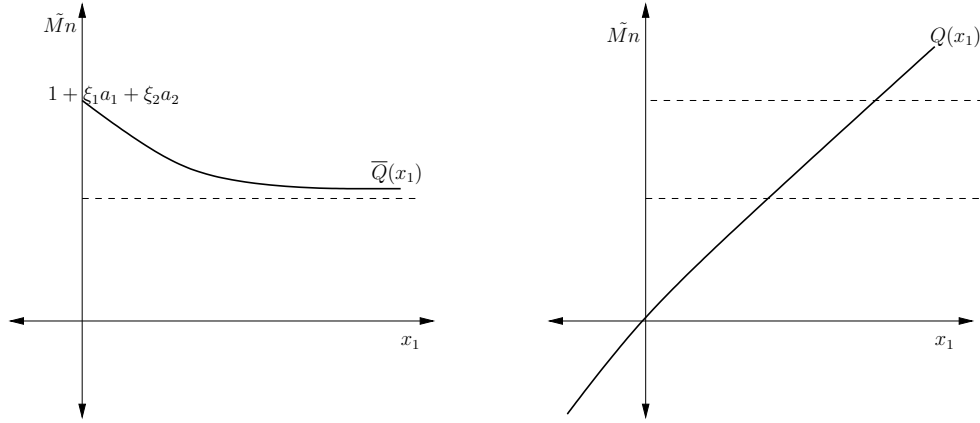
Figure 4.8: Left: plot of the polynomial $\overline{Q}(x_1)$. Right: plot of the polynomial $Q(x_1)$.

□

Class $U(II)$:

In the analysis of the Mn/Fe module class $U(II)$, we proceed similarly as in Cu/Zn module class $E(II)$. From equations $\dot{x}_{15} = 0$ and $\dot{x}_{16} = 0$ we deduce that

$$-K_{ZA}(x_{10} - x_3)x_{15} + \mathbf{R}_6(x_1) = 0$$

and

$$-K_{FU}(x_{13} - x_4)x_{16} + \mathbf{R}_7(x_2) = 0.$$

This implies that the variables Mn_{int}, Fe_{int}, Mn_{ext} and Fe_{ext} are different from zero in the equilibrium and depend on the initial external amount of both metal ions. So, in the rest of the subsection we will compute their values. Moreover, it is important to note that the analysis for the other variables remains as before with the exceptions of $x_{10} = ZurA$ and

$x_{13} = FeU$ because both x_3 and x_4 are now different from zero.

Let M_{int} be the sum of Mn_{int} (free internal manganese), $ZurAMn$, $SirRMn$ and $FeRMn$, that is, formally we write $M_{int} = x_1 + x_3 + x_5 + x_7$, and we obtain that:

$$(4.4.28) \qquad \dot{M}_{int} = -\mathbf{R}_6(x_1) + K_{ZA}(x_{10} - x_3)x_{15} = -\dot{Mn}_{ext} = -\dot{x}_{15}.$$

Let F_{int} be the sum of Fe_{int} (free internal iron), $FeUFe$, $SirRFe$, $FeRFe$, $DpsAFe$, whose derivative has the form $\dot{F}_{int} = \dot{x}_2 + \dot{x}_4 + \dot{x}_6 + \dot{x}_8 + \dot{x}_9$. Using the last equation we can deduce the following expression:

$$(4.4.29) \qquad \dot{F}_{int} = -\mathbf{R}_7(x_2) + K_{FU}(x_{13} - x_4)x_{16} = -\dot{Fe}_{ext} = -\dot{x}_{16}.$$

Equations (4.4.28) and (4.4.29) imply a conservation equation for the total amount of metal ions in the system, that is,

$$(4.4.30) \qquad M_{int} + x_{15} = Mn_{ext}(0) = \tilde{M}n,$$
$$(4.4.31) \qquad F_{int} + x_{16} = Fe_{ext}(0) = \tilde{F}e,$$

where constants $\tilde{M}n$ and $\tilde{F}e$ correspond to the initial conditions for external manganese and iron respectively. In what follows we will find expressions for the rest of the variables.

If we make the following sum $\dot{x}_1 + \dot{x}_5 + \dot{x}_7 = 0$, we conclude that

$$-\mathbf{R}_6(x_1) + (D_{ZA} + \delta_{ZA})x_3 = 0,$$

implying that

$$x_3 = \frac{\mathbf{R}_6(x_1)}{D_{ZA} + \delta_{ZA}}.$$

In the same way we can deduce that x_4 depends exclusively on x_2, making the sum $\dot{x}_2 + \dot{x}_6 + \dot{x}_8 + \dot{x}_9 = 0$, that is

$$x_4 = \frac{\mathbf{R}_7(x_2)}{D_{FU} + \delta_{FU}}.$$

Replacing the previous expressions for x_3 and x_4 in $\dot{x}_{10} = 0$ and $\dot{x}_{13} = 0$ respectively, we obtain that

$$x_{10} = \frac{1}{\bar{\delta}_{ZA}} \left\{ \frac{G}{1 + \gamma_1 \frac{\delta_{SR}x_5}{CC_{SR}x_1}} + (\bar{\delta}_{ZA} - \delta_{ZA}) \frac{\mathbf{R}_6(x_1)}{\delta_{ZA} + D_{ZA}} \right\}$$

and

$$x_{13} = \frac{1}{\bar{\delta}_{FU}} \left\{ \frac{x_7}{A_2 + x_7} + (\bar{\delta}_{FU} - \delta_{FU}) \frac{\mathbf{R}_7(x_2)}{\delta_{FU} + D_{FU}} \right\}.$$

Using the previous values we can compute the external metal ion concentration at the equilibrium as a function of x_1 and x_2. It follows that

$$x_{15} = \frac{\mathbf{R}_6(x_1)}{\frac{K_{ZA}}{\delta_{ZA}} \left(\frac{G}{1 + \gamma_1 \frac{\delta_{SR}x_5}{CC_{SR}x_1}} - \delta_{ZA} \frac{\mathbf{R}_6(x_1)}{\delta_{ZA} + D_{ZA}} \right)}$$

and

$$x_{16} = \frac{\mathbf{R}_7(x_2)}{\frac{K_{FU}}{\delta_{FU}} \left(\frac{x_7}{A_2 + x_7} - \delta_{FU} \frac{\mathbf{R}_7(x_2)}{\delta_{FU} + D_{FU}} \right)}.$$

Finally, from (4.4.30) and (4.4.31) we get the following two polynomial depending exclusively on x_1 and x_2:

$$(4.4.32) \quad \begin{cases} x_1 + x_3(x_1) + x_5(x_1) + x_7(x_1) + x_{15}(x_1) &= \tilde{M}n, \\ x_2 + x_4(x_1) + x_6(x_2) + x_8(x_2) + x_9(x_2) + x_{16}(x_2) &= \tilde{F}e. \end{cases}$$

The values for x_1 and x_2 at the equilibrium can be calculated from (4.4.32) as the positive real roots. Summarizing, the following proposition can be established taking into account all the previous results,

Proposition 4.4.9. *The class $U(II)$ for the Mn/Fe module satisfies:*

1. *At the equilibrium, x_1 and x_2 correspond to the positive real solutions of the following two polynomial:*

$$\begin{cases} x_1 + x_3(x_1) + x_5(x_1) + x_7(x_1) + x_{15}(x_1) &= \tilde{M}n \\ x_2 + x_4(x_2) + x_6(x_2) + x_8(x_2) + x_9(x_2) + x_{16}(x_2) &= \tilde{F}e \end{cases},$$

where constants $\tilde{M}n$ and $\tilde{F}e$ are the initial amounts for external manganese and iron respectively.

2. *Since all the variables depend on x_1 and x_2, we have that for each couple of values of the initial external metal ions concentrations $\tilde{M}n$ and $\tilde{F}e$ there exists a finite number of possible equilibrium states.*

Observation 4.4.10. *From the last proposition we conclude that the number of steady states is finite and that eventually, depending on the real parameters, is unique.*

Observation 4.4.11. *In Figure 4.24 we have the simulation that confirm the existence of the stationary state depending on the initial external condition.*

4.4.2 A comment on homeostatic behavior

In the previous subsection we have proved that both systems for metals extrusion and uptake present a unique steady state in the most simple case without recycling (class $E(I)$ and $U(I)$). In this context, we can infer that the dynamical systems reach an equilibrium or balance in which internal change continuously compensates for external change (adaptive under stress to environmental conditions) in a feedback control process to keep conditions relatively uniform, that is, the system present an homeostatic behavior.

The homeostasis phenomenon is particularly important in biological systems [N99]. The biological term of homeostasis, introduced by Claude Bernard $(1813 - 1878)$ and coined by Cannon, refers to the organisms ability to maintain steady states of operation in a changing internal and external environment. It has been formalized by Ross Ashby in his book "Design for a brain" where he exposed the study of biological systems like homeostatic or adaptative systems in terms of dynamical systems.

From a purely mathematical point of view, in a system of differential equations as in our case, the homeostasis phenomenon is determined either by the convergence to a steady state or small oscillations around a given value, independent of the considered parameters (or little, weak homeostasis condition [P06]). In our case these parameters correspond to the external source of metals (σ_i).

Nevertheless, the nonlinearity of the biological networks under study makes usually very difficult to prove the existence of such situations and an alternative strategy is used. As we discussed before, in 1981 René Thomas ([Th81]) has conjectured that a necessary condition for homeostatic behavior is the existence of negative circuits in the interaction graph.

Negative circuits

Thomas condition about negative circuits in the regulatory graph gives only a necessary condition and in practice it is a very weak condition. Nevertheless, we will study in the following the existence of negative circuits in the different modules, in order to determine what are the key elements that maintain the homeostasis under metal stress.
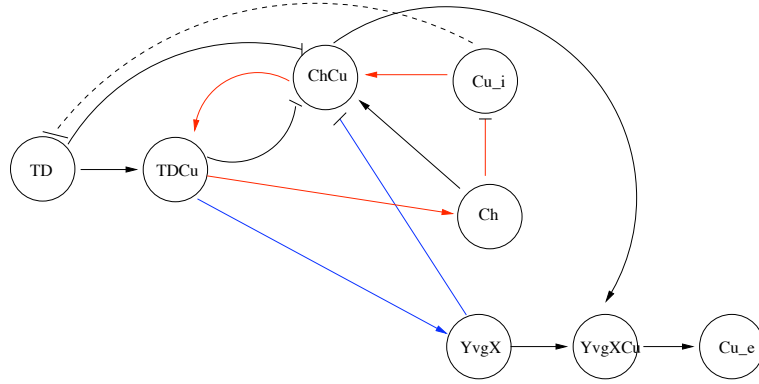
Figure 4.9: Negative circuits in the local interaction graph associated to the Cu/Zn module, in the copper section, independent of the x value. The blue and red edges correspond to the two negative circuits.

Using the system $\dot{x} = F(x)$ we recall that the local interaction graph $G = (V, E)$ at the point $\bar{x}$ is defined in the following way: the set of vertices V is $\{1, \ldots, n\}$, one for each variable, and the set of edges E is generated by the following rule: there is an oriented edge between vertices i to j if and only if the value of $\frac{dF_j}{dx_i}(\bar{x}) \neq 0$; this edge is labelled with the sign of the partial derivative at $\bar{x}$.

In the simplified graph of Figure 4.9 we can see two negative circuits. The first circuit through Cu_{int}, $ChCu$, $TDCu$ and Ch, and the second through $TDCu$, $YvgX$ and $ChCu$. This shows that the regulation of the internal copper model needs the activation of both the metallo-chaperone Ch and the protein $YvgX$. Moreover, we can see in both circuits that it is strictly necessary the existence of $ChCu$. This emphasizes the importance of the chaperone protein to obtain copper homeostasis ([Mo05], [To05]).

A similar situation is observed for the zinc. In Figure 4.10 there exists a negative circuit between $ChZn$, $ZntRZn$ and $ZntA$. Here the negative edge is produced by the relation between the protein $ZntA$ and the compound $ChZn$, which implies that for a high concentration of $ZntA$ less will be the quantity of $ChZn$.

In the Mn/Fe module (uptake system) we can observe the same behavior. In Figure 4.11 there exist two negative circuits. The first negative circuit through $SirRMn$ and $SirR$, and the second one through Mn_{int}, $SirRMn$, $ZurA$ and $ZurAMn$. In both circuits we can see, as it was predicted in the biological model, that the $SirR$ protein causes a double negative regulation in presence of Mn, and for that reason it is the main responsible of the homeostasis in the Mn section of the module for the metal uptake mechanism.

In Figure 4.12 we can see the existence of a negative circuit between Fe_{int}, $FeRFe$ and $DpsA$. All the edges in the circuit are positive with the exception of the interaction between

Figure 4.10: Negative circuit in the partial interaction graph associated to the Cu/Zn module, in the zinc section, independent of the x value. The red edges correspond to the negative circuit.
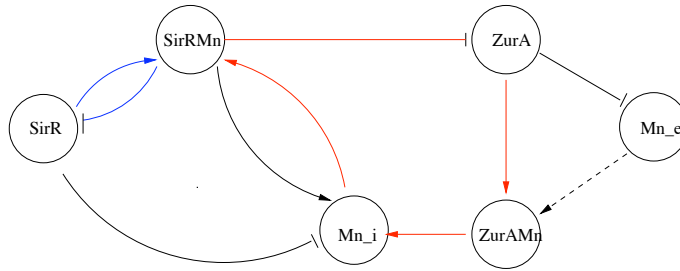
Figure 4.11: Negative circuit in the partial interaction graph associated to the Mn/Fe module, in the manganese section, independent of the x value. The blue and red edges correspond to the two negative circuits.

$DpsA$ and Fe_{int}, because of the detoxification process (Fe^{+3}). So if we increase the quantity of $DpsA$ protein there will be less internal Fe^{+2}, taking care of the excess of the metals.

Finally, it is important to note that this is only a preliminary study about the homeostasis property in *Halobacterium NRC-1* because as we said before Thomas rule gives us only a necessary condition.

As we have mentioned before in the homeostasis we can observe two types of stabilities. The first is related with the convergence towards an equilibrium state or eventually small oscillations around a steady state. In contrast, the second is related with the condition that the steady state remains the same or suffer variations of small amplitude when an external parameter is changed, and as we have seen previously this parameter corresponds to the σ_i value.

Meanwhile, the local stability of fixed points for non-linear autonomous differential equa-
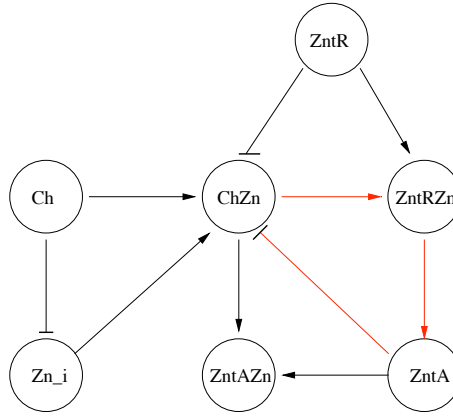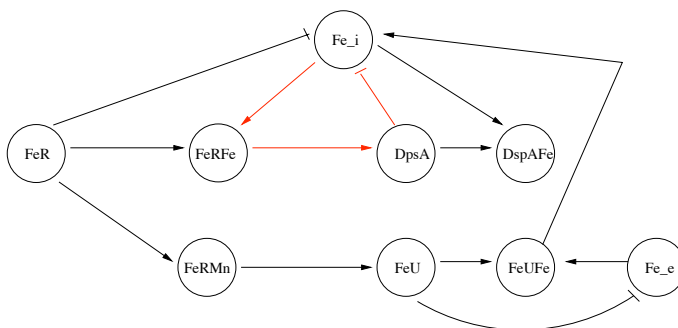
Figure 4.12: Negative circuit in the partial interaction graph associated to the Mn/Fe module, in the iron section, independent of the x value. The red edges correspond to the negative circuit.

tions can be analyzed by linearization of the system. In this case we need to calculate the associated Jacobian matrix for both modules and analyze the nature of its eigenvalues. In our case these matrices have a great number of zero values but the size still remains big enough. An alternative approach is the study of a Taylor development in the neighborhood of the equilibrium that maybe give us the result more quickly.

Nevertheless, we have decided to study the global stability response. For that reason, in order to obtain a global stability condition for both modules it is necessary to apply novel results for monotone and near monotone systems as we will see in the next section.

4.5 Monotonicity, convergence and global stability

In order to study global convergence properties of the metal stress resistance model, we proceed to the study of its monotonicity. The concept of monotonicity has been studied by several authors but the latest results obtained belong to novel works of Sontag, Angeli, Enciso and Smith ([AS03], [ES06], [ESS06], [Sg07]).

Monotonicity in a system is a very important property because it reflects the fact that a system responds consistently to perturbations on its components (in this case environmental perturbations). Consider for example a regulatory graph associated to three genes: g_1 activates g_2, g_2 represses g_3 and g_1 represses g_3 (positive cycle). If we assume that for certain reasons (external perturbation) gene 1 is activated then it is obvious that the response of the system will be coherent, because gene 2 will be activated and later gene 3 will be repressed by both gene 1 and gene 2, and this unambiguous global effect is independent of the constant parameters of the system.

For that reason, continuous-time monotone systems have convergent behavior, for example, they cannot admit any stable oscillation. Moreover, if there is only one steady state, a theorem of Dancer [D98] shows (under some assumptions which are often satisfied for biological systems) that every solution converges to this unique steady state (monostability).

Another central point with respect to the study of monotonicity is that in many situations we can characterize the behavior of an entire system, based upon the "qualitative" knowledge represented by the general network topology. That is, there is no need to know the precise form of the dynamics or the value of the kinetic or other kind of parameters in order to obtain global stability conclusions.

In the following we will introduce the main concepts and results for monotone systems. Then we will show a strategy of decomposition for non-monotone systems using external control variables in which the new controlled closed system is monotone and satisfies a small gain condition. Finally, we prove that the modules $E(I)$ (extrusion) and $U(I)$ (uptake) of *Halobacterium NRC-1* verify a global stability condition.

4.5.1 Monotone systems

The main results about convergence in monotone controlled systems described here have been developed in [AS03] for monotone control systems described by differential equations and in [ES06] which extends the theory for abstract dynamical systems with a nice strategy for decomposing systems into subsystems of the required type. Before explaining the main theorems, we proceed with some notations and definitions.

Definitions

Let $K \subset \mathbb{R}^n$ be a cone, by which is meant a set that is nonempty, convex, closed under multiplication by positive scalars and pointed (i.e. $K \cap -K = \emptyset$). K induces three natural order relations in $\mathbb{R}^n$: a partial order given by $x \leq_K y \iff y - x \in K$, $x <_K y \iff x \leq_K y$ and $x \neq y$, and a stronger order $x <<_K y \iff y - x \in intK$.

Definition 4.5.1 (Orthant cones). *In the case $B = \mathbb{R}^n$, a tuple $s = (s_1, \ldots, s_n)$, where $s_i = \pm 1$, $\forall i \in \{1, \ldots, n\}$, defines the orthant cone $K = \mathbb{R}^{s_1} \times \ldots \times \mathbb{R}^{s_n}$. The canonic orthant cone defined by $s = (+1, \ldots, +1)$ is called the cooperative cone.*

The order induced by the tuple s, denoted $\leq_s$, will be defined as

$$x \leq_s y \text{ iff } s_i x_i \leq s_i y_i, \forall i \in \{1, \ldots, n\}.$$

Definition 4.5.2. *Let K_1 and K_2 be cones in $\mathbb{R}^n$ and $\mathbb{R}^m$ respectively. A function $\gamma :$ $\mathbb{R}^n \to \mathbb{R}^m$ is said to be increasing with respect to the orders (K_1, K_2) if $x \leq_{K_1} y$ implies $\gamma(x) \leq_{K_2} \gamma(y)$, and it is said to be decreasing with respect to (K_1, K_2) if $x \leq_{K_1} y$ implies $\gamma(x) \geq_{K_2} \gamma(y)$ (similarly with the other order relations).*

In what follows, let $X \subset \mathbb{R}^n$ and $U \subset \mathbb{R}^m$ be two open sets. The set U is referred as the set of input values, and an input is defined as a function $u : \mathbb{R}^+ \to U$ that is Borel measurable and locally bounded. The set U_∞ is defined as the set of all inputs taking values in U. The set of all constant inputs $\hat{u}(\cdot) \equiv u \in U$ is denoted by $\hat{U}$, and we abuse of notation saying that $\hat{U} \subseteq U$.

Definition 4.5.3. *A controlled dynamical system (or just a dynamical system in the sequel) is a function*

$$\text{(4.5.1)} \qquad\qquad \Phi : \mathbb{R}^+ \times X \times U_\infty \to X$$

which satisfies the following hypotheses:

(1) Φ is continuous on its first two variables, and the restriction of Φ to the set $\mathbb{R}^+ \times X \times \hat{U}$ is continuous.

(2) For every $u, v \in U_\infty$ such that $u(s) = v(s)$ for almost every s, $\Phi(t, x_0, u) = \Phi(t, x_0, v)$ for all $x_0 \in X$, $t \in \mathbb{R}^+$.

(3) $\Phi(0, x_0, u) = x_0$ for any $x_0 \in X$, $u \in U_\infty$.

(4) If $\Phi(s, x, u) = y$ and $\Phi(t, y, v) = z$, then by appending $u|_{[0,s]}$ to the beginning of v to form the input w, it holds that $\Phi(s + t, x, w) = z$.

An autonomous system is a function $\Phi : \mathbb{R}^+ \times X \to X$ such that $(1), (3)$ and (4) are verified erasing the U points.

Given a controlled dynamical system Φ and a measurable set $Y \subset \mathbb{R}^k$, an output function is any continuous function $h : X \to Y$. The pair (Φ, h) consisting of:

$$\text{(4.5.2)} \qquad\qquad \Phi : \mathbb{R}^+ \times X \times U_\infty \to X, \quad h : X \to Y$$

is called a dynamical system with input and output.

Fix Φ a controlled dynamical system (with notations given above). Consider $Y = U$ and $h : X \to U$ a continuous function, and $K_X \subseteq \mathbb{R}^n$, $K_U \subseteq \mathbb{R}^m$ cones.

Definition 4.5.4 (Negative feedback function). *The pair (Φ, h) is called a controlled dynamical system with feedback. If $h : X \to U$ is decreasing (with respect to the cones K_X and K_U), then we say (Φ, h) is a controlled dynamical system with negative feedback.*

Definition 4.5.5 (Monotone systems). *The dynamical system Φ is said to be* **monotone** *(with respect to the cones K_X and K_U) if for any $u, v \in U_\infty$ such that $u(t) \leq_{K_U} v(t)$ for almost all times t, and $x_1 \leq_{K_X} x_2$ in X we have*

$$\Phi(t, x_1, u) \leq_{K_X} \Phi(t, x_2, v), \forall t \geq 0.$$

An autonomous system Φ is monotone if $x_1 \leq_{K_X} x_2$ implies $\Phi(t, x_1) \leq_{K_X} \Phi(t, x_2), \forall t \geq 0.$

Definition 4.5.6 (I/S characteristic). *The dynamical system Φ is said to have an input to state characteristic $k^X : U \to X$, denoted I/S, if for every constant input $u(\cdot) = \bar{u} \in \hat{U}$ and for every initial condition $x_0 \in X$,*

$$\lim_{t \to \infty} \Phi(t, x_0, \bar{u}) = k^X(\bar{u}).$$

Definition 4.5.7 (Feedback characteristic). *If Φ has an I/S characteristic function then $k = h \circ k^X : U \to U$ is called the feedback characteristic of the system. Moreover, if the autonomous system is monotone then k^X is an increasing function with respect to the cones.*

Definition 4.5.8 (Closed loop trajectory). *Given $x_0 \in X$ and a continuous function $x : \mathbb{R}^+ \to X$, it is said that $x(\cdot)$ is a closed loop trajectory of (Φ, h) with initial conditions x_0 if $x(0) = x_0$ and $x(t) = \Phi(t, x_0, h \circ x(\cdot))$ for all $t \geq 0$.*

Definition 4.5.9 (Closed loop system). *Suppose that the controlled system is such that, for each $x_0 \in X$, there is a unique continuous closed loop trajectory $x(t)$ so that $x(0) = x_0$. The function*

$$\Psi : \mathbb{R}^+ \times X \to X, \ \Psi(t, x_0) := x(t)$$

will be called the closed-loop behavior associated to (Φ, h). If this function itself constitutes a dynamical system, then it is denoted as the closed loop system associated to (Φ, h).

The assumptions

In the following we show the hypotheses used in the main theorem for controlled monotone systems proved by Sontag et al. We will start by introducing the concept of ϵ-box property:

Definition 4.5.10 (ϵ-box property)**.** *Consider a subset A of an ordered metric space $(T, \leq)$. If $a, b \in A$, we let $[a, b] = \{x \in A : a \leq x \leq b\}$ denote the order interval. A is said to satisfy the ϵ-box property if for every $\epsilon > 0$ and $x \in A$, there are $y, z \in A$ such that $diam[y, z] < \epsilon$ and $[y, z] \cap A$ is a neighborhood of x.*

Let Φ, h, K_X, K_U as before. Consider the following hypotheses:

$(H1)$ K_X and K_U are closed cones with nonempty interior.

$(H2)$ U is closed and convex. Moreover, for every bounded set $C \subset U$, there exist $a, b \in U$ such that $a \leq_{K_U} c \leq_{K_U} b$, $\forall c \in C$.

$(H3)$ X and U satisfy the ϵ-box property.

$(H4)$ The dynamical system Φ is monotone, with a completely continuous I/S characteristic k^X. Furthermore, h is a decreasing feedback function w.r.t. K_X and K_U that sends bounded sets to bounded sets.

Observation 4.5.11. *We recall a function $f : C \subset \mathbb{R}^n \rightarrow \mathbb{R}^n$ is completely continuous if and only if it is continuous and $\overline{f(A)}$ is compact for every bounded set $A \subset C$. Assumption $(H4)$ implies that the feedback characteristic function $k = h \circ k^X$ is completely continuous as k^X.*

4.5.2 Small gain theorem

We will mention the three main theorems used in this section in order to prove global convergence. The first result is about the "converging input converging state property" ($CICS$).

Theorem 4.5.12 (Enciso, Sontag: Theorem 1, $CICS$)**.** *Consider a monotone system Φ with a continuous I/S characteristic function k^X. Assume hypotheses $(H1)$ and $(H3)$. If $u(\cdot) \in U_\infty$ converges to $\bar{u} \in U$ as $t \rightarrow \infty$, then $\Phi(t, x_0, u)$ converges to $\bar{x} := k^X(\bar{u})$ as $t \rightarrow \infty$, for any $x_0 \in X$.*

To study closed loop trajectories we need to introduce the "small gain condition".

Definition 4.5.13. *For Φ and h as before with I/S characteristic k^X and feedback characteristic $k = h \circ k^X$, the small gain condition is satisfied when the following properties hold:*

1. *The sequence $u_n = k^n(u_0) = k \circ \ldots \circ k(u_0), n \geq 0$, has bounded orbits.*

2. *The equation $k^2(u) = k(k(u)) = u$ has a unique solution.*

Theorem 4.5.14 (Enciso, Sontag: Theorem 2, SGT)**.** *Let Φ, h, K_X, K_U as before. Assume $(H1), (H2), (H3), (H4)$ and the small gain condition are verified. Then all bounded closed loop trajectories $x(t)$ of (Φ, h) converge towards $\bar{x} = k^X(\bar{u})$, where $\bar{u}$ is such that $k^2(\bar{u}) = \bar{u}$. That is,*

$$\lim_{t \to \infty} x(t) = \lim_{t \to \infty} \Phi(t, x_0, h \circ x(t)) = k^X(\bar{u}) = \bar{x}.$$

4.5.3 Our setting: differential equations

As we have seen before, a controlled dynamical system is specified by a state space X, an input set U, and a mapping $\Phi : \mathbb{R}^+ \times X \times U_\infty \to X$ such that some continuity properties are required and the usual semigroup properties hold, i.e. $\Phi(0, x, u) = x$ and $\Phi(t, \Phi(s, x, u_1), u_2) = \Phi(s + t, x, v)$, where v is the restriction of u_1 to the interval $[0, s]$ concatenated with u_2 shifted to $[s, \infty)$.

We interpret $\Phi(t, x, u)$ as the state at time t obtained if the initial condition is x and the external input is $u(\cdot)$. Moreover, we write $x(t, x_0, u)$ or just $x(t)$ instead of $\Phi(t, x_0, u)$ when the context is clear. In this context, when there is no risk of confusion, we use x to denote states (i.e., elements of X) as well as trajectories. Similarly, u may refer to an input value or an input function.

From now on, we will specialize to the case of systems defined by ordinary differential equations of the form:

(4.5.3) $$\dot{x} = f(x, u), \ x(0) = x_0 \in X.$$

We make the following technical assumptions. The map f is defined on $X \times U$, where $X \subseteq \mathbb{R}^n$ and $U \subseteq \mathbb{R}^m$ are some open sets. We assume that $f(x, u)$ is continuous in (x, u) and locally Lipschitz continuous in x locally uniformly in u. This last property means that for compact subsets $C_1 \subseteq X$ and $C_2 \subseteq U$ there exists a constant k such that $|f(\psi, u) - f(\zeta, u)| \leq k|\psi - \zeta|$ for all $\psi, \zeta \in C_1$ and all $u \in C_2$. We will also implicitly assume that f is locally Lipschitz in (x, u), so that the full system has unique solution.

In order to obtain a well defined controlled dynamical system on X, we will assume that the solution $x(t) = \Phi(t, x_0, u)$ of $\dot{x} = f(x, u)$ with initial condition $x(0) = x_0$ is defined for all inputs $u(\cdot)$ and all times $t \geq 0$ and is unique. This means that solutions with initial states in X must be defined for all $t \geq 0$.

In what follows, we will adopt the nomenclature we introduced in Subsection 4.5.1 for controlled systems to the context of ordinary differential equations, using the dictionary just introduced. Moreover, we will describe the decomposition procedure which is similar to replacing one of the variables in the autonomous system $\dot{x} = g(x), x(0) = x_0$, by a real parameter u producing a controlled system of the form (4.5.3). Roughly speaking, consider (4.5.3), together with a function $h(x)$, such that $\dot{x} = f(x, h(x))$. The main idea is to prove monotonicity in this new system and the steady state response property: for every constant function $\bar{u} \in U_\infty$, the system $\dot{x} = f(x, \bar{u})$ converges globally towards $k^X(\bar{u})$ for all $t \geq 0$.

The region of attraction of an asymptotically stable equilibrium point refers to the set of all initial conditions that converge to that equilibrium point. An equilibrium point is said to be **globally asymptotically stable** if all initial conditions converge to that equilibrium point.

4.5.4 Decomposition of non-monotone systems

In order to prove if a dynamical system coming from a biological system is monotone, Sontag [Sg07] has shown that there exists a relation between the property of monotonicity and the existence of positive cycles in its associated regulatory graph. As we have seen before, it is common to associate a signed digraph $\mathcal{G}$ to a system of differential equations dealing with some biological processes, using the Jacobian matrix. In this signed digraph the vertices represent the species (genes, proteins or complexes) and the edges represent the interaction between the species that could be positive or negative. The main definitions on regulatory graphs have been made in Chapter 2.

In what follows we introduce the concepts of spin assignments and consistency to establish an alternative definition for monotone systems.

Definition 4.5.15 (Spin assignment)**.** *A spin assignment Σ for a signed digraph $G = (V, E)$ is an assignment, to each node $v \in V$, of a number σ equals to -1 or $+1$. If there is an edge from node v_i to node v_j, with sign ϵ_{ij}, we say that this edge is consistent with the spin assignment Σ if:*

$$\epsilon_{ij} = \sigma_i \sigma_j.$$

We will say that Σ is a consistent spin assignment for the signed digraph G if every edge of G is consistent with Σ.

It is not complicated to prove that a consistent spin assignment exists if and only if every undirected loop in the signed digraph G has positive sign [Sg07] (even number of negative arrows). The proof is similar to the one showed in Chapter 2, Proposition 2.4.3, but for undirected graphs and it uses an annihilation property for the multiplication of the σ numbers in the circuit.

Definition 4.5.16 (Monotone system). *A dynamical system is said to be monotone if there exists at least one consistent spin assignment for its associated digraph $\mathcal{G} = \mathcal{G}(f) = \cup \mathcal{G}(x)$ (see Definition 2.3.8 in Chapter 2).*

Nonetheless, in general there is no reason for large biochemical networks to have consistent sign assignment. For that reason it was developed the concept of near-monotone system.

Let us call the consistency deficit (CD) of a digraph G the smallest possible number of edges that should be removed from G in order that there exists at least one consistent spin assignment, and, correspondingly, the system is monotone. In this sense, a near-monotone system is a system closer to be monotone, and in practice with small CD [Sg07]. In what follows we will explain a decomposition technique for near-monotone systems.

The decomposition approach for non-monotone systems is a really useful technique since it permits to locate and characterize the stability of steady states based upon input/output behaviors of components. In this sense, one may "pull out" inconsistent connections among monotone components, in such a manner that the original system can then be viewed as a "negative feedback" loop around an otherwise consistent system (in our case interconnections of monotone subsystems).

For that reason, it is of interest to know whether one can decompose an autonomous system, $\dot{x} = f(x)$, not necessarily monotone, into negative feedback loops of a monotone controlled system.

Consider the following autonomous system

$$(4.5.4) \qquad\qquad \dot{x} = g(x),\ x \in X = (\mathbb{R}^+)^n$$

Definition 4.5.17 (Sign definite system). *We say that a system of the form (4.5.4) is sign definite if for each $i \neq j$, it holds that $\frac{\partial g_i}{\partial x_j}(x) \nabla 0$ for all $x \in X$, where the relation ∇ stands for either $>$, $<$, or $=$, and of course different signs are allowed for different pairs (i, j).*

If the autonomous system (4.5.4) is sign definite with associated regulatory graph $\mathcal{G}$, then one can find an n-dimensional controlled system

$$(4.5.5) \qquad \dot{x} = f(x, u), \; h : X \to U \text{ with } X = (\mathbb{R}^+)^n, U = (\mathbb{R}^+)^m,$$

such that:

  (i) is monotone with respect to some orthant cones in the inputs and the states;

  (ii) h is decreasing with respect to such cones (negative feedback);

  (iii) its closed loop system is well defined and is (4.5.4).

In what follows we will describe the decomposition method which tries to minimize the number of inputs and outputs involved, so as to make the reduced model in Theorem 4.5.14 (SGC) as simple as possible. Additionally, sufficient conditions for a well defined characteristic k^X can be found for controlled systems.

Let $A \subset \{x_1, \ldots, x_n\}$ be an arbitrary set of variables called agonists. These variables may be unrelated with each other, but it is better to choose them so that their dynamics are positively correlated, that is, most edges in the regulatory graph connecting two nodes from A are positive. The remainder variables (A^c) are called antagonists, and they will also be thought of as being mostly positively correlated to each other.

Definition 4.5.18 (Discordant edges). *In the labeled regulatory graph an edge will be called "discordant" if any of these situations occur: the edge is positive and joins vertices agonists with antagonists, or the edge is negative and joins two vertices agonists or two antagonists.*

Let $D_j := \{x_i/ \text{ there is a discordant edge from } x_i \text{ to } x_j\}$, and let $D := \cup_j D_j$, $m := |D|$ and $U := (\mathbb{R}^+)^m$. Now enumerate the elements of D as $x_{l_1}, \ldots, x_{l_m}$. Define the function $f_j(x, u)$ as the result of replacing in $g_j(x)$ all appearances of x_{l_i} by u_i, for each $x_{l_i} \in D_j$. The controlled system (4.5.5) thus defined has a regulatory graph $\mathcal{G}'$ that can be described as the result of removing all discordant edges from $\mathcal{G}$, where $\mathcal{G}$ is the regulatory graph obtained from the function g in 4.5.4.

Now we will define the output function $h : X \to U$ as $h_k(x) := x_{l_k}$ and close the loop by letting $u(t) = h(x(t))$. Let the vector s be defined as

$$s(i) = \begin{cases} 1 & \text{if } x_i \in A \\ -1 & \text{if } x_i \notin A \end{cases},$$

and let K_X be the orthant cone induced by s, that is $K_X = \mathbb{R}^s := \mathbb{R}^{s(1)} \times \ldots \times \mathbb{R}^{s(n)}$. Let $p(k) = -s(l_k)$, $k = 1, \ldots, m$, and let K_U be the orthant cone defined by p, that is $K_U = \mathbb{R}^p := \mathbb{R}^{p(1)} \times \ldots \times \mathbb{R}^{p(m)}$. Using the above decomposition method the next result follows.

Theorem 4.5.19 (Ensiso-Sontag Theorem 6). *Let $h : X \to U$, $u(t) = h(x(t))$, K_X and K_U be defined as above. Then, the controlled system Φ deduced from the previous construction, having the form 4.5.5, is monotone, h is a decreasing function respect to the cones, and the closed loop system is well defined and equal to the autonomous system. Furthermore, if for each strongly connected component of $\mathcal{G}'$ with vertices $S \subset \{x_1, \ldots, x_n\}$ the associated system has a well defined I/S characteristic, then the controlled system Φ allows an I/S characteristic.*

Example of Decomposition method

Consider the following system of differential equations which corresponds to the Goodwin model, negative feedback oscillator, for circadian rhythms (for a detailed description see Chapter 3).

$$(G_\lambda) = \begin{cases} \dot{x} &= K_1 R_\lambda^-(z) - \gamma_1 x &= g_1(x, y, z) \\ \dot{y} &= K_2 x - \gamma_2 y &= g_2(x, y, z) \\ \dot{z} &= K_3 y - \gamma_3 z &= g_3(x, y, z) \end{cases}$$

where the constants K_i are rates of synthesis and the constants γ_i are rates of degradation, and $R_\lambda^-(z) = \frac{\lambda^n}{\lambda^n + z^n}$ with n the cooperative index.

It is not difficult to see that the steady states satisfy the polynomial equation:

$$R_\lambda^-(z) - \frac{\gamma_1 \gamma_2 \gamma_3}{K_1 K_2 K_3} z = 0$$

Moreover, the Jacobian matrix has the following form:

$$J_{G_\lambda} = \begin{pmatrix} -\gamma_1 & 0 & K_1 \frac{dR_\lambda^-(z)}{dz} \\ K_2 & -\gamma_2 & 0 \\ 0 & K_3 & -\gamma_3 \end{pmatrix}$$

whose regulatory graph $\mathcal{G}$ at $(x, y, z) \in \mathbb{R}^3$ can be seen in Figure 4.13. The graph corresponds to an isolated negative circuit, for that reason we have an inconsistent sign assignment, implying that the autonomous system is not monotone.
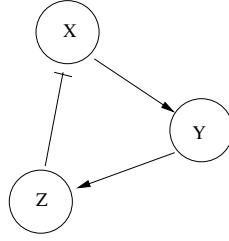
Figure 4.13: Regulatory graph $\mathcal{G}$ associated to the Goodwin model equations in Example 4.5.4. In this graph we have omitted self-loops

In this model, we have considered as agonist the variables x and y, and as antagonist the variable z. Using these sets we observe that the edge between y and z is positive and it joins an agonist with an antagonist, concluding that there exists one discordant edge. It holds that $D_x = D_y = \emptyset$ and $D_z = \{y\}$; thus $D = \{y\}$. The variable y is replaced by u in the function g_3 to form the function $f_3(x, u, z)$. The resulting controlled dynamical system is given by

$$
\begin{cases}
\dot{x} & = & K_1 R_\lambda^-(z) - \gamma_1 x \\
\dot{y} & = & K_2 x - \gamma_2 y \qquad\qquad h(x(t), y(t), z(t)) = (y(t)) \\
\dot{z} & = & K_3 u - \gamma_3 z
\end{cases}
$$

which is monotone with respect to the cones defined by $s = (+1, +1, -1)$ and $p = (-1)$, that is, $K_X = \mathbb{R}^s = \mathbb{R}^+ \times \mathbb{R}^+ \times \mathbb{R}^-$ and $K_U = \mathbb{R}^p = \mathbb{R}^-$.

4.5.5 Monotonicity in *Halobacterium NRC-1*

In the following we will show that the autonomous systems of differential equations related to Cu/Zn and Mn/Fe modules are near-monotone, because the associated regulatory graphs present negative circuits. However, using the decomposition technique (Subsection 4.5.4) it is possible to prove that the controlled dynamical system is monotone and conclude with this the desired property of global stability.

Finally, for both modules we will only consider the classes $E(I)$ and $U(I)$ without recycling of extruded metal ions. This is because, in both classes we have proved the existence of a unique equilibrium point. Therefore, the result about monotonicity in this context will ensure the global stability and convergence to that point.

Finally, given open sets $X \subseteq \mathbb{R}^n$, $U \subseteq \mathbb{R}^m$ and the underlying cones K_X, K_U, and a monotone system $\dot{x} = f(x, u)$, $u = h(x)$, with characteristic k^X, f continuous and locally Lipschitz function on x, and $h \leq_X$-decreasing and continuous, conditions $(H1), (H2), (H3), (H4)$ are

necessarily satisfied. Indeed, the only condition that still needs verification is that k^X is continuous which has been done in [AS03] Proposition 5.

Proposition 4.5.20 (Angeli, Sontag: Proposition 5)**.** *Under the previous assumptions, if (4.5.3) is a monotone system which is endowed with an input to state characteristic k^X, then k^X is a continuous map. Moreover for each $\bar{u} \in U$, $\bar{x} = k^X(\bar{u})$, the following properties hold:*

1. *For each neighborhood P of $\bar{x}$ in X there exist a neighborhood P_0 of $\bar{x}$ in X, and a neighborhood Q_0 of $\bar{u}$ in U, such that $\Phi(t, x_0, u) \in P$ for all $t \geq 0$, all $x_0 \in X$, and all inputs u such that $u(t) \in Q_0$ for all $t \geq 0$.*

2. *If, in addition, the order on the state space X is bounded, then, for each input u all whose values $u(t)$ lie in some interval $[c, d] \subseteq U$ and with the property that $u(t) \to \bar{u}$, and all initial states $x_0 \in X$, necessarily $x(t) = \Phi(t, x_0, u) \to \bar{x}$ as $t \to \infty$.*

Global stability in Cu/Zn module class $E(I)$

The system of ODE associated to Cu/Zn module in class $E(I)$ is given by:

$$(4.5.6) \qquad \qquad \dot{x} = g(x),\ x \in (\mathbb{R}^+)^{19},$$

where $g(x)$ corresponds to the right hand side functions depending on all the variables and parameters of the model (Subsection 4.3.2).

Let us associate to this system of ODE a signed graph denoted by $\mathcal{G}_1$. In $\mathcal{G}_1$ we define the set of vertices as the variables $\{x_1, \ldots, x_{19}\}$ and the edges are defined using the transpose of the Jacobian matrix J of g, i.e. there is an edge between x_i and x_j, $i \neq j$, with positive sign if $J_{ji} > 0$ and with negative sign if $J_{ji} < 0$. In Figure 4.14 we can see an illustration of this graph.

The discordant edges are associated to inconsistent minimal circuits. In $\mathcal{G}_1$ (Figure 4.14), these edges have been marked with blue color. In order to find the discordant edges we first made a partition of the set of vertices in agonists and antagonists. Since the graph $\mathcal{G}_1$ has a great number of double positive feedback loops, we have that the discordant edges correspond predominantly to negative edges. In our case, the variables in the antagonists set are $A^c = \{x_{12} = TD, x_{14} = ZntR\}$ and the other variables belong to the agonists set $A = \{x_1, \ldots, x_{19}\} \backslash \{x_{12}, x_{14}\}$.

From this set partition, we can conclude that there are 6 discordant edges, and using previous definitions we are able to construct the sets D_j. In our case it holds that $D_1 = \{x_{11}\}$,
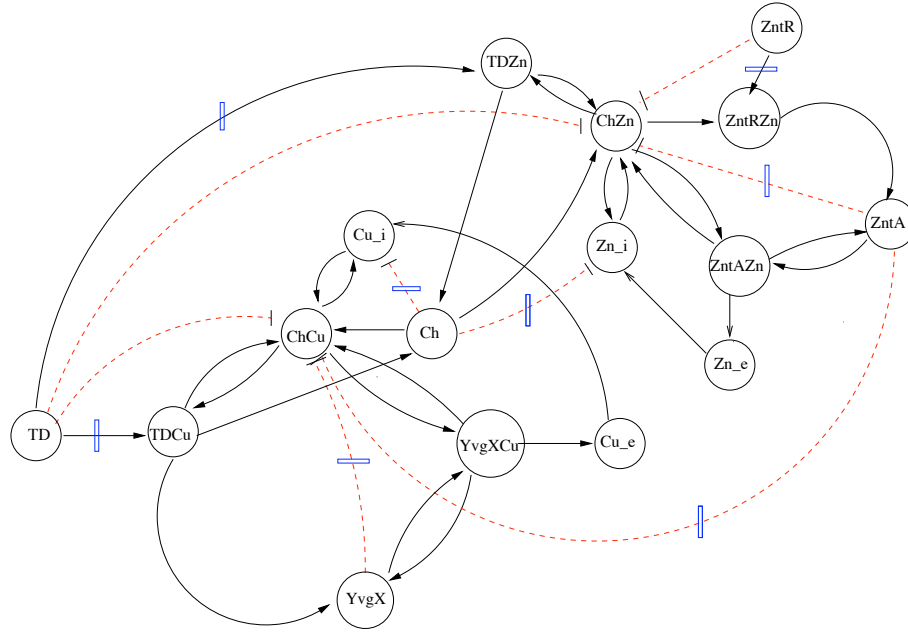
Figure 4.14: Regulatory graph associated to the Cu/Zn module class $E(I)$ obtained from the Jacobian matrix of the differential system. Red arrows correspond to negative interactions and blue lines to the discordant edges that need to be removed in order to obtain a graph without negative circuits.

$D_2 = \{x_{11}\}$, $D_3 = \{x_{13}, x_{15}\}$, $D_4 = \{x_{15}\}$, $D_5 = \{x_{12}\}$, $D_6 = \{x_{12}\}$ and $D_8 = \{x_{14}\}$, and the remainder sets D_i are empty. Thus $D = \{x_{11}, x_{12}, x_{13}, x_{14}, x_{15}\}$ and $m = |D| = 5$.

Finally, to obtain a controlled system with input output feedback function, the variables x_{11}, x_{12}, x_{13}, x_{14}, and x_{15} are replaced in functions g_j, $j \in \{1, 2, 3, 4, 5, 6, 8\}$, by the control variables $u_1, \ldots, u_5$ to form the functions $f_j(x, u)$. As a result we obtain the functions $f_1(x, u_1)$, $f_2(x, u_1)$, $f_3(x, u_3, u_5)$, $f_4(x, u_5)$, $f_5(x, u_2)$, $f_6(x, u_2)$ and $f_8(x, u_4)$ respectively, which have the following form:

$$
\begin{aligned}
\dot{x}_1 = f_1(x, u_1) \quad &= \quad \mathbf{R}_1(x_{18}) + \delta_{Ch}x_3 + \delta_{TD}x_5 + \delta_Y x_7 + \delta_{ZA}x_9 - CC_{Ch}(u_1 - x_3 - x_4)x_1 \\
\dot{x}_2 = f_2(x, u_1) \quad &= \quad \mathbf{R}_2(x_{19}) + \delta_{Ch}x_4 + \delta_{TD}x_6 + \delta_{ZR}x_8 + \delta_{ZA}x_{10} - CC_{Ch}(u_1 - x_3 - x_4)x_2 \\
\dot{x}_3 = f_3(x, u_3, u_5) \quad &= \quad CC_{Ch}(x_{11} - x_3 - x_4)x_1 - K_{TD}(x_{12} - x_5 - x_6)x_3 - K_Y(u_3 - x_7)x_3 \\
& \quad\quad -K_{ZA}(u_5 - x_9 - x_{10})x_3 - \delta_{Ch}x_3 \\
\dot{x}_4 = f_4(x, u_5) \quad &= \quad CC_{Ch}(x_{11} - x_3 - x_4)x_2 - K_{TD}(x_{12} - x_5 - x_6)x_4 - K_{ZR}(x_{14} - x_8)x_4 \\
& \quad\quad -K_{ZA}(u_5 - x_9 - x_{10})x_4 - \delta_{Ch}x_4 \\
\dot{x}_5 = f_5(x, u_2) \quad &= \quad K_{TD}(u_2 - x_5 - x_6)x_3 - \delta_{TD}x_5 \\
\dot{x}_6 = f_6(x, u_2) \quad &= \quad K_{TD}(u_2 - x_5 - x_6)x_4 - \delta_{TD}x_6 \\
\dot{x}_8 = f_8(x, u_4) \quad &= \quad K_{ZR}(u_4 - x_8)x_4 - \delta_{ZR}x_8
\end{aligned}
$$

and the other equations remain as in the original module, that is $\dot{x}_k = f_k(x) = g_k(x)$, $k \neq \{1, 2, 3, 4, 5, 6, 8\}$. Additionally, the function $h : X \to U$ has the following form $h(x) = (x_{11}, x_{12}, x_{13}, x_{14}, x_{15})$

Finally, we need to construct the vectors s and p to define the sign of the orthant cones. From the variables in A and A^c we obtain that

$$(4.5.7) \qquad s = (1, \ldots, 1, \underbrace{-1}_{TD}, 1, \underbrace{-1}_{ZntR}, 1, \ldots, 1)$$

with -1 at positions 12 and 14. On the other hand, as $D = \{x_{11}, x_{12}, x_{13}, x_{14}, x_{15}\}$ we get that

$$(4.5.8) \qquad p = (-1, +1, -1, +1, -1).$$

Using the previous equations, the controlled system for the Cu/Zn module class $E(I)$ is defined by

$$(4.5.9) \qquad \dot{x} = f(x, u_1, \ldots, u_5), \ x \in (\mathbb{R}^+)^{19}, \ u \in (\mathbb{R}^+)^5, \ h : X \to U$$

Proposition 4.5.21. *The controlled system (4.5.9) for the Cu/Zn module class $E(I)$ is monotone with respect to the orthant cones $K_X = \mathbb{R}^s$, $K_U = \mathbb{R}^p$, and it induces a globally asymptotically stable equilibrium depending on the control variables $u_1, \ldots, u_5$.*

Proof. By construction (decomposition method), system (4.5.9) is monotone with respect to the orthant cones $K_X = \mathbb{R}^s$ and $K_U = \mathbb{R}^p$ (where vectors s and p have been defined in equations (4.5.7),4.5.8)) because its associated regulatory graph $\mathcal{G}_1$ does not have any undirected negative cycle. Moreover, the output function h, which is defined as $h(x) = (x_{11}, x_{12}, x_{13}, x_{14}, x_{15})$, is a decreasing function with respect to these cones.

In order to characterize the equilibrium, it is necessary to solve

$$\dot{x} = f(x, u) = 0$$

for $x = (x_1, \ldots, x_{19})$ and fixed control variables $u = (u_1, \ldots, u_5)$.

Using the new differential equation it is possible to deduce, as we did before for the autonomous system (Subsection 4.4.1), that the variables x_{18}, x_{19}, x_7, x_9 and x_{10} are zero.

From the last assertion, equation $\dot{x}_7 = 0$ reads:

$$K_Y(x_{13} - x_7)x_3 - \mathbf{R}_3(x_7) - \delta_Y x_7 = 0$$

which implies $x_3 = 0$ or $x_{13} = 0$, since $x_7 = 0$. In the same way equations $\dot{x}_9 = 0$ and $\dot{x}_{10} = 0$ read:

$$K_{ZA}(x_{15} - x_9 - x_{10})x_3 - \mathbf{R}_4(x_9) - \delta_{ZA}x_9 = 0$$

which implies $x_3 = 0$ or $x_{15} = 0$, and $\dot{x}_{10} = 0$ leads to

$$K_{ZA}(x_{15} - x_9 - x_{10})x_4 - \mathbf{R}_5(x_{10}) - \delta_{ZA}x_{10} = 0$$

which implies $x_4 = 0$ or $x_{15} = 0$. Let us examine all different possibilities.

1. If $YvgX = x_{13} = 0$. By equation $\dot{x}_{13} = 0$, it follows that

$$\frac{Ax_5 + Bx_6}{AB + Ax_5 + Bx_6} = 0,$$

then we deduce that $x_5 = x_6 = 0$, since constants $A, B > 0$. From equation $\dot{x}_{12} = 0$, we get immediately that x_{12} is the positive solution of a second degree polynomial $\alpha_2 \bar{\delta}_{TD} x_{12}^2 + \bar{\delta}_{TD} x_{12} - G = 0$, whose solution is

$$x_{12} = \frac{-1 + \sqrt{1 + \frac{4G\alpha_2}{\bar{\delta}_{TD}}}}{2\alpha_2} > 0,$$

because all the constants are positive.

On the other hand, equations $\dot{x}_5 = 0$ implies $x_3 = 0$ or $u_2 = 0$. Equally, $\dot{x}_6 = 0$ gives $x_4 = 0$ or $u_2 = 0$.

Assuming $u_2 \neq 0$, then $x_3 = x_4 = 0$ and we conclude from equation $\dot{x}_{11} = 0$ that x_{11} is the positive solution of a second degree polynomial $\alpha_1 \bar{\delta}_{Ch} x_{11}^2 + \bar{\delta}_{Ch} x_{11} - G = 0$, whose solution is

$$x_{11} = \frac{-1 + \sqrt{1 + \frac{4G\alpha_1}{\bar{\delta}_{Ch}}}}{2\alpha_1} > 0.$$

As $x_4 = 0$, we easily derive that $x_8 = 0$ and as we have done before from $\dot{x}_{14} = 0$

$$x_{14} = \frac{-1 + \sqrt{1 + \frac{4G\alpha_3}{\bar{\delta}_{ZR}}}}{2\alpha_3} > 0.$$

From equation $\dot{x}_3 = 0$ we obtain $x_1 = 0$ and, in parallel, $x_2 = 0$ since $x_{11} \neq 0$. Finally, we get $x_{15} = 0$, and $x_{16} = Cu^*$ and $x_{17} = Zn^*$ (external amount of extruded copper and zinc) are constant and equal to the initial external amount of metal ions $\tilde{C}u$ and $\tilde{Z}n$, respectively.

2. If $x_{13} \neq 0$. Then $x_3 = 0$. Using equation $\dot{x}_5 = 0$, we find $x_5 = 0$.

- *First step:* Using the last five equations, we express x_{11}, x_{12}, x_{13}, x_{14} and x_{15} in terms of the other variables. We find:

$$x_{15} = \frac{1}{\bar{\delta}_{ZA}} \frac{x_8}{\beta + x_8}; \quad x_{13} = \frac{1}{\bar{\delta}_Y} \frac{x_6}{A + x_6};$$

$$x_{14} = \frac{-(\bar{\delta}_{ZR} + \alpha_3 \delta_{ZR} x_8) + \sqrt{(\bar{\delta}_{ZR} + \alpha_3 \delta_{ZR} x_8)^2 + 4\alpha_3 \bar{\delta}_{ZR}[(\bar{\delta}_{ZR} - \delta_{ZR})x_8 + (\delta_{ZR} - \bar{\delta}_{ZR})\alpha_3 x_8^2 + G]}}{2\alpha_3 \bar{\delta}_{ZR}}$$

$$x_{12} = \frac{-(\bar{\delta}_{TD} + \alpha_2 \delta_{TD} x_6) + \sqrt{(\bar{\delta}_{TD} + \alpha_2 \delta_{TD} x_6)^2 + 4\alpha_2 \bar{\delta}_{TD}[(\bar{\delta}_{TD} - \delta_{TD})x_6 + (\delta_{TD} - \bar{\delta}_{TD})\alpha_2 x_6^2 + G]}}{2\alpha_2 \bar{\delta}_{TD}}$$

$$G - \left[-\frac{x_6}{A + x_6} + \bar{\delta}_{Ch}(x_{11} - x_4) + \delta_{Ch} x_4 \right] (1 + \alpha_1(x_{11} - x_4)) = 0$$

- *Last step:* The only non trivial remaining equations are $\dot{x}_1 = \dot{x}_2 = \dot{x}_4 = \dot{x}_6 = \dot{x}_8 = 0$. Equation $\dot{x}_1 = 0$ gives $x_1 = 0$ or $x_4 = u_1$. But if the second option holds, then, by equation $\dot{x}_2 = 0$, we have $x_4 = x_6 = x_8 = 0$ and consequently $x_{13} = 0$, which is excluded. Thus $x_1 = 0$.

The next four equations are not independent and they have the following form:

$$0 = \delta_{CH} x_4 + \delta_{TD} x_6 + \delta_{ZR} x_8 - CC_{Ch}(u_1 - x_4) x_2$$
$$0 = CC_{Ch}(x_{11} - x_4)x_2 - K_{TD}(x_{12} - x_6)x_4 - K_{ZR}(x_{14} - x_8)x_4 - K_{ZA} u_5 x_4 - \delta_{Ch} x_4$$
$$0 = K_{TD}(u_2 - x_6)x_4 - \delta_{TD} x_6$$
$$0 = K_{ZR}(u_4 - x_8)x_4 - \delta_{ZR} x_8,$$

and if we sum them we obtain that

$$(4.5.10) \quad -CC_{Ch}(x_{11}-u_1)x_2 - K_{TD}(x_{12}-u_2)x_4 - K_{ZR}(x_{13}-u_4)x_4 - K_{ZA}u_5x_4 = 0$$

which implies since all the expressions are negative that $x_2 = 0$ and $x_4 = 0$, or $x_{11} = u_1$, $x_{12} = u_2$, $x_{14} = u_4$ and $u_5 = 0$.

If x_2 and $x_4 = 0$, then from $\dot{x}_8 = 0$ we get that $x_8 = 0$. Additionally, since $x_7 = x_9 = x_{10} = 0$, from $\dot{x}_{15} = 0$ we have that $x_{15} = 0$.

On the other hand, if $u_5 = 0$, $x_2 \neq 0$ and $x_4 \neq 0$ again from $\dot{x}_{10} = 0$ we get that $x_{15} = 0$ and then from $\dot{x}_{15} = 0$ we get that $x_8 = 0$. Hence, whatever the case, the only possible solutions are $x_6 = 0$, because $u_1 = x_{11} \neq 0$, $u_2 = x_{12} \neq 0$ and $u_4 = x_{14} \neq 0$. Moreover, $x_{13} = 0$ and $x_8 = 0$.

Since $C_{int} + x_{16} + x_{18} = \tilde{C}u$ and $Z_{int} + x_{17} + x_{19} = \tilde{Z}n$, we have that the external amount of extruded metal ions are $x_{16} = \tilde{C}u$ and $x_{17} = \tilde{Z}n$, where $\tilde{C}u = Cu_{ext}(0)$ and $\tilde{Z}n = Zn_{ext}(0)$, respectively. Concluding that the fixed control $(u_1, \ldots, u_5)$ induces a globally asymptotically stable equilibrium, because the controlled system is a finite dimensional system.

Finally, the I/S characteristic $k^X(u_1, \ldots, u_5) = (x_1, \ldots, x_{19})$ is well defined. In fact, we note that from the previous results it is evident that the state $k^X(u_1, \ldots, u_5)$ is a globally asymptotically stable state.

$\square$

To conclude the main property we prove the following proposition for the autonomous system.

Proposition 4.5.22. *The autonomous system (4.5.6) for the Cu/Zn module class $E(I)$ is globally attractive to its unique equilibrium.*

Proof. In order to prove the proposition we need to check that all the hypotheses in Theorem 4.5.14 are satisfied. That is, the small gain condition (SGC) and the hypotheses $(H1), \ldots, (H4)$.

Let $X \subseteq (\mathbb{R}^+)^{19}$, $U \subseteq (\mathbb{R}^+)^5$ be the set for initial conditions. From the decomposition method we have deduced the sets $U = (\mathbb{R}^+)^5$; $X = (\mathbb{R}^+)^{19}$, and the orthant cones $K_U = \mathbb{R}^p \subset \mathbb{R}^5$; $K_X = \mathbb{R}^s \subset \mathbb{R}^{19}$. We note that Proposition 4.5.20 can be directly applied to prove $(H1), (H2), (H3)$. Additionally, the monotonicity and existence of the characteristic have

been proved in Proposition 4.5.21, and since function $k^X : U \to X$ sends bounded sets to bounded sets (in fact k^X is constant) condition $(H4)$ also holds.

For the small gain condition, we need to prove that the discrete system $u_{n+1} = k(u_n)$ has bounded orbits and that the equation $k \circ k(u) = u$ has a unique solution $\bar{u} \in \mathbb{R}^5$. Since the components of $k(u_1, \ldots, u_5)$ are bounded it is easy to see that the orbits of the discrete system are bounded, therefore the first part of the SGC is satisfied.

In order to prove the second part of the SGC it is necessary to prove that $k(u_1, \ldots, u_5)$ has a unique fixed point. From Proposition 4.5.21 we can deduce that the feedback characteristic function $k : U \to U$ of the system is:

(4.5.11)

$$k(u_1, u_2, u_3, u_4, u_5) = \left(\frac{-1 + \sqrt{1 + \frac{4G\alpha_1}{\bar{\delta}_{Ch}}}}{2\alpha_1}, \frac{-1 + \sqrt{1 + \frac{4G\alpha_2}{\bar{\delta}_{TD}}}}{2\alpha_2}, 0, \frac{-1 + \sqrt{1 + \frac{4G\alpha_3}{\bar{\delta}_{ZR}}}}{2\alpha_3}, 0 \right)$$

where $\alpha_1, \alpha_2, \alpha_3, G$ and $\bar{\delta}$ are positive constants. It is important to note that the previous expression proves that $k(u_1, \ldots, u_5)$ has a unique fixed point. Moreover, since $k(u_1, \ldots, u_5)$ has a unique fixed point, we have that the discrete system is globally attractive.

It follows directly from Theorem 4.5.14 that the autonomous systems (4.5.6) for Cu/Zn module class $E(I)$ is globally attractive to its unique equilibrium $(x_1, \ldots, x_{19}) = k^X(u_1, \ldots, u_5)$.
□

Global stability in Mn/Fe module class $U(I)$

As before, using the system of differential equations in Subsection 4.3.4, class $U(I)$,

(4.5.12)
$$\dot{x} = g(x), \, x \in (\mathbb{R}^+)^{16},$$

we can construct the signed graph $\mathcal{G}_2$ (Figure 4.15). In $\mathcal{G}_2$ the vertices correspond to the variables of the Mn/Fe module which have been divided in two groups before defined agonists and antagonists. The variables x_8, x_{10}, x_{11}, x_{12} and x_{14} can be labeled as antagonists, that is $A^c = \{x_8, x_{10}, x_{11}, x_{12}, x_{14}\}$, and the other variables are labeled as agonists.

From this set partition we can conclude that there are 6 discordant edges, blue boxes in Figure 4.15, and with them we are able to define the sets D_j. In our case it holds that $D_3 = \{x_{10}\}$, $D_5 = \{x_{11}\}$, $D_7 = \{x_{14}\}$, $D_8 = \{x_2\}$, $D_9 = \{x_{12}\}$, $D_{16} = \{x_{13}\}$, and the remainder D_j are empty sets. Thus $D = \{x_2, x_{10}, x_{11}, x_{12}, x_{13}, x_{14}\}$.
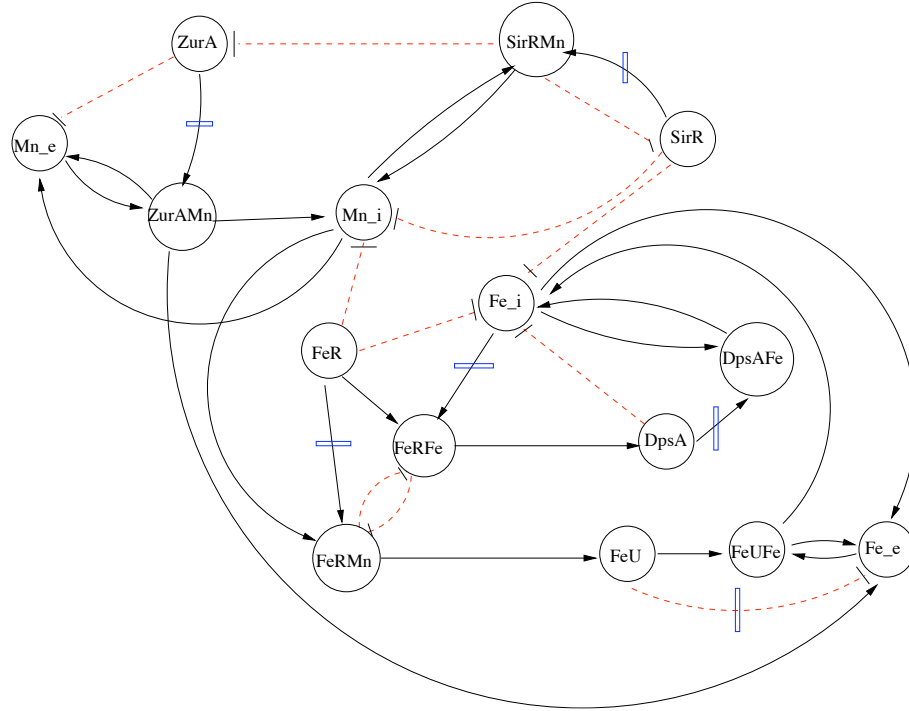
Figure 4.15: Regulatory graph associated to the Mn/Fe module obtained from the Jacobian matrix of the differential system, independent of the x value. The red arrows correspond to negative interactions and the blue lines to the discordant edges that need to be removed, in order to obtain a signed graph without negative circuits.

Finally, to obtain our controlled system with input output feedback function, the variables x_2, x_{10}, x_{11}, x_{12}, x_{13} and x_{14} are replaced by the control variables $u_1, \ldots, u_6$ to form the functions $f_8(x, u_1)$, $f_3(x, u_2)$, $f_5(x, u_3)$, $f_9(x, u_4)$, $f_{16}(x, u_5)$ and $f_7(x, u_6)$ respectively. The new functions have the following form:

$$
\begin{aligned}
\dot{x}_3 = f_3(x, u_2) &= K_{ZA}(u_2 - x_3)x_{15} - \delta_{ZA}x_3 - D_{ZA}x_3 \\
\dot{x}_5 = f_5(x, u_3) &= CC_{SR}(u_3 - x_5 - x_6)x_1 - \delta_{SR}x_5 \\
\dot{x}_7 = f_7(x, u_6) &= CC_{FR}(u_6 - x_7 - x_8)x_1 - \delta_{FR}x_7 \\
\dot{x}_8 = f_8(x, u_1) &= CC_{FR}(x_{14} - x_7 - x_8)u_1 - \delta_{FR}x_8 \\
\dot{x}_9 = f_9(x, u_4) &= CC_{DA}(u_4 - x_9)x_2 - \delta_{DA}x_9 \\
\dot{x}_{16} = f_{16}(x, u_5) &= -K_{FU}(u_5 - x_4)x_{16}
\end{aligned}
$$

and the other equations remain as in the original module, that is $\dot{x}_k = f_k(x) = g_k(x)$, $k \neq \{3, 5, 7, 8, 9, 16\}$. Additionally, the function $h : X \to U$ has the following form $h(x) = (x_2, x_{10}, x_{11}, x_{12}, x_{13}, x_{14})$.

Finally, we need to construct the vectors s and p to define the sign of the orthant cones

K_X and K_U, respectively. From the variables in A and A^c we obtain that

(4.5.13) $$s = (\underbrace{+1, \ldots, +1}_{1 \ldots 7}, -1, +1, -1, -1, -1, +1, -1, +1, +1) \in \{-1, 1\}^{16}$$

with -1 at the positions $\{8, 10, 11, 12, 14\}$. In contrast, as $D = \{x_2, x_{10}, x_{11}, x_{12}, x_{13}, x_{14}\}$ we get that

(4.5.14) $$p = (-1, +1, +1, +1, -1, +1) \in \{-1, 1\}^6.$$

With the previous information the controlled system is defined as

(4.5.15) $$\dot{x} = f(x, u_1, \ldots, u_6), \ x \in (\mathbb{R}^+)^{16}, \ u \in (\mathbb{R}^+)^6, \ h : X \to U.$$

Proposition 4.5.23. *The controlled system for the model $U(I)$ of the Mn/Fe module with fixed control is monotone with respect to the orthant cones $K_X = \mathbb{R}^s$, $K_U = \mathbb{R}^p$, and it induces a globally asymptotically stable equilibrium depending on the control variables $u_1, \ldots, u_6$.*

Proof. By construction (decomposition method), system (4.5.15) is monotone with respect to the orthant cones $K_X = \mathbb{R}^s$ and $K_U = \mathbb{R}^p$ (where vectors s and p have been defined in equations (4.5.13),(4.5.14)) because its associated regulatory graph $\mathcal{G}_2$ does not have any undirected negative cycle. Moreover, the output function h, which is defined as $h(x) = (x_2, x_{10}, x_{11}, x_{12}, x_{13}, x_{14})$, is a decreasing function with respect to these cones.

Using the new set of differential equations for the controlled system (4.5.15) it is possible to deduce, as we did before for the autonomous system (Subsection 4.4.1), that the equilibrium depends on the control variables. In order to characterize the steady states it is necessary to solve the following system

$$\dot{x} = f(x, u) = 0$$

for $x = (x_1, \ldots, x_{16})$ and fixed control variables $u = (u_1, \ldots, u_6)$.

From equations $\dot{x}_{15}$ and $\dot{x}_{16}$ we conclude that $x_{15} = 0$ or $x_{10} = x_3$ and $x_{16} = 0$ or $u_5 = x_4$. As we have done in Subsection 4.4.1, let us assume that $x_{15} = 0$, $x_{16} = 0$, and $x_{10} \neq x_3$, $u_5 \neq x_4$. It follows directly from $\dot{x}_3 = 0$ and $\dot{x}_4 = 0$ that

$$x_3 = x_4 = 0$$

Since $x_3 = 0$ and $x_4 = 0$, solutions $x_{10} = x_3 = 0$ and $u_5 = x_4 = 0$ are not allowed. In fact, from equations $\dot{x}_{10} = 0$ we conclude that the unique possibility would be that the constant

G equals to zero. This confirm our assumption that $x_{10}x_3$ and $u_5 \neq x_4$ and with them

$$x_{15} = x_{16} = 0.$$

As we have done before in the analysis of steady states for the Mn/Fe module class $U(I)$, we define the total amount of intracellular manganese, denoted by M_{int}, as the sum of Mn_{int} (free manganese), $ZurAMn$, $SirRMn$ and $FeRMn$. That is, in terms of the variables we have that $M_{int} = x_1 + x_3 + x_5 + x_7$ and we obtain that:

(4.5.16) $$\dot{M}_{int} = K_{ZA}(u_2 - x_3)x_{15} + CC_{SR}(u_3 - x_{11})x_1 + CC_{FR}(u_6 - x_{14})x_1.$$

At the equilibrium and assuming $x_{15} = x_3 = 0$ and $x_1 \neq 0$ we conclude from $\dot{M}_{int} = 0$ that

$$x_{11} = u_3 \text{ and } x_{14} = u_6.$$

Now, we define F_{int} as the total amount of intracellular ferric ions, that is, the sum of Fe_{int} (free iron), $FeUFe$, $SirRFe$, $FeRFe$, $DpsAFe$. Its derivative is $\dot{F}_{int} = \dot{x}_2 + \dot{x}_4 + \dot{x}_6 + \dot{x}_8 + \dot{x}_9$ and as before we get that

(4.5.17) $$\dot{F}_{int} = K_{FU}(x_{13} - x_4)x_{16} + CC_{FR}(x_{14} - x_7 - x_8)(u_1 - x_2) + CC_{DA}(u_4 - x_{12}).$$

At the equilibrium and assuming $x_{16} = x_4 = 0$ and $x_2 \neq 0$, we obtain from $\dot{F}_{int} = 0$ that

$$x_{12} = u_4 \text{ and } x_2 = u_1,$$

because $(x_{14} - x_7 - x_8) \neq 0$. As we have seen before if $(x_{14} - x_7 - x_8) = 0$ then from $\dot{x}_7 = 0$, $x_7 = 0$, and from $\dot{x}_8 = 0$, $x_8 = 0$. Both, together with equation $\dot{x}_{14} = 0$ implies that the constant G needs to be zero, which is not allowed.

Assuming the above results, in what follows we will obtain expressions for x_5, x_6, x_7, x_8 and x_9. From equation $\dot{x}_5 \cdot x_2 - \dot{x}_6 \cdot x_1 = 0$ we get that

$$\frac{x_1}{x_2} = \frac{x_5}{x_6} = C.$$

Since $x_2 = u_1$, we have that $x_1 = Cu_1$. Using $x_5 = Cx_6$ and replacing this expression in $\dot{x}_6 = 0$ we get that

$$x_6 = \frac{CC_{SR}u_3u_1}{CC_{SR}u_1(1+C) + \delta_{SR}} \text{ and } x_5 = \frac{CC_{SR}u_3u_1C}{CC_{SR}u_1(1+C) + \delta_{SR}}.$$

In the same way, from $\dot{x}_7 \cdot x_2 - \dot{x}_8 \cdot x_1 = 0$ we get that

$$\frac{x_7}{x_8} = C.$$

Using $x_7 = Cx_8$ and replacing this expression in $\dot{x}_8 = 0$ we get that

$$x_8 = \frac{CC_{FR}u_6u_1}{CC_{FR}u_1(1+C) + \delta_{FR}} \quad \text{and} \quad x_7 = \frac{CC_{FR}u_6u_1C}{CC_{FR}u_1(1+C) + \delta_{FR}}.$$

Additionally, from $\dot{x}_9 = 0$ we conclude that

$$x_9 = \frac{CC_{DA}u_4u_1}{CC_{DA}u_1 + \delta_{DA}}.$$

It still remains to compute x_{10} and x_{13}. From $\dot{x}_{10} = 0$ we obtain that

$$x_{10} = \frac{G}{\bar{\delta}_{ZA}\left(1 + \gamma_1\left(u_3 - (1+C)\frac{CC_{SR}u_3u_1}{CC_{SR}u_1(1+C)+\delta_{SR}}\right)\right)}.$$

To conclude, from $\dot{x}_{13} = 0$ we get that

$$x_{13} = \frac{1}{\bar{\delta}_{FU}} \frac{\frac{CC_{FR}u_6u_1C}{CC_{FR}u_1(1+C)+\delta_{FR}}}{A_2 + \frac{CC_{FR}u_6u_1C}{CC_{FR}u_1(1+C)+\delta_{FR}}}$$

Finally, the above results show that the I/S characteristic $k^X(u_1, \ldots, u_6) = (x_1, \ldots, x_{16})$ is well defined. In fact, since $x_1, \ldots, x_{16}$ depend on $u_1, \ldots, u_6$, it is evident that the state $k^X(u_1, \ldots, u_6)$, for a constant input, is a globally asymptotically stable state.

$\square$

To conclude the main property for the autonomous system we prove the following proposition:

Proposition 4.5.24. *The autonomous system (4.5.12) for the Mn/Fe module class $U(I)$ is globally attractive to its unique equilibrium.*

Proof. In order to prove the proposition we need to check that all the hypotheses in Theorem 4.5.14 are satisfied. That is, the small gain condition (SGC) and the hypotheses $(H1), \ldots, (H4)$.

Let $X \subseteq (\mathbb{R}^+)^{16}$, $U \subseteq (\mathbb{R}^+)^6$ be the set for initial conditions. From the decomposition

method we obtain the sets $U = (\mathbb{R}^+)^6$; $X = (\mathbb{R}^+)^{16}$, and the orthant cones $K_U = \mathbb{R}^p \subset \mathbb{R}^6$; $K_X = \mathbb{R}^s \subset \mathbb{R}^{16}$ (equations $(4.5.13),4.5.14)$). We note that Proposition 4.5.20 can be directly applied to prove $(H1), (H2), (H3)$. Additionally, the monotonicity and existence of the I/S characteristic have been proved in Proposition 4.5.21, and since function $k^X : U \to X$ sends bounded sets to bounded sets condition $(H4)$ also holds.

For the small gain condition we need to prove that the system $u_{n+1} = k(u_n)$ has bounded orbits and that the equation $k \circ k(u) = u$ has a unique solution $\bar{u} \in \mathbb{R}^6$. Since the components of $k(u_1, \ldots, u_6)$ are bounded it is easy to see that the orbits of the discrete system are bounded, therefore the first part of the SGC is satisfied.

In order to prove the second part of the SGC it is necessary to prove that $k(u_1, \ldots, u_6)$ has a unique fixed point. However, from Proposition 4.5.23 we can deduce that the feedback characteristic function $k : U \to U$ of the system is: $k(u_1, u_2, u_3, u_4, u_5, u_6) =$

$$\left(u_1, \frac{G}{\bar{\bar{\delta}}_{ZA}\left(1 + \gamma_1\left(u_3 - (1+C)\frac{CC_{SR}u_3u_1}{CC_{SR}u_1(1+C)+\delta_{SR}}\right)\right)}, u_3, u_4, \frac{1}{\bar{\bar{\delta}}_{FU}}\frac{\frac{CC_{FR}u_6u_1C}{CC_{FR}u_1(1+C)+\delta_{FR}}}{A_2 + \frac{CC_{FR}u_6u_1C}{CC_{FR}u_1(1+C)+\delta_{FR}}}, u_6 \right)$$

It is important to note that the previous expression proves that $k(u_1, \ldots, u_6)$ has a unique fixed point. Moreover, since $k(u_1, \ldots, u_6)$ has a unique fixed point, we have that the discrete system is globally attractive.

It follows directly from Theorem 4.5.14 that the autonomous system $(4.5.12)$ for the Mn/Fe module class $U(I)$ is globally attractive to its unique equilibrium $(x_1, \ldots, x_{16}) = k^X(u_1, \ldots, u_6)$.

$\square$

Observation 4.5.25. *It is important to note that in both modules Cu/Zn class $E(I)$ and Mn/Fe class $U(I)$ the control variables have been associated with proteins playing a central role in the mechanisms of traffic and uptake, as the case of TD, $YvgX$, $ZurA$, $SirR$ or $DpsA$, confirming the importance of these proteins in the cellular response to external metal ion stress.*

4.6 Simulations

In this section we will show the most important results obtained by the different simulations, putting emphasis in the principal proteins involved in the mechanisms of metal resistance,

such as $VNG1179C$ (with Trash domain), $VNG0702H/VNG2582H$ (Chaperones), $YvgX$, $ZntA$, $SirR$ and $DpsA$. All the simulations have been made using the programs $xDim$ [MM] to solve numerically the differential equations with unknown parameters and $CellDesigner$ ([K03], [K07]) to draw the interaction model.

In the first part we will show the standard global response of $Halobacterium\ NRC\text{-}1$ to metal stress. In this direction, we have done simulations for each one of the modules, which are consistent with the known experimental behavior. Then we will explore some relevant questions based in some observations made by the authors of the biological model such as:

1. Cellular response to the change in external metal concentrations (Baliga personal communication).

2. How the system works when we change the order in which we incorporate the metals, either at the same time or with a delay (Baliga personal communication).

3. How to measure the cellular growth and growth arrest incorporating a new differential equation to the model taking into account some experimental data of optical density versus external metal concentrations [B06].

4.6.1 Internal metal ions variation

The mathematical proof of the homeostatic property is difficult in general and Thomas rule gives us only a necessary condition. For that reason, it is important to obtain numerical results depending basically on the nature of the parameters in the models. In this direction the parametric stability of the steady state characteristics of the gene network components was analyzed.

In this part, it is demonstrated numerically, that the stationary concentration of internal metal is robust to changes in environmental conditions. For both modules, in order to test the property of homeostasis, it is important to know the variation of internal metal ions concentration at the equilibrium as a function of the parameters in the non trivial case. In our analysis we have distinguished two cases: (i) re-utilization of the extruded metal ions, and (ii) use of constant rates $\sigma_i \neq 0$.

(i) As we have seen before, in the steady state analysis (see Section 4.4.1) for both modules, the most relevant case occurs when there exists re-utilization of the extruded metal ions (class $E(II)$ and $U(II)$). This is because in the other cases (class $E(I)$) the only equilibrium is constant and equal to zero, with the exception of the unregulated

proteins with constant non zero production. In the following we will show the numerical behavior of both modules:

1. Cu/Zn **module:**

   In Figure 4.16 we can see that the concentrations for the external metal ions of Cu and Zn, x and y axis respectively, converge to a steady state that depends on the initial external concentration, as we have proved previously.
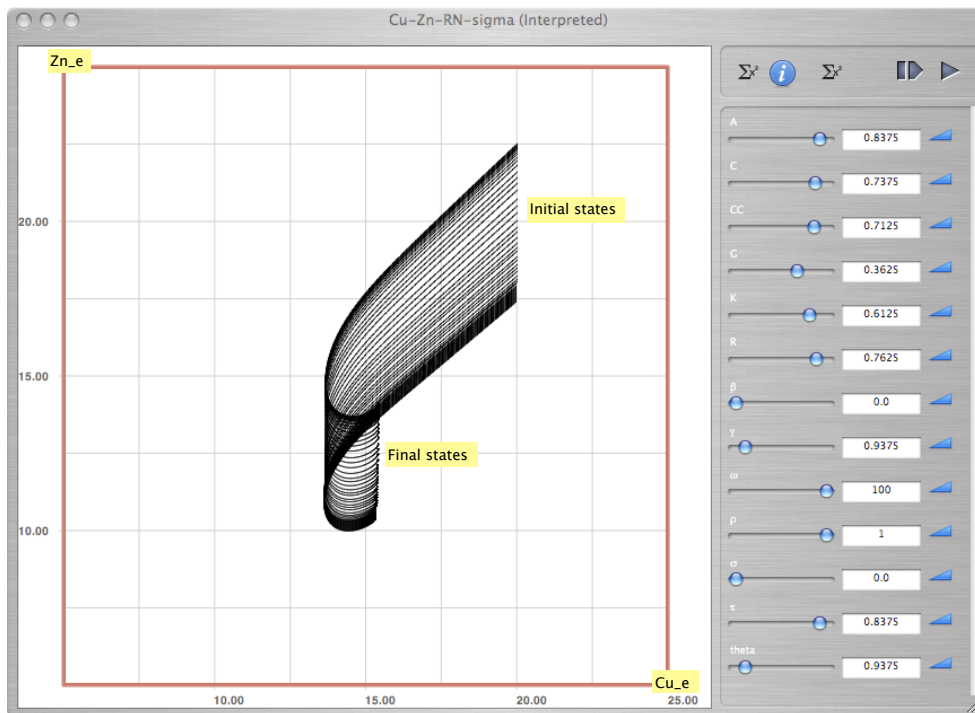

Figure 4.16: *xDim* simulation: convergence of external metal ions concentration for the Cu/Zn module, depending on the initial external metal concentration. The x axis corresponds to the external copper concentration and the y axis corresponds to the external zinc concentration.

2. Mn/Fe **module:**

   In Figure 4.17 as before we can observe that the external amount of Mn and Fe, x and y axis respectively, converges to an equilibrium that depends on the initial condition.

(ii) In previous analysis (Subsection 4.4.1), we have assumed for convenience that the parameter σ_i, rate at which the external metal ions enter to the system, remains constant and equal to zero.

For that reason a natural question, that needs to be addressed, is to understand the
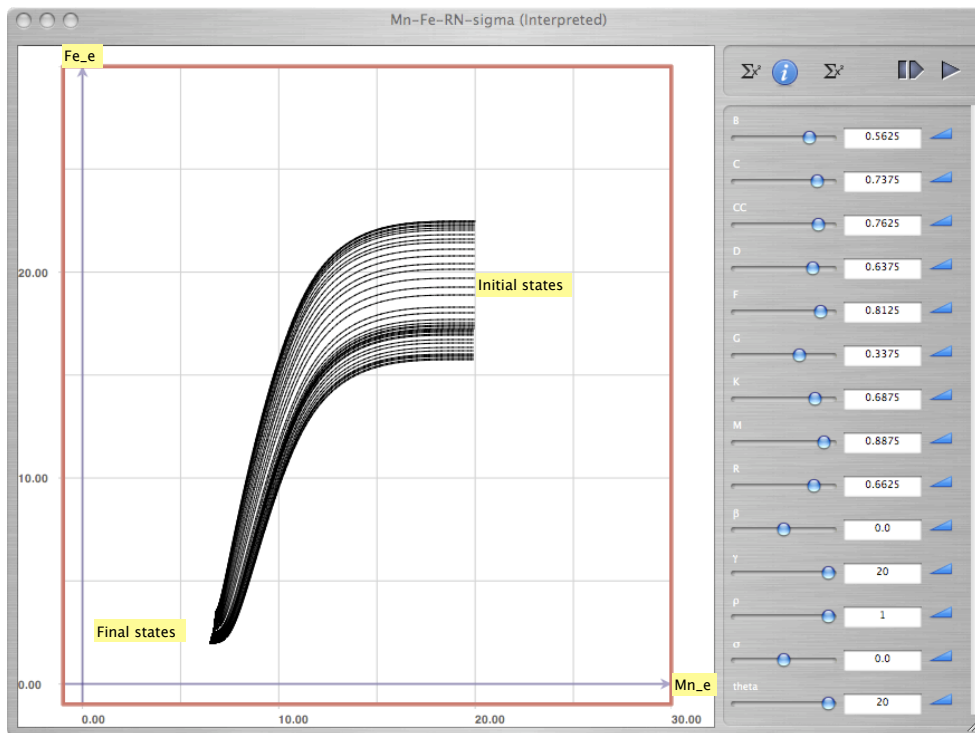
Figure 4.17: *xDim* simulation: convergence of external metal ions concentration for the Mn/Fe module, depending on the initial external metal concentrations. The x axis corresponds to the external manganese concentration and the y axis corresponds to external iron concentration.

typical behavior of both modules in the case $\sigma_i \neq 0$.

In this scenario, it is possible to prove (numerically) that for a range of values both modules preserve the property of convergence toward the equilibrium. Additionally, this demonstrates the robustness of the cellular system under external variations.

In the following we will see some of the most relevant simulations when we change the value of the parameter σ_i in both modules.

1. Cu/Zn **module:**

   We have developed several simulations in which we move the parameters σ_1 and σ_2 in order to preserve the convergence of internal and external metal concentrations. As a result we have found two threshold values, $\sigma_1^* = 0.186$ and $\sigma_2^* = 0.106$ (for the artificial values of our parameters), at which we lost the internal stability, which implies an increasing amount of metal ions that produce finally cellular death.

   In Figure 4.18 we observe the convergence of free internal copper ions independent of the initial external copper concentration. In this case the copper extrusion

mechanism is robust under external variations. This is because of the two proteins $YvgX$ and $ZntA$ that participate in the copper exportation process.
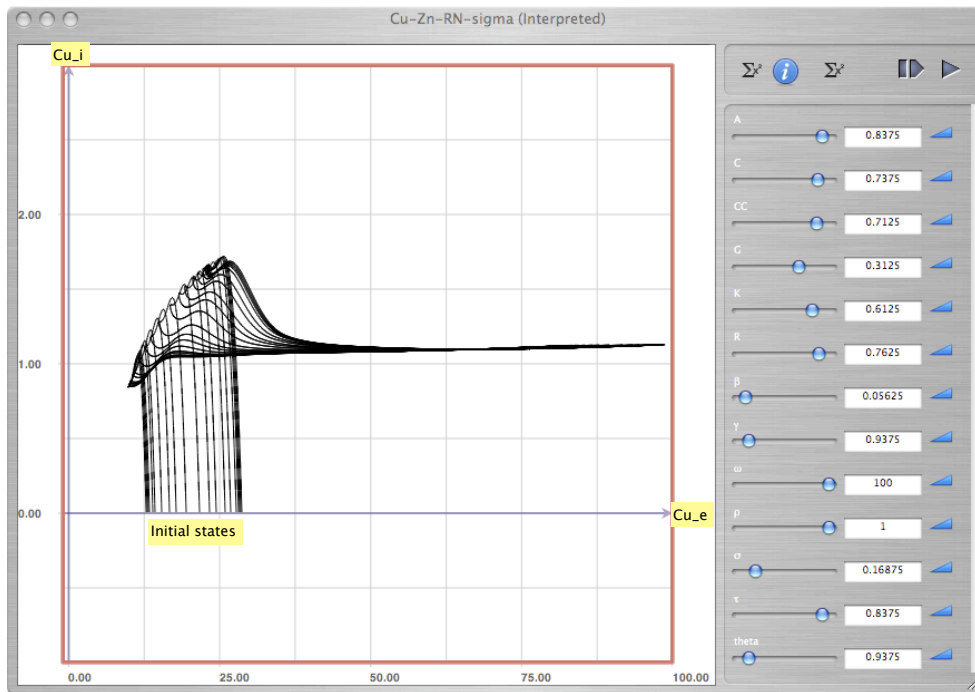

Figure 4.18: Convergence: Cu_e versus Cu_i. Internal copper remains constant independent of the initial condition for external metal ions using $\sigma_1 = \sigma = 0.186$ (copper) and $\sigma_2 = \beta = 0.056$ (zinc). The x axis represents external copper concentration and the y axis represents free internal copper concentration. The other parameters (degradation, affinity and synthesis) can be seen in the right hand side of the figure.

In contrast, for the internal zinc variation (see Figure 4.19) it is necessary that the degradation parameters to be less than a threshold (here artificially 0.2), because if it is not the case there are not convergence and the amount of internal metal ions would grow linearly. One possible explanation for this phenomenon could be that the zinc exportation mechanism is exclusive to the $ZntA$ protein and therefore it is less robust under environmental variations than the copper system.

2. Mn/Fe **module:**

In the Mn/Fe module we have found some particularities in the study of the internal metal ions variation. Specifically we have observed that the ferric uptake system is not robust under changes on the rate of iron concentration (σ_4). For that reason all the simulations have been obtained independently by changing only one parameter at once.

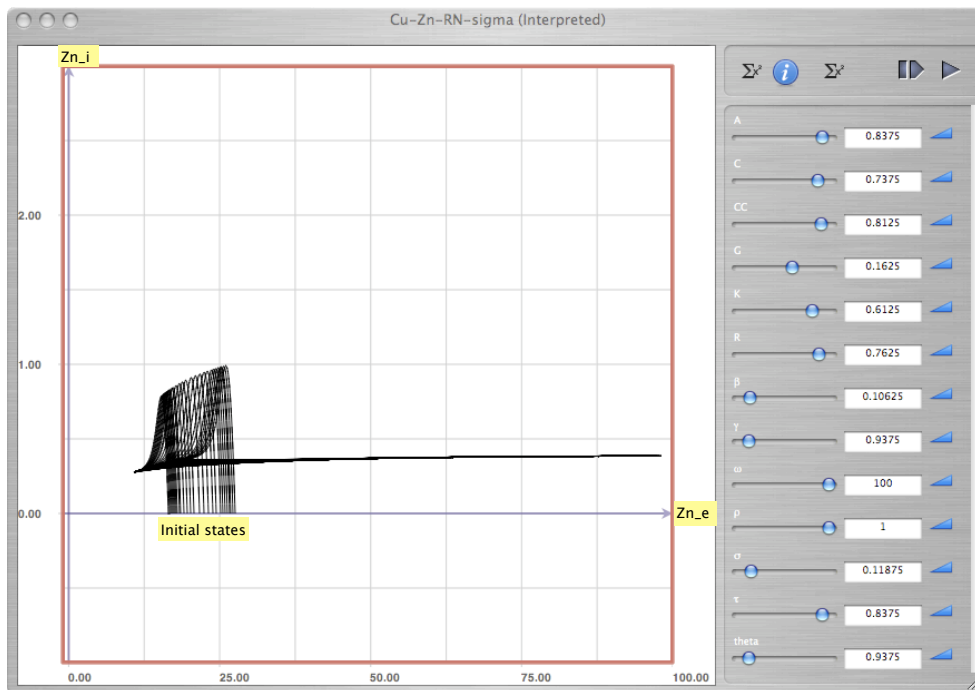If we only analyze the manganese mechanism (Figure 4.20) with $\sigma_3 \neq 0$, we can

Figure 4.19: Convergence: Zn_e versus Zn_i. Internal copper remains constant independent of the initial condition for external metal ions using $\sigma_2 = 0.106$ (zinc) and $\sigma_1 = 0.118$ (copper). The x axis represents external zinc concentration and the y axis represents free internal zinc concentration. The other parameters (degradation, affinity and synthesis) can be seen in the right hand side of the figure.

conclude that there exists again a threshold value for such rate at which the amount of internal manganese ions converge to the same equilibrium point independently of the initial external condition. This proves that the manganese mechanism is robust under external environmental variations.

In the case of internal iron ions, as Mn mimics iron deficiency if both σ_3 and σ_4 are constant but different from zero, the amount of internal iron increases steadily, i.e. there is not limit situation. In Figure 4.21 we can observe that for $\sigma_{3,4} = 0$ the amount of external and internal metal ions converge to a value different from zero. Besides, the amount of $DpsAFe$ is different from zero, which implies that the mechanism for detoxification works.

Additionally, we can observe in the small picture of Figure 4.21 the trajectories for Fe_i, Mn_i and $DpsAFe$, deployed in the same decreasing order. In this case the internal amount of iron is bigger than the internal amount of manganese because the latest is necessary in both uptake regulatory mechanisms.
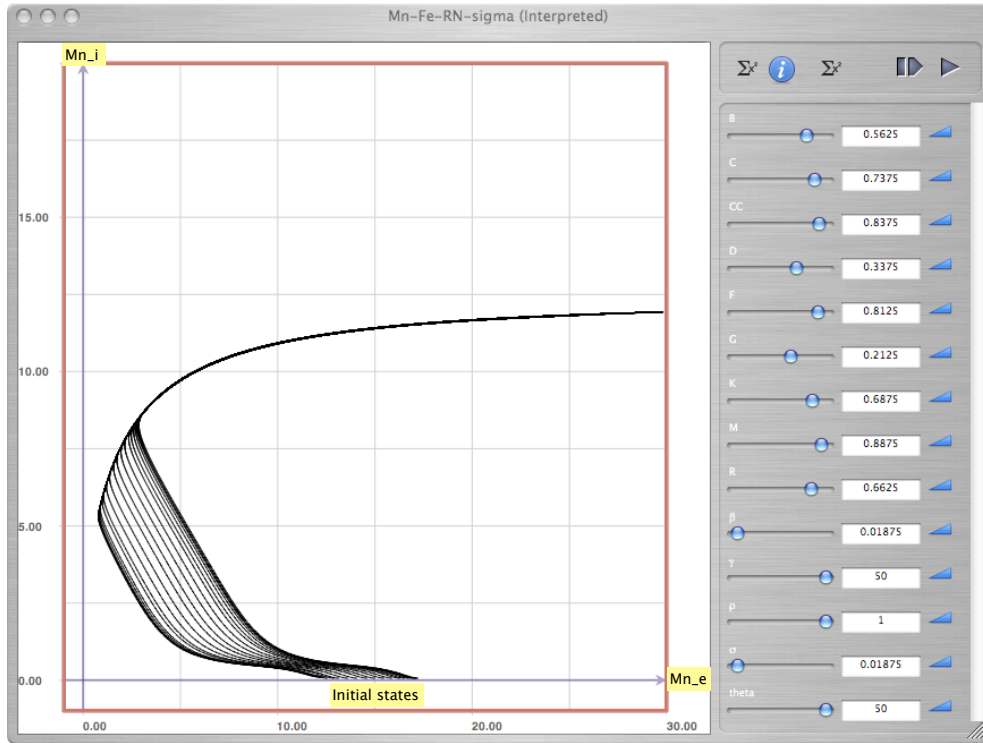
Figure 4.20: Convergence: Mn_e versus Mn_i. Internal manganese remains constant independent of the initial condition for external metal ions using $\sigma_3 = \sigma = 0.018$ (manganese) and $\sigma_4 = \beta = 0.018$ (iron). The x axis represents external manganese concentration and the y axis represents free internal manganese concentration. The other parameters (degradation, affinity and synthesis) can be seen in the right hand side of the figure.

It is important to note that in all the previous simulations the internal amount of metals ions at steady state are different from zero. This is crucial because *Halobacterium NRC-1* needs the metal ions to maintain their internal processes but at the same time it needs to be robust under external variations (maintain their values below a certain level).

4.6.2 Global response

As we have mentioned in Section 4.2 the complete model has been divided in two modules because we want to observe two independent processes, traffic and uptake of heavy metals respectively, which are essential at cellular level. Additionally, we have simplified the model eliminating the action of the zinc into the $Fe(II)$ resistance system. In fact in our final model we have only considered four metal interactions $Cu(II)$, $Zn(II)$, $Mn(II)$ and $Fe(II)$ from the six proposed in the original model (i.e. without $Co(II)$ and $Ni(II)$).

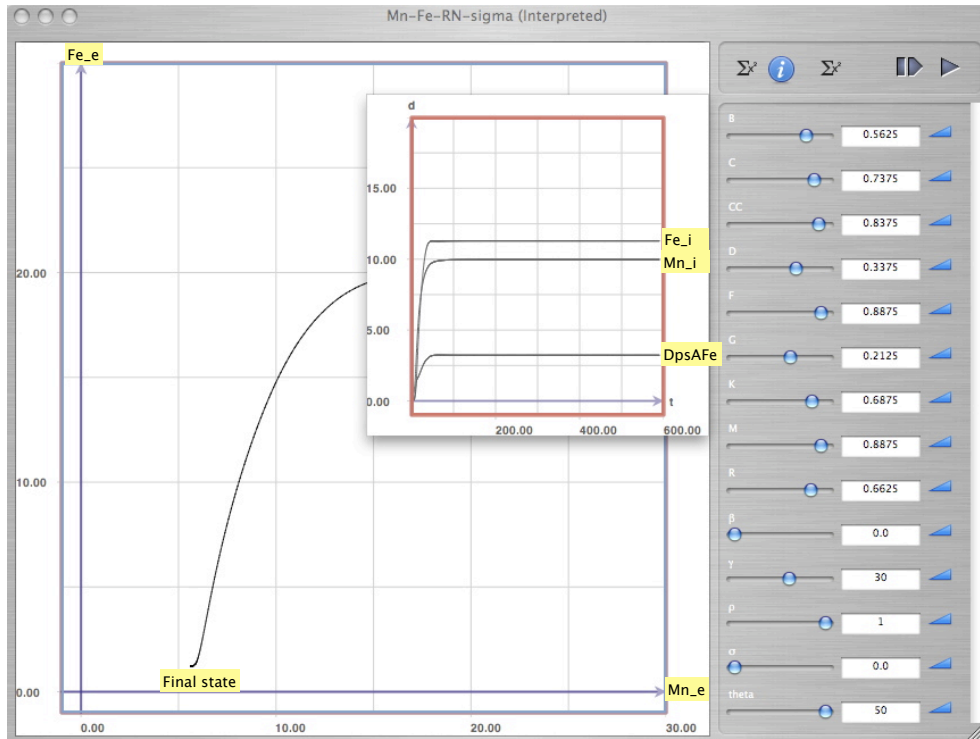In order to understand the global response we proceed to describe the trajectories obtained

Figure 4.21: Convergence: Mn_e versus Fe_e in the main picture and in the secondary picture we have the trajectories for Fe_i, Mn_i and $DpsAFe$ in the same order from top to button. Internal iron remains constant independently of the initial condition for external metal ions using $\sigma_3 = \sigma_4 = 0$. The other parameters (degradation, affinity and synthesis) can be seen in the right hand side of the figure.

numerically in the simulation of each module.

Cu/Zn module

We will begin with the traffic response, as we can see in Figure 4.22. The first conclusion deals with the variation in metals concentrations. The amount of external metals Cu_e and Zn_e decreases until reaching a value near to zero (the limit is zero). As we have explained before, in the first module we do not know the uptake mechanism, so for the simulations we have used a positive regulatory function with a threshold parameter.

The exported metals have been measured with the variables Cu^* and Zn^*, which increased, indicating that the exporting mechanism works. The only difference between the two metals is that the final amount of copper ions is greater than the amount of zinc ions, this happens mainly by two reasons: (i) For the copper we have two mechanisms exporting a bigger quantity of the metal outside the cell, $YvgX$ and $ZntA$ proteins, (ii) The zinc is used by the cell in the regulation of the copper mechanism.

In contrast, the function describing the solution for the internal metals Cu_{int} and Zn_{int} is concave and reach a maximum which coincides with the minimum of the external concentrations, then it decreases until a level next to zero. This evidence confirm the hypotheses about how the cell reacts under metal stress: at the beginning the metal enter to the cell, activates the proteins involved in the traffic process and then it is exported, reducing its toxicity. To complete the module we present a detailed description of the principal proteins in the process:

1. $VNG1179C$ acts as an activator with either $Cu(II)$ or $Zn(II)$ cofactors bound to the TRASH domain, and it is important for the up-regulation of both $YvgX$ and the chaperones. In our model we have made the assumption of the initial and constant concentration value, because we do not know the regulators for the gene. In [B06] there exists empirical evidence of inhibition under copper's presence but we did not have found a proof or references of such behavior in other articles. So we exclude this in the final model. As we can see in the simulations and in the mathematical steady state the final concentrations are different from zero.

2. The two chaperones $VNG0702H$ and $VNG2582H$ play a central role in the traffic mechanism because they initialize the complete process and transport the ions. In our simulations we have observed that a basal transcription rate concentration is necessary for the traffic of copper, so we can respond one of the hypotheses: the chaperone is constitutively present in the cell at a basal level. The simulations reveal that without the action of the chaperones we can obtain a higher internal concentration of the heavy metals.

3. $YvgX$ protein is important for withstanding copper toxicity and it is up-regulated by the complex $TDCu$ and $TDZn$. As a function of the time it grows until reaching a constant value obtained numerically in the steady state section. Meanwhile for the other protein $ZntA$ we have the same behavior, because both perform the same function. It is possible that this cause a problem in a more robust model but we do not have more information about the kinetic constants so mathematically there are no difference in the regulation.

Mn/Fe **module**

In the second module, dealing with the uptake mechanism, we have obtained a completely different behavior, mainly because we have down-regulations (negative interactions) and with them opposite results in the simulations. Here the manganese plays a central role in the
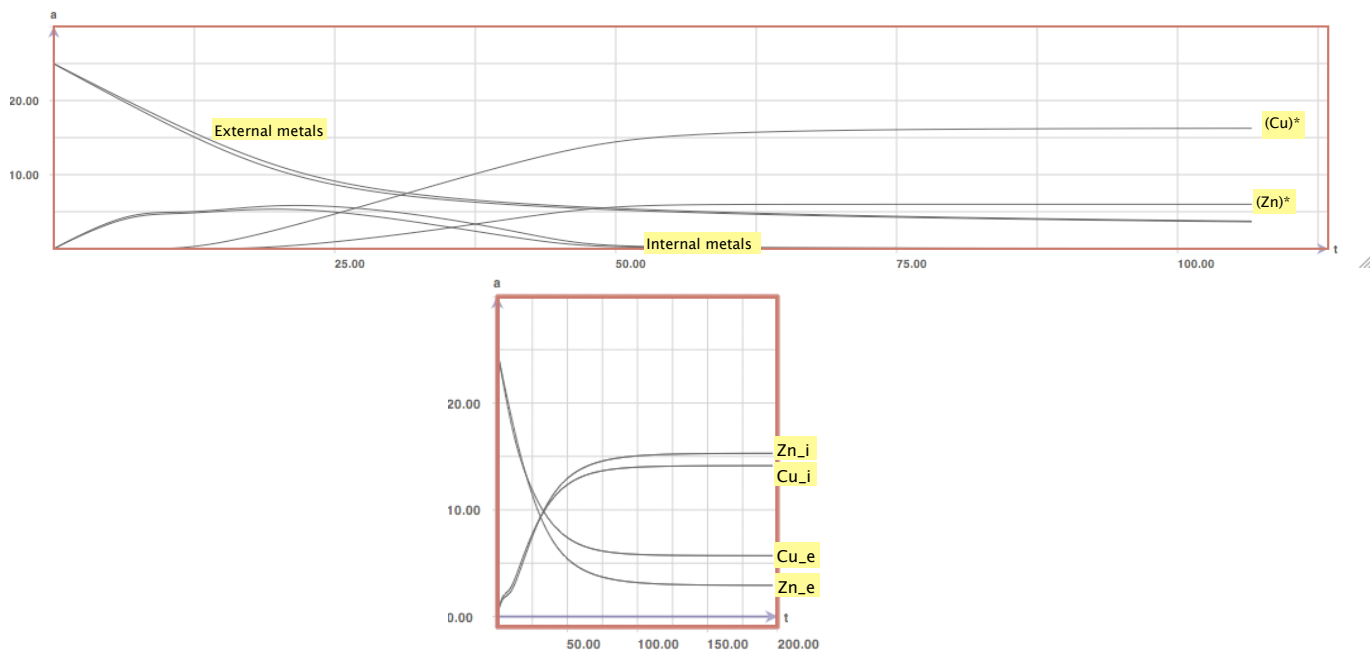
Figure 4.22: Simulation of the traffic mechanism in the Cu/Zn module for both classes $E(I)$ (up) and $E(II)$ (down).

control of Fe metabolism, because it mimics a $Fe(II)$ starvation condition in *Halobacterium NRC-1*.

The first conclusion has to do with the amount of external and internal metals. In the Mn/Fe module we have only considered the uptake mechanism proposed by Baliga et al. and for the simulation we have used a positive regulatory function that does not change the final results. As we can see in Figure 4.24 the external amount of metals ions Mn_e and Fe_e decreases as a function of time, as a cause of the negative sign. Additionally we can observe that both trajectories differ. This is because the uptake mechanism of Fe needs Mn, so it is natural that the manganese is depleted before.

On the other hand, the final internal quantity of $Fe(II)$ and $Mn(II)$ is near zero, this effect is desired since both metals are essentially toxic for the cell. This shows that the mechanism responds under external changes. So we can prove numerically that a big quantity of ferric ions are joined with the $DpsA$ protein which store it in a less toxic $Fe(III)$ form ($DpsAFe$ variable). In contrast the manganese is used by the cell in the ferric system and on its own mechanism. This is important because in some sense the manganese is used to help in other processes. To conclude we present the most relevant consequences for the other elements:

1. $SirR$ protein is the principal regulator of the uptake system for the manganese. In the presence of Mn and Fe, it down-regulates the production of $ZurA$ and of itself.
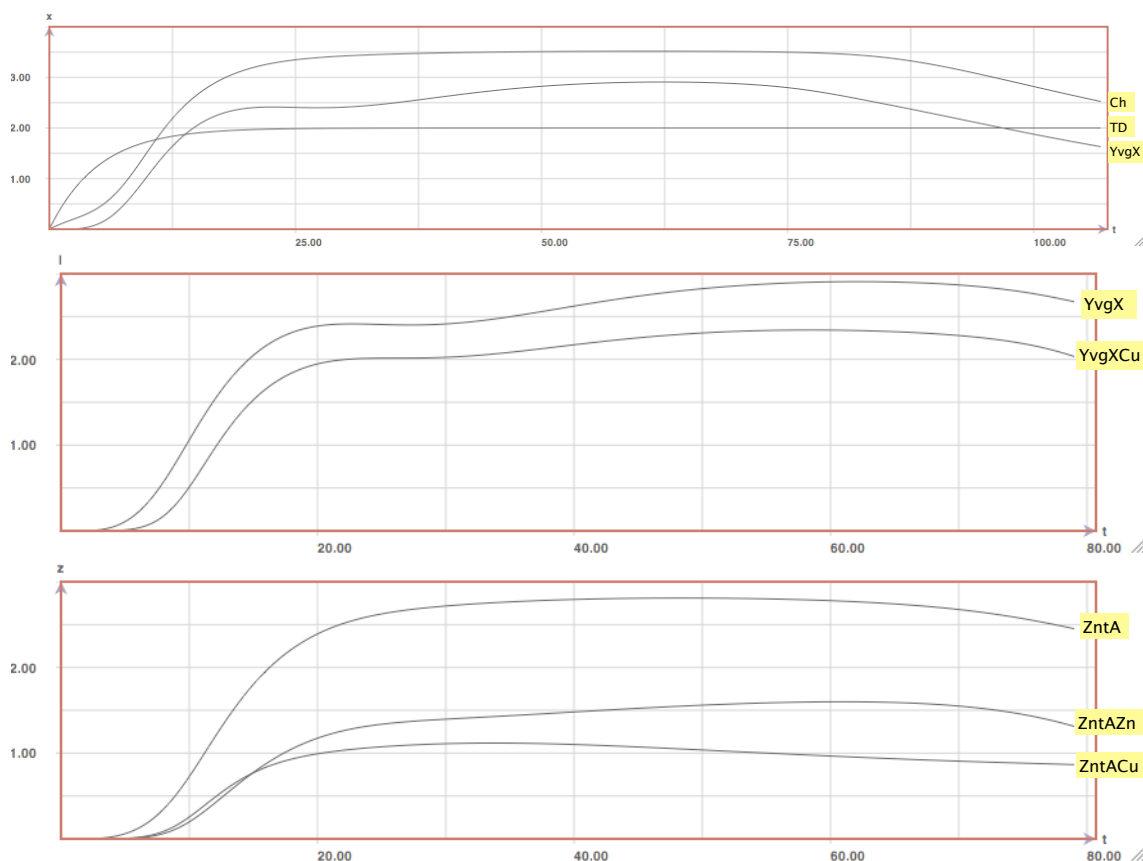
Figure 4.23: Proteins variation in the Cu/Zn module: The first graph shows the trajectory of the three proteins in the copper system: TD, Ch and $YvgX$. The second graph shows $YvgX$ and $YvgXCu$. Finally, the third graph shows $ZntA$, $ZntAZn$ and $ZntACu$.

This double negative regulation was proposed by Baliga et al., in our model we can observe the same behavior, in fact we can see that the trajectory reach a maximum, then decrease until external manganese is depleted and finally grows to reach an steady state value different from zero.

2. $ZurA$ represents the unit involved in the uptake of Mn_e, of the three proteins we have chosen one to characterize the system. In this case the final trajectory is similar to that for the $SirR$ protein, and this constitute an explanation about why both profiles, $SirR$ and $ZurA$, are similar. In Baliga's experiments they have thought at the beginning that there exists activation of the protein, but in reality the most credible explanation was double down-regulation. In the simulations we have obtained the same experimental results, so we have confirmed mathematically the hypotheses of down-regulation of $Mn(II)$ uptake to control toxicity.

3. The detoxification of the $Fe(II)$ by oxidation is made by the $DpsA$ protein. In the

graph we have a complex trajectory with a maximum and a minimum to end with a constant non zero maximum value in the stationary state. At the beginning we observe that the curve grows but when the internal amount of manganese increases then the $DpsA$ level decreases, we can see that the minimum value corresponds to the maximum value of internal $Mn(II)$. This effect coincides with the down-regulation exhibited in the biological experiments. Then when the amount of internal manganese is depleted, the curve grows again to reach the maximum at a steady state. This coincides with the experimental knowledge and with the regulation parameters. In the last point there is still a lot of work to do because we do not know exactly how the cell uses the up or down regulation in this case. To measure the quality of the detoxification process we have the variable $DpsAFe$, in the simulation we can see that the final value is near to the external ferric quantity, this means that the ferric uptake mechanism responds to the metal stress in an appropriate way.
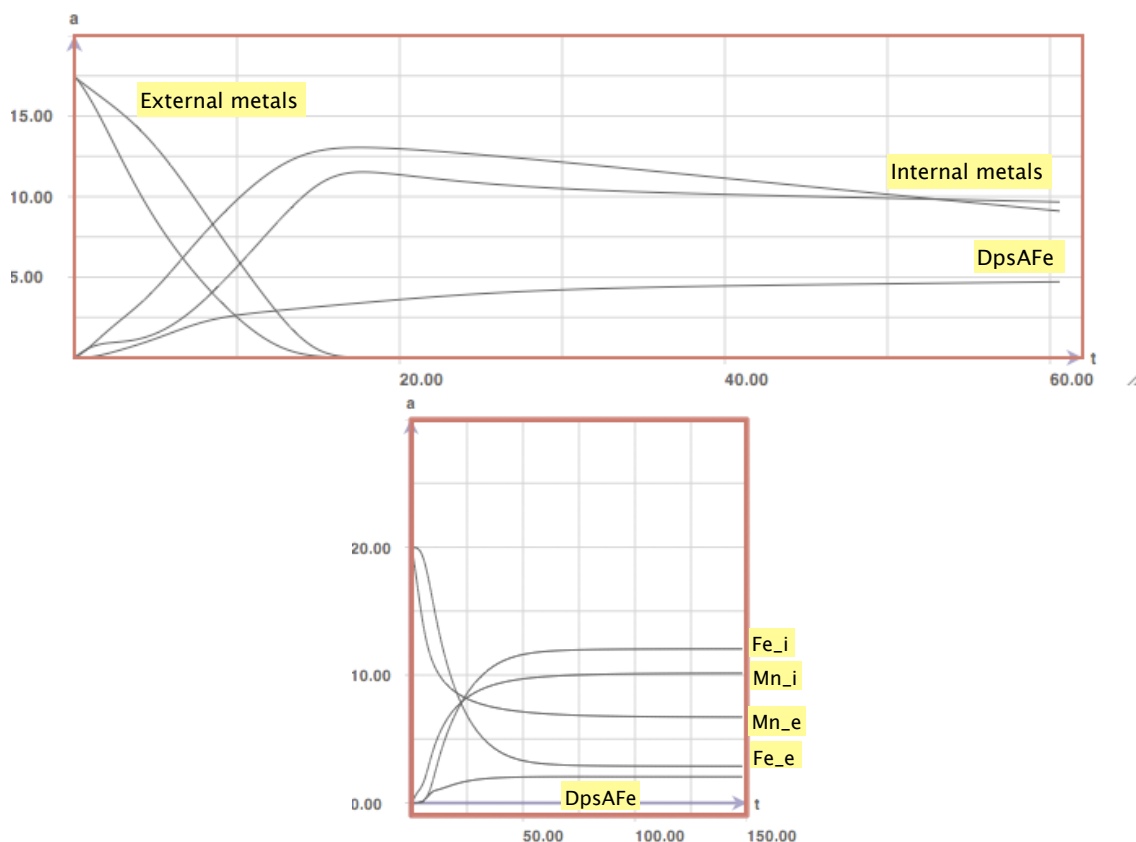

Figure 4.24: Simulation of the uptake mechanism in the Mn/Fe module for both classes $U(I)$ (up) and $U(II)$ (down). In this graph we have only considered the metal ions presented in the module and the complex $DpsAFe$ (detoxification).

4.6.3 Metal stress response

In general, when we study mechanisms dealing with the traffic and uptake of heavy metal ions, it is important not only to try to understand the proteins and genes involved in the processes, but also try to understand how the external conditions of metal ions in the medium control and damage the cellular response.

For that reason, one of the main questions in the Cu/Zn module is try to measure the cellular effect under multiple stress. That is, we try to understand how the cell responds under different stress scenarios. In our case, this scenarios are presented as successive variations of the external metal ions concentrations, and as time delay in the order of the ions.

In order to answer these questions, in our simulations we have considered three possible external variations:

1. Put both copper and zinc at the same time in the exterior: this simulation gives us the usual response, i.e., it is some kind of positive control in order to realize a comparison between the possible scenarios.

2. Put first copper and then zinc: this simulation gives us the effect of copper in the zinc mechanism.

3. Put first zinc and then copper: this simulation gives us the effect of the zinc in the copper mechanism.

4. Put copper in a successive way, that is, pulses of external ions with constant time delay.

The idea is to compare these three different conditions as we can see in the following simulation results showed in Figure 4.25:

In the simulations we have observed that the main difference is the time response. Under the third condition the copper response is faster because the zinc participate in the regulation of the copper system producing $YvgX$ protein. So when the copper enter to the cell in second place quickly is drawn to the outside. In contrast, if we put the copper first the zinc system is not initiated, since the regulation of $zntA$ depends exclusively on $ZntR$ plus $Zn(II)$. So the response is the same as we have seen before (see Figure 4.26).

In the Mn/Fe module we can do the same experiment, proving that manganese simulates iron deficiency increasing its response. In the manganese uptake system we can see the same effect because $Fe(II)$ regulates $SirR$ and $ZurA$. By contrast, stress in the $Fe(II)$ system
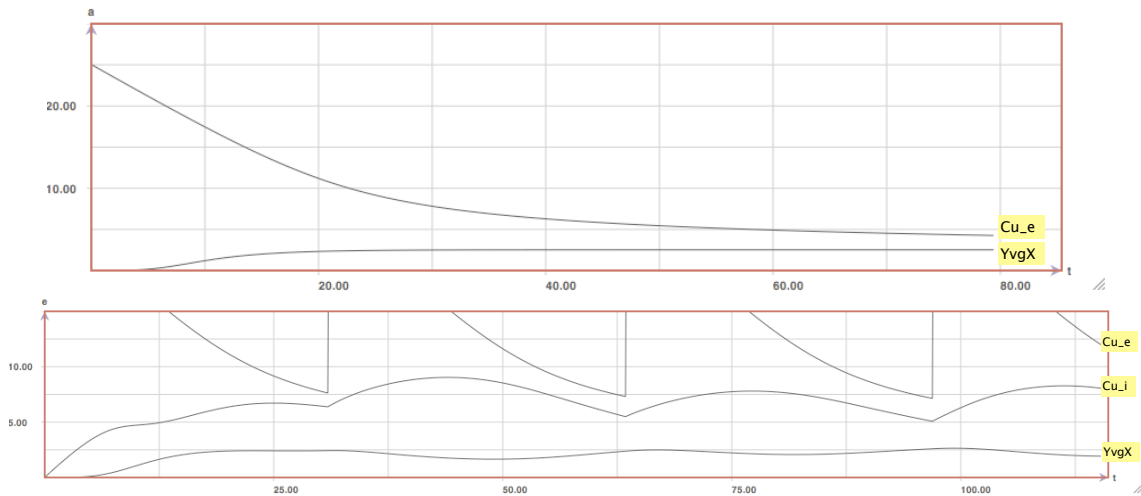
Figure 4.25: Stress response in time when we have applied three pulses of punctual external copper. The main fact is the behavior of protein $YvgX$. At each time that the pulse acts, its concentration decreases and then increases at the same time that the free internal copper change, showing that the system is robust under external variations.

is only effective until a certain threshold of the internal free iron concentrations, before this threshold the system fails. Basically, because the concentration of $DpsAFe$ maintains a constant value meanwhile the concentration of free internal $Fe(II)$ remains high (see Figure 4.27).

4.6.4 Incorporating a growth equation

Another important question extracted from the paper of Baliga et al. [B06] is to measure in some sense how the cellular growth depends on the external metal stress variations. To consider this problem, it is necessary to incorporate a new equation to the differential model, consisting mainly of a function that approximate how the cell grows and dies in the medium. Several experiments have been made in *Halobacterium NRC-1* showing growth rates assays when different metals concentrations are presented. In all of them growth was measured as the increment of the cell density (OD_{600}). The prediction says that at high concentrations of copper and zinc (bigger than 1.25 nM unit) there exists growth arrests. Besides, the experiments corroborate that the proteins $YvgX$ and $ZntA$ are necessaries because without them the cell dies at very low metal concentrations.

For that reason we have designed a growth function for the variable $\rho_{0,i}$, constant in the above simulations, in such a manner that for each one of the modules it is necessary to incorporate an additional differential equation for the region coding the main protein involved
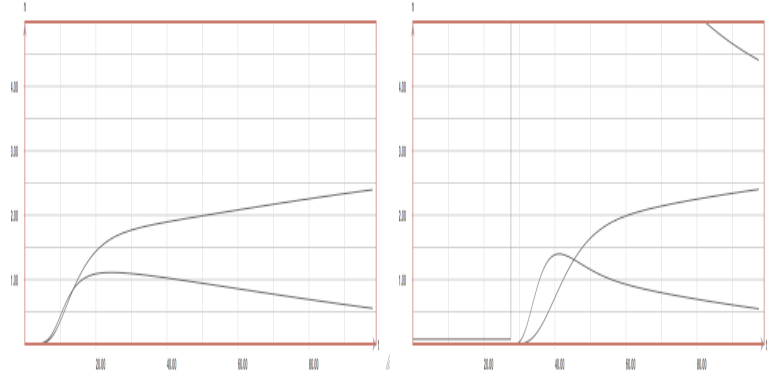
Figure 4.26: Stress by zinc in the Cu/Zn module: we have measured the effect of cellular stress resistance using $ZntA$ as a variable.
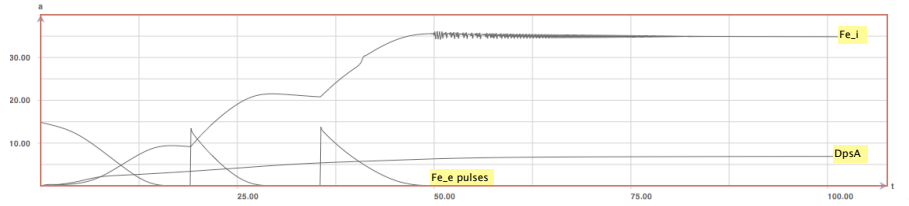

Figure 4.27: Stress by three pulses of iron: In the plot we can see the existence of a certain threshold in the iron concentration implying that the system for detoxification fails because $DpsA$ remains constant.

in the key regulatory mechanism, such as $YvgX$, $ZntA$, $ZurA$ and $DpsA$, because we know from the monotonicity property that they are essential to survive. Based in the graphical information, we have constructed the new function $G(\cdot)$ as the sum of two functions, one dealing with the growth at low metal concentrations and the other with the growth arrest at high metal concentrations. It is given by,

$$G(Cu_{int}) := \frac{K_1}{1 + \left(\frac{Cu_{int}}{Cu^*}\right)^n} + \frac{K_2\left(\frac{Cu_{int}}{Cu'}\right)^m}{1 + \left(\frac{Cu_{int}}{Cu'}\right)^m}$$

where K_1 and K_2 are two constants obtained to fit the same curve as for defective growth, and n, m are the cooperative coefficients. Finally we can see the plot of the function in Figure 4.28 for the copper case and constants $Cu' = 1.25$, $Cu^* = 8.5$, $n = 8$, $m = 2$, $K_1 = 0.6$ and $K_2 = 0.2$.

As the main idea behind the growth function is to measure the availability of the promotor region coding for the essential proteins, at the beginning, when we do not have metal ions inside the cell, the promotor region operates at some constant level. If the amount of internal metal growth until a first threshold, the promotor region increases its rate showing that the
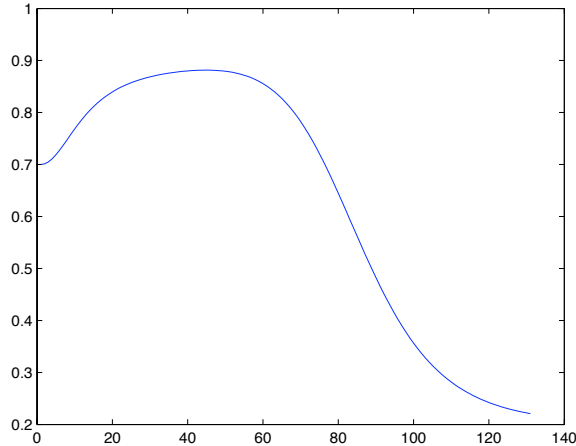
Figure 4.28: Scheme of the growth function depending on the variable for internal metal concentration and two constants indicating growth and death.

metal is necessary for the cell. But if the internal metal concentrations pass the second threshold then the function decreases until another constant level showing that high internal copper concentrations are harmful for the cell (see Figure 4.29).
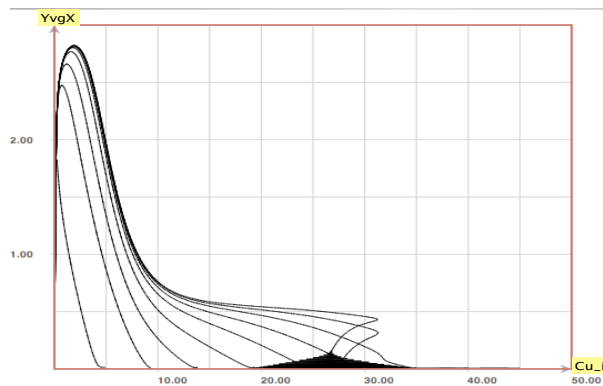
Figure 4.29: Limit behavior in the copper system with the additional growth equation: we have observed a threshold for the amount of internal free copper at which the cell arrest its growth.

So the new differential equation needed to be incorporated, for the copper model for example, has the form:

$$\dot{\rho} = G(Cu_{int})\rho - \gamma\rho$$

In general, we can incorporate independently to each module one equation modeling the cellular growth effect, because it depends on each internal metal concentration variable, regulating only the partial mechanism but with global effect, as we show in the compared

simulations. With all this information we are able to propose a more realistic model for the metal stress phenomena.

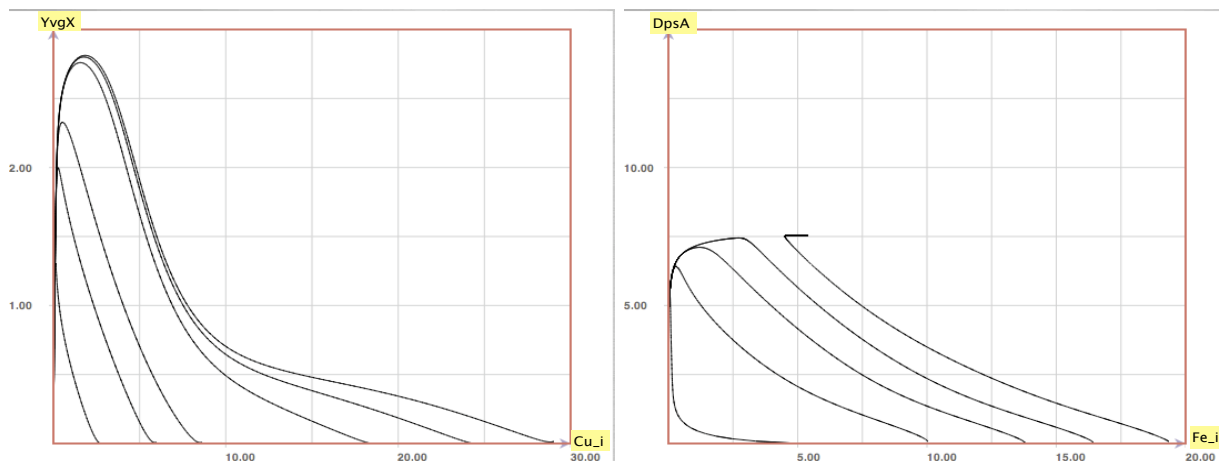Figure 4.30: Left: $YvgX$ versus Cu_{int}. At a bigger concentration of metal the slope of the curve decreases because we are in the right part of the growth function G. Right: $DpsA$ versus Fe_{int}. We can see a limit phenomenon, if the amount of free internal iron is bigger than a certain threshold, the mechanism did not work and the cell arrest its growth.

In the simulations we have measured the variation of essential proteins concentrations versus the variation of the free internal metal condition as we can see in Figure 4.30. In the case of $YvgX$ protein production versus free internal copper concentration, we can observe that at a bigger concentration of metal the slope of the curve decreases because we are in the right part of the growth function G. Meanwhile, in the case of $DpsA$ protein production versus free internal iron concentration, we can see a limit phenomenon. If the concentration of Fe_{int} is bigger than a certain threshold, the mechanism did not work and the cell arrest its growth.

In summary, we numerically test that high internal copper concentrations are harmful for the cell and the same behavior is true for iron where if the free internal amount of $Fe(II)$ pass a critical value the cell arrest its growth. These evidences corroborate that the trafficking (copper) and detoxification (iron) mechanisms are necessary for cellular survival.

4.7 Conclusions and discussions

The mathematical model for metal stress response constructed in this chapter has been mainly achieved from previous biological results of Baliga and coworkers, besides an exhaustive searching in the literature. Using this information we have derived some of the chemical

reactions governed by mass-action kinetics and with them we have proposed two modules, each one of them with more than 16 differential equations, dealing with essential cellular mechanisms such as traffic, uptake, efflux, detoxification and extrusion of heavy metal ions.

Once both modules are designed two questions arise naturally: a mathematical analysis in order to capture unknown information and simulations in order to answer and corroborate essential biological questions. In this direction, since metal resistance to external stress is a phenomenon of "equilibrium", we have made a steady state analysis with global convergence results, and we have studied the homeostasis property of the system. Additionally, several simulations confirm biological knowledge and reveal new evidence for metal stress resistance.

In the construction of both modules we have considered some restrictions as the elimination of the effect of nickel and cobalt. Moreover, we have introduced some interpretations and simplifications of the biological data in order to isolate the dynamical behaviors that we want to describe. In this context, for example, we have defined a variable for free internal metal ion (for the four metals) to represent the internal metal which is not bounded to a protein, that could be involved at the same time in storage or metabolic activities that remains unknown and independent of our model.

Some of the main questions are based in some observations made by the authors of the biological model such as: (i) Cellular response to the change in external metal concentrations (Baliga personal communication), (ii) How the system works when we change the order in which we incorporate the metals, either at the same time or with a constant time delay (Baliga personal communication), and (iii) How to measure the cellular growth and growth arrest incorporating a new differential equation to the model taking into account some experimental data of optical density versus external metal concentrations.

In the Cu/Zn module we have seen that the curve for the concentration of external copper grows faster than the curve for the concentration of external zinc. This behavior is consistent with two biological forces: zinc is necessary inside the cell because it is used in multiple regulatory mechanisms and copper is exported by two different proteins $YvgX$ and $ZntA$. In the simulations we have corroborated that the chaperone is necessary at basal concentration in order to initiate the main processes.

Dealing with alternate changes in external metal ion concentrations we have observed that the most important difference is the time response. Under the third condition, put first zinc and then copper, the copper response is faster because the zinc participate in the regulation of the copper system producing $YvgX$ protein. Hence when copper ions enter to the cell in second place quickly are drawn to the outside. In contrast, if we first put the copper, the zinc system is not initialized since the regulation of $zntA$ depends exclusively on the complex

ZntR plus *Zn(II)*.

In the Mn/Fe module we can do the same experiment, proving that manganese simulates iron deficiency increasing its response. In the manganese uptake system we can see the same effect because $Fe(II)$ regulates $SirR$ and $ZurA$. By contrast, stress in the $Fe(II)$ system is only effective until a certain threshold of the internal free iron concentrations, before this threshold the system fails. Basically, because the concentration of $DpsAFe$ maintains a constant value meanwhile the concentration of free internal $Fe(II)$ remains high.

From the mathematical point of view we have proved that both modules, class $E(I)$ and $U(I)$, present a unique steady state depending on the initial external amount of metal ions. Meanwhile, the other two classes, $E(II)$ and $U(II)$, present a finite number of equilibrium states. The simulations and rigorous mathematical proofs confirm that the system attains an equilibrium, and that the machinery determined by the trafficking and uptake mechanisms allow to adapt the internal state of the cell to changes in the external level of heavy metal ions.

Homeostasis and internal metal response have been studied. It is well known that these kind of systems dealing with resistance mechanisms are homeostatic. The homeostasis phenomenon is determined either by the convergence to a steady state or small oscillations around a given value. Nevertheless, it is difficult to answer positively these questions due to the complexity and nonlinearity of the differential equations. For that reason we have studied the existence of negative circuits (necessary condition) to identify the essential proteins involved in cellular maintaining. Here it was crucial to consider the effect of σ_i, rate at which the external metal ions enter to the system, constant but different from zero.

Together with the steady state analysis, the property of global convergence have been proved using the approach developed for near-monotone systems [ES06]. In this context it is possible to prove that both modules are near monotone due to the presence of inconsistent edges (negative undirected cycles) in its regulatory graph. Nonetheless, it is possible to decompose both modules into controlled monotone systems and using a small gain condition prove the desire property.

Finally, we have incorporated independently to each module one equation modeling the cellular growth effect in order to propose a more realistic model. For that reason, using previous biological evidence we have constructed a growth function to measure the availability of the promotor region coding for the essential proteins. Additionally, cellular growth effect depends on each internal metal concentration variable, regulating only the partial mechanism but with global effect. In different simulations we have observed that there exists critical values (thresholds) for the internal metal ion concentrations. For example, we are able to

test that high internal copper concentrations are harmful for the cell and the same behavior is true for iron where if the free internal amount of $Fe(II)$ pass a critical value the cell arrest its growth. These evidences corroborate that the trafficking and detoxification mechanisms are necessary for cellular survival.

In the future we expect to clarify some important questions that have not been taken into account in this work. In this direction, it would be interested to find a critical range for the unknown parameters values, test the model against new observations to see the prediction power and lately extend the model incorporating new biological information as reactions that involve new differential equations specially to particular mechanisms for nickel and cobalt, which have not been taken into consideration in this work.

Bibliography

[AS03] Angeli, D., Sontag, E.D.: Monotone control systems. IEEE Trans. Autom. Control, 48, 1684-1698, 2003.

[B02] Baliga, N.S., Pam, M., Goo, Y.A., Yi, E.C., Goodlett, D.R., Dimitrov, K., Shannon, P., Aebersold, R., Ng, W.V., Hood, L.: Coordinat regulation of energy transduction modules in *Halobacterium NRC-1* sp. analyzed by a global system approach. Proc. Natl. Acad. Sci. 99, 14913-14918, 2002.

[B04] Baliga, N.S., Bjork, S.J., Bonneau, R., Pan, M., iloanusi, C., Kottemann, M.C.H., Hood, L., DiRuggiero, J.: System level insights into the stress response to UV radiation in the halophilic archaeon *Halobacterium NRC-1*. Genome Research 14, 1025-1035, 2004.

[B06] Baliga, N.S., Kaur, A., Pan, M., Meislin, M., Facciotti, M., El-Gewely, R.: A system view of haloarchaeal strategies to withstand stress from transition metals. Genome Research 16, 841-854, 2006.

[B07] Baliga, N.S., Schmid A.: Prokaryotic System Biology. System Biology, 395-423, Springer Netherlands 2007.

[B08] Baliga, N.S.: Personal communication in Congress. 6th International Conference on Pathways, Networks, and Systems Medicine. Crete, Greece, June 16-21 2008.

[Bo06] Bonneau, R., Reiss, D., Shannon, P., Facciotti, M., Hood, L., Baliga, N., Thorsson, V.: The Inferelator: an algorithm for learning parsimonious regulatory networks from systems-biology data sets de novo. Genome Biology, 7(5): R36, 2006.

[Ch07] Chivers, P. T.: A Galvanizing story Protein stability and Zinc homeostasis. Journal of Bacteriology, 2953-2954, 2007.

[D98] Dancer, E.N.: Some remarks on a boundedness assumption for monotone dynamical systems. Proc. of the AMS126, 801-807, 1998.

[ES04] Enciso, G.A., Sontag, E.: Monotone systems under positive feedback: multistability and a reduction theorem. Systems and control letters. 2006.

Bibliography

[ES06] Enciso, G.A., Sontag, E.: Global attractivity, I/O monotone small-gain theorems, and biological delay systems. Discrete and continuous dynamical systems, Volume 14, number 3, March 2006.

[ESS06] Enciso, G.A., Smith, H.L., Sontag, E.: Nonmonotone systems decomposable into monotone systems with negative feedback. J. Differential equations 224, 205-227, 2006.

[E03] Ettema, T.J., Huynen, M.A., de Vos, W.M., van der Oost, J.: TRASH: A novel metal-binding domain predicted to be involved in heavy-metal sensing, traffic and resistance. Trends Biochem. Sci. 28, 170-173, 2003.

[E06] Ettema, T.J., Brinkman, A., Lamers, P., Kornet, N., W.M., de Vos, W.M., van der Oost, J.: Molecular characterization of a conserved archaeal copper resistance (cop) gene cluster and its copper-responsive regulator in Sulfolobus solfataricus P2. Microbiology 152, 1969-1979, 2006.

[F99] Forbes, J., Hsi, G., Cox, D.: Role of the Copper-binding domain in the copper transport function of ATP7B, the P-type ATPase defective in Wilson Disease. The Journal of biological chemistry 274(18), 12408-12413, 1999.

[G98] Gouzé, J.-L.: Positive and negative circuits in dynamical systems. Journal of Biolo-gycal Systems, 6:11-15, 1998.

[H99] Hamza, I., Schaefer, M., Klomp, L.W., Gitlin, J.D.: Interaction of the copper chap-erone HAH1 with the Wilson disease protein is essential for copper homeostasis. Proc, Natl. Acad. Sci. 96, 13363-13368, 1999.

[Ha01] Hantke, K.: Iron and metal regulation in bacteria. Curr. Opin. Microbiol. 4, 172-177, 2001.

[He99] Héchard, Y., Dalet, K., Gouin, E., Cenatiempo, Y., Cossart, P.: Characterisation of a new operon encoding a Zur-like protein and an associated ABC zinc permease in Listeria monocytogenes. FEMS Microbiology Letters 174, 111-116, 1999.

[Hi85] Hirsch, M.: Systems of differential equations that are competitive or cooperative: Convergence almost everywhere. SIAM J. Mathematical Analysis, 16:423-439, 1985.

[K03] Funahashi, A., Tanimura, N., Morohashi, M., and Kitano, H.: CellDesigner: a process diagram editor for gene-regulatory and biochemical networks. BIOSILICO, 1:159-162, 2003.

[K07] Funahashi, A., Jouraku, A., Matsuoka, Y., Kitano, H.: Integration of CellDesigner and SABIO-RK. In Silico Biol. 7(2 Supple), S81-90, 2007.

[L99] Larin, D., Mekios, C., Das, K., Ross, B., Yang, A.S., Gilliam, T.C.: Characterization of the interaction between the Wilson and Menkes disease proteins and the cytoplasmic copper chaperone, HAH1p. Journal Biol. Chem. 274, 28497-28504, 1999.

[M01] Mercer, J. F.: The molecular basis of copper-transport diseases. Trends Mol. Med. 7, 64-69, 2001.

[MM] Monticelli, Marc: *xDim*, Interactive Numerical Experimentation software.

[Mo05] Moore, C.M., Gaballa, A., Hui, M., Ye, R.W., Helmann, J.D.: Genetic and physiological responses of Bacillus subtilis to metal ion stress. Molecular Microbiology 57(1), 27-40, 2005.

[N99] Nelson, N.: Metal ion transporters and homeostasis. The EMBO Journal Vol.18 (16), 4361-4371, 1999.

[P06] Pécou, E., Maass, A., Remenik, D., Briche, J., Gonzalez, M.: A Mathematical Model for Copper Homeostasis in Enterococcus hirae. Mathematical Biosciences 203(2), 222-239, 2006.

[Pe05] Pennella, M., Giedroc, D.: Structural determinants of metal selectivity in prokaryotic metal-reponsive transcriptional regulators. BioMetals 18, 413-428, 2005.

[R02] Reindel, S., Anemuller, S., Sawaryn, A., Matzanke, B.F.: The DpsA-homologue of the archaeon *Halobacterium* salinarum is a ferretin. Biochim. Biophys. Acta 1598, 140-146, 2002.

[R05] Reindel, S., Schmidt, C.L., Anemuller, S., Matzanke, B.F.: Expression and regulation pattern of ferritin-like DpsA in the archaeon *Halobacterium* Salinarum. Biometals 18, 387-397, 2005.

[Se00] Sen, A., Dwivedi, K., Rice, K.A.: Growth phase and metal-dependent regulation of the dpsA gene in Synechococcus sp. strain PCC7942. Arch. Microbiol 173, 352-357, 2000.

[Sa01] Savageau, M.A.: Design principles for elementary gene circuits: Elements, methods and examples. Chaos 11(1), 141-159, 2001.

[So01] Soulé, C.: Graphic requeriments for multistability. ComplexUs 1, 123-133, 2003.

[SKT07] Soulé, C., Kaufman, M., Thomas, R.: A new necessary condition on interaction graphs for multistationarity. Journal of Theoretical Biology, 248: 67585, 2007.

[Sz03] Solioz, M., Stoyanov, J.V.: Copper homeostais in Enterococcus hirae. FEMS Microbiology Reviews 27, 183-195, 2003.

Bibliography

[Sg07] Sontag, E.: Monotone and near-monotone biochemical networks. Syst. Sybth. Biol 1, 59-87, 2007.

[To05] Tottey, S., Harvie, D.R., Robinson, N.J.: Understanding how cells allocate metals sensors and metallochaperones. Acc. Chem. Res. 38, 775-783, 2005.

[Th81] Thomas, R.: On the relation between the logical structure of systems and their ability to generate multiple steady states and sustained oscillations. In Series in Synergetics, volume 9, pages 180-193. Springer, 1981.

[Y05] Yamamoto, K., Ishihama, A.: Transcriptional response of Escherichia coli to external zinc. Journal Bacteriology 187, 6333-6340, 2005.

[Z04] Zeth, K., Offermann, S., Essen, L.O., Oesterhelt, D.: Iron-oxo clusters biomineralizing on protein surfaces: Structural analysis of *Halobacterium* salinarum DpsA in its low- and high-iron states. Proc. Natl. Acad. Sci. 101, 13780-13785, 2004.